LA-UR- 09-01414

Approved for public release; distribution is unlimited.

Title:	A Fully Relativistic Approach for Calculating Atomic Data for Highly Charged Ions
Author(s):	Douglas H. Sampson, Hong Lin Zhang and Christopher J. Fontes
Intended for:	Submission for publication to Physics Reports

Los Alamos
NATIONAL LABORATORY
EST. 1943

Form 836 (7/06)

A FULLY RELATIVISTIC APPROACH FOR CALCULATING ATOMIC DATA FOR HIGHLY CHARGED IONS

Douglas H. Sampson *

Department of Astronomy and Astrophysics, The Pennsylvania State University, University Park, PA 16802, USA

Hong Lin Zhang and Christopher J. Fontes **

Applied Physics Division, Los Alamos National Laboratory, Los Alamos, NM 87545, USA

Abstract

We present a review of our fully relativistic approach to calculating atomic data for highly charged ions, highlighting a research effort that spans twenty years. Detailed discussions of both theoretical and numerical techniques are provided. Our basic approach is expected to provide accurate results for ions that range from approximately half ionized to fully stripped. Options for improving the accuracy and range of validity of this approach are also discussed. In developing numerical methods for calculating data within this framework, considerable emphasis is placed on techniques that are robust and efficient. A variety of fundamental processes are considered including: photoexcitation, electron-impact excitation, electron-impact ionization, autoionization, electron capture, photoionization and photorecombination. Resonance contributions to a variety of these processes are also considered, including discussions of autoionization, electron capture and dielectronic recombination. Ample numerical examples are provided in order to illustrate the approach and to demonstrate its usefulness in providing data for large-scale plasma modeling.

Key words: relativistic, atomic structure, excitation, ionization, dielectronic recombination, Breit interaction
PACS: 31.15.Ar, 31.30.Jv, 32.80.Dz, 32.80.Fb, 34.80.Kw, 34.80.Lx

* Posthumous.
**Corresponding author.
Email addresses: zhang@lanl.gov (Hong Lin Zhang), cjf@lanl.gov (Christopher J. Fontes).

Contents

1 Introduction and purpose

The purpose of this review is to describe a fully relativistic approach we have developed over the past twenty years for calculating atomic data pertaining to highly charged ions. By fully relativistic, we mean that all orbitals, bound and free, are solutions of the single-electron Dirac equation with a central potential.

The method used in calculating the atomic data is a relativistic distorted-wave (RDW) approach. Since our principal motivation has been to provide atomic data needed for modeling and diagnostics of high-temperature plasmas, for which a very large amount of data is needed, we have emphasized the development of very rapid procedures, while maintaining accuracy within the distorted-wave framework. However, we have also used procedures for improving distorted-wave results by including resonance contributions to a variety of atomic processes. For example, the resonance contribution to electron-impact excitation can be calculated by considering the two-step process of electron capture to form a doubly excited state, followed by autoionization to the final level. The alternate outcomes associated with autoionization to a different final level or radiative decay of the doubly excited level are also taken into account via the use of branching ratios.

Although radiative processes are also considered, in the majority of our work we have focused on the development of very rapid procedures for the calculation of cross sections for excitation and ionization by electron impact because these processes tend to be, by far, the most lengthy to calculate. This trend occurs because, in order to determine a collision rate, the cross section must be known for several incident-electron energies and for each energy one must determine the scattering matrix elements for many initial and final values of the angular momentum quantum numbers associated with the incident and scattered electrons (plus those associated with the ejected electron for ionization). In addition, particularly for relatively high density plasmas, such as laser-produced plasmas used in inertial confinement fusion experiments and research to produce x-ray lasers, transitions between excited levels and ionization from excited levels are important. Then, collision rates for thousands, or even millions, of transitions are sometimes needed for treating a particular case involving ion stages associated with a single nuclear charge Z, or possibly several values of Z.

The range of validity of our approach is restricted to the region of Z values from 92 down to a value a little less than $2N$, where N is the number of bound electrons per ion. For these conditions, we have been able to develop procedures by which excitation and ionization cross sections for a given class of transitions can be rapidly calculated for the entire isoelectronic sequence

within the range of Z values. It should be noted that this range of Z values appears to cover essentially all cases in which a fully relativistic treatment is necessary for plasma applications.

For most of these plasma applications, only total cross sections averaged over initial magnetic sublevels and summed over final magnetic sublevels are needed. However, a second purpose of the present review is to describe the application of our approach to the more detailed cross sections for transitions between magnetic sublevels of an ion due to impact with an electron beam. Such cross sections are needed for application to plasmas with an anisotropic electron distribution and for study of electron beam ion trap (EBIT) experiments. The latter also have the benefit of providing experimental tests of the accuracy of our approach.

The present review is organized according to the various fundamental atomic processes for which we have developed theoretical expressions and numerical procedures for calculating useful data. Emphasis is placed on basic theoretical formulae for these data, such as cross sections, associated with each of these processes, as well as on the numerical procedures that were implemented to compute these quantities. Derivations are provided for a variety of expressions in order to illustrate certain techniques that are useful in manipulating expressions within a fully relativistic approach. Numerical examples are provided along with a comprehensive reference list of all the calculations that we have performed using the RDW method. In chapter 2, a description is provided of our approach for generating the atomic structure within the Dirac-Fock-Slater (DFS) approximation. A solution of the wave equation for atomic structure provides the fundamental wave functions and energies that are necessary to compute more involved quantities, such as cross sections and rate coefficients, that describe collisional and radiative processes. A discussion of photoexcitation is provided in chapter 3, while chapter 4 addresses the process of electron-impact excitation. Chapter 5 deals with electron-impact ionization and chapter 6 deals with photoionization. The concepts of resonances and dielectronic recombination, which involve the process of autoionization, are handled in chapter 7. Chapter 8 deals with transitions between hyperfine-structure levels for the process of electron-impact excitation. Chapter 9 deals with transitions between magnetic sublevels for the processes of electron-impact excitation and electron-impact ionization. Finally, some concluding remarks are provided in chapter 10. Except where explicitly noted, Rydberg atomic units have been used throughout this work.

2 A Dirac-Fock-Slater atomic structure program

In section 2.1, we summarize the general procedures used in our relativistic atomic structure program [1]. These procedures are very similar to those used in most relativistic atomic structure programs and, hence, are quite standard. The differences in the various programs are principally in the different numerical procedures used to determine the radial functions and the different methods used to determine the central potentials employed in solving the single-electron Dirac equation. The particular procedures we use are described in detail in sections 2.2 and 2.3. In later sections, we discuss improvements for computing the atomic structure of heavy ions, such as the generalized Breit interaction, and the configuration-average approximation. While the ability to calculate radiative oscillator strengths is generally included in atomic structure programs, our procedures for computing quantities such as the electric dipole oscillator strength are described in chapter 3.

2.1 General procedure

We omit, for the present, quantum electrodynamics (QED) corrections, which will be considered in section 2.5. Then, the Hamiltonian H for an ion with N bound electrons and nuclear charge Z is assumed to be given by

$$H = \sum_{i=1}^{N} H_D(i) + \sum_{\substack{i,j \\ i<j}} \frac{2}{r_{ij}}, \tag{2.1}$$

where $H_D(i)$ is the single-electron Dirac-Hamiltonian for a pure Coulomb potential $-2Z/r_i$ due to the nucleus of the ion. Here, energies are in Rydbergs and distances are in units of the Bohr radius a_0. We add and subtract the electron-electron electrostatic contributions, $V^{\mathrm{ee}}(r_i)$, to the central potential $V(r_i)$ so that H is rewritten as

$$H = \sum_{i=1}^{N} H'_D(i) - \sum_{i=1}^{N} V^{\mathrm{ee}}(r_i) + \sum_{\substack{i,j \\ i<j}} \frac{2}{r_{ij}}, \tag{2.2}$$

where

$$H'_D = H_D + V^{\mathrm{ee}}(r_i) \; . \tag{2.3}$$

Thus, H'_D is the single-electron Dirac Hamiltonian with the central potential

$$V(r_i) = \frac{-2Z}{r_i} + V^{\rm ee}(r_i)\,. \tag{2.4}$$

The specific form of $V^{\rm ee}$ that we use in our calculations will be discussed in section 2.3 (see the discussion following eq. (2.18)).

It is well known [2,3] that the Dirac equation for a central potential

$$H'_D u_{n\kappa m} = \epsilon_{n\kappa} u_{n\kappa m}\,, \tag{2.5}$$

has bound state solutions, the so-called Dirac spinors, which can be written in the form

$$u_{n\kappa m}(x) = \frac{1}{r}\begin{bmatrix} P_{n\kappa}(r) & \chi_{\kappa m}(\theta,\phi,\sigma) \\ {\rm i}Q_{n\kappa}(r) & \chi_{-\kappa m}(\theta,\phi,\sigma)\end{bmatrix}\,, \tag{2.6}$$

where x stands for all coordinates, spatial and spin, of the electron. Here, $P_{n\kappa}$ and $Q_{n\kappa}$ are the large and small components of the radial function, respectively, and $\epsilon_{n\kappa}$ is the corresponding energy eigenvalue. The $\chi_{\kappa m}$ are the usual spin-angular functions [4], also known as spherical spinors [5], given by

$$\chi_{\kappa m}(\theta,\phi,\sigma) = \sum_{m_l,m_s} C(l\tfrac{1}{2}m_l m_s; jm) Y_{lm_l}(\theta,\phi)\chi^{m_s}(\sigma) \tag{2.7}$$

in which C and Y represent Clebsch-Gordan coefficients and spherical harmonics, respectively. The $\chi^{m_s}(\sigma)$ represent the eigenvectors of the 2×2 Pauli spin matrix σ_z [3] and the relativistic quantum number κ has the values

$$\kappa = l, \quad j = l - \tfrac{1}{2}; \quad \kappa = -(l+1), \quad j = l + \tfrac{1}{2}\,. \tag{2.8}$$

The coupled Dirac radial equations determining $P_{n\kappa}$ and $Q_{n\kappa}$ are

$$\left[\frac{\rm d}{{\rm d}r} + \frac{\kappa}{r}\right]P_{n\kappa}(r) = \frac{\alpha}{2}\left[\epsilon_{n\kappa} - V(r) + \frac{4}{\alpha^2}\right]Q_{n\kappa}(r) \tag{2.9}$$

and

$$\left[\frac{\rm d}{{\rm d}r} - \frac{\kappa}{r}\right]Q_{n\kappa}(r) = \frac{\alpha}{2}[V(r) - \epsilon_{n\kappa}]P_{n\kappa}(r)\,, \tag{2.10}$$

where α is the fine-structure constant.

As is standard (e.g. Grant et al. [6]) in multi-configuration relativistic programs, in treating an ion with N bound electrons one uses basis states $\Phi_\nu(1,2,...,N)$

that are single-configuration state functions (SCSFs). These are antisymmetric sums of the products of N single-electron Dirac spinors $u_{n\kappa m}$ given by eq. (2.6). In forming the Φ_ν, the standard jj-coupling scheme is followed. In this scheme, the j values of all electrons in a subshell $n_r l_r j_r$ are coupled together to form a total angular momentum J_r of the subshell. Then, these total, subshell values for the angular momentum are successively coupled together, starting with the lowest subshell, to form the total angular momentum J of the ion. By the lower of the two subshells $n_1 l_1 j_1$ and $n_2 l_2 j_2$, one means the subshell with the smaller n value, or if $n_1 = n_2$, the subshell with the smaller l value, or if $n_1 l_1 = n_2 l_2$, the subshell with the smaller j value. Here, of course, the l values are those associated with the angular function of the large component.

One then obtains approximate, fine-structure ion wave functions Ψ given by

$$\Psi = \sum_{\nu=1}^{N_{\rm SCSF}} b_\nu \Phi_\nu \,, \tag{2.11}$$

where the mixing coefficients b_ν and the corresponding eigenenergies are obtained by diagonalizing the Hamiltonian, given by eq. (2.2), expressed in the Φ_ν basis. Since the Φ_ν are antisymmetric products of the Dirac spinor $u_{n\kappa m}$, which are eigenfunctions of H_D' that satisfy eq. (2.5), the first term on the right-hand side of eq. (2.2) contributes only to the diagonal matrix elements of H. Specifically, this term gives a contribution equal to the sum of the N energy eigenvalues $\epsilon_{n\kappa}$ associated with the N spinors contained in Φ_ν. The second term, $-\sum_i V^{\rm ee}(r_i)$, also contributes only to the diagonal matrix elements, provided one includes mixing only among the states in a complex, i.e. those states having the same total angular momentum J, parity and set of n values, as is often done for highly charged ions. However, in cases where additional states have energies near or overlapping with those in the complex, mixing with those additional states should also be included. For these cases, this term also contributes to off-diagonal matrix elements of H that are taken between states with the same angular functions, but different n values.

The final electron-electron electrostatic interaction term in eq. (2.2) contributes to both diagonal and non-diagonal matrix elements of H. In evaluating this term, one employs the standard expansion of the Coulomb interaction between two electrons, in terms of Racah tensors, such that

$$\frac{1}{r_{12}} = \sum_{\lambda=0}^{\infty} \frac{r_<^\lambda}{r_>^{\lambda+1}} \boldsymbol{C}^{(\lambda)}(\hat{\boldsymbol{r}}_1) \cdot \boldsymbol{C}^{(\lambda)}(\hat{\boldsymbol{r}}_2) \,, \tag{2.12}$$

where $\boldsymbol{C}^{(\lambda)}$ is the renormalized spherical harmonic of rank λ, $\hat{\boldsymbol{r}}_1$ and $\hat{\boldsymbol{r}}_2$ represent the angular coordinates of $\boldsymbol{r}_1$ and $\boldsymbol{r}_2$, respectively, and $r_<$ ($r_>$) is the lesser (greater) of r_1 and r_2. The matrix element of each term in eq. (2.12) can

be expressed as a product of an angular and radial part. The angular part is determined using irreducible tensor techniques (e.g. Appendix C of Messiah [7]). The results are similar to those arising in the calculation of scattering matrix elements, which are considered in more detail in later chapters. In our atomic structure program [1], we simply used the angular package from the program of Grant and coworkers [6] (hereafter referred to as the Grant code) in determining the angular coefficient associated with a particular value of λ. Due to selection rules arising from the angular contribution, only a few values of λ contribute to the sum in each case. We note that, because the operator corresponding to the electron angular-momentum quantum number j commutes with H'_D, the evaluation of the angular part of the matrix elements of eq. (2.12) is the same as that encountered when jj coupling is used in non-relativistic calculations. However, the radial part of the matrix elements is more complex in the relativistic case because the radial functions depend on j, as well as n and l, and because the small component makes a contribution. Specifically, these radial matrix elements, or so-called relativistic Slater integrals, are given by

$$R^\lambda(ab,cd) = 2\int_0^\infty\int_0^\infty [P_{n_a\kappa_a}(r_1)P_{n_c\kappa_c}(r_1) + Q_{n_a\kappa_a}(r_1)Q_{n_c\kappa_c}(r_1)]$$
$$\times\frac{r_<^\lambda}{r_>^{\lambda+1}}[P_{n_b\kappa_b}(r_2)P_{n_d\kappa_d}(r_2) + Q_{n_b\kappa_b}(r_2)Q_{n_d\kappa_d}(r_2)]\mathrm{d}r_1\mathrm{d}r_2\,. \qquad (2.13)$$

2.2 Numerical determination of the radial functions

We use eq. (2.9) to express $Q_{n\kappa}$ in terms of $P_{n\kappa}$ and substitute the result into eq. (2.10) to obtain a second-order differential equation for $P_{n\kappa}$,

$$\left\{-\frac{\mathrm{d}^2}{\mathrm{d}r^2} + \frac{l(l+1)}{r^2} + V(r) - \frac{\alpha^2}{4}[\epsilon_{n\kappa} - V(r)]^2\right.$$
$$\left.-\frac{\alpha^2}{4}\left[1+\frac{\alpha^2}{4}[\epsilon_{n\kappa}-V(r)]\right]^{-1}\frac{\mathrm{d}V(r)}{\mathrm{d}r}\left[\frac{1}{P_{n\kappa}}\frac{\mathrm{d}P_{n\kappa}}{\mathrm{d}r} + \frac{\kappa}{r}\right]\right\}P_{n\kappa} = \epsilon_{n\kappa}P_{n\kappa}\,, \qquad (2.14)$$

where use has been made of the relation

$$\kappa(\kappa+1) = l(l+1)\,, \qquad (2.15)$$

which follows from eq. (2.8). Eq. (2.14) is similar to the usual non-relativistic Schrödinger equation except that it has a much more complicated effective potential. The radial part of the Hartree-Fock relativistic (HFR) option of Cowan's widely used program [8] corresponds to solving eq. (2.14) with κ

replaced by its j-averaged value of -1, so that the large component does not depend on j. Then, the small component is neglected and the large component is normalized as though it were the total radial function. In our case, we are interested in retaining both the κ dependence and the small component of the wave function. Therefore, we simply used the radial part of Cowan's HFR program modified to retain the κ (or j) dependence and modified to also obtain $Q_{n\kappa}$. The latter is readily done because, as seen from eq. (2.9), $Q_{n\kappa}$ is essentially given by the final term in the effective potential of eq. (2.14). Of course, we also use the correct relativistic normalization

$$\int_0^\infty [P_{n\kappa}^2(r) + Q_{n\kappa}^2(r)]\,\mathrm{d}r = 1\,. \tag{2.16}$$

We found it necessary to separately consider the $-2Z/r$ nuclear contribution to the potential and determine its contribution to $\mathrm{d}V(r)/\mathrm{d}r$ analytically in order to obtain $Q_{n\kappa}(r)$ with sufficient accuracy for large Z values. In addition, we employ an initial mesh size that is 1/8 the value typically used with Cowan's program. Specifically,

$$\Delta\rho_{\mathrm{init}} = 3.125 \times 10^{-4},\ \rho = 4\Big(\frac{2Z}{9\pi^2}\Big)^{1/3} r \tag{2.17}$$

was used. This choice did not add much to the computing time because a linear mesh is used with a doubling of the interval size every 40 points, which added only 120 points to a usual total of 640 points. Actually, in providing atomic structure data for collision processes, we stop the doubling at the largest mesh size that satisfies eq. (4.47) in chapter 4 of the present work.

The method for solving eq. (2.14) is quite standard and can be found, for example, in ref. [8]. The result is a set of radial functions and corresponding eigenvalues for each orbital denoted by the quantum numbers $n\kappa$, along with a self-consistent potential, $V(r)$, given by eq. (2.4). The principal manner in which speed is obtained in our atomic structure calculations is through our choice for this central potential, which we discuss next.

2.3 Choice for the central potential

The reason we call our relativistic atomic structure program a Dirac-Fock-Slater program is that we choose the Dirac-Fock-Slater potential for the central potential $V(r)$ appearing in eqs. (2.9), (2.10) and (2.14). That is, we use the relativistic version of the Hartree-Fock-Slater potential introduced by Slater

[9], except that we use the Kohn-Sham [10] value for the coefficient of the exchange term. In particular, we use

$$V(r) = -\frac{2Z}{r} + V_c(r) - \left[\frac{24}{\pi}\rho(r)\right]^{1/3}, \tag{2.18}$$

where the first term is the potential due to the nucleus. In a later upgrade of our relativistic atomic structure code, discussed near the end of section 2.5, this term is replaced by $-2Z(r)/r$. That is, the point nuclear charge Z is replaced with a distributed nuclear charge $Z(r)$, which differs from Z only for extremely small values of r. The remaining two terms in eq. (2.18) are the electron-electron contribution previously called $V^{\rm ee}(r)$ in eqs. (2.2)–(2.4). The $V_c(r)$ term is the spherically averaged classical potential due to the bound electrons,

$$V_c(r) = \sum_{n'\kappa'} w_{n'\kappa'} \int_0^\infty \frac{2}{r_>}[P^2_{n'\kappa'}(r_2) + Q^2_{n'\kappa'}(r_2)]{\rm d}r_2\,, \tag{2.19}$$

where $w_{n'\kappa'}$ is the occupation number of subshell $n'\kappa' = n'l'j'$. The summation is over all occupied subshells and, again, $r_>$ is the greater of r_1 and r_2. The final term in eq. (2.18) is the exchange energy of an electron in a free-electron gas of density ρ, averaged over all possible momenta of the electron. Following Slater [9], we use for ρ the electron number density at a distance r from the nucleus,

$$\rho(r) = \frac{1}{4\pi r^2}\sum_{n'\kappa'} w_{n'\kappa'}[P^2_{n'\kappa'}(r) + Q^2_{n'\kappa'}(r)]\,. \tag{2.20}$$

One sees that, if $w_{n'\kappa'}$ were replaced by $w_{n'\kappa'} - 1$ when $n'\kappa' = n\kappa$, where $P_{n\kappa}$ and $Q_{n\kappa}$ represent the orbitals being solved for in eqs. (2.9) and (2.10), then eq. (2.19) would give the relativistic version of the Hartree potential. The undesirable feature that self-interaction is included in $V_c(r)$ is at least partially canceled by the fact that the self-exchange energy is also included in the calculation because eq. (2.20) contains the contribution from all of the electrons, including those residing in subshell $n\kappa$.

In considering a particular class of transitions, we use a single mean configuration with fractional occupation numbers in evaluating the central potential given by eqs. (2.18)–(2.20). The prescription generally used in determining this mean configuration is that the occupation number of the active electron is split equally between the initial and final subshells. For example, in obtaining structure results for oscillator strengths and collision strengths for transitions from the $n = 2$ shell of the ground level to the excited levels with $n = 3$ occupancy in neon-like ions, we could use for the mean configuration

$$1s^2 2s_{1/2}^{1.9} 2p_{1/2}^{1.9} 2p_{3/2}^{3.7} 3s_{1/2}^{0.1} 3p_{1/2}^{0.1} 3p_{3/2}^{0.1} 3d_{3/2}^{0.1} 3d_{5/2}^{0.1} \,. \tag{2.21}$$

However, if transitions among the $n = 3$ excited levels were also being considered, then

$$1s^2 2s_{1/2}^{1.8} 2p_{1/2}^{1.8} 2p_{3/2}^{3.6} 3s_{1/2}^{0.16} 3p_{1/2}^{0.16} 3p_{3/2}^{0.16} 3d_{3/2}^{0.16} 3d_{5/2}^{0.16} \tag{2.22}$$

would be a more appropriate choice. It should be noted that slight shifts in the occupation numbers, especially among the subshells of a given shell, have little effect on the numerical results.

It should be emphasized that our calculations are generally multi-configuration calculations in which, at least, the mixing between all states in a complex is included. The single mean configuration is used solely in determining the potential and the resulting radial functions that comprise the Dirac spinors in eq. (2.6). (When computing a physically relevant quantity, the appropriate integer occupation numbers are assigned to each spinor before performing a calculation.) This procedure, coupled with the use of eqs. (2.18)–(2.20), has many advantages. For example, the potential is then the same for all electrons, so all orbitals are automatically orthogonal and the calculations are much more rapid than with a fully multi-configuration Dirac-Fock program, such as that of the Grant code [6]. We also use this same potential in calculating free-electron orbitals for other electron-ion and photon-ion processes, as discussed in later chapters.

In addition to the fully relativistic (FR) approach that we have discussed, a quasi-relativistic (QR) option has also been included in our atomic structure program [1]. This option corresponds to simply solving eq. (2.14) for $P_{n\kappa}$ and normalizing this function as though it were the total radial function, i.e.

$$\int_0^\infty [P_{n\kappa}(r)]^2 \, \mathrm{d}r = 1 \qquad \text{(QR approach)} \,. \tag{2.23}$$

Then, $Q_{n\kappa}$ is omitted everywhere, such as in eqs. (2.13), (2.19) and (2.20). Hence, this method is like Cowan's HFR approach [8], except that the j dependence is retained, which is quite important for large Z values. It was thought initially that the QR approach would be somewhat faster than the FR option of our program, but it turned out to be only 5–10% more rapid than the FR option. This outcome results because, as noted previously, the small component of the wave function, $Q_{n\kappa}$, is essentially already computed in calculating the final term in the effective potential of eq. (2.14). Nevertheless, as seen from the sample results given below in tables 1 and 3, the QR approach gives rather accurate structure results, even for very large values of

Z, and is useful in rapidly computing collision strengths when coupled with an additional approximation for the free electron, as discussed in chapter 4.

2.4 Some comparisons of energies for neon-like ions

In table 1, a sample comparison, taken from ref. [1], is made of excited-level energies relative to the ground level for neon-like uranium ($Z = 92$). Each level is labeled by the pure SCSF in eq. (2.11) that makes the dominant contribution that level's wave function. Specifically, we use the following state abbreviations:

$$(2p3l)_J = (1s^2\,2s^2\,2p^{*2}\,2p^3\,3l)_J\,, \quad (2p3l^*)_J = (1s^2\,2s^2\,2p^{*2}\,2p^3\,3l^*)_J \tag{2.24}$$

$$(2p^*3l)_J = (1s^2\,2s^2\,2p^*\,2p^4\,3l)_J\,, \quad (2p^*3l^*)_J = (1s^2\,2s^2\,2p^*\,2p^4\,3l^*)_J \tag{2.25}$$

$$(2s3l)_J = (1s^2\,2s\,2p^{*2}\,2p^4\,3l)_J\,, \quad (2s3l^*)_J = (1s^2\,2s\,2p^{*2}\,2p^4\,3l^*)_J\,, \tag{2.26}$$

where use has been made of the orbital shorthand notation

$$nl^* = nlj, \quad j = l - \tfrac{1}{2} \qquad \text{and} \qquad nl = nlj, \quad j = l + \tfrac{1}{2}\,,$$

so that

$$1s = 1s_{1/2}, \quad 2s = 2s_{1/2}, \quad 2p^* = 2p_{1/2}, \quad 2p = 2p_{3/2}, \quad \text{etc.}$$

In this table, results computed with our QR and FR approaches are compared with those obtained with the "average level" option of the Grant code [6,11], labeled G and G**, and the HFR option of Cowan's program [8]. Comparisons for lower values of Z and for Ni-like ions ($N = 28$) are also provided in ref. [1]. The FR and FR* results differ slightly because FR* values correspond to using eq. (2.21) in determining the potential, while FR (and also the QR) values are obtained using eq. (2.22). The G** values correspond to including the generalized Breit interaction plus other QED corrections and use of a finite nuclear size (all of which are discussed in the next section), while the G values are obtained without these additions or corrections. Hence, the G values are calculated similarly to our FR and FR* values, except that the more elaborate multi-configuration Dirac-Fock potential is used. Also, a logarithmic radial grid is used in calculating the G and G** results, while we use a linear

Table 1
Comparison of energies (in eV) for excited-state levels relative to the ground level for neon-like ions with $Z = 92$. The levels are designated by the pure jj-coupled state making the dominant contribution using the abbreviations of eqs. (2.24)–(2.26). The following labeling is used: QR and FR are present quasi-relativistic and fully relativistic results using eq. (2.22) in determining the potential. FR* differs from FR only in that eq. (2.21) is used in place of eq. (2.22). G** and G are results obtained from the Grant code [6,11] with and without inclusion of the generalized Breit interaction, QED corrections and a finite nuclear size, respectively. HFR are results obtained using Cowan's [8] HFR program.

Level	QR	FR	FR*	G	G**	HFR
$(2p3s)_2$	12890.5	12871.4	12872.7	12877.1	12860.3	12596.1
$(2p3s)_1$	12901.9	12882.4	12883.7	12888.1	12872.0	12607.0
$(2p3p^*)_1$	13103.6	13096.7	13097.9	13097.8	13075.8	12777.8
$(2p3p^*)_2$	13108.8	13101.6	13102.8	13102.6	13075.9	12782.2
$(2p3p)_1$	14221.9	14204.2	14205.5	14206.0	14167.0	13971.4
$(2p3p)_3$	14222.1	14204.5	14205.8	14206.0	14165.4	13971.6
$(2p3p)_2$	14236.5	14219.1	14220.4	14220.7	14184.1	13985.4
$(2p3p)_0$	14308.2	14295.4	14296.6	14294.9	14262.7	14051.1
$(2p3d^*)_0$	14426.5	14409.6	14411.0	14411.4	14378.5	14092.2
$(2p3d^*)_1$	14445.8	14428.6	14430.0	14430.5	14391.1	14109.3
$(2p3d^*)_3$	14448.5	14431.2	14432.5	14432.8	14389.5	14111.4
$(2p3d^*)_2$	14454.9	14438.4	14439.8	14440.1	14401.6	14117.4
$(2p3d)_4$	14688.2	14667.0	14668.4	14668.4	14619.9	14359.5
$(2p3d)_2$	14694.8	14673.6	14675.0	14675.3	14630.5	14365.7
$(2p3d)_3$	14707.9	14686.6	14688.0	14688.2	14644.2	14378.1
$(2p3d)_1$	14746.7	14725.1	14726.3	14726.3	14679.0	14413.5
$(2p^*3s)_0$	16886.6	16820.4	16822.3	16828.3	16764.8	16836.6
$(2p^*3s)_1$	16893.0	16826.6	16828.5	16834.4	16768.1	16842.7
$(2p^*3p^*)_1$	17097.8	17043.4	17045.2	17046.6	16970.0	17020.1
$(2p^*3p^*)_0$	17158.1	17110.9	17112.7	17112.7	17043.1	17065.9
$(2s3s)_1$	17581.0	17561.9	17563.1	17553.4	17458.5	17504.6
$(2s3s)_0$	17623.7	17621.1	17613.3	17602.8	17511.8	17463.9
$(2s3p^*)_0$	17797.7	17790.7	17791.8	17777.4	17678.0	17648.3
$(2s3p^*)_1$	17801.8	17794.3	17795.4	17781.0	17676.1	17651.2
$(2p^*3p)_1$	18221.1	18158.1	18160.0	18161.9	18077.5	18217.7
$(2p^*3p)_2$	18225.3	18160.9	18162.8	18164.7	18076.0	18220.3
$(2p^*3d^*)_2$	18444.4	18382.1	18384.0	18385.8	18295.1	18351.6
$(2p^*3d^*)_1$	18474.8	18411.9	18413.8	18415.6	18322.5	18385.8
$(2p^*3d)_2$	18692.5	18626.1	18628.1	18629.7	18535.9	18605.9
$(2p^*3d)_3$	18697.7	18630.9	18632.9	18634.5	18540.2	18612.8
$(2s3p)_2$	18918.5	18901.2	18902.3	18888.4	18772.9	18843.4
$(2s3p)_1$	18926.8	18909.2	18910.4	18896.5	18781.0	18850.5
$(2s3d^*)_1$	19135.3	19119.8	19121.1	19107.3	18991.6	18974.5
$(2s3d^*)_2$	19145.6	19129.5	19130.7	19116.8	18996.4	18983.9
$(2s3d)_3$	19383.4	19363.3	19364.6	19350.5	19225.5	19299.9
$(2s3d)_2$	19399.4	19379.0	19380.3	19366.3	19244.7	19246.0

grid. The larger discrepancies between the G values and the FR and FR* values, of up to 14 eV for levels involving s orbitals, appear to be due to our use of a linear grid. For other levels, and all levels for $Z \lesssim 60$, the differences are generally within 2 eV, which is about the same as the differences between the most accurately computed G** values and measurements performed by

Beiersdorfer et al. [12]. Eventually, we plan to modify our program to use a logarithmic grid. However, the resulting error in energies due to the use of a linear grid is much less than 1% and it appears that this discrepancy is not very important in determining accurate oscillator strengths, collision strengths or ionization cross sections. The much larger differences between the G** entries and the FR, FR* and G entries indicate that the extra corrections used in the G** calculations are important for large Z values. We later included these effects in our structure and oscillator strength calculations, as will be discussed in sections 2.5 and 3.3. Finally, one sees that the QR values are moderately good even for $Z = 92$ and are a considerable improvement over the HFR values. Both the HFR and QR values should be compared with the G entries because neither of them contain the additional corrections included in the G** values. This comparison indicates that including the j dependence in the radial functions is important for large Z values, which becomes more apparent when oscillator strengths are compared, as done in section 3.3.

2.5 Inclusion of the generalized Breit interaction and other corrections in the atomic structure

In order to improve the accuracy of our calculations for high-Z ions, it was necessary to include the effect of the generalized Breit interaction. This interaction can be derived from quantum electrodynamics (QED) via first-order perturbation theory, and represents the lowest-order Feynman diagram for the exchange of a single virtual photon between two electrons. Specifically, the generalized Breit interaction, which is to be added to the Coulomb interaction expressed as $2/r_{ij}$ in eq. (2.1), is given by

$$B(i,j) = -2(\boldsymbol{\alpha}_i \cdot \boldsymbol{\alpha}_j)\frac{\exp(\mathrm{i}\omega r_{ij})}{r_{ij}} + 2(\boldsymbol{\alpha}_i \cdot \boldsymbol{\nabla}_i)(\boldsymbol{\alpha}_j \cdot \boldsymbol{\nabla}_j)\frac{\exp(\mathrm{i}\omega r_{ij}) - 1}{\omega^2 r_{ij}}\,, \tag{2.27}$$

where ω is the wavenumber of the exchanged virtual photon and the $\boldsymbol{\alpha}_i$ are the usual Dirac matrices. An appropriate value for ω will be discussed in section 4.10 of chapter 4. In writing eq. (2.27), as usual, we have used distances in units of the Bohr radius and energies in Rydbergs.

Other interactions that are related to the one above also appear in the literature. For example, for intermediate Z values, an accurate approximation to the generalized Breit interaction can be obtained by taking the $\omega \longrightarrow 0$ limit

of eq. (2.27). The result is the original Breit interaction [13–15],

$$H_{\rm Br}(i,j) = -\frac{1}{r_{ij}}[\boldsymbol{\alpha}_i \cdot \boldsymbol{\alpha}_j + (\boldsymbol{\alpha}_i \cdot \hat{\boldsymbol{r}}_{ij})(\boldsymbol{\alpha}_j \cdot \hat{\boldsymbol{r}}_{ij})], \tag{2.28}$$

where $\hat{\boldsymbol{r}}_{ij}$ is a unit vector along $\boldsymbol{r}_{ij}$. We shall refer to this interaction simply as "the Breit interaction". This interaction represents one of the earliest attempts to take into account the lowest-order relativistic effects, to $O(v^2/c^2)$, that are associated with retardation and the magnetic interaction. The latter effect is similar to the well-known spin-orbit interaction, but arises from the interaction between an electron, traveling with speed v, and the magnetic field arising from a different electron, rather than the field that arises from the nucleus. Retardation is the term used to describe the delay in the electromagnetic interaction, which is mediated by photons, due to the finite value of the speed of light. In this case, as the electron velocities approach the speed of light, the effect of retardation becomes more important. This original form of the Breit interaction has the advantage of being computationally simpler to calculate, as compared to eq. (2.27), but its range of validity is limited due to the approximation of taking the limit $\omega \rightarrow 0$.

Yet another interaction that takes into account, to lowest order, the exchange of a virtual photon between two electrons is the Møller interaction. While the various flavors of the Breit interaction mentioned above were derived within the context of resolving discrepancies in bound-electron energies, Møller considered the problem of scattering between two continuum electrons [16]. And while the various forms of the Breit interaction were derived in the Coulomb gauge, the Møller interaction, given by

$$M(i,j) = \frac{2}{r_{ij}}(1 - \boldsymbol{\alpha}_i \cdot \boldsymbol{\alpha}_j)\exp(\mathrm{i}\omega r_{ij})\,, \tag{2.29}$$

was derived in the Lorentz gauge. We note that the Møller interaction represents the entire, lowest-order interaction between two electrons, while the Breit interaction is a perturbation to the Coulomb interaction and must be added to the usual $2/r_{ij}$ expression.

More detailed information on these various interactions and their application to bound-state calculations can be found in a number of references, e.g. refs. [17–21]. In the current body of work, we primarily consider the generalized Breit interaction given by eq. (2.27), and occasionally consider the more approximate expression in eq. (2.28). A detailed evaluation of the matrix elements of the generalized Breit interaction is not considered in this section because the approach is essentially the same as that employed in evaluating the excitation scattering matrix elements, which is described in detail in chapter 4. The only essential difference is that a free electron replaces one of the

bound electrons for the case of collisional excitation.

In order to compare more favorably with results produced by the Grant code [6,11], we also added options in our program to include the additional QED effects of vacuum polarization and self-energy, along with a finite nuclear size. The QED corrections were implemented in the same manner as in the Grant code, using the work of Fullerton and Rinker [22] and Mohr [23,24]. The numerical procedure for including these corrections in our program is that the diagonal matrix elements of these interactions are added after diagonalization of the Dirac-Coulomb Hamiltonian, eq. (2.2), has occurred, but before the final diagonalization of Hamiltonian that includes the Breit interaction has been performed. This approach is the procedure used in the default option of the GRASP program [25]. Thus, these additional QED corrections affect the mixing coefficients slightly, but the principal effect is on the energies for high Z values, where the QED corrections sometimes contribute nearly as much as the generalized Breit interaction. For the finite nuclear size, we used the Fermi charge distribution of Chen et al. [26]. This choice causes the nuclear charge, Z, appearing in eq. (2.4) to be replaced with $Z(r_i)$, which differs from Z only for extremely small values of r_i. Again, this procedure is the same as that used in various versions of the Grant code [6,11,25].

In table 2 a comparison is provided between our DFS results that were computed with all of the above corrections (denoted by FR**) and the corresponding G** and FR* results that were presented in table 1. As expected, the agreement between the FR** and G** energies is considerably better than the agreement between the FR* and G** results for most of the levels considered. (The FR* and G** data that appear in table 2 are the result of a more recent calculation, performed on a different computing platform, than the corresponding values that appear in table 1. The disparity between the data appearing in tables 1 and 2 is attributed to these issues.)

2.6 The configuration-average approximation

The previous sections provide a detailed treatment for obtaining fine-structure quantities associated with the wave functions in eq. (2.11). When considering a large amount of fine-structure data, the configuration-average approximation can be a useful approach for drastically reducing the number of states to be considered. Furthermore, these results can be obtained in a manner that is far less computationally demanding. The concept of a configuration-average energy has existed for some time (see, for example, refs. [8,27,28]). In this section, we provide an expression for the configuration-average energy associated with a particular relativistic configuration c denoted by

$$c \equiv (n_\alpha \kappa_\alpha)^{w_\alpha} (n_\beta \kappa_\beta)^{w_\beta} (n_\gamma \kappa_\gamma)^{w_\gamma} \cdots , \tag{2.30}$$

Table 2
Comparison of energies (in eV) for excited-state levels relative to the ground level for neon-like ions with $Z = 92$. The notation is the same as that used in table 1, except that FR** refers to FR-type calculations that include the generalized Breit interaction, other QED corrections and a finite nuclear size.

Level	FR*	FR**	G**
$(2p3s)_2$	12872.2	12840.4	12856.3
$(2p3s)_1$	12883.3	12852.4	12868.2
$(2p3p^*)_1$	13096.8	13068.4	13061.5
$(2p3p^*)_2$	13101.7	13068.7	13061.8
$(2p3p)_1$	14204.0	14158.4	14152.4
$(2p3p)_3$	14204.2	14159.6	14153.6
$(2p3p)_2$	14218.8	14176.9	14170.7
$(2p3p)_0$	14295.0	14257.1	14250.2
$(2p3d^*)_0$	14409.4	14371.0	14363.4
$(2p3d^*)_1$	14428.4	14380.8	14373.1
$(2p3d^*)_3$	14430.9	14383.5	14375.9
$(2p3d^*)_2$	14438.2	14393.8	14386.2
$(2p3d)_4$	14666.7	14611.9	14604.3
$(2p3d)_2$	14673.3	14622.6	14615.0
$(2p3d)_3$	14686.3	14635.5	14627.9
$(2p3d)_1$	14724.8	14672.0	14664.3
$(2p^*3s)_0$	16820.2	16744.9	16762.9
$(2p^*3s)_1$	16826.5	16748.1	16766.2
$(2p^*3p^*)_1$	17042.5	16962.3	16957.7
$(2p^*3p^*)_0$	17109.9	17036.5	17031.1
$(2s3s)_1$	17558.2	17482.1	17418.4
$(2s3s)_0$	17608.2	17535.6	17471.5
$(2s3p^*)_0$	17786.3	17712.2	17625.6
$(2s3p^*)_1$	17789.9	17714.1	17627.5
$(2p^*3p)_1$	18156.8	18068.3	18064.5
$(2p^*3p)_2$	18159.6	18069.9	18066.0
$(2p^*3d^*)_2$	18380.8	18287.0	18281.6
$(2p^*3d^*)_1$	18410.6	18314.8	18309.2
$(2p^*3d)_2$	18624.8	18528.0	18522.2
$(2p^*3d)_3$	18629.6	18531.3	18525.8
$(2s3p)_2$	18896.3	18808.5	18723.1
$(2s3p)_1$	18904.4	18817.1	18731.3
$(2s3d^*)_1$	19115.0	19027.4	18940.1
$(2s3d^*)_2$	19124.7	19032.3	18944.9
$(2s3d)_3$	19358.5	19261.6	19174.3
$(2s3d)_2$	19374.1	19280.5	19193.2

where w_α represents the occupation number of subshell α. In eq. (2.30), as well as the subsequent discussion, we have adopted a notation similar to that of Peyrusse [28], who provided a detailed treatment of the configuration-average approximation (for both structure and scattering quantities) for non-relativistic configurations.

In the context of the present work, the most general expression for the configuration-average energy can be defined as

$$E_c \equiv \frac{\sum\limits_{\text{levels}\in c}(2J+1)\langle\Psi^J|H|\Psi^J\rangle}{\sum\limits_{\text{levels}\in c}(2J+1)} = \frac{\sum\limits_{\text{levels}\in c}(2J+1)E^J}{\sum\limits_{\text{levels}\in c}(2J+1)}, \tag{2.31}$$

where H is the N-electron Hamiltonian defined in eq. (2.1), Ψ^J is a fine-structure level, described by eq. (2.11), with total angular momentum J, and E^J is the energy corresponding to Ψ^J. The summations are performed over all such levels that are characterized by a dominant single-configuration state function (SCSF) that arose from configuration c. However, this definition is not particularly useful because there is no way to remove the dependence on the mixing coefficients that appear in eq. (2.11) for an arbitrary amount of configuration interaction (CI). Thus, in order to evaluate eq. (2.31), one must still proceed with the usual diagonalization of H, which defeats the purpose of defining a configuration-average energy. Nevertheless, eq. (2.31) is useful to compare with energies obtained from more approximate, configuration-average expressions. Some attempts to approximate the effect of CI in configuration-average calculations have been made in the context of unresolved-transition-array theory (see, for example, ref. [29]), but no further discussion will be provided in this work.

A more traditional, and practical, definition of the configuration-average energy is obtained by replacing the fine-structure levels in eq. (2.31) with the pure SCSFs in eq. (2.11), so that

$$E_c \equiv \frac{\sum\limits_{\text{SCSF}\in c}(2J+1)\langle\Phi^J|H|\Phi^J\rangle}{\sum\limits_{\text{SCSF}\in c}(2J+1)} = \frac{\sum\limits_{\text{SCSF}\in c}(2J+1)E^J_{\text{SCSF}}}{\sum\limits_{\text{SCSF}\in c}(2J+1)}. \tag{2.32}$$

The advantage of using the expression in eq. (2.32) is that it can be rewritten in terms of quantities that are readily available from the solution of the coupled radial equations given by eqs. (2.9) and (2.10). To be as general as possible, the definition in eq. (2.32) could have included summations over mixed levels, provided that mixing was considered only among those pure SCSFs that result from configuration c. When the amount of mixing is restricted in this way, the resulting set of mixed levels represents an alternative, orthonormal basis that spans exactly the same space (with the same dimensionality) as that spanned by the corresponding pure SCSFs. Therefore, any formal average computed within this space can be computed equivalently with either basis. In practice, it is easier to use the pure SCSF basis in deriving a convenient form for the

configuration-average energy. The result is given by

$$E_c = \sum_{\alpha \in c} w_\alpha \langle \alpha \rangle + \sum_{\alpha,\beta \in c} w_\alpha (w_\beta - \delta_{\alpha\beta}) \langle \alpha, \beta \rangle \tag{2.33a}$$

$$\begin{aligned} \langle \alpha \rangle &= \epsilon_{n_\alpha \kappa_\alpha} + \langle u_{n_\alpha \kappa_\alpha m_\alpha} | [-V(r) - 2Z/r] | u_{n_\alpha \kappa_\alpha m_\alpha} \rangle \\ &= \epsilon_{n_\alpha \kappa_\alpha} + \int_0^\infty [P^2_{n_\alpha \kappa_\alpha}(r) + Q^2_{n_\alpha \kappa_\alpha}(r)][-V(r) - 2Z/r]\, \mathrm{d}r \end{aligned} \tag{2.33b}$$

$$\begin{aligned} \langle \alpha, \beta \rangle = \frac{1}{2} \frac{g_\alpha}{g_\alpha - \delta_{\alpha\beta}} \Big[& R^0(\alpha\beta, \alpha\beta) - \\ & \sum_\lambda \begin{pmatrix} j_\alpha & \lambda & j_\beta \\ \frac{1}{2} & 0 & -\frac{1}{2} \end{pmatrix}^2 R^\lambda(\alpha\beta, \beta\alpha) \Big] . \end{aligned} \tag{2.33c}$$

In eq. (2.33c), $(\cdots)$ represents a Wigner 3-j symbol, $V(r)$ is the central potential from eq. (2.4) and $\epsilon_{n_\alpha \kappa_\alpha}$ represents the energy eigenvalue of orbital α from eq. (2.5). If the finite-nucleus option described in section 2.5 is used, then the Coulomb interaction, $-2Z/r$, should be replaced with $-2Z(r)/r$. In eq. (2.33c), $R^\lambda(\alpha\beta, \alpha\beta)$ is a Slater integral of the form given in eq. (2.13) and $g_\alpha = 2j_\alpha + 1$ is the statistical weight of subshell α.

In practice, once a self-consistent set of orbitals and eigenvalues, along with the corresponding potential, have been determined, eq. (2.33a) above can be evaluated to determine the configuration-average energy for any configuration of the form given in eq. (2.30). These energies, in turn, will be useful in computing configuration-average quantities associated with radiative and collisional processes that are described in upcoming chapters. We note that the occupation numbers in eqs. (2.30) and (2.33a) are integers, as these configurations represent the basis from which the physically meaningful, pure SCSFs are constructed. In contrast, the occupation numbers used in solving the coupled radial eqs. (2.9) and (2.10) are typically chosen to be fractional, as described in the discussion that follows eq. (2.20). Of course, one could instead compute a different set of wave functions, eigenvalues and potential for each configuration of interest, using the appropriate integral occupation numbers from eq. (2.30). However, this approach can require significantly more computing time and does not produce a set of orbital wave functions that are automatically orthogonal, since the orbitals arise from different self-consistent potentials.

3 Oscillator strengths and line strengths

Radiative transitions that occur between two bound states are typically characterized by oscillator strengths and line strengths. Since these quantities depend only on the wave functions of the ion, the capability to calculate them is

included in most atomic structure programs. However, because our discussion of this topic is somewhat lengthy, we devote a separate chapter to this subject matter here.

3.1 General relations for optically allowed transitions

The electric dipole, or optically allowed, transitions generally have much larger transition probabilities, or rates, than the other, so-called forbidden, radiative transitions and are the only kind we consider here. However, the forbidden transitions can be important for very low-density plasmas. Nevertheless, we have not included them in our relativistic atomic structure program for several reasons. As noted in chapter 1, our principal interest is in collision processes involving free electrons, which are much more lengthy to calculate than radiative processes. Also, relativistic values for the latter, including forbidden transitions, are available by use of most relativistic programs, such as the Grant code [6,11,25]. On the other hand, in addition to the direct use for radiative processes, the results for optically allowed transitions are required for other purposes. For example, they enter in some of our approximations for the large angular momentum (or top-up) contribution to electron-impact excitation cross sections for the corresponding transitions, as will be described in chapter 4. Also, the expressions obtained here for optically allowed transitions can be readily extended to give an expression for the photoionization cross section, as will be shown in chapter 6. Finally, these results are used in the expression for the branching ratio associated with autoionizing resonance contributions to various processes and for dielectronic recombination, since radiative decay competes with autoionization in this case. This topic will be addressed in chapter 7.

Radiative decay rates and the contribution of spectral lines to the radiative absorption coefficient are generally expressed in terms of the line strength S or the related dimensionless oscillator strength f. Specifically, for the transition $i \rightarrow j$, the contribution to the radiative absorption coefficient μ is

$$\mu_{ij}(\nu) = N_i \frac{\pi e^2}{mc} f_{ij} \phi_{ij}(\nu), \qquad \int \mathrm{d}\nu \, \phi_{ij}(\nu) = 1 \,, \tag{3.1}$$

where ϕ is the line shape function, ν is the photon frequency and N_i is the number of ions per unit volume in level i. For the inverse transition $j \rightarrow i$, the radiative decay rate is

$$A_{ji} = \frac{8\pi^2 e^2 \nu^2}{mc^3} \frac{g_i}{g_j} f_{ij} \,, \tag{3.2}$$

where g_i and g_j are the statistical weights of the lower and upper levels, respectively. Eqs. (3.1) and (3.2) are provided in regular units, and the fundamental constants e, m and c have their customary meanings. When cgs units are used, A_{ji} is in s^{-1} and μ_{ij} is in cm^{-1}. The relation between the oscillator strength and line strength is

$$f_{ij} = \frac{\Delta E}{3g_i} S_{ij}\,, \tag{3.3}$$

where ΔE is the transition energy in Rydbergs. Another useful quantity that is sometimes considered is the weighted oscillator strength,

$$gf = (2J_i + 1)f_{ij} = -(2J_j + 1)f_{ji}, \tag{3.4}$$

which is symmetric in the indices that denote the initial and final levels of the transition.

3.1.1 Transitions between fine-structure, magnetic sublevels

Before considering the usual transitions of the form $\Delta_t J_t - \Delta'_t J'_t$ between fine-structure energy levels, we first consider the more detailed transitions of the type $\Delta_t J_t M_t - \Delta'_t J'_t M'_t$ between magnetic sublevels, where the summation of the line strength over the magnetic quantum numbers M_t and M'_t has not been performed. Here, J_t and M_t are the total angular momentum and its z component, associated with the initial sublevel, respectively. The symbol Δ_t indicates all additional quantum numbers required to specify the lower energy sublevel. Primes on quantities indicate corresponding quantum numbers for the higher energy sublevel. These detailed transitions are of interest when polarization of the radiation is involved, as in EBIT experiments and the study of anisotropic plasmas. In this case, the g_i and g_j in eqs. (3.2) and (3.3) are unity, and for an ion with N bound electrons the line strength is given by

$$S(\Delta_t J_t M_t - \Delta'_t J'_t M'_t) = \left| \langle \Delta_t J_t M_t \mid \sum_{i=1}^{N} \boldsymbol{r}_i \mid \Delta'_t J'_t M'_t \rangle \right|^2 , \tag{3.5}$$

where, as in sections 2.1–2.3, distances are in units of the Bohr radius.

It is convenient to express the electron positions in standard irreducible tensor form [8] according to

$$\boldsymbol{r}_i = r_i \boldsymbol{C}^{(1)}(\hat{\boldsymbol{r}}_i) = r_i \sum_q \boldsymbol{C}^{(1)}_q(\hat{\boldsymbol{r}}_i)\,, \tag{3.6}$$

where $\boldsymbol{C}^{(1)}$ is the renormalized spherical harmonic of rank one. This result can be used to express the electric dipole operator, $\boldsymbol{P}^{(1)}$, in the useful form

$$\boldsymbol{P}^{(1)} \equiv \sum_{i=1}^{N} \boldsymbol{r}_i = \sum_q \boldsymbol{P}_q^{(1)} , \tag{3.7}$$

where

$$\boldsymbol{P}_q^{(1)} = \sum_{i=1}^{N} r_i \boldsymbol{C}_q^{(1)}(\hat{\boldsymbol{r}}_i) . \tag{3.8}$$

Then, applying eqs. (3.6)–(3.8) to the matrix element in eq. (3.5), one obtains

$$\langle \Delta_t J_t M_t \mid \sum_{i=1}^{N} \boldsymbol{r}_i \mid \Delta_t' J_t' M_t' \rangle = \sum_q \langle \Delta_t J_t M_t \mid \boldsymbol{P}_q^{(1)} \mid \Delta_t' J_t' M_t' \rangle . \tag{3.9}$$

Application of the Wigner-Eckart theorem [7,8] to the matrix element on the right-hand side of eq. (3.9) gives

$$\begin{aligned} \langle \Delta_t J_t M_t \mid \boldsymbol{P}_q^{(1)} \mid \Delta_t' J_t' M_t' \rangle = (-1)^{J_t - M_t} & \begin{pmatrix} J_t & 1 & J_t' \\ -M_t & q & M_t' \end{pmatrix} \\ & \times \langle \Delta_t J_t \parallel \boldsymbol{P}^{(1)} \parallel \Delta_t' J_t' \rangle , \end{aligned} \tag{3.10}$$

where $(\cdots)$ represents a Wigner 3-j symbol and $\langle \Delta_t J_t \parallel \boldsymbol{P}^{(1)} \parallel \Delta_t' J_t' \rangle$ is called the reduced matrix element, which will be discussed shortly in more detail.

Now we apply eqs. (3.9) and (3.10) to eq. (3.5) and use the fact that $J_t - M_t$ is an integer so that $(-1)^{2J_t - 2M_t} = 1$. Also,

$$\sum_{q,q'} \begin{pmatrix} J_t & 1 & J_t' \\ -M_t & q & M_t' \end{pmatrix} \begin{pmatrix} J_t & 1 & J_t' \\ -M_t & q' & M_t' \end{pmatrix} = \sum_q \begin{pmatrix} J_t & 1 & J_t' \\ -M_t & q & M_t' \end{pmatrix}^2 \tag{3.11}$$

because q' must equal q in order to satisfy the 3-j property

$$-M_t + q + M_t' = 0 . \tag{3.12}$$

Hence,

$$S(\Delta_t J_t M_t,\ \Delta_t' J_t' M_t') = \sum_q \begin{pmatrix} J_t & 1 & J_t' \\ -M_t & q & M_t' \end{pmatrix}^2$$

$$\times |\langle \Delta_t J_t \parallel \boldsymbol{P}^{(1)} \parallel \Delta'_t J'_t \rangle|^2 . \tag{3.13}$$

Actually, in order to satisfy eq. (3.12), q is fixed for given values of M_t and M'_t. The possible values of q and corresponding polarizations for the radiation field are provided by Cowan [8] and are as follows: (1) For $M_t = M'_t$, $q = 0$, the polarization is linear, parallel to the z axis. (2) For $M_t = M'_t + 1$, $q = +1$, the polarization is circular, clockwise in the (x, y) plane. (3) For $M_t = M'_t - 1$, $q = -1$, the polarization is circular, counterclockwise in the (x, y) plane. Cases (2) and (3) pertain to radiation as seen looking in the negative z direction. When viewed from other directions, the radiation field is elliptically polarized, except that when viewed from a point in the (x, y) plane it is plane polarized, perpendicular to the z axis.

3.1.2 Transitions between fine-structure levels

In typical plasma applications, where no anisotropy is assumed, the line strength for a transition between fine-structure energy levels, $\Delta_t J_t \rightarrow \Delta'_t J'_t$, is given by

$$\begin{aligned} S(\Delta_t J_t,\ \Delta'_t J'_t) &= \sum_{M_t, M'_t} S(\Delta_t J_t M_t,\ \Delta'_t J'_t M'_t) \\ &= |\langle \Delta_t J_t \parallel \boldsymbol{P}^{(1)} \parallel \Delta'_t J'_t \rangle|^2 , \end{aligned} \tag{3.14}$$

where use has been made of eq. (3.13) and the fact that

$$\sum_{M_t, q, M'_t} \begin{pmatrix} J_t & 1 & J'_t \\ -M_t & q & M'_t \end{pmatrix}^2 = 1 . \tag{3.15}$$

This last result is obtained by noting that the summation over M_t and q yields $(2J'_t + 1)^{-1}$, which is ultimately canceled by the summation over M'_t. Of course, in this case the statistical weights in eqs. (3.2) and (3.3) are $g_i = 2J_t + 1$ and $g_j = 2J'_t + 1$.

The procedure we have been discussing for obtaining the oscillator strength employs the so-called length form, i.e. the line strength in eq. (3.5) involves the matrix elements of the position vectors $\boldsymbol{r}_i$. Two other forms, called the velocity form and the acceleration form, give results identical to those obtained with the length form, if exact wave functions are used in the calculation. However, these are generally not available. Since these two other forms depend more sensitively on the wave functions for small r values, where the wave functions are generally least accurately known, the length form is usually the most accurate. This is also the form that occurs naturally in the expression for the Coulomb-Bethe approximation of the very large angular momentum contribution to the electron-impact excitation cross section for optically allowed

transitions, as discussed in section 4.9.

3.1.3 Selection rules for optically allowed transitions

From the properties of the 3-j symbol appearing in eq. (3.13), one obtains the familiar selection rule for allowed transitions

$$J_t - J'_t = \pm 1 \text{ or } 0\,, \tag{3.16}$$

but $J_t = J'_t = 0$ is forbidden. Also, since parity must be conserved and $\boldsymbol{P}^{(1)}$ has odd parity, only transitions in which the parity changes are allowed. In addition, there is the weak selection rule that only single-electron jumps occur. However, as will be seen from the discussion in the next section, this rule is strictly valid only when configuration mixing does not occur.

3.2 Detailed expressions for the line strength

Now we consider evaluation of the reduced matrix element $\langle \Delta_t J_t \parallel \boldsymbol{P}^{(1)} \parallel \Delta'_t J'_t \rangle$ appearing in eq. (3.14). As discussed in section 2.1, we obtain approximate wave functions by expanding them in terms of a set of single-configuration state functions (SCSFs), as given by eq. (2.11). Then, using more explicit notation, we have

$$\begin{aligned}\langle \Delta_t J_t \parallel \boldsymbol{P}^{(1)} \parallel \Delta'_t J'_t \rangle = \sum_{\beta_t, \beta'_t} & b^{J_t}(\Delta_t, \beta_t) b^{J'_t}(\Delta'_t, \beta'_t) \\ & \times \langle \beta_t J_t \parallel \boldsymbol{P}^{(1)} \parallel \beta'_t J'_t \rangle\,,\end{aligned} \tag{3.17}$$

where β_t represents all quantum numbers in addition to J_t and M_t necessary to specify the pure SCSF basis state $\beta_t J_t M_t$ with corresponding mixing coefficient $b^{J_t}(\Delta_t, \beta_t)$. Of course, only states with the same parity, as well as total angular momentum J_t, mix because these are good quantum numbers. As usual, primes on symbols indicate corresponding quantities in the final state, assumed to be the higher energy state in determining the oscillator strength. The case of no mixing will first be addressed, which requires only the pure-state, reduced matrix element appearing in eq. (3.17). Some additional details concerning the mixed case are provided at the end of this section.

Before proceeding, we provide a rather lengthy, explanatory note in order to avoid possible confusion concerning the jargon that is used when referring to SCSFs, states and fine-structure levels. Note that, in general, a complete description of an SCSF basis state or magnetic sublevel requires the specification

of a magnetic quantum number M, as provided in the description immediately following eq. (3.17). However, the reduce matrix elements and mixing coefficients in eq. (3.17) are independent of the magnetic quantum numbers associated with the particular SCSFs from which these quantities were derived. In this case, it can be confusing when a magnetic quantum number does not explicitly appear in a mathematical expression, but it does appear in the subsequent discussion. When this situation occurs, it is *understood* that the relevant quantity was determined from wave functions that depend on M, but the quantity itself is independent of M. A related situation sometimes occurs when reference is made to the initial and final "states" (denoted by $\beta_t J_t$ and $\beta'_t J'_t$) or "levels" (denoted by $\Delta_t J_t$ and $\Delta'_t J'_t$) of a particular process, matrix element, etc. These states or levels can not be expressed in an explicit mathematical form, although it is not uncommon to see expressions such as $|\beta_t J_t\rangle$ or $|\Delta_t J_t\rangle$. A common occurrence of this type of notation is encountered when referring to matrix elements of the Hamiltonian in eq. (2.1). In this case, the matrix elements in the SCSF basis are independent of M, so it is convenient to refer to the energy associated with a state denoted by the quantum numbers β_t, J_t. However, it is *understood* that this energy is actually associated with each of the $2J_t + 1$ (degenerate) sublevels that are described by the additional quantum numbers β_t, J_t. As a different example, the concept of states or levels typically arises when considering some sort of summing or averaging process over quantities that depend on the more fundamental SCSFs or magnetic sublevels (see, for example, eq. (3.14)). In this context, we will sometimes refer to the initial and final "states" or "levels" as if they can be described by an explicit wave function. Technically, this is not true, but it is a convenient terminology when properly understood. Furthermore, "states" are often referred to as SCSFs in this context, even though this usage is technically incorrect because the labeling of these "states" does not include the requisite magnetic quantum number associated with any SCSF. Once again, in this case, it is *understood* that we are referring to some quantity that was derived from SCSFs, but that is ultimately found to be independent of any magnetic quantum number. Thus, it is sufficient to simply specify the appropriate "state" quantum numbers, without providing a specific magnetic quantum number. When confusion may arise from these types of situations, we have attempted to provide a cautionary remark and refer the reader to this explanatory note.

Moving along to a consideration of the reduced matrix element, $\langle \beta_t J_t \parallel \boldsymbol{P}^{(1)} \parallel \beta'_t J'_t \rangle$, we first discuss the case of ions with initially only empty or closed subshells, in addition to the active subshell, which is designated by subscript a. Since the orbital wave functions entering the SCSF basis states are orthogonal and normalized to unity, and $\boldsymbol{P}^{(1)}$ is given by eq. (3.7), one sees that non-vanishing matrix elements will occur only when the same electrons occur initially and finally in each inactive, closed subshell. Of course, there will be many terms of this kind resulting from permutations of the electrons between

the different subshells due to the requirement of a completely antisymmetric wave function, but the presence of these identical terms is exactly canceled by the normalization factors in the SCSFs. Thus, the form of the results for the matrix element is completely unaffected by the presence of closed subshells of the inactive electrons. Hence, we hereafter ignore the inactive subshells, except that, of course, they must be included in determining the central potential appearing in eqs. (2.9), (2.10) and (2.14) when calculating the radial functions.

Now we consider the construction of the SCSFs, following closely the analogous discussion in ref. [30]. It is well known that for two equivalent electrons an antisymmetric wave function is given by

$$\Psi[(n_a l_a j_a)^2 J_a M_a \mid x_1 x_2] = \sum_{m_1,m_2} C(j_a j_a m_1 m_2; J_a M_a) \times u_{n_a l_a j_a m_1}(x_1) u_{n_a l_a j_a m_2}(x_2)\,, \qquad (3.18)$$

where x_i stands for the coordinates, spatial and spin, of electron i. Although eq. (3.18) appears to have the form of an unsymmetrized function, the Clebsch-Gordan coefficients ensure antisymmetry. Analogously, for three equivalent electrons an antisymmetrized wave function is given by

$$\Psi[(n_a l_a j_a)^3 J_a M_a \mid x_1 x_2 x_3] = \sum_{J_1} (j_a^2 J_1 \mid\} j_a^3 J_a) \sum_{M_1,m_a} C(J_1 j_a M_1 m_a; J_a M_a) \times \Psi[(n_a l_a j_a)^2 J_1 M_1 \mid x_1 x_2] u_{n_a l_a j_a m_a}(x_3)\,, \qquad (3.19)$$

where $\Psi[(n_a l_a j_a)^2 J_1 M_1 \mid x_1 x_2]$ is given by eq. (3.18), with $J_1 M_1$ replacing $J_a M_a$, and the $(\cdots \mid\} \cdots)$ are coefficients of fractional parentage (CFP). Although eq. (3.19) has the appearance of an unsymmetrized function, it is actually completely antisymmetric in all three electrons due to the properties of the Clebsch-Gordan coefficients and the CFP. One can continue this procedure for any number of equivalent electrons, w. Thus, the completely antisymmetric wave function for w electrons in subshell a can be written

$$\Psi[(n_a l_a j_a)^w \alpha_a J_a M_a \mid x_1 x_2 \cdots x_w] = \sum_{J_1,\alpha_1} (j_a^{w-1} \alpha_1 J_1 \mid\} j_a^w \alpha_a J_a) \sum_{M_1,m_a} C(J_1 j_a M_1 m_a; J_a M_a) \times \Psi[(n_a l_a j_a)^{w-1} \alpha_1 J_1 M_1 \mid x_1 x_2 \cdots x_{w-1}] u_{n_a l_a j_a m_a}(x_w)\,, \qquad (3.20)$$

where the electrons are in the definite increasing order $1, 2, 3, ..., w$, but the CFP and Clebsch-Gordan coefficients maintain complete antisymmetry. Here, α_1 represents any additional quantum numbers, such as the seniority numbers, required to completely specify a state when there are several states

arising from the j_a^{w-1} configuration, with the same J_1 value. An analogous statement applies for α_a and the j_a^w configuration. Of course, the functions given by eq. (3.20) are assumed to be orthogonal and normalized to unity, which requires the CFP to obey

$$\sum_{J_1,\alpha_1} (j_a^{w-1}\alpha_1 J_1 \,|\}\, j_a^w \alpha_a J_a)(j_a^{w-1}\alpha_1 J_1 \,|\}\, j_a^w \alpha_a' J_a) = \delta_{\alpha_a \alpha_a'} \,. \tag{3.21}$$

Labeling the final upper (initially empty) subshell as $n_a' l_a' j_a'$, one can write the final completely antisymmetrized wave function in a form similar to eq. (3.20), but with the following changes: (1) the CFP and summation over J_1 and α_1 is omitted, (2) an orbital $u_{n_a' l_a' j_a' m_a'}$ replaces $u_{n_a l_a j_a m_a}$, (3) one must include an antisymmetrized sum over all the possible states with any of the w electrons transitioning to the subshell $n_a' l_a' j_a'$, and, (4) in order to have a normalized function, one must multiply by the factor $1/\sqrt{w}$. The result is

$$\begin{aligned}
&\Psi[(n_a l_a j_a)^{w-1} \alpha_a'' J_a'' n_a' l_a' j_a' J_t' M_t' \mid x_1 x_2 \cdots x_w] \\
&\quad = \frac{1}{\sqrt{w}} \sum_{p=1}^{w} (-1)^{w-p} \sum_{M_a'', m_a'} C(J_a'' j_a' M_a'' m_a'; J_t' M_t') \\
&\quad \times \Psi[(n_a l_a j_a)^{w-1} \alpha_a'' J_a'' M_a'' \mid x_1 x_2 \cdots x_{p-1} x_{p+1} \cdots x_w] u_{n_a' l_a' j_a' m_a'}(x_p) \,,
\end{aligned} \tag{3.22}$$

where the $w-1$ electrons in $\Psi[(n_a l_a j_a)^{w-1} \alpha_a'' J_a'' M_a'' \mid x_1 x_2 \cdots x_{p-1} x_{p+1} \cdots x_w]$ are in the definite increasing order $1, 2, 3, ..., w$, with, of course, the value p omitted.

Now we use eqs. (3.20) and (3.22) as the initial and final states in the reduced matrix element $\langle \beta_t J_t \parallel \boldsymbol{P}^{(1)} \parallel \beta_t' J_t' \rangle$. However, as noted previously, the additional filled subshells of inactive electrons make no contribution. Hence, in the summation that appears in the expression for $\boldsymbol{P}^{(1)}$ given by eq. (3.7), we can replace N with w. Also, in eq. (3.20) the replacements $J_a \rightarrow J_t$ and $M_a \rightarrow M_t$ should be made. In addition, due to the orthogonality of the Dirac spinors, denoted by u, only terms with the index i in eq. (3.8) equal to the index p in eq. (3.22) will contribute to the matrix element. As noted previously, even though the initial wave function given by eq. (3.20) has all the electrons in the definite increasing order $1, 2, ..., w$, it is actually an antisymmetric function due to the properties of the CFP and the Clebsch-Gordan coefficients. Hence, in evaluating $\langle \beta_t J_t \parallel \boldsymbol{P}^{(1)} \parallel \beta_t' J_t' \rangle$, one can permute the coordinates in the initial ion wave function such that they are in the same positions as the final ion wave function given by eq. (3.22) in determining the contribution of each term in the summation over p. This procedure introduces a phase factor, $(-1)^{w-p}$, that exactly cancels the effect of the similar phase factor in eq. (3.22). Then, the sum over p yields w contributions, all with the same value. Using eq. (3.8) with $N = w$ and $i = p$, one obtains the result

$$\langle \beta_t J_t \parallel \boldsymbol{P}^{(1)} \parallel \beta'_t J'_t \rangle = \sqrt{w} \langle n_a l_a j_a \mid r \mid n'_a l'_a j'_a \rangle \times \sum_{J_1, \alpha_1} (j_a^{w-1} \alpha_1 J_1 \mid\} j_a^w \alpha_a J_a) \times \langle j_a^{w-1} \alpha_1 J_1 j_a J_t \parallel \boldsymbol{C}^{(1)} \parallel j_a^{w-1} \alpha''_a J''_a j'_a J'_t \rangle \,, \tag{3.23}$$

which separates into a product consisting of an angular part that can be evaluated using irreducible tensor techniques, and a radial integral given by

$$\langle n_a l_a j_a \mid r \mid n'_a l'_a j'_a \rangle = \int_0^\infty [P_{n_a l_a j_a}(r) P_{n'_a l'_a j'_a}(r) + Q_{n_a l_a j_a}(r) Q_{n'_a l'_a j'_a}(r)] r \, \mathrm{d}r \,. \tag{3.24}$$

As mentioned earlier, J_t has been used in place of J_a in the above angular matrix element. However, the substitution has not been made in the CFP, for reasons that will be made explicit below.

In order to evaluate the angular part of eq. (3.23), we use eq. (C.90) of Messiah [7] to obtain

$$\langle j_a^{w-1} \alpha_1 J_1 j_a J_t \parallel \boldsymbol{C}^{(1)} \parallel j_a^{w-1} \alpha''_1 J''_a j'_a J'_t \rangle = \delta_{\alpha_1 \alpha''_a} \delta_{J_1 J''_a} (-1)^{J_t + J_1 + j'_a + 1} [(2J_t + 1)(2J'_t + 1)]^{1/2} \times \begin{Bmatrix} j_a & 1 & j'_a \\ J'_t & J_1 & J_t \end{Bmatrix} \langle j_a \parallel \boldsymbol{C}^{(1)} \parallel j'_a \rangle \,, \tag{3.25}$$

where $\{\cdots\}$ represents a Wigner 6-j symbol and

$$\langle j_a \parallel \boldsymbol{C}^{(1)} \parallel j'_a \rangle = (-1)^{j_a + 1/2} [(2j_a + 1)(2j'_a + 1)]^{1/2} \begin{pmatrix} j_a & 1 & j'_a \\ \frac{1}{2} & 0 & -\frac{1}{2} \end{pmatrix} . \tag{3.26}$$

Applying eq. (3.25) to eq. (3.23), we obtain

$$\langle \beta_t J_t \parallel \boldsymbol{P}^{(1)} \parallel \beta'_t J'_t \rangle = \sqrt{w} [(2J_t + 1)(2J'_t + 1)]^{1/2} (-1)^{J'_t + J''_a + j'_a} \times \begin{Bmatrix} j_a & 1 & j'_a \\ J'_t & J''_t & J_t \end{Bmatrix} (j_a^{w-1} \alpha''_a J''_a \mid\} j_a^w \alpha_a J_a) \times \langle j_a \parallel \boldsymbol{C}^{(1)} \parallel j'_a \rangle \langle n_a l_a j_a \mid r \mid n'_a l'_a j'_a \rangle \,. \tag{3.27}$$

In writing the phase factor in eq. (3.27), we replaced $(-1)^{J_t+1}$ with $(-1)^{J'_t}$. This choice is obviously valid when $J_t = J'_t \pm 1$. For the remaining case of $J_t = J'_t$ (see eq. (3.16)), a factor of (-1) remains, but it will not contribute to the line strength, S, given by eq. (3.14) because it will lead to an overall factor of $(-1)^2 = 1$. Our reason for making this replacement is that our results then take on a form very similar to that obtained in chapter 4 for electron-impact excitation when the convenient factorization method of ref. [31] is used.

Also, in addition to using $J_t = J_a$ in eq. (3.27), we have used $J''_t = J''_a$, where J''_t is the final total angular momentum of the core, which, when coupled to j'_a, gives J'_t. For the present case of initially filled or empty subshells, in addition to the active subshell, this choice is obviously valid. The reason we used J_t in place of J_a, and J''_t in place of J''_a, everywhere except in the CFP, is that when one considers more complex cases of additional partially filled subshells, the form of eq. (3.27) remains unchanged, except for inclusion of additional angular factors that arise from the presence of these extra partially filled subshells. Many of these angular factors were worked out in ref. [30] and given in ref. [32]. However, eq. (3.27) is applicable for many of the transitions of greatest interest.

We note that the weak selection rule mentioned in subsection 3.1.3 follows from the derivation of eq. (3.27). Specifically, a non-zero value is obtained only when the initial and final states are connected by a one-electron jump. However, as is apparent from eq. (3.17), this rule is strictly valid only when there is no mixing. A useful form of the line strength, when mixing becomes necessary, is provided next.

In order to simplify the notation and make it similar to that used in chapter 4, we let $U = \Delta_t J_t$ and $U' = \Delta'_t J'_t$ for the initial and final levels. Also, we let $S = \beta_t J_t$ to indicate a pure SCSF state contributing to U, while $S' = \beta'_t J'_t$ indicates a pure SCSF state contributing to U'. (The omission of the magnetic quantum number in describing an SCSF is potentially confusing. See the explanatory note following eq. (3.17).) Thus,

$$U = \sum_S b(U,S)|S\rangle, \quad U' = \sum_{S'} b(U',S')|S'\rangle\,, \tag{3.28}$$

where the b's in eq. (3.28) are the mixing coefficients formerly referred to as $b^{J_t}(\Delta_t, \beta_t)$ and $b^{J'_t}(\Delta'_t, \beta'_t)$ in eq. (3.17). In addition, we let

$$F^{(1)}(US, U'S') = b(U,S) f^{(1)}(S,S') b(U',S')\,, \tag{3.29}$$

where

$$\begin{aligned} f^{(1)}(S,S') = {} & [(2J_t+1)(2J'_t+1)]^{1/2}(-1)^{J'_t+J''_t+j'_a} \\ & \times \left\{ \begin{matrix} j_a & 1 & j'_a \\ J'_t & J''_t & J_t \end{matrix} \right\} \sqrt{w}(j_a^{w-1}\alpha''_a J''_a \,|\}\, j_a^w \alpha_a J_a)\,. \end{aligned} \tag{3.30}$$

For more complex cases, extra angular factors will enter eq. (3.30), as mentioned previously. Alternatively, we note that it was unnecessary for us to work out the values of $f^{(1)}(S,S')$ for the most general case because we found [33] that $f^{\lambda}(S,S')$ equals the quantity $d^{\lambda}_{a,a'}(S,S')$ that is defined in ref. [34].

Thus, these coefficients are readily available, in complete generality, from the MCT module of the Grant code.

Applying eq. (3.29) to eqs. (3.27) and (3.17) yields the expression

$$\begin{aligned}\langle \Delta_t J_t \parallel \boldsymbol{P}^{(1)} \parallel \Delta'_t J'_t \rangle &\equiv \langle U \parallel \boldsymbol{P}^{(1)} \parallel U' \rangle \\ &= \sum_{S,S'} F^{(1)}(US, U'S') L_{\mathrm{H}}^{\mathrm{ps}}(n_a l_a j_a, n'_a l'_a j'_a)\,, \end{aligned} \tag{3.31}$$

where

$$L_{\mathrm{H}}^{\mathrm{ps}} = \langle n_a l_a j_a \mid r \mid n'_a l'_a j'_a \rangle \langle j_a \parallel \boldsymbol{C}^{(1)} \parallel j'_a \rangle \tag{3.32}$$

in which $\langle n_a l_a j_a \mid r \mid n'_a l'_a j'_a \rangle$ and $\langle j_a \parallel \boldsymbol{C}^{(1)} \parallel j'_a \rangle$ are given by eqs. (3.24) and (3.26). (The "ps" superscript and "H" subscript denote a pseudo-hydrogenic quantity that will be explained in more detail in the upcoming subsection 3.2.1.) Applying eq. (3.31) to eq. (3.14) for the line strength, we obtain

$$\begin{aligned} S(U,U') = \sum_{\substack{S,S' \\ S_1,S'_1}} & B^{(1)}(U, SS_1; U', S'S'_1) \\ & \times L_{\mathrm{H}}^{\mathrm{ps}}(n_a l_a j_a, n'_a l'_a j'_a) L_{\mathrm{H}}^{\mathrm{ps}}(n_{a_1} l_{a_1} j_{a_1}, n'_{a_1} l'_{a_1} j'_{a_1})\,, \end{aligned} \tag{3.33}$$

where

$$B^{(1)} = F^{(1)}(US, U'S') F^{(1)}(US_1, U'_1 S'_1)\,. \tag{3.34}$$

It is interesting to note that $B^{(1)}$ is a special case of the quantity B^{λ} (with $\lambda = 1$) that appears in the expression for the excitation collision strength to be obtained in chapter 4. For the case of transitions between magnetic sublevels, eq. (3.33) is easily generalized. In particular, the right-hand side of eq. (3.33) must be multiplied by the factor

$$\begin{pmatrix} J_t & 1 & J'_t \\ -M_t & q & M'_t \end{pmatrix}^2\,, \tag{3.35}$$

and it is understood that the state summation indices, as well as the level indices U and U', each contain a valid magnetic quantum number. As stated previously, there is no need to include a summation over q, since its value is fixed for given values of M_t and M'_t. (See the discussion immediately following eq. (3.13).)

3.2.1 *Special simple cases*

Among the several cases for which there are no partially filled subshells, in addition to the active one, in the initial state, so that no extra angular factors enter into eq. (3.30), there are two of particular interest for which $f^{(1)}$ becomes especially simple. These are: (1) the case in which the active subshell initially contains a single electron, and (2) the case in which the active subshell is initially filled. For case (1), which applies to hydrogenic ions and transitions involving the valence electron outside of a closed shell, such as in Li-like and Na-like ions, $J_t'' = 0$ and, consequently, the 6-j symbol in eq. (3.30) becomes [7]

$$\left\{ \begin{matrix} j_a & 1 & j_a' \\ J_t' & 0 & J_t \end{matrix} \right\} = \left\{ \begin{matrix} j_a & J_t & 0 \\ J_t' & j_a' & 1 \end{matrix} \right\} = \frac{(-1)^{j_a + J_t' + 1} \delta_{J_t j_a} \delta_{J_t' j_a'}}{[(2J_t + 1)(2J_t' + 1)]^{1/2}} . \tag{3.36}$$

Also, since both w and the CFP are equal to one, $f^{(1)}$ reduces to $(-1)^{j_a + 3j_a' + 1}$. Moreover, no mixing can occur for hydrogenic ions or for the alkali-like ions, provided one considers mixing only among the states in a complex and only the valence electron is active. Therefore, the quadruple sum in eq. (3.33) reduces to a single term and the square of $f^{(1)}$, which is equal to one, enters into the final expression for the line strength. Consequently, the factor $B^{(1)} = 1$ and eq. (3.33) reduces to the expression for the pseudo-hydrogenic line strength

$$S_{\mathrm{H}}^{\mathrm{ps}}(n_a l_a j_a, n_a' l_a' j_a') = L_{\mathrm{H}}^{\mathrm{ps}}(n_a l_a j_a, n_a' l_a' j_a')^2 . \tag{3.37}$$

The corresponding oscillator strength is given by

$$f_{\mathrm{H}}^{\mathrm{ps}}(n_a l_a j_a, n_a' l_a' j_a') = \frac{\Delta E}{3(2j_a + 1)} L_{\mathrm{H}}^{\mathrm{ps}}(n_a l_a j_a, n_a' l_a' j_a')^2 . \tag{3.38}$$

This last expression is precisely the form that one obtains when considering radiative transitions in hydrogenic ions. Of course, for alkali-like ions, the radial functions used in determining $L_{\mathrm{H}}^{\mathrm{ps}}$ must be obtained from the approximate potential displayed in eq. (2.18) that includes the electron-electron contribution, rather than just the pure $-2Z/r$ Coulomb potential due to the nucleus, which applies to hydrogenic ions. That is why the superscript "ps" (for pseudo) has been added to the quantity L_{H}.

Next, we consider the second case, which applies to He-like, Ne-like and Ni-like ions. These ion stages are very important in plasma applications because each one tends to be the dominant stage of ionization over a wide range of temperatures. For this situation, the CFP is again unity. Also, $J_t = 0$ so that the 6-j symbol in eq. (3.30) reduces to

$$\left\{ \begin{matrix} j_a & 1 & j'_a \\ J'_t & J''_t & 0 \end{matrix} \right\} = \left\{ \begin{matrix} j_a & J''_t & 0 \\ J'_t & 1 & j'_a \end{matrix} \right\} = \frac{(-1)^{j_a+J'_t+j'_a}\,\delta_{J''_t j_a}\delta_{J'_t 1}}{[(2J'_t+1)(2j_a+1)]^{1/2}}\,. \tag{3.39}$$

Thus, eq. (3.30) becomes

$$f^{(1)} = \frac{w^{1/2}}{(2j_a+1)^{1/2}}(-1)^{2J'_t+J''_t+2j'_a+j_a} = (-1)^{2(J'_t+j_a+j'_a)}\,, \tag{3.40}$$

where the final form applies because $w = 2j_a + 1$ for a filled subshell, and j_a has been substituted for J''_t, according to eq. (3.39). One can ignore the phase factor $(-1)^{2J'_t}$, which must be equal to one, because $J'_t = 1$ due to the selection rule in eq. (3.16). Similarly, since j_a and j'_a are half integers, the phase factor $(-1)^{2(j_a+j'_a)}$ is also equal to one. Finally, it is usually a good approximation to omit mixing for these closed-shell ground states, specifically for highly charged ions, so that there is mixing only among the upper states. Hence, the line strength obtained from eqs. (3.33) and (3.34) becomes

$$\begin{aligned} S(U,U') = \sum_{S',S'_1} & b(U',S')b(U',S'_1) \\ & \times L_{\rm H}^{\rm ps}(n_a l_a j_a, n'_a l'_a j'_a) L_{\rm H}^{\rm ps}(n_{a_1} l_{a_1} j_{a_1}, n'_{a_1} l'_{a_1} j'_{a_1})\,. \end{aligned} \tag{3.41}$$

In the present case, the statistical weight g_i in eq. (3.3) is $2J_t + 1 = 1$. Hence, if mixing can also be ignored among the upper states, the corresponding oscillator strength could be put in the pseudo-hydrogenic form of eq. (3.38), but multiplied by an additional factor of $w = 2j_a + 1$. This result is precisely what one would intuitively expect when the initial state contains only closed shells.

It may seem odd that different orbitals for the lower state enter into eq. (3.41), when there is no mixing included in the lower level. However, this notation takes into account the possibility that an electron jump may occur from different subshells in the ground-state wave function, depending on the amount of mixing included among the upper states. As a simple illustration, when considering $n = 2$ to 3 transitions from the ground state of Ne-like ions, it is possible for orbital transitions of the type $2p_{1/2} \rightarrow 3s$ and $2p_{3/2} \rightarrow 3s$ to contribute to a particular fine-structure transition, if mixing is included among the $1s^2 2s^2 2p_{1/2} 2p_{3/2}^4 3s$ and $1s^2 2s^2 2p_{1/2}^2 2p_{3/2}^3 3s$ configurations. In these cases, the particular lower orbital that appears in the argument of $L_{\rm H}^{\rm ps}$ is fixed by the upper orbital, in concert with the fixed J'_t-value of unity, plus the fixed odd parity of the upper level.

3.2.2 Configuration-average case

For configuration-average transitions, we consider an electron jump from subshell α of configuration c to subshell β of configuration c'. We write this

transition in the symbolic form

$$(n_\alpha\kappa_\alpha)^{w_\alpha}(n_\beta\kappa_\beta)^{w_\beta-1}(n_\gamma\kappa_\gamma)^{w_\gamma}\cdots \longrightarrow (n_\alpha\kappa_\alpha)^{w_\alpha-1}(n_\beta\kappa_\beta)^{w_\beta}(n_\gamma\kappa_\gamma)^{w_\gamma}\cdots . \quad (3.42)$$

The multitude of fine-structure transitions that can arise from eq. (3.42) is sometimes referred to as a "transition array". Analogous to the discussion in section 2.6, the most general expression for the configuration-average oscillator strength, or line strength, would include an average over all of the corresponding fine-structure values that comprise the transition array. In this case, the presence of mixing coefficients is not so problematic due to the existence of powerful line-strength sum rules and, in theory, an expression could be obtained in terms of more fundamental quantities when an arbitrary amount of CI is considered. (See, for example, pp. 423–424 of ref. [8].) However, here we limit the discussion to the single-configuration approximation, which results in the so-called "array oscillator strength". It is most convenient to begin with the line strength, rather than the oscillator strength, because the expression for the line strength does not explicitly contain the transition energy. The presence of the transition energy, which can be different for each SCSF transition that comprises the array, further complicates the averaging process.

Thus, we write the formal expression for the configuration-average line strength between configurations c and c' as

$$S_{c-c'} \equiv \sum_{i\in c}\sum_{j\in c'} S_{i-j}\,, \quad (3.43)$$

where S_{i-j} is the line strength for the transition between two pure SCSFs labeled i and j. Note that the outer and inner summations consider only those SCSFs that arise from configurations c and c', respectively. After some manipulation eq. (3.43) can be simplified according to

$$\begin{aligned} S_{c-c'} &= g_c\frac{w_\alpha}{g_\alpha}\frac{g_\beta-(w_\beta-1)}{g_\beta}S_{\rm H}^{\rm ps}(n_\alpha l_\alpha j_\alpha, n_\beta l_\beta j_\beta) \\ &= g_c\frac{w_\alpha(2j_\beta+2-w_\beta)}{(2j_\alpha+1)(2j_\beta+1)}S_{\rm H}^{\rm ps}(n_\alpha l_\alpha j_\alpha, n_\beta l_\beta j_\beta)\,, \end{aligned} \quad (3.44)$$

where $S_{\rm H}^{\rm ps}$ is the pseudo-hydrogenic line strength given by eq. (3.37), $g_\alpha = 2j_\alpha+1$ is the statistical weight of subshell α (with a similar expression for g_β) and g_c is the statistical weight of configuration c. A detailed expression for this last quantity is given by

$$g_c = \prod_\alpha \frac{(2j_\alpha+1)!}{(2j_\alpha+1-w_\alpha)!w_\alpha!}\,, \quad (3.45)$$

where the product is over each open subshell α, which contains w_α electrons.

In order to obtain an expression for the configuration-average oscillator strength, we must make the additional approximation that the energy associated with each SCSF transition in the transition array is approximately equal to the configuration-average transition energy, $\Delta E_{c-c'} = E_{c'} - E_c$, where the energy associated with a particular configuration is given by eq. (2.33a). Then, with the use of eq. (3.3), the configuration-average oscillator strength can be written as

$$\begin{aligned} f_{c-c'} &\equiv \sum_{i\in c}\sum_{j\in c'} g_i f_{i-j}/g_c = \frac{1}{3g_c}\sum_{i\in c}\sum_{j\in c'} \Delta E_{i-j} S_{i-j} \\ &\approx \frac{\Delta E_{c-c'}}{3g_c}\sum_{i\in c}\sum_{j\in c'} S_{i-j} = \frac{\Delta E_{c-c'}}{3g_c} S_{c-c'} \,. \end{aligned} \tag{3.46}$$

Thus, the relationship between the configuration-average oscillator strength and corresponding line strength is formally identical to the relationship between the fine-structure (or SCSF) quantities, as given by eq. (3.3). With the use of eqs. (3.37), (3.38) and (3.44), the configuration-average oscillator strength can be expressed in the useful form

$$f_{c-c'} = \frac{w_\alpha(2j_\beta + 2 - w_\beta)}{(2j_\beta + 1)} f_{\rm H}^{\rm ps}(n_\alpha l_\alpha j_\alpha, n_\beta l_\beta j_\beta) \,, \tag{3.47}$$

where $f_{\rm H}^{\rm ps}$ is the pseudo-hydrogenic oscillator strength given by eq. (3.38). It is easily verified that, for hydrogenic ions (i.e. when $w_\alpha = w_\beta = 1$), the configuration-average oscillator strength reduces to the correct hydrogenic expression. We also note that eq. (3.47) is the relativistic analog of the configuration-average expression given by Peyrusse [28] and by Cowan in eq. (14.97) of ref. [8].

3.3 Some comparisons of oscillator strengths

In table 3, a sample comparison, taken from ref. [1], is made between oscillator strengths obtained in various ways for transitions from the ground level to the $n = 3$ levels in Ne-like ions. The notation is the same as that used in table 1 of section 2.4, which compared energies of excited levels relative to the ground level in Ne-like uranium. However, there are a few additional symbols in the oscillator strength table. The HBS values were obtained using the fairly crude approximation of non-relativistic hydrogenic basis states. However, this approximation is seen to give fairly good results for $Z = 26$. The R entries were obtained by Reed [35] using the fully relativistic program of Hagelstein and

Table 3
Comparison of oscillator strengths for transitions from the ground level to certain excited levels in neon-like ions. The notation is as in table 1 of section 2.4, except that HBS indicates results using hydrogenic basis states and R indicates results obtained by Reed [35] using the relativistic program of Hagelstein and Jung [36]. Also G, G* and G** are results obtained with the Grant code [6,11] without retardation, with retardation, and with retardation plus the generalized Breit interaction, other QED corrections and finite nuclear size, respectively.

				$Z = 26$			
	$(2p3s)_1$	$(2p^*3s)_1$	$(2p3d^*)_1$	$(2p3d)_1$	$(2p^*3d^*)_1$	$(2s3p^*)_1$	$(2s3p)_1$
QR	0.1093	0.0919	0.0097	0.6140	2.5325	0.0369	0.2875
FR	0.1081	0.0922	0.0098	0.5900	2.5516	0.0358	0.2880
FR*	0.1102	0.0937	0.0099	0.6095	2.5514	0.0358	0.2868
G	0.1051	0.0890	0.0076	0.6049	2.3779	0.0342	0.2648
G*	0.1051	0.0888	0.0074	0.6036	2.3743	0.0343	0.2642
G**	0.1047	0.0896	0.0072	0.5900	2.3844	0.0337	0.2638
HFR	0.121	0.103	0.010	0.682	2.582	0.039	0.322
HBS	0.116	0.099	0.010	0.659	2.651	0.041	0.344

				$Z = 47$			
	$(2p3s)_1$	$(2p^*3s)_1$	$(2p3d^*)_1$	$(2p3d)_1$	$(2p^*3d^*)_1$	$(2s3p^*)_1$	$(2s3p)_1$
QR	0.1262	0.1010	0.0003	2.0531	1.5905	0.1214	0.3273
FR	0.1239	0.0971	0.0001	2.0460	1.5797	0.1210	0.3253
FR*	0.1250	0.0978	0.0001	2.0557	1.5828	0.1207	0.3248
G	0.1223	0.0957	0.0003	2.0013	1.5491	0.1165	0.3132
G*	0.1222	0.0947	0.0004	1.9839	1.5420	0.1166	0.3097
G**	0.1232	0.0947	0.0005	1.9897	1.5305	0.1166	0.3050
HFR	0.1238	0.1156	0.0005	2.0336	1.6826	0.1084	0.3647

				$Z = 56$			
	$(2p3s)_1$	$(2p^*3s)_1$	$(2p3d^*)_1$	$(2p3d)_1$	$(2p^*3d^*)_1$	$(2s3p^*)_1$	$(2s3p)_1$
QR	0.1304	0.0066	2.3117	0.0214	1.4733	0.1083	0.3268
FR	0.1268	0.0057	2.2688	0.0534	1.4477	0.1128	0.3232
FR*	0.1278	0.0058	2.2798	0.0508	1.4511	0.1123	0.3229
G	0.1256	0.0065	2.2320	0.0457	1.4299	0.1086	0.3138
G*	0.1254	0.0073	2.2026	0.0452	1.4208	0.1088	0.3084
G**	0.1267	0.0083	2.1624	0.0897	1.4068	0.1114	0.3025
R	0.1369	0.0068	2.326	0.0564	1.475	0.1050	0.3121
HFR	0.1217	0.0079	2.2865	0.0000	1.6042	0.0867	0.3744

				$Z = 74$			
	$(2p3s)_1$	$(2p^*3s)_1$	$(2p3d^*)_1$	$(2p3d)_1$	$(2p^*3d^*)_1$	$(2s3p^*)_1$	$(2s3p)_1$
QR	0.1527	0.0640	2.3918	0.0280	0.3962	1.0370	0.2899
FR	0.1451	0.0599	2.3787	0.0266	0.4196	0.9725	0.2829
FR*	0.1460	0.0603	2.3847	0.0269	0.4186	0.9759	0.2826
G	0.1441	0.0611	2.3413	0.0269	0.4081	0.9726	0.2722
G*	0.1441	0.0648	2.2827	0.0260	0.4068	0.9600	0.2676
G**	0.1456	0.0704	2.2783	0.0256	0.4809	0.8756	0.2609
HFR	0.127	0.064	2.225	0.062	0.306	1.319	0.364
HBS	0.078	0.065	2.474	0.028	0.802	1.047	0.534

				$Z = 92$			
	$(2p3s)_1$	$(2p^*3s)_1$	$(2p3d^*)_1$	$(2p3d)_1$	$(2p^*3d^*)_1$	$(2s3p^*)_1$	$(2s3p)_1$
QR	0.2045	0.1297	2.3564	0.0306	0.2985	0.9947	0.2143
FR	0.1893	0.1197	2.3393	0.0287	0.2768	0.9517	0.2041
FR*	0.1902	0.1202	2.3445	0.0289	0.2768	0.9535	0.2039
G	0.1878	0.1202	2.3087	0.0288	0.2725	0.9498	0.2012
G*	0.1886	0.1271	2.2143	0.0272	0.2725	0.9299	0.1882
G**	0.1895	0.1356	2.2020	0.0268	0.2775	0.9177	0.1834
HFR	0.1496	0.1167	2.0645	0.0928	0.1851	1.4323	0.3187

Jung [36]. This code includes the Breit interaction plus other QED corrections and a finite nuclear size.

Also, some further clarification on the differences between the G, G* and G** data is required. These values were all obtained using the "average level" approximation of the Grant code [6,11,25]. As mentioned previously, the G**

values include the effects of the generalized Breit interaction, other QED corrections and a finite nuclear size. When considering oscillator strengths, the G* and G** entries also contain the effect of retardation, while the G entries do not. Analogous to the previous description associated with the Breit interaction, this effect takes into account the delay in the electromagnetic interaction between the incident photon and the transitioning bound electron due to the finite value of the speed of light. More precisely, we note that the correct form of the photon interaction with the ith electron contains a factor of $e^{i(\boldsymbol{k}_\lambda \cdot \boldsymbol{r}_i)}$, where $\boldsymbol{k}_\lambda$ is the photon wave vector. When the photon wavelength is much larger than r_i, this factor can be expanded in powers of $(\boldsymbol{k}_\lambda \cdot \boldsymbol{r}_i)$, and retention of the lowest-order surviving term produces the unretarded dipole oscillator strength, which becomes less accurate for increasing values of Z. The retention of the complete exponential allows for a consideration of higher-order multipole terms along with the effect of retardation [5,37]. A more detailed discussion of retardation, as it applies to the oscillator strength, will be provided in the next section.

One sees that the effect of retardation is small in all cases covered by table 3, but, as expected, it is generally seen to be more important for large values of Z. All of the results in table 3 are generally in quite close agreement, except that the HFR and HBS values differ appreciably from the other results for some transitions where Z is very large. Presumably, this discrepancy is largely due to the omission of the j dependence in the radial functions in those calculations. Also, there is the noticeable trend among the QR, FR, FR* and G values that the agreement between FR, FR* and G results improves with increasing Z, while that between QR and FR results improves with decreasing Z. The former is expected because the difference in the physics of the FR, FR* and G calculations is solely in the treatment of the electron-electron contribution $V^{\mathrm{ee}}(r)$ to the central potential. Since $V^{\mathrm{ee}}(r)$ becomes smaller relative to the nuclear contribution as Z increases, the effect on f values decreases as Z increases. Of course, the quasi-relativistic approximations made in the QR approach, discussed near the end of section 2.3, increase in significance as Z increases and relativistic effects become more important. Thus, one expects the difference between QR and FR results to increase with Z. Nevertheless, one sees that, even for $Z = 92$, the QR results for oscillator strengths appear to be quite good.

One case in which the G** values do differ appreciably from the other fully relativistic values is for the weak transition to the $(2p_{1/2}3s_{1/2})_1$ level where $Z = 56$. When the upper level of a weak transition lies close in energy to the upper level of one or more strong transitions with which it can mix, as in this case, slight differences in the method of calculation can sufficiently affect the mixing of the level to provide an appreciable change in the f value for the weak transition. The principal reason for the difference in results for this transition appears to be the inclusion of the generalized Breit interaction in

the G** calculations.

3.4 Inclusion of the generalized Breit interaction and other corrections in calculating oscillator strengths

The necessity to include the generalized Breit interaction (see section 2.5) in order to obtain more accurate results for oscillator strengths of weak transitions in high-Z ions became very clear when we considered the much more complex case of F-like ions in ref. [38]. Before doing large-scale calculations for a wide range of Z values, we generally do some preliminary checks. In ref. [38], results for energies and f values for the $n = 2$ to $n = 3$ transitions for F-like ions, with $Z = 34$ and 92, were compared with other work. For our FR calculations, the mean configuration used in determining the central potential described by eqs. (2.18)–(2.20) was

$$1s^2 2s_{1/2}^{1.9} 2p_{1/2}^{1.9} 2p_{3/2}^{2.7} 3s_{1/2}^{0.1} 3p_{1/2}^{0.1} 3p_{3/2}^{0.1} 3d_{3/2}^{0.1} 3d_{5/2}^{0.1} . \tag{3.48}$$

The agreement, associated with f values and energies, that was obtained by comparing results determined from various relativistic codes and experiment was generally very good for $Z = 34$. For $Z = 92$, we could only make comparisons with results obtained from the Grant code. In this case the G, G* and G** values were obtained with the newer, more efficient version of the Grant code called GRASP [25]. Good agreement was found between our FR results and the G values, but somewhat worse agreement was found between our FR values and the G** results for many of the weak transitions. Although inclusion of retardation had some effect, much of the discrepancy was traced to the effect on mixing coefficients due to inclusion of the generalized Breit interaction in the G** results. This discrepancy provided the original motivation for including the generalized Breit interaction plus other QED corrections, a finite nuclear size and retardation effects in performing large-scale calculations for high-Z ions. The implementation of all but the retardation correction was described previously in section 2.5. In the context of computing oscillator strengths, the finite nuclear size option produced very little effect on this quantity, but can significantly alter the energy associated with a particular level for very high-Z values.

As for retardation, we included this effect when calculating oscillator strengths by computing results in the Babushkin gauge [37,39], which reduces to the length form in the non-relativistic limit. Specifically, in order to include the effect of retardation, the radial integral in eq. (3.24) should be replaced with

$$\langle n_a l_a j_a \mid r \mid n'_a l'_a j'_a \rangle \rightarrow (3/k_\lambda)\{J_1 + [(\kappa_a - \kappa_{a'})/2] I_2^+ + I_2^-\}, \tag{3.49}$$

where k_λ is the wavenumber of the photon and

$$I_2^{\pm} = \int_0^\infty [P_{n_a l_a j_a}(r) Q_{n'_a l'_a j'_a}(r) \pm Q_{n_a l_a j_a}(r) P_{n'_a l'_a j'_a}(r)] j_2(k_\lambda r)\, dr \quad (3.50a)$$

$$J_1 = \int_0^\infty [P_{n_a l_a j_a}(r) P_{n'_a l'_a j'_a}(r) + Q_{n_a l_a j_a}(r) Q_{n'_a l'_a j'_a}(r)] j_1(k_\lambda r)\, dr\,. \quad (3.50b)$$

The function $j_L(k_\lambda r)$ is the spherical Bessel function of order L, which can be expanded for small arguments according to

$$j_L(z) = \frac{z^L}{(2L+1)!!} + \cdots\,, \quad (3.51)$$

where !! denotes the double factorial, which contains products of only even, or odd, positive integers. Using this expansion in eq. (3.49), and retaining only the lowest-order term, which is of $O(k_\lambda r)$, reproduces the unretarded integral in eq. (3.24).

A comparison of oscillator strengths and transition energies that were calculated with the above improvements is presented in table 4 for F-like ions. The notation used in labeling the levels can be found in ref. [38], along with a more complete set of tables. With the inclusion of all these additions to our program, we obtained very good agreement with the Grant code for oscillator strengths for $n = 2$ to $n = 3$ transitions in F-like ions with $Z = 92$, as well as 34. Also, the agreement for transition energies was typically within about 2 or 3 eV, except for transitions to $n = 3$ levels involving a 3s or 2s electron, for which the discrepancies for $Z = 92$ were typically about 8 eV or 40 eV, respectively. However, even in the worst cases, the discrepancy in transition energies was only about 0.38%. As in the discussion of energies for neon-like ions in section 2.4, we attribute these discrepancies for transitions involving s orbitals to numerical imprecision, occurring at small values of r and due to our use of a linear grid in solving for the radial functions. This behavior can likely be eliminated by using a logarithmic grid. However, it appears that this inaccuracy has a negligible effect on line strengths and collision strengths, which was confirmed, for example, by the fact that we were able to reproduce exactly Grant's hydrogenic line strengths for $Z = 90$, even for the 1s-$2p_{1/2}$ and 1s-$2p_{3/2}$ transitions, to within 1%. On the other hand, for $\Delta n = 0$ transitions, where the transition energy can be very small, and hence the percentage error larger, we have used energies provided by the Grant code. This approach added little time to collision strength calculations because the atomic structure part of such calculations, even with the slower Grant code, required only a small portion of the total run time.

Table 4
Comparison of our DFS transition energies and oscillator strengths, computed with various options, against those obtained with the Grant code (labeled "Grant") for selected transitions from the ground level (A1) in F-like ions with $Z = 34$ and 92. The labeling for the excited states can be found in ref. [38]. The columns labeled "1", "2" and "3" display our results computed with none of the new options, with all of the new options, except inclusion of retardation in calculating the f values, and with all the new options, respectively.

	ΔE(eV)			f			
Transition	1	2	Grant	1	2	3	Grant
			$Z = 34$				
A1 - D1	1519.5	1518.4	1516.6	0.0129	0.0128	0.0128	0.0124
A1 - D2	1545.8	1543.8	1541.8	0.0125	0.0127	0.0127	0.0122
A1 - D3	1604.1	1601.4	1599.5	0.0010	0.0011	0.0011	0.0011
A1 - D4	1615.1	1613.4	1611.6	0.0022	0.0020	0.0020	0.0022
A1 - D5	1623.2	1621.2	1619.4	0.0851	0.0847	0.0845	0.0818
A1 - D7	1672.6	1669.6	1667.8	0.2031	0.2031	0.2028	0.1986
A1 - E1	1505.6	1504.0	1501.9	0.0615	0.0619	0.0618	0.0599
A1 - E2	1542.0	1540.0	1537.9	0.0159	0.0160	0.0160	0.0156
A1 - E3	1556.8	1554.2	1552.1	0.0042	0.0040	0.0040	0.0039
A1 - E4	1613.4	1611.8	1609.7	0.0002	0.0001	0.0001	0.0001
A1 - E5	1626.9	1625.1	1623.0	0.1672	0.1751	0.1739	0.1719
A1 - E7	1656.3	1653.9	1651.8	0.0130	0.0117	0.0117	0.0117
A1 - E8	1663.4	1660.7	1658.7	0.0042	0.0031	0.0031	0.0033
A1 - F1	1500.8	1499.2	1497.1	0.0093	0.0091	0.0091	0.0088
A1 - F2	1555.4	1552.8	1550.7	0.0447	0.0450	0.0448	0.0440
A1 - F3	1613.3	1611.4	1609.3	0.0002	0.0001	0.0001	0.0001
A1 - F4	1630.4	1628.4	1626.3	0.3552	0.3703	0.3688	0.3646
A1 - F5	1638.5	1636.9	1634.8	0.2585	0.2402	0.2390	0.2316
A1 - F6	1661.1	1658.5	1656.4	0.0979	0.1032	0.1030	0.1016
A1 - F7	1662.7	1660.1	1658.0	0.2069	0.1977	0.1971	0.1957
A1 - F8	1673.1	1670.1	1668.0	0.0319	0.0331	0.0329	0.0328
			$Z = 92$				
A1 - D1	13134	13127	13136	0.0239	0.0240	0.0240	0.0236
A1 - D2	14599	14599	14598	0.0520	0.0528	0.0545	0.0541
A1 - D3	14859	14813	14811	0.1003	0.0994	0.0953	0.0942
A1 - D4	17050	16986	16994	0.0053	0.0053	0.0050	0.0049
A1 - D5	18008	17927	17890	0.0465	0.0478	0.0478	0.0467
A1 - D7	18623	18527	18524	0.1569	0.1549	0.1518	0.1524
A1 - E1	13075	13051	13059	0.0934	0.0939	0.0943	0.0925
A1 - E2	14588	14553	14551	0.0080	0.0080	0.0083	0.0082
A1 - E3	14666	14641	14639	0.0119	0.0120	0.0127	0.0126
A1 - E4	14893	14846	14843	0.5381	0.5369	0.5143	0.5081
A1 - E5	17036	16972	16980	0.0047	0.0045	0.0042	0.0041
A1 - E7	17895	17811	17773	0.0338	0.0355	0.0355	0.0349
A1 - E8	18011	17928	17890	0.0580	0.0580	0.0580	0.0568
A1 - F1	13061	13036	13044	0.0234	0.0236	0.0237	0.0232
A1 - F2	14598	14554	14552	0.0453	0.0491	0.0516	0.0512
A1 - F3	14892	14845	14842	0.5780	0.6978	0.6686	0.6643
A1 - F4	14931	14898	14896	0.5294	0.4051	0.3880	0.3836
A1 - F5	17072	16991	16998	0.0145	0.0144	0.0136	0.0133
A1 - F6	17902	17810	17771	0.1395	0.1414	0.1415	0.1388
A1 - F7	18586	18499	18496	0.1258	0.1140	0.1116	0.1126
A1 - F8	18629	18529	18526	0.3562	0.3618	0.3541	0.3535

4 Electron-impact excitation cross sections and collision strengths

4.1 General features

Before going into the details of our relativistic distorted-wave approach that was developed in ref. [40] for the rapid calculation of cross sections for excitation of highly charged ions, we give some general features of the relativistic distorted-wave method. It is convenient to express the cross section $Q(i-f)$ (in units of a_0^2) for a transition $i-f$ in terms of the (dimensionless) collision strength $\Omega(i-f)$ by the relation

$$Q(i-f) = \frac{\pi}{k^2 g_i}\Omega(i-f)\,. \tag{4.1}$$

Here, k is the relativistic wavenumber of the impact electron and g_i is the statistical weight of the initial level of the N-electron ion. The relation between k (in units of $1/a_0$) and the kinetic energy ϵ of the impact electron is

$$k^2 = \epsilon[1 + \frac{\alpha^2}{4}\epsilon]\,, \tag{4.2}$$

where α is the fine-structure constant $e^2/(\hbar c)$ and ϵ is in Rydbergs. As written, eq. (4.1) is of a general form that applies to transitions between configurations, states, fine-structure levels or magnetic sublevels. For most of this chapter, we will be interested in fine-structure transitions of the type that were discussed in chapter 3. Thus, we will consider here transitions from level $i = \Delta_t J_t$ to level $f = \Delta_t' J_t'$. The configuration-average case will be discussed at the end of this chapter, while a treatment of transitions between magnetic sublevels is reserved for chapter 9.

In any distorted-wave approach to collisional excitation, the cross section or collision strength in eq. (4.1) is typically expressed in terms of matrix elements involving the initial and final wave functions that represent the $(N+1)$-electron systems formed by the incident electron and the initial ion, and by the scattered electron and the final ion. Appropriate expressions for the ion wave functions were previously described in chapter 3. On the other hand, the free-electron wave functions are represented as an expansion over an infinite number of partial waves, which are coupled to the ion wave functions, in order to describe the initial and final $(N+1)$-electron systems. In the most general case, the cross section or collision strength is often expressed in terms of the transmission matrix, denoted by $\boldsymbol{T}$. For example, the collision strength can be written in the nonspecific form

$$\Omega = \tfrac{1}{2}\sum(2J+1)\,|T|^2\,, \tag{4.3}$$

where T represents a particular element of the $\boldsymbol{T}$ matrix. The $\boldsymbol{T}$ matrix can alternatively be expressed in terms of the reactance matrix, denoted by $\boldsymbol{R}$, which is commonly used in distorted-wave theory. For the highly charged ions of interest in the present work, the reactance matrix elements associated with these system wave functions are sufficiently small that unitarization is unnecessary. In this case, the relation between $\boldsymbol{T}$ and $\boldsymbol{R}$ reduces to

$$\boldsymbol{T} = \frac{-2\mathrm{i}\boldsymbol{R}}{1-2\mathrm{i}\boldsymbol{R}} \simeq -2\mathrm{i}\boldsymbol{R} \tag{4.4}$$

and the collision strength can be written as

$$\Omega = 2\sum(2J+1)\,|R|^2\,. \tag{4.5}$$

The precise form of the reactance matrix elements will be provided shortly. For the moment, we consider a more specific form of eq. (4.5) that provides an expression for the relativistic distorted-wave collision strength for a transition between fine-structure levels,

$$\Omega(\Delta_t J_t - \Delta'_t J'_t) = 8\sum_J (2J+1)\sum_{\kappa,\kappa'}\left|\left\langle \Psi_i \left| \sum_{\substack{p,q\\ p<q}}^{N+1} \frac{1}{r_{pq}} \right| \Psi_f \right\rangle\right|^2, \tag{4.6}$$

which can be obtained, for example, from first-order time-dependent perturbation theory. We first note that an extra factor of four appears in this formula, relative to other expressions that one might encounter in the literature, such as eq. (4.5), due to the use of Rydberg atomic units. With this choice of units, distances are in units of the Bohr radius and energies in Rydbergs, so that the electron-electron interaction is $2/r_{pq}$, analogous to $2/r_{ij}$ in eq. (2.1).

As for the physical quantities in eq. (4.6), κ and κ' are the initial and final relativistic quantum numbers that represent the partial waves associated with the incident and scattered electrons, respectively. We have employed the customary practice of using unsubscripted quantum numbers to describe the free electrons. Thus, κ is related to the orbital and total angular momentum quantum numbers l and j for the incident free electron according to eq. (2.8). Similarly, the quantum-number relations

$$\kappa' = l', \quad j' = l' - \tfrac{1}{2}; \quad \kappa' = -(l'+1), \quad j' = l' + \tfrac{1}{2} \tag{4.7}$$

apply to the scattered free electron. The symbol J refers the total angular momentum of the complete $(N+1)$-electron system that is formed by coupling

J_t of the initial ion with j of the incident electron, or J'_t of the final ion with j' of the scattered electron. The resulting value of J must be the same in both cases in order for the matrix element in eq. (4.6) to be non-zero. The Ψ_i and Ψ_f in eq. (4.6) are the initial and final antisymmetric wave functions for the total $(N+1)$-electron system consisting of the target ion plus a free electron. For example,

$$\Psi_i = \frac{1}{(N+1)^{1/2}} \sum_{p=1}^{N+1} (-1)^{N+1-p} \sum_{M_t,m} C(J_t j M_t m; JM) \times \Psi_{\Delta_t J_t M_t}(x_p^{-1}) u_{\epsilon l j m}(x_p) \tag{4.8}$$

with an analogous expression applying for Ψ_f in which Δ'_t, J'_t, M'_t, ϵ', l', j' and m' replace the corresponding unprimed quantities. Here, as in chapter 3, x_p designates the space and spin coordinates of electron p, while x_p^{-1} means the space and spin coordinates of all N electrons other than p. The $\Psi_{\Delta_t J_t M_t}$ and $\Psi_{\Delta'_t J'_t M'_t}$ are the initial and final target-ion wave functions of the kind given by eq. (2.11), and in more detail in chapter 3. Of course, Δ_t, J_t, M_t, Δ'_t, J'_t and M'_t have the same meaning as in chapter 3. The $u_{\epsilon l j m}$ in eq. (4.8) is the distorted-wave Dirac spinor or orbital for a free electron in a central potential $V(r)$ due to the target ion. In particular, analogous to eq. (2.6) for a bound electron,

$$u_{\epsilon l j m}(x) \equiv u_{\epsilon \kappa m}(x) = \frac{1}{r} \begin{bmatrix} P_{\epsilon\kappa}(r) & \chi_{\kappa m}(\theta,\phi,\sigma) \\ \mathrm{i}Q_{\epsilon\kappa}(r) & \chi_{-\kappa m}(\theta,\phi,\sigma) \end{bmatrix}, \tag{4.9}$$

where $\chi_{\kappa m}$ are the usual spin-angular functions given by eq. (2.7), and the large and small components $P_{\epsilon\kappa}$ and $Q_{\epsilon\kappa}$ satisfy the coupled Dirac equations

$$\left[\frac{\mathrm{d}}{\mathrm{d}r} + \frac{\kappa}{r}\right] P_{\epsilon\kappa}(r) = \frac{\alpha}{2}\left[\epsilon - V(r) + \frac{4}{\alpha^2}\right] Q_{\epsilon\kappa}(r) \tag{4.10}$$

$$\left[\frac{\mathrm{d}}{\mathrm{d}r} - \frac{\kappa}{r}\right] Q_{\epsilon\kappa}(r) = -\frac{\alpha}{2}[\epsilon - V(r)] P_{\epsilon\kappa}(r)\,. \tag{4.11}$$

These expressions are similar to eqs. (2.9) and (2.10) for bound electrons, except that ϵ is positive and is the kinetic energy of the electron in Rydbergs when $r \to \infty$. The numerical procedures we use in solving these equations for the radial functions will be discussed in detail in section 4.5.

As stated previously, the distorted-wave collision strength is often expressed in terms of the reactance matrix elements, e.g.

$$\Omega(\Delta_t J_t - \Delta'_t J'_t) = 2\sum_J (2J+1) \sum_{\substack{l,j \\ l',j'}} |R(\Delta_t J_t \epsilon l j J;\ \Delta'_t J'_t \epsilon' l' j' J)|^2 , \qquad (4.12)$$

which is an alternative form of eq. (4.6), and a more explicit form of eq. (4.5) applied to transitions between fine-structure levels. In general, the initial and final wave functions associated with the fine-structure levels of the ion are each mixtures of the wave functions for pure SCSF states with the same total angular momentum and parity, as in eq. (2.11). It is convenient to express the reactance matrix in terms of a pure-state representation

$$R(\Delta_t J_t \epsilon l j J;\ \Delta'_t J'_t \epsilon' l' j' J) = \sum_{\beta_t, \beta'_t} b^{J_t}(\Delta_t, \beta_t) b^{J'_t}(\Delta'_t, \beta'_t) \times R(\beta_t J_t \epsilon l j J;\ \beta'_t J'_t \epsilon' l' j' J) , \qquad (4.13)$$

where the additional symbols have the same meanings as in chapter 3. (See, for example, eq. (3.17).) The reactance matrix has a direct and an exchange part

$$\boldsymbol{R} = \boldsymbol{R}^d - \boldsymbol{R}^e , \qquad (4.14)$$

for which the detailed matrix elements can be written as

$$R^d(\beta_t J_t \epsilon l j J;\ \beta'_t J'_t \epsilon' l' j' J) = 2 \sum_{\substack{M_t, m \\ M'_t, m'}} C(J_t j M_t m; JM) C(J'_t j' M'_t m'; JM) \times \int \mathrm{d}x_1 \int \mathrm{d}x_2 \cdots \int \mathrm{d}x_{N+1} \Psi^\dagger_{\beta_t J_t M_t}(x_i^{-1}) u^\dagger_{\epsilon l j m}(x_i) \times \left[\sum_{q(\neq i)}^{N+1} \frac{1}{r_{qi}} \right] \Psi_{\beta'_t J'_t M'_t}(x_i^{-1}) u_{\epsilon' l' j' m'}(x_i) \qquad (4.15)$$

and

$$R^e(\beta_t J_t \epsilon l j J;\ \beta'_t J'_t \epsilon' l' j' J) = 2N \sum_{\substack{M_t, m \\ M'_t, m'}} C(J_t j M_t m; JM) C(J'_t j' M'_t m'; JM) \times \int \mathrm{d}x_1 \int \mathrm{d}x_2 \cdots \int \mathrm{d}x_{N+1} \Psi^\dagger_{\beta_t J_t M_t}(x_i^{-1}) u^\dagger_{\epsilon l j m}(x_i) \times \left[\sum_{q(\neq i)}^{N+1} \frac{1}{r_{qi}} \right] \Psi_{\beta'_t J'_t M'_t}(x_j^{-1}) u_{\epsilon' l' j' m'}(x_j) , \ j \neq i . \qquad (4.16)$$

Actually, only the single term with $q = j$ can contribute to the exchange contribution due to the orthogonality of the u spinors.

A word should be said about how eqs. (4.12)–(4.16) follow from eqs. (4.6) and (4.8). In particular, one might question how the normalization factor

$(N+1)^{-1/2}$ in eq. (4.8), and the similar factor in the final $(N+1)$-electron wave function, Ψ_f, were removed, and how the factor N in eq. (4.16) arises. In evaluating eq. (4.6), one starts with the electrons ordered in the same way in both the initial and final system wave functions, so that the phase factor $(-1)^{N+1-p}$ in eq. (4.8), and the identical one in the analogous expression for Ψ_f, cancel. Each permutation gives rise to non-vanishing matrix elements of the same value. Altogether, there are $N+1$ of these terms, which cancels out the product of the two normalization factors $(N+1)^{-1/2}$, and leads to eq. (4.15). Furthermore, for each of the N non-vanishing matrix elements in eq. (4.15), one could alternatively obtain a non-vanishing matrix element in which there was a permutation between the electron in the final active orbital and the electron in the final free (scattered) orbital. There are N such terms, each with an extra factor of -1 due to the permutation of two electrons, which leads to eq. (4.16) and the minus sign in eq. (4.14).

Now we turn to a discussion of our particular approach to electron-impact excitation between fine-structure levels. Descriptions are provided for two versions of our collision strength program that contain the same physics, but the angular portion of the calculations is performed in different ways. For treating a single ion, with a definite Z value, there is usually little difference in the speed in calculating the radial part by the two procedures. However, the second version, which will be described in detail, requires less computing time in the angular part of the calculation (especially for the $\Delta n = 0$ transitions), and has an added advantage. Specifically, it can treat a given class of transitions simultaneously for all of an iso-electronic sequence for which our method is valid, i.e. for ions having a Z value of 92, down to a value that is a little less than $Z = 2N$. Hence, the second procedure is the one we use for large-scale production of atomic data. Having two different excitation programs that contain the same physics, but in which the angular part is performed differently, provides the additional benefit of a numerical check by using both methods in test cases to help ensure that no numerical errors are being made in the calculations.

4.2 Version 1 of our collision strength program: non-factorized method

From inspection, the Ψ_i given by eq. (4.8) has the same form as the wave function for an $(N+1)$-electron ion with an N-electron core and a single electron in a very high subshell. An analogous statement applies for Ψ_f. Thus, as far as the angular part is concerned, the matrix elements appearing in eq. (4.6), or more precisely those in eqs. (4.15) and (4.16), are of the same form as those occurring in atomic structure calculations for an $(N+1)$-electron ion when determining the off-diagonal matrix elements of the electron-electron electrostatic interaction prior to diagonalization of the Hamiltonian. Therefore, in

evaluating the right-hand side of eq. (4.6) we simply used the angular part of the Grant code [6], except that a few modifications had to be made, such as allowing the outer electron (free electron in our case) to have much larger angular momenta than occur in ordinary atomic structure calculations. Also, the radial part is similar to that of atomic structure calculations and takes the form of Slater integrals similar to eq. (2.13). Specifically, there are "direct" terms

$$D^{\lambda}(n_a l_a j_a \epsilon l j; n'_a l'_a j'_a \epsilon' l' j') = \int_0^{\infty}\int_0^{\infty} [P_{n_a l_a j_a}(r_1) P_{n'_a l'_a j'_a}(r_1) + Q_{n_a l_a j_a}(r_1) Q_{n'_a l'_a j'_a}(r_1)] \times \frac{r_<^{\lambda}}{r_>^{\lambda+1}} [P_{\epsilon l j}(r_2) P_{\epsilon' l' j'}(r_2) + Q_{\epsilon l j}(r_2) Q_{\epsilon' l' j'}(r_2)]\, \mathrm{d}r_1 \mathrm{d}r_2 \qquad (4.17)$$

and "exchange" terms

$$E^{\lambda}(n_a l_a j_a \epsilon l j; n'_a l'_a j'_a \epsilon' l' j') = \int_0^{\infty}\int_0^{\infty} [P_{n_a l_a j_a}(r_1) P_{\epsilon' l' j'}(r_1) + Q_{n_a l_a j_a}(r_1) Q_{\epsilon' l' j'}(r_1)] \times \frac{r_<^{\lambda}}{r_>^{\lambda+1}} [P_{\epsilon l j}(r_2) P_{n'_a l'_a j'_a}(r_2) + Q_{\epsilon l j}(r_2) Q_{n'_a l'_a j'_a}(r_2)]\, \mathrm{d}r_1 \mathrm{d}r_2 \,, \qquad (4.18)$$

where, as in chapter 3, $r_<$ ($r_>$) is the lesser (greater) of r_1 and r_2. We note that these integrals also occur in version 2 of our program.

In the evaluation of eq. (4.6), or, equivalently, eqs. (4.12)–(4.16), it is assumed that all orbitals, bound and free, are orthogonal. This quality, and a completely consistent treatment of exchange between bound and free electrons, are automatically achieved in the present approach because the central potential used in eqs. (4.10) and (4.11) is exactly the same as that used in eqs. (2.9) and (2.10) for the bound electrons. That is, we use the same Dirac-Fock-Slater potential given by eqs. (2.18)–(2.20), coupled with the use of a mean configuration, such as that given by eq. (2.21) for neon-like ions, to obtain the radial functions for both bound and free electrons. This approach, as well as the numerical procedures we use to calculate the radial functions, is the same for both versions of our collision strength program. These numerical procedures will be described in detail in section 4.5.

Bar-Shalom, Klapisch and Oreg [31] showed how the relativistic distorted-wave approach for highly charged ions could be expressed in a factorized form (see eq. (4.31) below) and used this approach to simplify the angular part of the calculations for complex cases. One such application is to the transitions occurring between the excited levels of neon-like and nickel-like ions, where the angular part of the calculation becomes very large in a conventional treatment. In addition to that advantage of the factorization method, we realized (see ref. [40]) that it is very convenient for calculating simultaneously the cross sections for a given class of transitions for many members of an iso-electronic sequence. In fact, we have used the method for all Z values within the expected range of validity of our approach. A few years after the publication of ref. [40], we published some details concerning the factorization method as it applies to collisional excitation (and ionization) [32]. The derivation provided below expands upon this later work. It provides an alternative derivation than the one originally presented in ref. [31], including previously unpublished details that might be of some use in various applications.

We start with eqs. (4.12)–(4.16) and, as in section 3.2, treat, in detail, the case of subshells that are initially filled or empty, in addition to the active one labeled a. By similar arguments to those given in section 3.2, one sees that filled inactive subshells make no contribution other than to the central potential $V(r)$. Hence, they can be ignored in the following derivation. Thus, the symbol N appearing in eqs. (4.15) and (4.16) can be replaced with w, the initial occupation number of the active subshell. First we consider R^d given by eq. (4.15) and substitute the expressions given by eqs. (3.20) and (3.22) for $\Psi_{\beta_t J_t M_t}(x_i^{-1})$ and $\Psi_{\beta'_t J'_t M'_t}(x_i^{-1})$, and choose coordinate $x_i = x_{w+1}$. The result is

$$
\begin{aligned}
&R^d(\beta_t J_t \epsilon l j J;\ \beta'_t J'_t \epsilon' l' j' J) = \\
&\frac{2}{\sqrt{w}} \sum_{J_1,\alpha_1} (j_a^{w-1}\alpha_1 J_1 \,|\}\, j_a^w \alpha_a J_a) \\
&\quad \times \sum_{M_t,m} C(J_t j M_t m; JM) \sum_{M'_t,m'} C(J'_t j' M'_t m'; JM) \\
&\quad \times \sum_{\substack{M_1,m_a \\ M''_a,m'_a}} C(J_1 j_a M_1 m_a; J_t M_t) C(J''_a j'_a M''_a m'_a; J'_t M'_t) \\
&\qquad \times \int \mathrm{d}x_1 \int \mathrm{d}x_2 \cdots \int \mathrm{d}x_{w+1} \\
&\qquad\quad \times \{\Psi^\dagger[(n_a l_a j_a)^{w-1}\alpha_1 J_1 M_1 \mid x_1 x_2 \cdots x_{w-1}] \\
&\qquad\quad \times u^\dagger_{n_a l_a j_a m_a}(x_w) u^\dagger_{\epsilon l j m}(x_{w+1}) \Big[\sum_{q=1}^{w} \frac{1}{r_{q(w+1)}}\Big]
\end{aligned}
$$

$$\times \sum_{p=1}^{w} (-1)^{w-p} \Psi[(n_a l_a j_a)^{w-1} \alpha_a'' J_a'' M_a'' \mid x_1 x_2 \cdots x_{p-1} x_{p+1} x_w]$$
$$\times u_{n_a' l_a' j_a' m_a'}(x_p) u_{\epsilon' l' j' m'}(x_{w+1})\} \,. \tag{4.19}$$

Of course, in this case $J_a = J_t$ and $M_a = M_t$, which we used in writing the third Clebsch-Gordan coefficient. One sees that, due to the orthogonality of the u spinors, only the terms with $q = p$ can contribute. Analogous to the discussion leading to eq. (3.23), we note that, although the electrons are all in the definite increasing order $1, 2, ..., w$ in the initial target-ion wave function, it is an antisymmetric function due to the properties of the Clebsch-Gordan coefficient and the CFP. Thus, in evaluating eq. (4.19) we can permute the coordinates in the initial target-ion wave function so that they are in the same positions as they are in the final target-ion wave function when determining the contribution of each term in the summation over p. This reordering introduces a phase factor, $(-1)^{w-p}$, that exactly cancels the effect of the similar phase factor in eq. (4.19). Then, the sum over p gives w contributions, all with the same value. Hence, a simplified expression for R^d is obtained from eq. (4.19) with the sums over p and q removed, the phase factor omitted, both p and q set equal to w, and the result multiplied by a factor of w.

Since both the initial and final wave functions of the total system have the electrons in the same order and with the same type of coupling, we can also use irreducible tensor techniques to further simplify R^d. In doing so, we use the standard expansion given by eq. (2.12) with w and $w+1$ replacing 1 and 2, respectively. The result is

$$\begin{aligned} &R^d(\beta_t J_t \epsilon l j J;\, \beta_t' J_t' \epsilon' l' j' J) \\ &= 2\sqrt{w} \sum_{J_1, \alpha_1} (j_a^{w-1} \alpha_1 J_1 \,|\} j_a^w \alpha_a J_a) \sum_{\lambda=0}^{\infty} D^\lambda(n_a l_a j_a \epsilon l j; n_a' l_a' j_a' \epsilon' l' j') \\ &\quad \times \langle j_a^{w-1} \alpha_1 J_1 j_a J_t j J M \mid \boldsymbol{C}^{(\lambda)}(\hat{\boldsymbol{r}}_w) \cdot \boldsymbol{C}^{(\lambda)}(\hat{\boldsymbol{r}}_{w+1}) \mid j_a^{w-1} \alpha_a'' J_a'' j_a' J_t' j' J M \rangle \,, \end{aligned} \tag{4.20}$$

where D^λ is given by eq. (4.17), $\boldsymbol{C}^{(\lambda)}$ is the renormalized spherical harmonic of rank λ, and $\hat{\boldsymbol{r}}_w$ and $\hat{\boldsymbol{r}}_{w+1}$ represent the angular coordinates of x_w and x_{w+1}, respectively. Using standard formulae given in ref. [8] or the Appendix of ref. [7], one obtains

$$\begin{aligned} &\langle j_a^{w-1} \alpha_1 J_1 j_a J_t j J M \mid \boldsymbol{C}^{(\lambda)}(\hat{\boldsymbol{r}}_w) \cdot \boldsymbol{C}^{(\lambda)}(\hat{\boldsymbol{r}}_{w+1}) \mid j_a^{w-1} \alpha_a'' J_a'' j_a' J_t' j' J M \rangle \\ &\qquad = (-1)^{J+j+J_t'} \begin{Bmatrix} J_t & \lambda & J_t' \\ j' & J & j \end{Bmatrix} \langle j \parallel \boldsymbol{C}^{(\lambda)} \parallel j' \rangle \\ &\qquad\quad \times \langle j_a^{w-1} \alpha_1 J_1 j_a J_t \parallel \boldsymbol{C}^{(\lambda)}(\hat{\boldsymbol{r}}_w) \parallel j_a^{w-1} \alpha_a'' J_a'' j_a' J_t' \rangle \end{aligned} \tag{4.21}$$

in which

$$\langle j_a^{w-1}\alpha_1 J_1 j_a J_t \parallel \boldsymbol{C}^{(\lambda)}(\hat{\boldsymbol{r}}_w) \parallel j_a^{w-1}\alpha_a'' J_a'' j_a' J_t'\rangle = \delta_{\alpha_1\alpha_a''}\delta_{J_1 J_a''}(-1)^{J_t+J_a''+j_a'+\lambda}$$
$$\times[(2J_t+1)(2J_t'+1)]^{1/2}\begin{Bmatrix} j_a & \lambda & j_a' \\ J_t' & J_a'' & J_t \end{Bmatrix}\langle j_a \parallel \boldsymbol{C}^{(\lambda)} \parallel j_a'\rangle\,, \quad (4.22)$$

where $\langle j_a \parallel \boldsymbol{C}^{(\lambda)} \parallel j_a'\rangle$ and $\langle j \parallel \boldsymbol{C}^{(\lambda)} \parallel j'\rangle$ can be evaluated by applying the general relation

$$\langle j_1 \parallel \boldsymbol{C}^{(\lambda)} \parallel j_2\rangle = (-1)^{j_1+1/2}[(2j_1+1)(2j_2+1)]^{1/2}\begin{pmatrix} j_1 & \lambda & j_2 \\ \frac{1}{2} & 0 & -\frac{1}{2}\end{pmatrix}. \quad (4.23)$$

Thus, applying eqs. (4.21) and (4.22) to eq. (4.20) we have

$$R^d(\beta_t J_t \epsilon l j J;\, \beta_t' J_t' \epsilon' l' j' J) = 2\sqrt{w}(j_a^{w-1}\alpha_a'' J_a'' \,|\}\, j_a^w \alpha_a J_a)$$
$$\times \sum_{\lambda=0}^{\infty} D^\lambda(n_a l_a j_a \epsilon l j; n_a' l_a' j_a' \epsilon' l' j')(-1)^{J+J_t+J_t'+j+j_a'+J_t''+\lambda}$$
$$\times[(2J_t+1)(2J_t'+1)]^{1/2}\begin{Bmatrix} J_t & \lambda & J_t' \\ j' & J & j \end{Bmatrix}\begin{Bmatrix} j_a & \lambda & j_a' \\ J_t' & J_t'' & J_t \end{Bmatrix}$$
$$\times\langle j_a \parallel \boldsymbol{C}^{(\lambda)} \parallel j_a'\rangle\langle j \parallel \boldsymbol{C}^{(\lambda)} \parallel j'\rangle\,, \quad (4.24)$$

where, analogous to eq. (3.27) and the discussion below it, we have used the fact that $J_a = J_t$ and $J_a'' = J_t''$ to substitute for J_a and J_a'' everywhere except in the CFP. In this way, when one considers more complicated cases with additional partially-filled subshells, the added complexity will only produce extra angular factors that do not involve the free electron (in fact they are the same factors as those that enter in the line strength formula for the corresponding radiative transition), leaving eq. (4.24) otherwise unchanged. (These same factors also enter the expression for R^e in complex cases.)

Now we consider R^e, given by eq. (4.16), for the same situation. Once again, we let $N = w$ and choose $x_i = x_{w+1}$, along with setting $x_j = x_w$. Only the single term for which $q = w$ can contribute due to the orthogonality of the u spinors. Thus, we obtain expressions similar to eqs. (4.19) and (4.20), except that E^λ replaces D^λ and in the final state wave function it is the orbital j_a' that is a function of x_{w+1} and orbital j' that is a function of x_w. However, in order to use irreducible tensor techniques, the electrons in the final state must be in the same order as they are in the initial state $(1, 2, ..., w, w+1)$. Also, the angular momentum coupling must be the same. Thus, we must recouple in such a way that both the same coupling scheme and the same ordering of the electrons occurs in the initial and final states. This objective is accomplished by using the standard recoupling formula [7,8]

$$|\, j_a^{w-1}\alpha_a'' J_a'' j_a' J_t' j' J M\rangle = \sum_{J_2}(-1)^{j'+j_a'+J_t'+J_2}[(2J_2+1)(2J_t'+1)]^{1/2}$$

$$\times \left\{ \begin{matrix} J_a'' & j' & J_2 \\ J & j_a' & J_t' \end{matrix} \right\} | \, j_a^{w-1} \alpha_a'' J_a'' j' J_2 \, j_a' J M \rangle \,. \quad (4.25)$$

Then we proceed in exactly the same manner that was used to obtain eq. (4.24). The result is

$$\begin{aligned} R^e(\beta_t J_t \epsilon l j J;\, \beta_t' J_t' \epsilon' l' j' J) &= 2\sqrt{w}(j_a^{w-1} \alpha_a'' J_a'' \,|\} j_a^w \alpha_a J_a) \\ &\times \sum_{\lambda=0}^{\infty} E^\lambda(n_a l_a j_a \epsilon l j; n_a' l_a' j_a' \epsilon' l' j') \sum_{J_2} (-1)^{J_t''+2J_2+J_t'+2j'+j+j_a'+J+J_t+\lambda} \\ &\times (2J_2+1)[(2J_t+1)(2J_t'+1)]^{1/2} \left\{ \begin{matrix} J_t'' & j' & J_2 \\ J & j_a' & J_t' \end{matrix} \right\} \\ &\times \left\{ \begin{matrix} J_t & \lambda & J_2 \\ j_a' & J & j \end{matrix} \right\} \left\{ \begin{matrix} j_a & \lambda & j' \\ J_2 & J_t'' & J_t \end{matrix} \right\} \langle j_a \,\|\, \boldsymbol{C}^{(\lambda)} \,\|\, j' \rangle \langle j \,\|\, \boldsymbol{C}^{(\lambda)} \,\|\, j_a' \rangle \,, \quad (4.26) \end{aligned}$$

where E^λ is given by eq. (4.18). Also, as with R^d, we used the fact that in this case $J_a = J_t$ and $J_a'' = J_t''$ to substitute for J_a and J_a'' everywhere, except in the CFP. This choice was made for the same reasons as given in the discussion following the expression for R^d given in eq. (4.24).

In a conventional treatment, one would simply obtain the collision strength by applying eqs. (4.24) and (4.26) to eqs. (4.12)–(4.14), except that one could replace the product of the three 6-j symbols in eq. (4.26) with a 9-j symbol using the formula [41]

$$\sum_{J_2} (-1)^{2J_2} (2J_2+1) \left\{ \begin{matrix} J_t'' & j_a' & J_t' \\ J & j' & J_2 \end{matrix} \right\} \left\{ \begin{matrix} J_t & j & J \\ j_a' & J_2 & \lambda \end{matrix} \right\} \left\{ \begin{matrix} j_a & \lambda & j' \\ J_2 & J_t'' & J_t \end{matrix} \right\} = \left\{ \begin{matrix} J_t'' & J_t & j_a \\ j_a' & j & \lambda \\ J_t' & J & j' \end{matrix} \right\} . \quad (4.27)$$

However, this 9-j symbol can be recast in terms of a different product of three 6-j symbols that allows one to obtain the collision strength in the convenient factorization form. Specifically, we use the formula [41]

$$\left\{ \begin{matrix} J_t'' & J_t & j_a \\ j_a' & j & \lambda \\ J_t' & J & j' \end{matrix} \right\} = \sum_\tau (-1)^{2\tau} (2\tau+1) \left\{ \begin{matrix} J_t & \tau & J_t' \\ j' & J & j \end{matrix} \right\} \times \left\{ \begin{matrix} j_a & \tau & j_a' \\ J_t' & J_t'' & J_t \end{matrix} \right\} \left\{ \begin{matrix} j_a & j' & \lambda \\ j & j_a' & \tau \end{matrix} \right\} , \quad (4.28)$$

where the factor $(-1)^{2\tau}$ can be ignored because τ is an integer. Applying eqs. (4.27) and (4.28) to eq. (4.26), and then substituting the resulting expression for R^e, along with R^d from eq. (4.24), into eq. (4.14) yields

$$
\begin{aligned}
&R(\beta_t J_t \epsilon l j J,\ \beta'_t J'_t \epsilon' l' j' J) = \\
&\quad 2\sqrt{w}(j_a^{w-1}\alpha''_a J''_a\ |\}j_a^w \alpha_a J_a)[(2J_t+1)(2J'_t+1)]^{1/2}(-1)^{J+J_t+J'_t+J''_t+j'_a+j} \\
&\quad \times\Bigg[\sum_\lambda (-1)^\lambda \begin{Bmatrix} J_t & \lambda & J'_t \\ j' & J & j \end{Bmatrix} \begin{Bmatrix} j_a & \lambda & j'_a \\ J'_t & J''_t & J_t \end{Bmatrix} \\
&\qquad \times D^\lambda(n_a l_a j_a \epsilon l j; n'_a l'_a j'_a \epsilon' l' j')\langle j_a \parallel \boldsymbol{C}^{(\lambda)} \parallel j'_a\rangle\langle j \parallel \boldsymbol{C}^{(\lambda)} \parallel j'\rangle \\
&\quad + \sum_{\lambda'}\sum_\tau (-1)^{\lambda'}(2\tau+1) \begin{Bmatrix} J_t & \tau & J'_t \\ j' & J & j \end{Bmatrix} \begin{Bmatrix} j_a & \tau & j'_a \\ J'_t & J''_t & J_t \end{Bmatrix} \begin{Bmatrix} j_a & j' & \lambda' \\ j & j'_a & \tau \end{Bmatrix} \\
&\qquad \times E^{\lambda'}(n_a l_a j_a \epsilon l j; n'_a l'_a j'_a \epsilon' l' j')\langle j_a \parallel \boldsymbol{C}^{(\lambda')} \parallel j'\rangle\langle j \parallel \boldsymbol{C}^{(\lambda')} \parallel j'_a\rangle\Bigg] . \qquad (4.29)
\end{aligned}
$$

In expressing the exchange contribution, we used the fact that, since j' is a half integer, $(-1)^{2j'} = -1$.

When eq. (4.29) is substituted in eqs. (4.13) and (4.12), and the labeling λ' and τ are interchanged so the results look more like those in ref. [31], one can perform the summation over J using the standard formula [41]

$$
\sum_J (2J+1) \begin{Bmatrix} J_t & C & J'_t \\ j' & J & j \end{Bmatrix} \begin{Bmatrix} J_t & C' & J'_t \\ j' & J & j \end{Bmatrix} = \frac{\delta_{CC'}}{2C+1} , \qquad (4.30)
$$

which is allowed because J_t, J'_t, j and j' are all good quantum numbers. The result is the factorized form for the collision strength. When the simplified notation given by eq. (3.28) is used, the factorized form can be written as

$$
\begin{aligned}
\Omega(U-U') = 8 \sum_{\substack{S,S' \\ S_1,S'_1}} \sum_\lambda & B^\lambda(U, SS_1; U', S'S'_1) \\
& \times Q^\lambda(n_a l_a j_a, n'_a l'_a j'_a; n_{a_1} l_{a_1} j_{a_1}, n'_{a_1} l'_{a_1} j'_{a_1}) . \qquad (4.31)
\end{aligned}
$$

Here,

$$
\begin{aligned}
&Q^\lambda(n_a l_a j_a, n'_a l'_a j'_a; n_{a_1} l_{a_1} j_{a_1}, n'_{a_1} l'_{a_1} j'_{a_1}) \\
&\quad = \sum_{\substack{l,l' \\ j,j'}} P^\lambda(n_a l_a j_a \epsilon l j; n'_a l'_a j'_a \epsilon' l' j') P^\lambda(n_{a_1} l_{a_1} j_{a_1} \epsilon l j; n'_{a_1} l'_{a_1} j'_{a_1} \epsilon' l' j') , \qquad (4.32)
\end{aligned}
$$

where the P^λ are given by

$$
\begin{aligned}
&P^\lambda(n_a l_a j_a \epsilon l j; n'_a l'_a j'_a \epsilon' l' j') \\
&\quad = (2\lambda+1)^{-1/2} D^\lambda(n_a l_a j_a \epsilon l j; n'_a l'_a j'_a \epsilon' l' j')\langle j_a \parallel \boldsymbol{C}^{(\lambda)} \parallel j'_a\rangle\langle j \parallel \boldsymbol{C}^{(\lambda)} \parallel j'\rangle \\
&\qquad + \sum_\tau (-1)^{\lambda+\tau}(2\lambda+1)^{1/2} \begin{Bmatrix} j_a & j' & \tau \\ j & j'_a & \lambda \end{Bmatrix} \\
&\qquad\quad \times E^\tau(n_a l_a j_a \epsilon l j; n'_a l'_a j'_a \epsilon' l' j')\langle j_a \parallel \boldsymbol{C}^{(\tau)} \parallel j'\rangle\langle j \parallel \boldsymbol{C}^{(\tau)} \parallel j'_a\rangle . \qquad (4.33)
\end{aligned}
$$

The B^λ are analogous to, but more general than, the $B^{(1)}$ given by eq. (3.34). In particular,

$$B^\lambda(U, SS_1; U', S'S'_1) = F^\lambda(US, U'S')F^\lambda(US_1, U'S'_1)\,, \tag{4.34}$$

where

$$F^\lambda(US, U'S') = b(U, S)f^\lambda(S, S')b(U', S') \tag{4.35}$$

and, in the present case,

$$\begin{aligned} f^\lambda(S, S') = {} & [(2J_t + 1)(2J'_t + 1)]^{1/2}(-1)^{J'_t + J''_t + j'_a} \\ & \times \sqrt{w}(j_a^{w-1}\alpha''_a J''_a \,|\}\, j_a^w \alpha_a J_a) \begin{Bmatrix} j_a & \lambda & j'_a \\ J'_t & J''_t & J_t \end{Bmatrix}. \end{aligned} \tag{4.36}$$

For more complex cases with initially one or more partially filled subshells, in addition to the active subshell, all that is required is to include extra angular factors involving only quantum numbers of the target ion. These factors are exactly the same as those that enter in the corresponding radiative transitions. When implementing this approach in our computer programs, it was unnecessary to derive the relevant factors for the general case because, as noted at the end of subsection 3.2.1, the $f^\lambda(S, S')$ are equal to the quantities denoted by $d^\lambda_{aa'}(S, S')$, which are available in complete generality from the MCT module [34] of the Grant code [6,11,25].

By comparing eqs. (4.34)–(4.36) with eqs. (3.29), (3.30) and (3.34), one sees that the $B^{(1)}$ of eq. (3.34) is just a special case of B^λ with $\lambda = 1$. Also, eq. (4.31) is very similar to, but more complex than, eq. (3.33) for the line strength. However, in general, only a few values of λ and τ in the expressions for the collision strength survive because of restrictions on them due to the properties of the 6-j symbols appearing in eqs. (4.33) and (4.36).

4.4 Improvements for computing the free-electron wave functions

In the previous two sections, we described some methods for making our collision strength codes more efficient. Now we describe ways to improve the accuracy of the data calculated with our codes. As noted in chapter 3, some level energies calculated by our DFS structure code still differ from those produced by the Grant code by a few eV, even after we included the generalized Breit interaction and other QED corrections. That discrepancy does not affect line strength or collision strength results very much for $\Delta n > 0$ transitions, as

the transition energies are usually large. However, for $\Delta n = 0$ transitions the results could be affected significantly for those transitions with the initial and final level energies close to each other. One way to correct this discrepancy is to replace the energies obtained from our structure code with those calculated by the Grant code, as was done in ref. [38] for F-like ions. With this approach, it is important to recognize that different numerical procedures, such as our using a linear radial grid versus the logarithmic grid in the Grant code, and different physics, such as our DFS potential vs. the multi-configuration Dirac-Fock (MCDF) potential in the Grant code, will not only affect the energies obtained, but also the resulting mixing coefficients that form the fine-structure wave functions. Different mixing coefficients could (and do) affect considerably the collision strength results for some weak transitions. For this reason, we decided [33] to include an option in our collision strength codes that would use all of the relevant structure data obtained from the Grant code, including level energies, mixing coefficients, radius-dependent nuclear charge $Z(r)$, radial wave functions and line strengths. Here we note that line strengths are used in the Coulomb-Bethe approximation for optically allowed transitions to obtain high partial-wave contributions, as described later in section 4.9. In addition to increasing the accuracy of collision strength results for high-Z ions, use of the Grant structure data also extends the range of the validity of our data from $Z \gtrsim 2N$ to $Z \gtrsim 1.5N$. This extension to lesser charged ions is possible because the electron-electron interaction becomes more important to the total potential, and the MCDF potential used in the Grant code should be more accurate than the DFS potential used in our structure code.

As mentioned previously, the Grant code uses a logarithmic radial grid while our collision codes use a linear grid. Therefore, in order to use Grant's $Z(r)$ values and radial wave functions, they have to be transformed from the logarithmic grid to a linear grid. We use a procedure based on a four-point Lagrange-polynomial interpolation scheme originally written by Moores [42] for this purpose. Then we construct the potential $V(r)$ for use in solving the Dirac equation, eqs. (4.10) and (4.11), for the free-electron radial functions. It is noted that, in using the Grant code, we typically use the "average level" option [6], which employs a set of effective fractional occupation numbers. However, if we were to construct a DFS potential to obtain the free-electron wave functions using our original approach, then we would choose a set of fractional occupation numbers for each class of transitions with the prescription described in section 2.3. Obviously, the DFS potential constructed in this way (based on eqs. (2.18)–(2.20)) will not be the same as the MCDF potential used in the Grant code to obtain the bound-state wave functions. Since this difference in potentials no longer guarantees orthogonality between the bound- and free-electron wave functions, we decided to use a new form of the potential when calculating the continuum functions, which has been shown to produce more accurate data. This new potential differs from our standard DFS potential in that the exchange contribution is the so-called semiclassical

exchange (SCE) term of Riley and Truhlar [43]. The resulting potential was employed extensively by Mann [44,45] and will be referred to as the Mann potential, $V_{\rm M}(r)$. The form of this potential is given by

$$V_{\rm M}(r) = \tilde{V}(r) + V_{\rm M}^{\rm ex}(r)\,, \tag{4.37}$$

where the direct part is the usual

$$\tilde{V}(r) = -\frac{2Z(r)}{r} + V_c(r) \tag{4.38}$$

and the exchange part is

$$V_{\rm M}^{\rm ex}(r) = -\frac{1}{2}\left[\epsilon({\rm Ry}) - \tilde{\rm V}({\rm r})\right]\left[(1+\beta^2(r))^{1/2} - 1\right]\,. \tag{4.39}$$

The classical potential, $V_c(r)$, in eq. (4.38) is given by eq. (2.19) and $\beta(r)$ in eq. (4.39) is defined by

$$\beta^2(r) = \frac{4\rho(r)}{r^2[\epsilon({\rm Ry}) - \tilde{\rm V}({\rm r})]^2}\,, \tag{4.40}$$

where $\rho(r)$ is given by eq. (2.20). Of course, in evaluating eqs. (2.19) and (2.20), the bound wave functions from the Grant code (transformed on to a linear grid) are used, along with a set of fractional occupation numbers $w_{n\kappa}$ that are chosen according to the prescription mentioned above.

In order to account for the lack of orthogonality that results from the use of different bound and continuum potentials, we note that, in general, the exchange integral E^λ given by eq. (4.18) should have an additional one-electron exchange term that contains the overlap of the active bound orbital and a free-electron orbital. In our version of the collision codes that uses the same DFS potential in calculating wave functions for both the bound and free electrons, this term vanishes due to orthogonality between the bound and free orbitals. In the current option of using the structure data obtained from the Grant code and the continuum wave functions computed with the Mann potential, this term should be retained.

As pointed out in ref. [44], there are two forms of this overlap integral, the so-called "prior" form that corresponds to an overlap between the initial bound and final scattered orbitals, and the "post" form that corresponds to an overlap between the final bound and initial impact orbitals. We use the post form in our codes, which is given by

$$E_1^{\lambda=0}(n_a l_a j_a \epsilon l j; n'_a l'_a j'_a \epsilon' l' j') =$$
$$-\int_0^\infty [\frac{V'_c(r_1)}{2N} P_{n_a l_a j_a}(r_1) P_{\epsilon' l' j'}(r_1) + Q_{n_a l_a j_a}(r_1) Q_{\epsilon' l' j'}(r_1)]\, \mathrm{d}r_1$$
$$\times \int_0^\infty [P_{\epsilon l j}(r_2) P_{n'_a l'_a j'_a}(r_2) + Q_{\epsilon l j}(r_2) Q_{n'_a l'_a j'_a}(r_2)]\, \mathrm{d}r_2\,, \qquad (4.41)$$

where $V'_c(r)$ is given by eq. (2.19). Here, the prime denotes that the occupation numbers to be used in eq. (2.19) are the same values that were used in determining the potential for the final continuum wave functions. This distinction is important because, for the current approach under consideration, we sometimes use two different sets of occupation numbers in order to determine the potential for the initial and final continuum wave functions. Of course, if our original fractional-occupation-number, mean-configuration approach is being used (see, for example, eq. (2.21)), then the initial and final configuration occupation numbers are always the same and $V'_c(r) \equiv V_c(r)$. The integral in eq. (4.41) is to be added to the right-hand side of eq. (4.18) when $\lambda = 0$. It should be mentioned that, as stated in ref. [45], it is a minor approximation to use $V'_c(r)$ above instead of $V'_c(r) + V'^{\mathrm{ex}}_{\mathrm{M}}(r)$, which is more generally correct.

For completeness, we also provide an expression for the prior form of the overlap integral, which is given by

$$E_1^{\lambda=0}(n_a l_a j_a \epsilon l j; n'_a l'_a j'_a \epsilon' l' j') =$$
$$-\int_0^\infty [P_{n_a l_a j_a}(r_1) P_{\epsilon' l' j'}(r_1) + Q_{n_a l_a j_a}(r_1) Q_{\epsilon' l' j'}(r_1)]\, \mathrm{d}r_1$$
$$\times \int_0^\infty \frac{V_c(r_2)}{2N} [P_{\epsilon l j}(r_2) P_{n'_a l'_a j'_a}(r_2) + Q_{\epsilon l j}(r_2) Q_{n'_a l'_a j'_a}(r_2)]\, \mathrm{d}r_2\,. \qquad (4.42)$$

An option to use either form of the one-electron exchange integral is available, for example, in the Los Alamos National Laboratory excitation code ACE [46]. Some numerical comparisons using the post and prior forms in non-relativistic Coulomb-Born and distorted-wave calculations are available in ref. [44].

4.5 Numerics of the free-electron radial functions

In this section, we discuss our method for obtaining the radial portion of the free-electron wave functions from eqs. (4.10) and (4.11). One could proceed in a manner similar to that described for the bound-electron case in section 2.2 by solving for $Q_{\epsilon\kappa}$ in eq. (4.10) and substituting the result into eq. (4.11). The result would be a second-order differential equation for $P_{\epsilon\kappa}$, analogous to

eq. (2.14). However, a more convenient approach is to follow Hagelstein and Jung [36] by transforming $P_{\epsilon\kappa}$ according to

$$F_{\epsilon\kappa}(r) = \sqrt{a_P(r)} P_{\epsilon\kappa}(r), \tag{4.43}$$

where

$$a_P(r) = \frac{\alpha}{2}\left[\epsilon - V(r) + \frac{4}{\alpha^2}\right]. \tag{4.44}$$

The result is a second-order differential equation of the form

$$\frac{\mathrm{d}^2}{\mathrm{d}r^2} F_{\epsilon\kappa}(r) + \omega(r) F_{\epsilon\kappa}(r) = 0\,, \tag{4.45}$$

where

$$\begin{aligned}\omega(r) = a_P(r) a_Q(r) - \frac{l(l+1)}{r^2} - \frac{\kappa}{r}\frac{1}{a_P(r)}\frac{\mathrm{d}}{\mathrm{d}r} a_P(r) \\ -\frac{3}{4}\left[\frac{1}{a_P(r)}\frac{\mathrm{d}}{\mathrm{d}r} a_P(r)\right]^2 + \frac{1}{2}\frac{1}{a_P(r)}\frac{\mathrm{d}^2}{\mathrm{d}r^2} a_P(r)\end{aligned} \tag{4.46a}$$

$$a_Q(r) = \frac{\alpha}{2}[\epsilon - V(r)]\,. \tag{4.46b}$$

In writing the second term on the right-hand side of eq. (4.46a), use has been made of the relation $\kappa(\kappa+1) = l(l+1)$, in order to facilitate the discussion in the upcoming section 4.7 concerning the quasi-relativistic approach. The advantage of solving eq. (4.45), rather than the analog of eq. (2.14) for continuum electrons, is that $\omega(r)$ does not depend on $F_{\epsilon\kappa}(r)$, in contrast to the effective potential in eq. (2.14), which does depend on $P_{\epsilon\kappa}(r)$. For bound orbitals, use of eq. (2.14), rather than the analog of eqs. (4.45)–(4.46b), does not tend to increase the difficulty in obtaining a solution because the bound orbitals also enter the Dirac-Fock-Slater potential given by eqs. (2.18)–(2.20) which, in any event, must be determined self-consistently with the solution of eq. (2.14).

Similar to the discussion in section 2.2, we separate out the nuclear contribution to the central potential, $-2Z/r$, and evaluate its contribution to $\mathrm{d}V/\mathrm{d}r$ and $\mathrm{d}^2V/\mathrm{d}r^2$ analytically. Additionally, the radial mesh is started with the same spacing given in eq. (2.17), and then doubling of this spacing occurs after every 40 points. The doubling is terminated for the largest value of Δr that satisfies

$$\Delta r \leq \frac{1}{4\sqrt{\epsilon_{\max}}}\,, \tag{4.47}$$

where $\epsilon_{\max}$ is the largest incident energy (in Rydbergs) being considered in the calculations. When this largest value of Δr is reached, the mesh is continued with this fixed spacing, typically for a total of 1800 points. Although only every fourth mesh point is used in calculating the radial integrals in eqs. (4.17) and (4.18), the use of eq. (4.47) ensures that a sufficient number of points are available to resolve the oscillatory nature of the radial functions at large values of r. For details on the appropriate normalization of these radial functions, the reader is referred to the appendix of ref. [40].

4.6 Procedures for minimizing the number of radial integrals

In this section, a description is provided for various numerical schemes that are used to accelerate the calculation of collision strengths. For most cases the time required to perform collision-strength calculations is principally determined by the number of radial wave functions and radial matrix elements or integrals. Therefore, it is important to keep the number of these quantities that are explicitly calculated to a minimum.

In our approach, as described previously (see the discussion surrounding eqs. (2.21) and (2.22)), we use a single set of fractional occupation numbers for each category of calculations which is usually determined by iso-electronic sequence and the type of $n - n'$ transition. This choice results in the use of the same potential for determining the orbitals of all the electrons, bound and free, which in turn produces just one set of bound wave functions for a particular type of transition. While greatly reducing the number of continuum orbitals that need to be computed, this procedure also helps to minimize the number of radial integrals, particularly when treating complex ions. More specifically, one can take advantage of the fact that the bound-electron contribution to the Coulomb integrals appearing in eqs. (4.17) and (4.18) (as well as to the integrals in eqs. (4.78) and (4.79), when the generalized Breit interaction is also considered) is the same for all transitions in which the same orbital transition $n_a l_a j_a - n'_a l'_a j'_a$ enters. In contrast, in some multi-configuration treatments, the bound-electron radial functions are different if they belong to different configurations, even if they are described by the same quantum numbers $n_a l_a j_a$ or $n'_a l'_a j'_a$. Since the number of times that a particular $n_a l_a j_a - n'_a l'_a j'_a$ transition occurs can be very large for complex ions, this sort of consideration can save a considerable amount of computing time.

Also, unlike the bound-electron contribution, the free-electron contribution to eqs. (4.17) and (4.18) differs for each pair of impact and scattered energies. This issue will impede the calculations for complex ions, for which many energy levels are typically present, and the resulting number of fine-structure transitions can be quite large. However, this concern can be addressed by

realizing that, in our approach, the radial matrix elements or integrals associated with a given $n_a l_a j_a - n'_a l'_a j'_a$ transition are smooth functions of the free-electron energy. Therefore, in order to minimize the number of integrals to be calculated, we implemented the following procedure: in considering a given class of transitions, results are calculated for a fixed set of scattered energies beginning from near zero and spanning the range needed to obtain accurate collisional rate coefficients, which are discussed in section 4.14. For each of these scattered energies, we calculate results for three impact energies spanning the range of fine-structure transition energies for the class of transitions being considered. Then we interpolate on these three sets of results to obtain the desired quantity at the specific transition energy for each fine-structure transition.

In version 1 of our collisional excitation code, the interpolation is done on the reactance matrix elements between the pure states that appear on the right-hand side of eq. (4.13). It should be mentioned that the results would be virtually the same if the interpolation were instead made on the direct and exchange integrals appearing in eqs. (4.15) and (4.16), according to the procedure described in ref. [40]. In version 2 of our excitation code, the interpolation is instead made on the Q^λ appearing in eq. (4.32). The interpolation scheme that we employed is a non-linear, Lagrange-polynomial interpolation scheme taken from the semi-relativistic program of Bottcher [47]. This interpolation procedure has been shown to work quite well in both versions of our codes and leads to a significant reduction in the number of radial integrals to be calculated for a given type of $n-n'$ transition. However, we should mention that, in the treatment of $\Delta n = 0$ transitions, we usually found it necessary to increase the number of impact-electron energies for which results were calculated for each scattered-electron energy to a number larger than three.

In principle, one could also apply the above interpolation scheme for a fixed set of impact energies, rather than a fixed set of scattered energies. Such an option is available in our codes, but no data have been published using this method because it is typically impossible to determine a single, compact set of impact-electron energies that can be used to calculate the rate coefficients for all of the fine-structure transitions that arise from a given type of $n - n'$ transition. Alternatively, we note that many authors calculate collision strengths for a fixed set of impact energies in threshold units, rather than absolute energies. With such an approach the problem of choosing a practical set of impact energies for calculating the rate coefficients is obviated. However, most of the above methods for accelerating the calculations can not be used with this approach, and the evaluations become more lengthy.

Finally, we mention that the contribution to the collision strength from those radial integrals or matrix elements that are characterized by large angular momentum values, associated with the incident- and scattered-electron partial

waves, can be significant. This statement is particularly relevant for optically allowed transitions, and especially those with $\Delta n = 0$. Some approximate procedures for calculating this contribution will be discussed in section 4.9.

4.7 The quasi-relativistic approach applied to continuum electrons

As mentioned in section 2.3, we also implemented a quasi-relativistic (QR) option in our electron-impact excitation codes that is analogous to the QR approach described for the atomic structure calculations. As in the structure case, the small component of the continuum-electron wave functions is ignored in all expressions and the large component is treated as the entire radial function. Thus, in this approach, the second term in each of the square brackets appearing in the radial integrals of eqs. (4.17) and (4.18) is omitted. Furthermore, the large component of the bound-electron wave functions is normalized according to eq. (2.23), while the large component of the continuum electron wave functions is normalized according to eq. (A23) in the appendix of ref. [40].

Similar to the reasoning provided in section 2.3, the above QR approach saves about 10% in computing time relative to the fully relativistic approach, which is not a terribly significant amount. However, a much larger reduction in computing time can be obtained by introducing an additional approximation for the continuum electrons. Specifically, one can replace the κ value associated with a continuum-electron wave function with its j-averaged value of -1, so that the large component no longer depends on j. (However, the dependence on l is retained.) This additional approximation is implemented by simply setting $\kappa = -1$ in eq. (4.46a). The appropriate normalization for the resulting radial wave functions is given by eq. (A24) or (A25) in the appendix of ref. [40]. The benefit of this approximation is a reduction in the number of radial functions to be computed by approximately a factor of two and the number of radial integrals by a factor of four, which leads to a reduction in the overall computing time by a factor of 2.5.

In ref. [40], numerical examples were provided that showed the QR approach with $\kappa = -1$ to be quite accurate. The success of this approximation is not unexpected if one realizes that the collision strength in eq. (4.12) contains a sum over the initial and final continuum-electron quantum numbers j and j'. Thus, replacing κ and κ' by their j-averaged value of -1 when computing the continuum wave functions is analogous to removing the double sum over j and j' in the expression for the collision strength and replacing the summand with a suitably averaged value.

4.8 The relativistic plane-wave-Born approximation

In anticipation of the upcoming discussion of the Kummer transformation in subsection 4.9.3, we present here the relativistic plane-wave-Born (RPWB) approximation for electron-impact excitation. The treatment closely follows that given in ref. [48], which, in turn, is based strongly on the non-relativistic approach of Cowan [8]. For clarity, we divide the discussion into two subsections, with the first describing an analytic approach and the second describing a partial-wave decomposition. The expressions presented in this section are written with all fundamental constants intact, except where noted, in order to facilitate the discussion of terms that arise from a relativistic treatment.

4.8.1 An analytic approach to the plane-wave-Born approximation

The goal of this subsection is to produce an analytic expression for the RPWB excitation cross section between two fine-structure levels. We begin by considering an excitation transition between an initial magnetic sublevel $|\Delta_t J_t M_t\rangle$ and final sublevel $|\Delta_t' J_t' M_t'\rangle$ of an atom or ion with N bound electrons. This sublevel notation is identical to that used in connection with the collision strength for transitions between fine-structure levels in eq. (4.6). However, when dealing with the approximation of representing the continuum electrons as plane waves, we also ignore antisymmetrization of the continuum function with the target in the $(N+1)$-electron system wave function. The RPWB matrix element that characterizes an excitation transition between these two sublevels can then be written in the form

$$H_{\alpha\alpha'} = \langle\alpha| \sum_{q=1}^{N} \frac{2}{|\boldsymbol{r}_q - \boldsymbol{r}|} |\alpha'\rangle \,, \tag{4.48}$$

where

$$\alpha \equiv |\Delta_t J_t M_t\rangle |\mathrm{e}^{i\boldsymbol{k}\cdot\boldsymbol{r}}, m_s\rangle, \quad \alpha' \equiv |\Delta_t' J_t' M_t'\rangle |\mathrm{e}^{i\boldsymbol{k}'\cdot\boldsymbol{r}}, m_s'\rangle \tag{4.49}$$

are direct products between the appropriate magnetic sublevel and a Dirac plane wave. The values $\boldsymbol{k}$ and $\boldsymbol{k}'$ represent the wave vectors of the incident and scattered plane waves, respectively, and the values m_s and m_s' represent the corresponding spin magnetic quantum numbers. The concept of spin arises in a natural, formal way when considering solutions of the Dirac equation, but does not occur when considering the non-relativistic case involving solutions to the Schrödinger equation. Of course, it is possible to manually insert spin wave functions into the non-relativistic theory (see, for example, eq. (7) of ref. [30]), but such an approach does not provide a fully relativistic description of spin, as described below.

While the matrix element in eq. (4.48) is similar to that appearing in eq. (4.6), there are some important differences. For example, the summation in eq. (4.48) needs to be carried out over only the N, bound-electron coordinates because we are dealing with product wave functions. Another important difference is that the plane waves in eq. (4.49) are written analytically, while those appearing in eq. (4.6) represent a single component of the partial-wave expansion of the complete distorted-wave continuum wave functions. A partial-wave analysis of the RPWB approach will be considered in the next subsection, but here we continue with the analytic representation, which can be expressed in a convenient closed form.

Employing the relationship between the momentum and wave vector of a continuum electron, $\boldsymbol{p} = \hbar\boldsymbol{k}$, the Dirac plane waves can be written in the form [3]

$$\psi_{\boldsymbol{k},m_s}(\boldsymbol{r}) = U(\boldsymbol{k},m_s)\mathrm{e}^{i\boldsymbol{k}\cdot\boldsymbol{r}} = N_k \begin{pmatrix} \chi^{m_s} \\ \dfrac{c\ \boldsymbol{\sigma}\cdot\boldsymbol{p}}{E+mc^2}\ \chi^{m_s} \end{pmatrix} \mathrm{e}^{i\boldsymbol{k}\cdot\boldsymbol{r}}, \tag{4.50}$$

where $\boldsymbol{\sigma}$ are the usual 2×2 Pauli matrices and χ^{m_s} are the eigenvectors of σ_z [3]. A value of $N_k = \sqrt{(E+mc^2)/2E}$, where $E = \sqrt{(pc)^2+(mc^2)^2}$ is the total energy of the incident electron, has been chosen such that the plane waves are orthonormal according to $\psi^\dagger_{\boldsymbol{k},m_s}\psi_{\boldsymbol{k},m'_s} = U^\dagger(\boldsymbol{k},m_s)U(\boldsymbol{k},m'_s) = \delta_{m_s m'_s}$. More generally, when $\boldsymbol{k}' \neq \boldsymbol{k}$, the relativistic plane waves satisfy the more comprehensive orthonormality condition

$$\langle \mathrm{e}^{i\boldsymbol{k}\cdot\boldsymbol{r}}, m_s | \mathrm{e}^{i\boldsymbol{k}'\cdot\boldsymbol{r}}, m'_s\rangle = (2\pi)^3 U^\dagger(\boldsymbol{k},m_s)U(\boldsymbol{k}',m'_s)\delta(\boldsymbol{k}-\boldsymbol{k}'), \tag{4.51}$$

where

$$U^\dagger(\boldsymbol{k},m_s)U(\boldsymbol{k}',m'_s) = N_k N'_k \left[\langle\chi^{m_s}|\chi^{m'_s}\rangle + \frac{c^2\langle\boldsymbol{\sigma}\cdot\boldsymbol{p}\,\chi^{m_s}|\boldsymbol{\sigma}\cdot\boldsymbol{p}'\,\chi^{m'_s}\rangle}{(E+mc^2)(E'+mc^2)}\right]. \tag{4.52}$$

Eq. (4.52) represents the scalar product between the 4-vector amplitudes of the incident and scattered plane waves, which has no analog in the non-relativistic case. The term on the far right that contains the two dot products results from the small components of the incident and scattered plane waves. It is well known that the small component differs from the large component by a factor of $O(v/c)$, where $v = pc^2/E$ is the speed of the electron. Therefore, in the non-relativistic limit, the term containing the dot products can be ignored, the normalization constants N_k and N'_k can be approximated by one and the scalar product in eq. (4.52) can be set to one, provided that $m'_s = m_s$, or to zero if $m'_s \neq m_s$.

The PWB and RPWB approaches were considered in detail by Bethe in a series of seminal articles [49–51]. This paradigm eventually became known as the Bethe high-energy theory and a comprehensive review of this approach has been written by Inokuti [52]. In the high-energy limit considered by Bethe, the scattering is strongly peaked in the forward direction for which $\boldsymbol{k}' \approx \boldsymbol{k}$. In this case, the scalar product above can also be set to one due to the orthonormalization condition, again provided that $m_s' = m_s$ (otherwise the result is zero). If the spin polarization of the incident and scattered electrons is not of interest, then the resulting scalar product obtained after performing the appropriate averaging and sums over the spin quantum numbers (see discussion below) can also be approximated as one in both the non-relativistic and high-energy limits. Approximations of this latter type have been used, for example, in eq. (52.23) of ref. [51] and eq. (13) of ref. [53].

In the present discussion, we are indeed interested in scattering by unpolarized electrons, as mentioned above. (A discussion of excitation by polarized electrons will be provided in chapter 9.) However, we do not introduce the Bethe approximation, $\boldsymbol{k}' \approx \boldsymbol{k}$, as our goal is to obtain an exact expression for the RPWB collision strength, analogous to the RDW expression given in eq. (4.6) for a transition between fine-structure levels, denoted by $\Delta_t J_t - \Delta_t' J_t'$. In order to obtain such a quantity, one must square the matrix element in eq. (4.48), then perform the appropriate sums and averages over the magnetic quantum numbers associated with the continuum electrons and the magnetic sublevels, and finally integrate over the angle of the scattered electron. The details of this procedure are provided in ref. [48] and additional details are also supplied in subsection 9.1.3 of the present work, which deals with transitions between magnetic sublevels. The resulting RPWB collision strength can be expressed (in Rydberg atomic units) in the closed form

$$\begin{aligned}\Omega^{\mathrm{RPWB}}(\Delta_t J_t - \Delta_t' J_t') &\equiv \frac{k^2 g_i}{\pi} Q^{\mathrm{RPWB}}(\Delta_t J_t - \Delta_t' J_t') \\ &= \frac{8}{\Delta E} \int_{K_{\mathrm{min}}}^{K_{\mathrm{max}}} F_{\mathrm{rel}}(K) g f(\Delta_t J_t - \Delta_t' J_t'; K)\, \mathrm{d}(\ln K)\,. \quad (4.53)\end{aligned}$$

As it is written, eq. (4.53) is formally identical to the usual non-relativistic PWB collision strength (see, for example, eq. (18.157) of ref. [8]), except for the appearance of the relativistic correction factor, $F_{\mathrm{rel}}(K)$, which will be discussed below. Specifically, $g_i = 2J_t + 1$ is the statistical weight of the initial level, ΔE is the transition energy in Rydbergs, k is the wave number of the incident electron in atomic units and K is the magnitude of the momentum transfer vector $\boldsymbol{K} = \boldsymbol{k}' - \boldsymbol{k}$. The quantity $gf(\cdots; K)$ is the generalized oscillator strength (GOS) between the two levels and is given by

$$gf(\Delta_t J_t - \Delta_t' J_t'; K)$$
$$= \frac{\Delta E}{K^2} \sum_{\nu} (2\nu+1) \langle \Delta_t J_t || \sum_{q=1}^{N} j_\nu(K r_q) \boldsymbol{C}_q^{(\nu)} || \Delta_t' J_t' \rangle^2 , \qquad (4.54)$$

where j_ν is the spherical Bessel function of order ν and $\boldsymbol{C}_q^{(\nu)}$ is the renormalized spherical harmonic of rank ν. In this case, the subscript q indicates that the angular variables associated with position vector $\boldsymbol{r}_q$ are the arguments of the renormalized spherical harmonic (q should not be confused with the component of $\boldsymbol{C}^{(\nu)}$ in this instance). This expression for the GOS also agrees formally with the corresponding non-relativistic formula, but when expanded in detail, the reduced matrix element must also contain the small component of the target wave functions. When describing an electric dipole allowed transition, eq. (4.54) has the desired property of reducing to the length form of the relativistic gf value (i.e. eq. (3.4), with substitutions from eqs. (3.3), (3.14), (3.17) and (3.27)) in the limit $K \rightarrow 0$.

The limits of integration are obtained from a consideration of the excitation process using relativistic kinematics. As in the non-relativistic case, these limits are found by taking the minimum and maximum allowed values of the magnitude of the momentum transfer vector $\boldsymbol{K}$. With the incident-electron kinetic energy given by $\epsilon = E - mc^2$, and a similar expression for the scattered-electron kinetic energy ϵ', the limits of integration can be written in the form

$$K_{\min} \equiv k - k' = \frac{1}{\hbar c} \left[\sqrt{\epsilon(\epsilon + 2mc^2)} - \sqrt{\epsilon'(\epsilon' + 2mc^2)} \right] \qquad (4.55a)$$

$$K_{\max} \equiv k + k' = \frac{1}{\hbar c} \left[\sqrt{\epsilon(\epsilon + 2mc^2)} + \sqrt{\epsilon'(\epsilon' + 2mc^2)} \right] , \qquad (4.55b)$$

where use has been made of eq. (4.2). Of course, ϵ' can always be eliminated in favor of ϵ in the above expression, as well as in any other formulae appearing in the subsequent discussion, via the energy conservation relationship, $\epsilon = \Delta E + \epsilon'$.

Lastly, we come to a discussion of the relativistic correction factor, $F_{\mathrm{rel}}(K)$. This factor arises from a product of the appropriately averaged scalar product in eq. (4.52) and an extra kinematic factor [52] that takes into account the relativistic relationship between the velocity and momentum, $\boldsymbol{v} = \boldsymbol{p}c^2/E$, for the incident and scattered electrons. The result is

$$F_{\mathrm{rel}}(K) = \left(\frac{EE'}{m^2c^4} \right) (N_k N_k')^2 \left[\left(1 + \frac{c^2}{D} \boldsymbol{p} \cdot \boldsymbol{p}' \right)^2 + \frac{c^4}{D^2} (\boldsymbol{p} \times \boldsymbol{p}')^2 \right]$$
$$= \frac{(\epsilon + 2mc^2)(\epsilon' + 2mc^2)}{4m^2c^4} \left[1 + \frac{(\hbar c)^2 [k^2 + (k')^2 - K^2)]}{(\epsilon + 2mc^2)(\epsilon' + 2mc^2)} \right.$$

$$+\frac{(\hbar c)^4(kk')^2}{(\epsilon+2mc^2)^2(\epsilon'+2mc^2)^2}\Bigg]\,, \quad (4.56)$$

where $D \equiv (E+mc^2)(E'+mc^2)$. With a small amount of manipulation, it is easy to show that the first line of eq. (4.56) reduces to one in the non-relativistic limit, since both p and $p' \ll mc$ in that case. Furthermore, in the Bethe high-energy case, $\boldsymbol{p}' \to \boldsymbol{p}$, and the first line of eq. (4.56) can again be greatly simplified. In particular, the factor arising from the scalar product can be set to one (as mentioned earlier in this subsection) and the only factor that survives is the extra kinematic piece $EE'/m^2c^4 \approx E^2/m^2c^4$, which appears regularly in the Bethe high-energy theory. However, in the present work, no such approximations are made. Eq. (4.53) represents an exact expression for the RPWB collision strength for an arbitrary transition between two fine-structure levels. All that is required to evaluate this expression are numerical values for the relativistic GOS and the associated transition energy, both of which are readily obtained from our atomic structure code, followed by a numerical integration over the appropriate range of K values.

4.8.2 A partial-wave approach to the plane-wave-Born approximation

In this subsection, we provide the details for calculating the RPWB collision strength using a partial-wave decomposition. The treatment is essentially the same as that used to compute RDW collision strengths in the earlier part of this chapter. For example, eqs. (4.6) and (4.8) can also be used to describe the partial-wave expansion of the RPWB collision strength, provided that allowance is made for the use of product wave functions to describe the $(N+1)$-electron system, rather than fully antisymmetrized wave functions, such as the one appearing in eq. (4.8). The main difference between the RPWB and RDW approaches resides in the choice of radial functions associated with each partial wave. In the RPWB case, the radial functions can be expressed in an analytic form, while the RDW radial functions must be solved for numerically. This analyticity arises from the fact that the exponential in eq. (4.50) can be expanded according to the well-known expression

$$\mathrm{e}^{i\boldsymbol{k}\cdot\boldsymbol{r}} = \sum_{\nu=0}^{\infty}(2\nu+1)\,\mathrm{i}^{\nu} j_\nu(kr)[\boldsymbol{C}^{(\nu)}(\hat{\boldsymbol{k}})\cdot\boldsymbol{C}^{(\nu)}(\hat{\boldsymbol{r}})]\,, \quad (4.57)$$

where j_ν is the spherical Bessel function of order ν. Alternatively, this analytic behavior could also have been deduced by setting the potential, $V(r)$, to zero in eqs. (4.10) and (4.11). The resulting second-order differential equation for $P_{\epsilon\kappa}$ or $Q_{\epsilon\kappa}$ is the radial equation that one obtains when the Helmholtz equation is expressed in spherical coordinates. The solutions of this equation are precisely the spherical Bessel functions. Thus, the Dirac spinors that appear in eq. (4.9) have the same functional form for both the RPWB and RDW cases, but the

RPWB functions can be written in the more explicit form

$$u^{\mathrm{RPWB}}_{\epsilon\kappa m}(x) = \frac{1}{r}\begin{bmatrix} P_{\epsilon\kappa}(r) & \chi_{\kappa m} \\ \mathrm{i}Q_{\epsilon\kappa}(r) & \chi_{-\kappa m} \end{bmatrix} = \frac{1}{r}\begin{bmatrix} krj_l(kr) & \chi_{\kappa m} \\ \dfrac{ipc}{E+mc^2}S_\kappa krj_{\bar{l}}(kr) & \chi_{-\kappa m} \end{bmatrix}, \quad (4.58)$$

in accordance with eq. (5.12) of Rose [3]. In eq. (4.58) $P_{\epsilon\kappa}$ and $Q_{\epsilon\kappa}$ are the large and small radial components of the RPWB spinor, κ is the usual relativistic quantum number that represents a particular pair of l and j values, $S_\kappa = \kappa/|\kappa|$ is the sign of κ and the symbol $\bar{l} = l - S_\kappa$ differs from the value of l by ± 1.

Combining the above results, a partial-wave expansion of the RPWB collision strength can be evaluated in terms of the reactance matrix, according to the relationship displayed in eq. (4.12). Therefore, the same computer code that is used to calculate RDW collision strengths from a numerically determined set of $P_{\epsilon\kappa}$ and $Q_{\epsilon\kappa}$ functions can also be used to calculate RPWB collision strengths via eq. (4.58) provided that: (1) only the "direct" Slater integrals are retained for the RPWB calculation and (2) the normalization for the plane waves is chosen such that they are consistent with the asymptotic form of the distorted waves. Condition (1) is necessary because, as mentioned previously, the total $(N+1)$-electron wave functions contain the plane-wave contribution in product form, rather than antisymmetrized form. Thus, the direct Slater integrals appearing in eq. (4.17) are retained, while the exchange integrals in eq. (4.18) are ignored for the RPWB calculation. Condition (2) is required so that the same mathematical expression for the collision strength can be applied to both the RDW and RPWB calculations. For example, if the energy normalization is chosen according to eq. (A1) of ref. [40], then the asymptotic form of the continuum wave functions, given by eq. (A7) of that same reference, determines the appropriate normalization for the corresponding plane waves. The result is that the plane-wave spinor on the right-hand side of eq. (4.58) must be multiplied by the factor

$$C_P(\epsilon) = \left(\frac{k}{\epsilon}\right)^{1/2}, \quad (4.59)$$

where k is in atomic units and ϵ is in Rydbergs.

4.9 The top-up: approximate treatments of the large angular momentum, partial-wave contribution

Upon choosing one of the previously described numerical procedures to compute the reactance matrix, the collision strength is then obtained by evaluating

the summations in eq. (4.12). However, the inner quadruple sum in this expression contains an infinite number of terms with different free-electron orbital quantum numbers. Each term, denoted by a pair of l and j values, is usually called a partial-wave contribution. (It is not necessary to consider separately the infinite pairs of l' and j' associated with the scattered electron because the allowed values are determined by selection rules imposed on them and on l, j, the expansion index λ appearing in eq. (2.12), and the corresponding quantum numbers associated with the active bound electrons.) Obviously, one can not include all of the infinite number of partial-wave contributions in a calculation. In practice, the summation is computed numerically up to some finite maximum value for l and j, and then a procedure must be adopted to estimate the remaining high partial-wave contributions. This remaining contribution, sometimes referred to as the "top-up" in the literature, can be a significant portion of the total sum, especially for high impact energies and for optically allowed transitions with $\Delta n = 0$. In this section, we describe the methods that have been used in our collision codes to compute the top-up contribution. These methods include the Coulomb-Bethe approximation, the ratio approximation and the Kummer transformation.

4.9.1 Coulomb-Bethe approximation for optically allowed transitions

The Coulomb-Bethe (CBe) approximation [54] is widely used to obtain the high partial-wave contribution for the optically allowed transitions. In this method one makes the following approximations: (1) neglect exchange; (2) approximate the electrostatic interaction between the active bound electron and the free electron with the replacement

$$\begin{aligned}\frac{1}{|\,\boldsymbol{r}_N - \boldsymbol{r}_{N+1}\,|} &= \sum_\lambda \frac{r_<^\lambda}{r_>^{\lambda+1}} \boldsymbol{C}^{(\lambda)}(\hat{\boldsymbol{r}}_N)\cdot\boldsymbol{C}^{(\lambda)}(\hat{\boldsymbol{r}}_{N+1}) \\ &\simeq \frac{r_N}{(r_{N+1})^2}\boldsymbol{C}^{(1)}(\hat{\boldsymbol{r}}_N)\cdot\boldsymbol{C}^{(1)}(\hat{\boldsymbol{r}}_{N+1})\,, \end{aligned} \tag{4.60}$$

where N and $N+1$ are used in this context to label the coordinates of the active bound electron and the free electron, respectively; and (3) use pure Coulomb wave functions to represent the free electron. These approximations should be valid for large angular momenta of the free electron.

A detailed derivation of the relativistic Coulomb-Bethe (RCBe) approximation will be given in subsection 9.1.2, which deals with transitions between magnetic sublevels. Here, we simply write down the form that is applicable for transitions between fine-structure levels, i.e. eq. (14) in [55]

$$\Omega^{\mathrm{RCBe}}(\Delta_t J_t - \Delta_t' J_t') = \tfrac{8}{3} S(\Delta_t J_t - \Delta_t' J_t')$$

$$\times \sum_{\substack{l,j \\ l',j'}} I^2(\epsilon l j, \epsilon' l' j') \langle j \parallel \boldsymbol{C}^{(1)} \parallel j' \rangle \,, \tag{4.61}$$

where $S(\Delta_t J_t - \Delta'_t J'_t)$ is the line strength given by eq. (3.14) and I is the relativistic Coulomb integral

$$I(\epsilon l j, \epsilon' l' j') = \int_0^\infty \frac{1}{r^2} [P_{\epsilon l j}(r) P_{\epsilon' l' j'}(r) + Q_{\epsilon l j}(r) Q_{\epsilon' l' j'}(r)] \, \mathrm{d}r \,. \tag{4.62}$$

In general, one evaluates the partial-wave contributions to the distorted-wave collision strength, given by eq. (4.12), up to some reasonably large value $l = l_0 - 1$ (where l_0 typically ranges from 10–70, depending on the type of transition and the impact energy), and designates the result as $\Omega^{\mathrm{RDW}}_{0,l_0-1}$. Then, the remaining high partial-wave contributions up to $l = \infty$ are evaluated in one of two ways. Since eq. (4.61) can not be further reduced to a simpler form, the first method involves making a further approximation by removing the small component Q and the j dependence in eq. (4.62). Specifically, the non-relativistic form of the Coulomb integral, $I(\epsilon l, \epsilon' l')$, is used, and the double sum over j, j' can be simplified according to

$$\sum_{j,j'} \langle j \parallel \boldsymbol{C}^{(1)} \parallel j' \rangle^2 \rightarrow 2 \langle l \parallel \boldsymbol{C}^{(1)} \parallel l' \rangle^2 \,, \tag{4.63}$$

where

$$\langle l \parallel \boldsymbol{C}^{(1)} \parallel l' \rangle = \pm (l_>)^{1/2} \,. \tag{4.64}$$

Combining these results yields a collision strength given by

$$\Omega^{\mathrm{PRCBe}}(\Delta_t J_t - \Delta'_t J'_t) = \tfrac{16}{3} S(\Delta_t J_t - \Delta'_t J'_t) \sum_{l,l'} l_> I^2(\epsilon l, \epsilon' l') \,, \tag{4.65}$$

which is identical in form to the well-known, non-relativistic version of the CBe approximation [54]. However, in our case, the line strength is computed in a fully relativistic manner, while the continuum electrons are treated in a non-relativistic manner. Thus, we refer to eq. (4.65) as the partial-relativistic Coulomb-Bethe (PRCBe) approximation in this work. The symbol $l_>$ in eqs. (4.64) and (4.65) is the greater of l and l', and the plus sign applies if $l = l' + 1$, while the minus sign applies if $l = l' - 1$ in eq. (4.64). Combining results, the complete RDW collision strength can be written as

$$\Omega^{\mathrm{RDW}} \approx \Omega^{\mathrm{RDW}}_{0,l_0-1} + \Omega^{\mathrm{PRCBe}}_{l_0,\infty} \,, \tag{4.66}$$

where the top-up contribution, $\Omega_{l_0,\infty}^{\mathrm{PRCBe}}$, is given by

$$\Omega_{l_0,\infty}^{\mathrm{PRCBe}} = \tfrac{16}{3} S(\Delta_t J_t - \Delta_t' J_t') \sum_{l=l_0}^{\infty} \sum_{l'=l\pm1}^{\infty} l_> I^2(\epsilon l, \epsilon' l') \,. \tag{4.67}$$

The double summations in eq. (4.67) can be evaluated using the convenient expression given by eq. (10) of Burgess [56], which, in the present notation, becomes

$$\sum_{l=l_0}^{\infty} \sum_{l'=l\pm1}^{\infty} l_> I^2(\epsilon l, \epsilon' l') = [I^2(\epsilon l_0, \epsilon'(l_0-1)) - I^2(\epsilon(l_0-1), \epsilon' l_0)] \frac{1+(k l_0/z)^2}{l_0[(k/z)^2 - (k'/z)^2]} \,, \tag{4.68}$$

where

$$z = Z - N \,, \tag{4.69}$$

and $k = \sqrt{\epsilon}$ and $k' = \sqrt{\epsilon'}$ are the non-relativistic wave numbers of the impact and scattered electrons, respectively.

In most of our calculations of collision strengths, we have used eq. (4.66) to obtain the complete RDW results. The data calculated should be quite accurate for $\Delta n > 0$ transitions and for most transitions with $\Delta n = 0$. However, after obtaining the more precise, fully relativistic expression in eq. (4.61), and using it to verify the total collision strengths obtained from eq. (4.66), we found some non-trivial inaccuracies for certain optically allowed transitions. These problematic cases typically occurred when the impact energies were very high, especially for high-Z ions, for which relativistic effects were very important.

Therefore, we added an option to use a second method, which will be described in more detail in subsection 9.1.2 when dealing with magnetic sublevel transitions, to obtain the top-up contribution for the total collision strength. In this method, after obtaining the distorted-wave contributions up to $l = l_0 - 1$, higher partial-wave contributions from $l = l_0$ to some very high value $l = l_0^* - 1$ are computed using the fully relativistic expression in eq. (4.61). This contribution can be written as

$$\Omega_{l_0,l_0^*-1}^{\mathrm{RCBe}} = \tfrac{8}{3} S(\Delta_t J_t - \Delta_t' J_t') \times \sum_{l=l_0}^{l_0^*-1} \sum_{l',j,j'} I^2(\epsilon l j, \epsilon' l' j') \langle j \parallel \boldsymbol{C}^{(1)} \parallel j' \rangle \,. \tag{4.70}$$

With l_0^* sufficiently large, up to 200 in most cases, the ratio of successive partial-wave contributions becomes very nearly constant. Assuming this ratio is exactly constant, and equal to some value C for a given transition and incident (or scattered) electron energy, the properties of the geometric series can be invoked to obtain a closed form result. Under this assumption, the contribution of all partial waves with $l \geq l_0^*$ can be written as

$$\Omega_{l_0^*,\infty}^{\mathrm{RATIO}} = \Omega_{l_0^*-1}^{\mathrm{RCBe}} \frac{C}{1-C}\,, \tag{4.71}$$

where $\Omega_{l_0^*-1}^{\mathrm{RCBe}}$ is the partial-wave, relativistic Coulomb-Bethe value evaluated at $l = l_0^* - 1$ (with l', j and j' taking on all allowed in eq. (4.70)). Hence, the complete RDW collision strength computed with the second top-up method is given by

$$\Omega^{\mathrm{RDW}} \approx \Omega_{0,l_0-1}^{\mathrm{RDW}} + \Omega_{l_0,l_0^*-1}^{\mathrm{RCBe}} + \Omega_{l_0^*,\infty}^{\mathrm{RATIO}}\,. \tag{4.72}$$

It is noted that values of the incident-electron orbital quantum number l have been used to label the approximate top-up contributions in the above equations. One could alternatively reformulate these equations such that the relevant label was the scattered-electron orbital quantum number l'. For example, the quadruple summation in eq. (4.70) can be reordered so that the scattered-electron orbital quantum number l' appears as the index of the outermost sum. If an appropriate range of values is prescribed for l', then the numerical values of the RCBe top-up contribution computed in this way are virtually the same as the results obtained from eq. (4.70). In fact, the latter approach is used predominantly in our production calculations, since collision strengths are computed for the final, or scattered, electron energies, instead of the incident-electron energies.

4.9.2 Ratio approximation for forbidden transitions

For forbidden transitions, the partial-wave contributions rapidly decrease with l and j and the ratio

$$C = \Omega_{l_0-2}^{\mathrm{RDW}} / \Omega_{l_0-1}^{\mathrm{RDW}} \tag{4.73}$$

becomes very small and almost constant. Similar to the second method in the previous discussion, the top-up contribution can be written in closed form according to the properties of the geometric series, and the complete collision strength is approximated by

$$\Omega^{\mathrm{RDW}} \approx \Omega^{\mathrm{RDW}}_{0,l_0-1} + \Omega^{\mathrm{RDW}}_{l_0-1}\frac{C}{1-C}\,. \tag{4.74}$$

This method is usually called the ratio, or geometric progression, approximation. In using this method to obtain the complete collision strength, one still needs to include the RDW partial-wave contributions up to some sufficiently large value, $l_0 - 1$, especially for $\Delta n = 0$ transitions and high impact energies, so that C is small and almost constant. It is noted that for some transitions that can occur only through exchange processes, the partial-wave contributions associated with large l values are negligible. In this case, the ratio approximation is typically not required.

4.9.3 The Kummer transformation

A third method for obtaining the top-up contribution to the RDW collision strength is to approximate this high-l portion with the corresponding RPWB result. This quantity is readily obtained from the expressions provided in section 4.8. As in the previous two subsections, the distorted-wave contributions to the RDW collision strength are summed up to a value of $l = l_0 - 1$. The same type of summation can be carried out for the RPWB partial-wave expansion described in subsection 4.8.2 to obtain $\Omega^{\mathrm{RPWB}}_{0,l_0-1}$. This latter quantity is then subtracted from the analytic expression for the RPWB collision strength given by eq. (4.53) of subsection 4.8.1 to obtain the RPWB top-up contribution. We refer to this top-up prescription as the Kummer transformation [57] and the resulting RDW collision strength can be expressed in mathematical form according to

$$\Omega^{\mathrm{RDW}} \approx \Omega^{\mathrm{RDW}}_{0,l_0-1} + (\Omega^{\mathrm{RPWB}} - \Omega^{\mathrm{RPWB}}_{0,l_0-1})\,. \tag{4.75}$$

We note that this approach has several advantages over the two previously described methods. For example, the Kummer transformation is not limited to a specific type of transition, such as dipole allowed transitions. It can be applied to any transition that is described by a non-zero RPWB collision strength. Also, the Kummer transformation has the desirable property of producing RDW collision strengths that naturally exhibit the correct RPWB behavior as the incident-electron energy approaches the appropriate high-energy limit. A disadvantage of this approach is that it provides a less accurate approximation for the top-up contribution at low impact energies. In this regime, the nuclear and electrostatic interactions have a stronger effect on the continuum electrons and, therefore, the high-l partial waves are more accurately represented by Coulomb waves rather than plane waves. This behavior suggests that, at least for optically allowed transitions, a combined approach that employs either the PRCBE or RCBe approximation at low impact energies and the Kummer transformation at higher energies would provide more accurate

values for the top-up contribution.

To clarify the above discussion, we present in figure 1 various calculations of the RDW collision strength for the $(1s\,2s)_1 \rightarrow (1s\,2p_{1/2})_1$ transition in He-like iron. These results were originally presented in ref. [48] and provide a

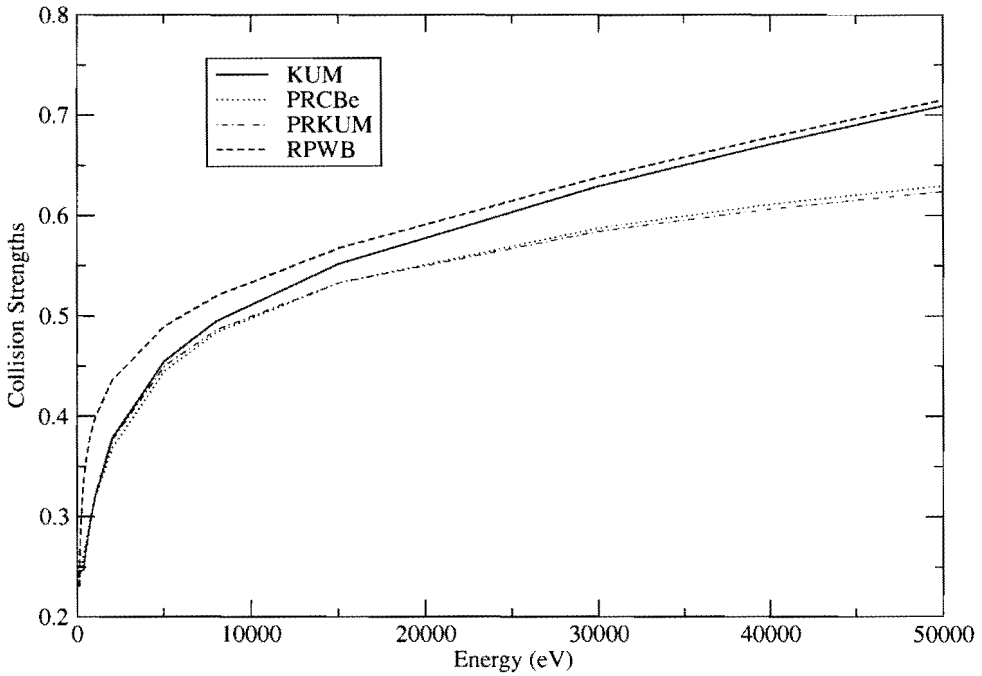

Fig. 1. RDW collision strengths obtained via different top-up methods as a function of impact energy for the $(1s\,2s)_1 \rightarrow (1s\,2p_{1/2})_1$ transition in He-like iron; solid curve: Kummer (KUM) top-up from eq. (4.75); dotted curve: partial-relativistic, Coulomb-Bethe (PRCBe) top-up from eq. (4.66); dot-dashed curve: partial-relativistic, Kummer (PRKUM) top-up [58]. The RPWB collision strength (dashed curve) obtained from eq. (4.53) is also provided for reference.

comparison between three separate methods for computing the top-up contribution. The Kummer (KUM) and PRCBe approximations have been discussed previously. The PRKUM curve represents a partial-relativistic Kummer approximation to calculating the top-up contribution. We have not discussed this approach here, but it is described in ref. [58]. By analogy with the PRCBe approach, the PRKUM approach is based on the fully relativistic Kummer transformation described in this subsection, but the additional approximation is made to treat the (plane-wave) continuum electrons in a non-relativistic manner, while the bound electrons are handled in a fully relativistic manner. (In ref. [48], the notation QRCBe and QRKUM appears in the legend of figure 1, instead of PRCBe and PRKUM. In the present work, we use "PR" rather than "QR" to avoid confusion with the quasi-relativistic approach discussed previously in chapters 3 and 4.) In the figure, one observes that the RDW result computed with the Kummer top-up merges nicely with the RPWB curve as the impact energy increases. On the other hand, there is a widening

divergence between this Kummer result and the two partial-relativistic calculations that starts at an energy of ~5 eV. At the lower impact energies, the RPWB collision strength is clearly too high due to the use of plane waves in a region where the distortion potential plays an important role. As expected, the KUM and PRKUM curves merge into each other as the impact energy decreases because the relativistic effects on the continuum electrons become less important. However, both of those curves are somewhat higher than the PRCBe curve, which suggests that a Coulomb-Bethe approach to calculating the top-up contribution might be more appropriate at these lower impact energies.

4.10 An option to include the generalized Breit interaction in the excitation scattering matrix elements

As described in section 2.5, we included the generalized Breit interaction in our structure calculations in order to improve the accuracy of our results for high-Z ions. Similar considerations led us to also include this interaction in our electron-impact excitation calculations, initially using the non-factorized approach [59] and eventually developing the factorization approach [60]. A formal derivation that includes this interaction in the scattering matrix elements begins with the substitution

$$\frac{2}{r_{qi}} \rightarrow \frac{2}{r_{qi}} + B(q,i) \tag{4.76}$$

in the matrix elements appearing in eq. (4.6) and the radial integrals appearing in eqs. (4.15) and (4.16). Here, $B(q,i)$ represents the generalized Breit interaction given by eq. (2.27). In practice, an operator that is slightly more complicated than $B(q,i)$ is used in our approach to atomic structure and electron-impact excitation. Instead of using $B(q,i)$, we replace it by the sum of two similar terms that differ only in their value of ω. It is convenient to describe this operator, denoted by the symbol B_{qi}, by considering its matrix element between pairs of Dirac spinors, i.e. the bound and continuum wave functions appearing in eqs. (2.6) and (4.9), respectively. If we let $|a_q\rangle$ represent the spinor $|a\rangle$ evaluated at coordinate q, then such a matrix element can be written in the shorthand notation

$$\langle a_q b_i | B_{qi} | c_q d_i \rangle = \langle a_q b_i | \tfrac{1}{2} \{ B_{\omega_{ca}}(q,i) + B_{\omega_{db}}(q,i) \} | c_q d_i \rangle \,, \tag{4.77}$$

where the wavenumbers ω_{ca} and ω_{db} denote the exchange of a virtual photon between two different pairs of spinors. For example, $\omega_{ca} = |\epsilon_c - \epsilon_a|/2c$, where c is the speed of light and ϵ_c, ϵ_a are the one-electron energies (in Rydbergs)

associated with spinors $|c\rangle$, $|a\rangle$, respectively. The operator $B_\omega(q,i)$ is the same as $B(q,i)$ in eq. (2.27), with the ω dependence stated explicitly.

The advantage in using B_{qi} is that it is valid for off-diagonal matrix elements as well as diagonal elements. On the other hand, $B(q,i)$ is valid only for diagonal elements and is equivalent to B_{qi} when $\omega_{ca} = \omega_{bd}$. Mittleman [61] derived this new operator by using a succession of contact transformations to decouple the electron and radiation fields and it is claimed to be correct to $O(\alpha^2)$ [19]. Use of B_{qi} will also take into account part of the fourth-order effects (two-photon exchange) [21]. In this work, however, only single-photon exchange is included in its entirety.

Upon implementing the substitutions that are implied by eqs. (4.76) and (4.77), the derivation proceeds in a manner very similar to that given for the Coulomb interaction in section 4.2 (non-factorized method) or section 4.3 (factorization method). The next two subsections are devoted to the treatment of these approaches.

4.10.1 Non-factorized method including the generalized Breit interaction

The non-factorized approach uses the angular package of McKenzie, Grant and Norrington [11] when evaluating the Breit contribution to the right-hand side of eq. (4.6), after the substitutions given by eqs. (4.76) and (4.77) have been performed. There are also two types of direct radial integrals that arise, analogous to the Slater integrals appearing in eq. (4.17). Using the notation of Grant and Pyper [19] and Grant and McKenzie [20], we write these integrals as

$$R^\nu(ac,bd) = \int_0^\infty \int_0^\infty \rho_{ac}(r_1)\,[\,V_\nu(r_1,r_2;\omega_{ac}) + V_\nu(r_1,r_2;\omega_{bd})]\rho_{bd}(r_2)\,\mathrm{d}r_1\,\mathrm{d}r_2 \tag{4.78}$$

and

$$S^k(ac,bd) = \int_0^\infty \int_0^\infty \rho_{ac}(r_1)\,[\,W_{k-1,k+1,k}(r_1,r_2;\omega_{ac}) + W_{k-1,k+1,k}(r_1,r_2;\omega_{bd})]\rho_{bd}(r_2)\,\mathrm{d}r_1\,\mathrm{d}r_2, \tag{4.79}$$

where the density $\rho_{ac}(r)$ is given by

$$\rho_{ac}(r) = P_a(r)Q_c(r) \tag{4.80}$$

with a similar expression for $\rho_{bd}(r)$. For the process of excitation considered here, orbitals a and c represent bound electrons while orbitals b and d represent free electrons. So, for example, $a \equiv n_a l_a j_a$ and $b \equiv \epsilon l j$, in the notation of eq. (4.17). For the structure calculations discussed in section 2.5, all four indices represent bound orbitals. A corresponding set of exchange integrals, analogous to those appearing in eq. (4.18), can be obtained by making the exchange $c \leftrightarrow d$ in the above equations.

The wavenumbers appearing in eqs. (4.78) and (4.79) are given by $\omega_{xy} = |\epsilon_x - \epsilon_y|/2c$, where c is the speed of light, and ϵ_x and ϵ_y are the one-electron spinor energies (in Rydbergs) associated with radial functions (P_x, Q_x) and (P_y, Q_y), respectively. The V and W functions are given by

$$V_\nu(r_1, r_2; \omega) = [\nu]\omega j_\nu(\omega r_<) n_\nu(\omega r_>)\,, \qquad r_</r_> = \min/\max(r_1, r_2) \tag{4.81}$$

and

$$W_{k-1,k+1,k}\,(r_1, r_2; \omega) = \begin{cases} [k]\omega j_{k-1}(\omega r_1) n_{k+1}(\omega r_2) + \dfrac{[k]^2}{\omega^2}\dfrac{r_1^{k-1}}{r_2^{k+2}}, & r_1 < r_2 \\ [k]\omega n_{k-1}(\omega r_1) j_{k+1}(\omega r_2), & r_1 > r_2\ , \end{cases} \tag{4.82}$$

where j_ν and n_ν are spherical Bessel functions of the first and second kind, respectively, and $[x] \equiv (2x+1)$.

Note, however, that the integrals appearing in eqs. (4.78) and (4.79) have no imaginary part, and yet the generalized Breit interaction in eq. (2.27) is complex. In fact, there is an additional set of integrals, very similar to R^ν and S^k, to be considered. Expressions for these additional integrals can be obtained by retaining all terms in eqs. (4.81) and (4.82) that contain spherical Bessel functions of the second kind, and then making the simple substitution $n_\nu \rightarrow -\mathrm{i} j_\nu$ in those terms. The explanation for this substitution becomes apparent when considering the expansion [62]

$$\frac{\exp(\mathrm{i}\omega r_{12})}{r_{12}} = \mathrm{i}\omega \sum_{\nu=0}^{\infty} [\nu]\, j_\nu(\omega r_<)\, [\, j_\nu(\omega r_>) + \mathrm{i} n_\nu(\omega r_>)] \times [\boldsymbol{C}^{(\nu)}(\hat{\mathbf{r}}_1) \cdot \boldsymbol{C}^{(\nu)}(\hat{\mathbf{r}}_2)]\,. \tag{4.83}$$

In atomic structure calculations, this imaginary part of the interaction is usually ignored when calculating energies and is attributed to the lifetime of a bound state [2]. However, the collision strength in eq. (4.6) allows for a scattering interaction that is complex and, consequently, these additional integrals should be considered for the process of excitation. The effect of this imagi-

nary contribution on the collision strength is typically small, as demonstrated below.

We are also interested in collision strengths that are computed with the original Breit interaction, eq. (2.28), which is accurate up to intermediate-Z values, but breaks down for sufficiently high-Z ions, as will be seen shortly. As mentioned in section 2.5, this interaction is the $\omega \rightarrow 0$ limit of the generalized Breit interaction. Therefore, the angular algebra is basically unchanged from that described above, but the V and W functions must be modified according to

$$V_\nu(r_1, r_2; \omega) \rightarrow r_<^\nu / r_>^{\nu+1} \tag{4.84}$$

and

$$W_{\nu-1,\nu+1,\nu}(r_1, r_2; \omega) \rightarrow -\frac{1}{2}[\nu][\overline{U}_{\nu-1}(r_1, r_2) - \overline{U}_{\nu+1}(r_1, r_2)], \tag{4.85}$$

where

$$\overline{U}_\nu(r_1, r_2) = \begin{cases} r_1^\nu / r_2^{\nu+1} & \text{if } r_1 < r_2 \\ 0 & \text{if } r_1 > r_2. \end{cases} \tag{4.86}$$

The resulting radial integrals are considerably simpler than those associated with the generalized Breit interaction and, therefore, require significantly less computing time to evaluate. Also, the Breit interaction has the additional simplification that it is independent of ω and, consequently, does not need to be split into two terms, as was done in eq. (4.77) for the generalized Breit interaction.

As far as actual calculations are concerned, it appears that Walker was the first person to compute detailed excitation cross sections that included the Breit and Møller interactions [63]. These results concerned hydrogenic ions and comparisons of our RDW (Z^4-scaled) cross sections with those provided by Walker displayed excellent agreement between the two sets of calculations [59]. Subsequent to Walker, hydrogenic results that included the Møller interaction were also computed by Pindzola, Moores and coworkers [64,65], providing us with additional opportunities to test our RDW calculations. Once again, the agreement was found to be excellent when comparing collision strengths at the appropriate impact energies [59].

However, the goal of our approach, with respect to the generalized Breit interaction, was to produce a completely general capability that would include this interaction in the excitation scattering matrix elements for an arbitrary number of bound electrons. Therefore, we also provided collision strengths for

Table 5
Collision strengths for the six $n = 1$ to $n = 2$ transitions from the ground state of He-like ions with $Z = 26$, 54 and 92. The final scattered energies are 70 eV, 300 eV and 1000 eV, respectively. $x[y] = x \times 10^y$.

Transition	C	B	GB	GBI
		$Z = 26$		
$1s^2$ - $(1s2s)_0$	7.687[-4]	8.102[-4]	8.101[-4]	8.101[-4]
$1s^2$ - $(1s2s)_1$	3.626[-4]	3.600[-4]	3.604[-4]	3.604[-4]
$1s^2$ - $(1s2p^*)_0$	2.267[-4]	2.108[-4]	2.108[-4]	2.108[-4]
$1s^2$ - $(1s2p^*)_1$	8.079[-4]	8.140[-4]	8.143[-4]	8.143[-4]
$1s^2$ - $(1s2p)_1$	2.122[-3]	2.077[-3]	2.077[-3]	2.077[-3]
$1s^2$ - $(1s2p)_2$	1.065[-3]	1.082[-3]	1.083[-3]	1.083[-3]
		$Z = 54$		
$1s^2$ - $(1s2s)_0$	2.260[-4]	2.777[-4]	2.772[-4]	2.773[-4]
$1s^2$ - $(1s2s)_1$	9.931[-5]	1.046[-4]	1.062[-4]	1.066[-4]
$1s^2$ - $(1s2p^*)_0$	6.211[-5]	4.468[-5]	4.474[-5]	4.477[-5]
$1s^2$ - $(1s2p^*)_1$	2.854[-4]	3.016[-4]	3.055[-4]	3.058[-4]
$1s^2$ - $(1s2p)_1$	4.113[-4]	3.769[-4]	3.798[-4]	3.804[-4]
$1s^2$ - $(1s2p)_2$	2.332[-4]	2.548[-4]	2.579[-4]	2.580[-4]
		$Z = 92$		
$1s^2$ - $(1s2s)_0$	1.503[-4]	2.321[-4]	2.311[-4]	2.319[-4]
$1s^2$ - $(1s2s)_1$	5.531[-5]	8.456[-5]	8.961[-5]	9.198[-5]
$1s^2$ - $(1s2p^*)_0$	3.383[-5]	1.198[-5]	1.246[-5]	1.289[-5]
$1s^2$ - $(1s2p^*)_1$	1.194[-4]	1.815[-4]	1.965[-4]	1.997[-4]
$1s^2$ - $(1s2p)_1$	1.156[-4]	9.763[-5]	1.041[-4]	1.087[-4]
$1s^2$ - $(1s2p)_2$	6.474[-5]	9.128[-5]	1.009[-4]	1.016[-4]

He-like and Li-like ions in ref. [59]. A sample of these results are provided in table 5 for the six $n = 1$ to $n = 2$ collision strengths from the ground state of He-like ions, with $Z = 26$, 54 and 92, and for near-threshold impact energies. The levels appearing in this table are described with the same notation that was used in table 1. The four columns of data in this table display collision strengths that were calculated with the Coulomb interaction (labeled C), with inclusion of the Breit interaction (labeled B), with inclusion of the real part of the generalized Breit interaction (labeled GB) and with inclusion of the real+imaginary parts of the generalized Breit interaction (labeled GBI).

The He-like data presented in table 5 exhibit the same trends that were observed for the H-like and Li-like data that were also provided in ref. [59]. The obvious main conclusion is that inclusion of the generalized Breit interaction has a significant impact on the collision strengths and, as expected, the importance of this interaction increases with Z. For example, the GBI results are greater than the Coulomb-only results by more than 50% for $Z = 92$ for a majority of the transitions. Another important conclusion is that the imaginary portion of the generalized Breit interaction does not produce a large contri-

bution to the collision strength, even for high-Z ions. For example, neglect of the imaginary part produces a maximum difference of 4.5% when comparing the GB and GBI data for $Z = 92$. This finding is of practical importance because the majority of the time required to calculate the collision strengths is taken up by the evaluation of the Breit integrals. Exclusion of the imaginary integrals reduces the total computing time by almost a factor of two. As for collision strengths computed with the original Breit interaction, which results from taking the $\omega = 0$ limit of the generalized Breit interaction, these results are found to be accurate for ions with intermediate-Z values, such as $Z = 54$. However, appreciable differences, on the order of 10%, are encountered when comparing the Breit-interaction (B) data with the GB data for $Z = 92$.

An unexpected conclusion that resulted from this work was that the inclusion of the generalized Breit interaction in the scattering matrix elements appeared to have a somewhat larger effect on collision strengths associated with more complex ions than for hydrogenic ions. For example, the near-threshold results for the 1s-2p* and 1s-2p transitions in H-like ions with $Z = 54$ were found to be affected by less than 1%. On the other hand, the collision strengths for one of the four analogous transitions in He-like ions with this same Z value was decreased by 28% and those associated with the remaining transitions were changed by $\pm 7\%$ and 11%. Of course, as one would expect, results obtained by summing these He-like data over the J values associated with the final levels exhibited decreased sensitivity to the various forms of the Breit interaction, very similar to the observed behavior for the corresponding results for hydrogenic ions. The explanation of this behavior is that the various forms of the Breit interaction do affect certain individual matrix elements appreciably, even for rather low-Z values, but the effect is largely canceled upon summation over a significant number of quantum numbers. For additional details concerning the effect of the various forms of the Breit interaction on collision strength calculations, the reader should consult ref. [59].

A comparison of our excitation data with experimental results for xenon ($Z = 54$) ions is also available. A comparison between our calculated cross sections and EBIT measurements performed at Lawrence Livermore National Laboratory (LLNL) was carried out by Beiersdorfer's group [66] for H-like and He-like xenon ions. For this moderately heavy element, the generalized Breit interaction was again found to exhibit a strong effect for certain transitions. Here, we reproduce tabular data from ref. [66] as table 6, in which three sets of distorted-wave results are compared with each other and against the EBIT-measured values for an incident energy of 112 keV, which is considerably greater than the energies considered in table 5. One set of the distorted-wave calculations was made in the non-relativistic approximation (our structure and collisional excitation codes include a non-relativistic option), while two of the data sets represent our relativistic (RDW) calculations. Furthermore, one of those relativistic calculations also included the generalized Breit interaction

in obtaining the scattering matrix elements.

Table 6
Comparison between measured (σ_{EE}) and calculated electron-impact excitation cross sections for H-like and He-like xenon ions at an excitation energy of 112 keV. The calculated cross sections produced by our distorted-wave code are: non-relativistic (denoted by $\sigma_{non-rel}$), relativistic (denoted by σ_{rel}) and relativistic plus the generalized Breit interaction (denoted by σ_{GBI}). All cross sections are provided in barns.

Line	σ_{EE}	$\sigma_{non-rel}$	σ_{rel}	σ_{GBI}
Ly-α_1	8.6 ± 1.5		8.256	8.109
Ly-$\alpha_{2,3}$	8.2 ± 3.4		6.541	6.787
w	7.0 ± 2.0	21.64	17.45	8.364
y	3.9 ± 1.5	0.127	7.313	3.842
z	1.08 ± 0.48	0.123	0.172	0.152

In this table, cross sections are presented for three H-like transitions and three He-like transitions for xenon ions. The three H-like transitions,

$$2p\,^2P_{3/2} \rightarrow 1s \quad \text{or} \quad 2p_{3/2} \rightarrow 1s_{1/2}\,,$$
$$2p\,^2P_{1/2} \rightarrow 1s \quad \text{or} \quad 2p_{1/2} \rightarrow 1s_{1/2}\,,$$
$$2s\,^2S_{1/2} \rightarrow 1s \quad \text{or} \quad 2s_{1/2} \rightarrow 1s_{1/2}\,,$$

are denoted by Ly-α_1, Ly-α_2 and Ly-α_3, respectively. (We note that the Ly-α_2 and Ly-α_3 lines appear as overlapping features in the EBIT experiment.) The three He-like transitions,

$$2\,^1P_1 \rightarrow 1\,^1S_0 \quad \text{or} \quad (1s2p)_1 \rightarrow (1s^2)_0\,,$$
$$2\,^3P_1 \rightarrow 1\,^1S_0 \quad \text{or} \quad (1s2p^*)_1 \rightarrow (1s^2)_0\,,$$
$$2\,^3S_1 \rightarrow 1\,^1S_0 \quad \text{or} \quad (1s2s)_1 \rightarrow (1s^2)_0\,.$$

are typically referred to as the w, y and z lines, respectively. The importance of relativistic effects for these cross sections is obvious when comparing the non-relativistic and relativistic data. For example, the relativistic cross section for the y line is more than a factor of 50 larger than the corresponding non-relativistic value.

In addition, the combination of a large incident energy for the continuum electron scattering off relativistic bound electrons produces a significant contribution from the generalized Breit interaction for some of the transitions. The relativistic cross section for the y line is reduced by about a factor of two

in this case, bringing the calculated value in excellent agreement with the experimental value. A similar, dramatic improvement in the agreement between theory and experiment is also observed for the w line when the cross sections are computed with the generalized Breit interaction. We note that the generalized Breit interaction affects the cross sections for these two transitions much more strongly for these conditions, in contrast to the trends observed when comparing C versus GBI results for the same two transitions in table 5. This difference underscores the sensitivity of the cross section to the generalized Breit interaction as a function of impact energy. In table 5, the incident energy was very close to the threshold value for these $n = 1$ to $n = 2$ transitions, while in table 6 the incident energy was approximately four times the threshold value. Returning to the remaining transitions in table 6, all of the calculations for the z cross section display rather poor agreement with experiment, while both sets of relativistic calculations of the hydrogenic, Ly-α data agree reasonably well with each other and with experiment. A possible explanation for this discrepancy is due to the inclusion of cascade effects in the experimental data. The z line is a result of emission from the lowest lying, metastable $n = 2$ level, which is the most sensitive to cascade effects. As noted in the previous analysis of the data in table 5, the hydrogenic cross sections in table 6 display considerably less sensitivity to the generalized Breit interaction than the He-like results.

4.10.2 Factorization method including the generalized Breit interaction

The motivation for adapting the factorization method described in section 4.3 to include the generalized Breit interaction was to further explore the effects of this interaction in more complex ions. An increase in the number of bound electrons in the target ion typically leads to a corresponding increase in the amount of angular coupling that is required to describe the levels involved in a given transition. Another motivation was that the factorization method provides an efficient means to compute large amounts of collision-strength data that are required for plasma modeling efforts.

The method for including the generalized Breit interaction in the factorization method is relatively straightforward. The details have been provided in ref. [60] and only a summary is given here. When the generalized Breit interaction is included in the scattering matrix elements, the resulting collision strength can be expressed in the same compact form given by eq. (4.31). The expression for the B^λ coefficients remains unchanged, but the expression for Q^λ in eq. (4.32) must be replaced with

$$Q^\lambda(n_a l_a j_a, n'_a l'_a j'_a; n_{a_1} l_{a_1} j_{a_1}, n'_{a_1} l'_{a_1} j'_{a_1})$$

$$= \sum_{\substack{l,l' \\ j,j'}} \{ \mathrm{Re}[P^\lambda(n_a l_a j_a \epsilon l j; n'_a l'_a j'_a \epsilon' l' j')] \times \mathrm{Re}[P^\lambda(n_{a_1} l_{a_1} j_{a_1} \epsilon l j; n'_{a_1} l'_{a_1} j'_{a_1} \epsilon' l' j')] + \mathrm{Im}[P^\lambda(n_a l_a j_a \epsilon l j; n'_a l'_a j'_a \epsilon' l' j')] \times \mathrm{Im}[P^\lambda(n_{a_1} l_{a_1} j_{a_1} \epsilon l j; n'_{a_1} l'_{a_1} j'_{a_1} \epsilon' l' j')] \}, \quad (4.87)$$

where $\mathrm{Re}[\cdots]$ and $\mathrm{Im}[\cdots]$ indicate that the real and imaginary parts of their respective arguments are to be taken. In the following discussion, we consider the complex interaction that appears in eq. (4.76). The generalization that is necessary to consider the more complicated interaction in eq. (4.77) is straightforward. The real portion of P^λ can be written in a form that is very similar to the Coulomb-only expression in eq. (4.33). Namely,

$$\begin{aligned}\mathrm{Re}[P^\lambda(n_a l_a j_a \epsilon l j; n'_a l'_a j'_a \epsilon' l' j')] &= (2\lambda+1)^{-1/2} \langle j_a || \boldsymbol{C}^{(\lambda)} || j'_a \rangle \langle j || \boldsymbol{C}^{(\lambda)} || j' \rangle (D^\lambda + D_1^\lambda + D_2^\lambda) \\ &\quad + \sum_\tau (-1)^{\lambda+\tau} (2\lambda+1)^{1/2} \langle j_a || \boldsymbol{C}^{(\tau)} || j' \rangle \langle j || \boldsymbol{C}^{(\tau)} || j'_a \rangle \\ &\quad \times \begin{Bmatrix} j_a & j' & \tau \\ j & j'_a & \lambda \end{Bmatrix} (E^\tau + E_1^\tau + E_2^\tau), \quad (4.88)\end{aligned}$$

where the arguments of the D and E integrals have been suppressed for convenience. The D^λ and E^τ integrals are identical to those appearing in eq. (4.33) for the Coulomb-only case (see eqs. (4.17) and (4.18) for explicit expressions), while the subscripted integrals arise from the generalized Breit interaction. Here, we present expressions for all of the direct integrals (with their respective arguments) in a single, consistent notation according to

$$\begin{aligned}D^\lambda(n_a \kappa_a \epsilon \kappa; n'_a \kappa'_a \epsilon' \kappa') &= \int_0^\infty \int_0^\infty \mathrm{d}r_1 \mathrm{d}r_2 \, r_1^2 r_2^2 [R_{a,+1}(r_1) R_{a',+1}(r_1) + R_{a,-1}(r_1) R_{a',-1}(r_1)] \\ &\quad \times \frac{r_<^\lambda}{r_>^{\lambda+1}} [R_{\epsilon,+1}(r_2) R_{\epsilon',+1}(r_2) + R_{\epsilon,-1}(r_2) R_{\epsilon',-1}(r_2)], \quad (4.89)\end{aligned}$$

$$\begin{aligned}&D_1^\lambda(n_a \kappa_a \epsilon \kappa; n'_a \kappa'_a \epsilon' \kappa') \\ &= \sum_{\nu=\lambda-1}^{\lambda+1} v_{\nu\lambda} \sum_{\beta,\beta'=\pm 1} (-\beta\beta') E^\nu_{-\beta}(\kappa_a, \kappa'_a; \lambda) \Pi(\kappa_a, \kappa'_a, \nu) E^\nu_{-\beta'}(\kappa, \kappa'; \lambda) \Pi(\kappa, \kappa', \nu) \\ &\times \int_0^\infty \int_0^\infty \mathrm{d}r_1 \mathrm{d}r_2 \, r_1^2 r_2^2 \, V_\nu(r_1, r_2; \omega) R_{a,\beta}(r_1) R_{a',-\beta}(r_1) R_{\epsilon,\beta'}(r_2) R_{\epsilon',-\beta'}(r_2) \quad (4.90)\end{aligned}$$

and

$$
\begin{aligned}
&D_2^{\lambda}(n_a\kappa_a\epsilon\kappa; n'_a\kappa'_a\epsilon'\kappa') \\
&\quad = \omega_\lambda \Bigg\{ \sum_{\beta,\beta'=\pm 1} (-\beta\beta') E_{-\beta}^{\lambda-1}(\kappa_a, \kappa'_a; \lambda)\Pi(\kappa_a, \kappa'_a, \lambda-1) \\
&\qquad\qquad \times E_{-\beta'}^{\lambda+1}(\kappa, \kappa'; \lambda)\Pi(\kappa, \kappa', \lambda+1) \\
&\qquad \times \int_0^\infty \int_0^\infty \mathrm{d}r_1 \mathrm{d}r_2\, r_1^2\, r_2^2\, W_{\lambda-1,\lambda+1,\lambda}(r_1, r_2; \omega) \\
&\qquad\qquad \times R_{a,\beta}(r_1) R_{a',-\beta}(r_1) R_{\epsilon,\beta'}(r_2) R_{\epsilon',-\beta'}(r_2) \\
&\qquad\qquad + [(\lambda+1) \leftrightarrow (\lambda-1)] \Bigg\}. \quad (4.91)
\end{aligned}
$$

The corresponding exchange integrals are obtained by making the usual exchange of coordinates in the direct integrals, i.e.

$$
E^\tau \equiv E^\tau(n_a\kappa_a\epsilon\kappa; n'_a\kappa'_a\epsilon'\kappa') = D^\tau(n_a\kappa_a\epsilon\kappa; \epsilon'\kappa' n'_a\kappa'_a), \quad (4.92)
$$

with similar expressions for E_1^τ and E_2^τ.

In eqs. (4.89)–(4.91), $R_{a,\beta}(r)$ is $1/r$ times the large (small) component of the radial wave function of the bound orbital $a \equiv n_a l_a j_a$, if $\beta = +1$ (-1). A similar statement holds for the continuum orbitals labeled $\epsilon \equiv \epsilon l j$, where ϵ is the electron kinetic energy. The functions V and W contain the radial pieces of the generalized Breit interaction and are given by eqs. (4.81) and (4.82), respectively. The remaining symbols, $v_{\nu\lambda}$, ω_λ, $E_{-\beta}^{\nu}(\kappa_a, \kappa'_a; \lambda)$ and $\Pi(\kappa_a, \kappa'_a, \nu)$ are simple numerical factors, all of which can be found in ref. [19]. The notation $[(\lambda+1) \leftrightarrow (\lambda-1)]$ in eq. (4.91) indicates that the entire summation to the left of the preceding plus sign should be repeated with the λ expressions exchanged.

All that remains is to define the imaginary part of P^λ. An expression for $\mathrm{Im}[P^\lambda]$ is obtained by discarding D^λ and E^τ in eq. (4.88) and then replacing the remaining Breit integrals with their imaginary counterparts. The imaginary Breit integrals are identical to those given in eqs. (4.90) and (4.91), except that the following two modifications must be performed: (1) the second term appearing in the first line of the expression for the W function in eq. (4.82), which does not contain any Bessel functions, must be discarded and (2) the substitution $n_\nu \rightarrow -ij_\nu$ must be made in all of the remaining terms that appear in the V and W functions, in accord with the discussion surrounding eq. (4.83) of the previous subsection.

As an application of the factorized form of the Breit interaction, we present table 7, which contains collision strengths for the 36 $n = 2$ to $n = 3$ transitions from the ground state of Ne-like uranium. These data were originally presented

Table 7
Collision strengths for $n = 2$ to $n = 3$ transitions from the ground state of Ne-like uranium. An explanation of the labels used for the levels appearing in each transition is provided in ref. [60]. $x[y] = x \times 10^y$.

Transition	ΔE(Ry)	$\epsilon' = 150$ eV			$\epsilon' = 30000$ eV		
		C	GB	GBI	C	GB	GBI
A1 - B1	1047.8	2.568[-3]	2.705[-3]	2.705[-3]	3.196[-3]	3.295[-3]	3.295[-3]
A1 - B2	1252.1	1.087[-3]	1.151[-3]	1.151[-3]	1.324[-3]	1.377[-3]	1.377[-3]
A1 - B3	1286.5	1.184[-3]	1.264[-3]	1.264[-3]	1.539[-3]	1.603[-3]	1.603[-3]
A1 - C1	960.5	1.435[-4]	1.205[-4]	1.206[-4]	3.815[-5]	3.439[-5]	3.439[-5]
A1 - C2	1040.7	1.708[-4]	2.013[-4]	2.014[-4]	4.359[-5]	7.814[-5]	7.814[-5]
A1 - C3	1246.7	1.301[-4]	1.413[-4]	1.413[-4]	3.842[-5]	4.719[-5]	4.720[-5]
A1 - C4	1282.6	1.033[-4]	1.121[-4]	1.122[-4]	2.890[-5]	3.672[-5]	3.673[-5]
A1 - C5	1328.1	1.377[-4]	1.099[-4]	1.100[-4]	4.153[-5]	3.526[-5]	3.527[-5]
A1 - C6	1395.3	1.025[-4]	9.760[-5]	9.761[-5]	2.687[-5]	2.803[-5]	2.803[-5]
A1 - D1	960.5	3.500[-4]	3.690[-4]	3.690[-4]	3.902[-4]	4.131[-4]	4.131[-4]
A1 - D2	1041.9	1.986[-4]	1.841[-4]	1.842[-4]	2.109[-4]	2.152[-4]	2.152[-4]
A1 - D3	1328.0	1.566[-4]	1.682[-4]	1.682[-4]	1.030[-4]	1.140[-4]	1.140[-4]
A1 - D4	1395.6	3.975[-4]	4.406[-4]	4.406[-4]	6.450[-4]	6.985[-4]	6.985[-4]
A1 - D5	1413.9	5.757[-4]	5.797[-4]	5.797[-4]	1.129[-3]	1.150[-3]	1.150[-3]
A1 - E1	1040.6	2.831[-4]	3.175[-4]	3.175[-4]	6.575[-5]	8.430[-5]	8.431[-5]
A1 - E2	1412.5	2.201[-4]	2.406[-4]	2.407[-4]	5.372[-5]	6.821[-5]	6.821[-5]
A1 - F1	1056.2	1.540[-4]	1.214[-4]	1.214[-4]	3.398[-5]	2.542[-5]	2.542[-5]
A1 - F2	1231.6	2.169[-5]	2.152[-5]	2.154[-5]	6.991[-6]	6.355[-6]	6.358[-6]
A1 - F3	1298.7	2.714[-5]	2.411[-5]	2.413[-5]	7.605[-6]	6.067[-6]	6.070[-6]
A1 - G1	945.5	2.481[-4]	2.418[-4]	2.422[-4]	8.034[-4]	7.814[-4]	7.819[-4]
A1 - G2	1057.1	6.699[-4]	6.401[-4]	6.404[-4]	8.399[-4]	8.078[-4]	8.083[-4]
A1 - G3	1078.3	6.175[-3]	5.777[-3]	5.782[-3]	1.326[-2]	1.261[-2]	1.261[-2]
A1 - G4	1231.9	6.625[-5]	8.194[-5]	8.207[-5]	8.365[-5]	9.395[-5]	9.404[-5]
A1 - G5	1298.6	3.007[-4]	2.890[-4]	2.896[-4]	7.558[-4]	7.199[-4]	7.208[-4]
A1 - G6	1346.1	1.818[-3]	1.682[-3]	1.684[-3]	3.796[-3]	3.573[-3]	3.576[-3]
A1 - G7	1379.8	7.075[-5]	7.986[-5]	8.029[-5]	2.893[-4]	2.907[-4]	2.914[-4]
A1 - H1	944.6	1.318[-4]	1.457[-4]	1.458[-4]	3.579[-5]	4.285[-5]	4.286[-5]
A1 - H2	1057.9	2.350[-4]	2.097[-4]	2.097[-4]	3.921[-5]	3.605[-5]	3.605[-5]
A1 - H3	1074.7	3.540[-4]	3.893[-4]	3.893[-4]	6.722[-5]	1.027[-4]	1.027[-4]
A1 - H4	1344.1	1.708[-4]	1.768[-4]	1.768[-4]	3.707[-5]	4.464[-5]	4.464[-5]
A1 - H5	1361.8	2.428[-4]	2.380[-4]	2.380[-4]	5.447[-5]	5.996[-5]	5.996[-5]
A1 - H6	1379.2	8.746[-5]	9.309[-5]	9.316[-5]	2.730[-5]	3.154[-5]	3.155[-5]
A1 - I1	1056.9	3.493[-4]	4.101[-4]	4.101[-4]	2.709[-4]	3.014[-4]	3.014[-4]
A1 - I2	1075.7	2.211[-4]	2.171[-4]	2.171[-4]	1.778[-4]	1.830[-4]	1.830[-4]
A1 - I3	1362.0	1.828[-4]	1.890[-4]	1.890[-4]	1.359[-4]	1.457[-4]	1.457[-4]
A1 - J1	1073.9	4.499[-4]	4.972[-4]	4.972[-4]	8.006[-5]	1.018[-4]	1.018[-4]

in ref. [60] and the level labeling scheme can be found in Table I of that reference. The column headings have the same meanings as those used in table 5 of the previous subsection in order to facilitate comparisons between calculations that considered only the Coulomb interaction and those that included various forms of the Breit interaction. The collision strengths are provided for two different kinetic energies of the scattered electron; a value of $\epsilon' = 150$ eV corresponds to the near-threshold region, while a value of $\epsilon' = 30000$ eV corresponds to an impact energy of about three times threshold.

First, we note that there is very little difference between the GB and GBI results presented in table 7, reinforcing the notion that the imaginary part of the generalized Breit interaction is not very important for obtaining accurate values of the collision strengths, even for high-Z ions. Next, we note that, since the transitions considered in table 7 refer to $n = 2$ to $n = 3$ transitions, the bound and continuum energies involved are somewhat less than those encoun-

tered for the $n = 1$ to $n = 2$ transitions for He-like uranium in the previous subsection. Therefore, the effect of the generalized Breit interaction is also expected to have less of an effect on the collision strengths. In fact, this trend is observed for the strongest transitions that are listed in the table, for which the GB results typically differ by, at most, a few percent from the Coulomb-only data. However, for those collision strengths that are approximately two orders of magnitude or more smaller than the largest values, the effect can be quite large. For example, the GB results are enhanced by 79% and 53% for the A1-C2 and A1-H3 transitions at $\epsilon' = 30000$ eV, and the interaction has more than a 10% effect for nearly half of all transitions. However, since the effect is strong only for such weak transitions, the importance to plasma modeling is not expected to be significant when considering excitation processes that involve $n = 2$ to $n = 3$ transitions. On the other hand, our results presented in the previous subsection, along with our work in refs. [59] and [60], indicate that the generalized Breit interaction should typically be included for excitation from the 1s subshell for all but low-Z values.

4.11 A summary of completed fine-structure excitation calculations

In this section, we summarize our production work that involved the calculation of collision strengths for various iso-electronic sequences. These calculations were performed by applying the fully relativistic distorted-wave methods described in the previous sections. These results have been published in Atomic Data and Nuclear Data Tables and include:

(1) 88 transitions from the ground level to $n = 3$ and $n = 4$ levels in 71 Ne-like ions with $22 \leq Z \leq 92$ [67];
(2) 3 transitions among $n = 2$ levels and 63 transitions from these levels to $n = 3$, $n = 4$ and $n = 5$ levels in 85 Li-like ions with $8 \leq Z \leq 92$ [68];
(3) 10 transitions among $n = 3$ levels and 80 transitions from these levels to $n = 4$ and $n = 5$ levels in 71 Na-like ions with $22 \leq Z \leq 92$ [69];
(4) 21 transitions among $n = 4$ levels and 63 transitions from these levels to $n = 5$ levels in 33 Cu-like ions with $60 \leq Z \leq 92$ [70];
(5) 3 transitions among $n = 2$ levels and 327 transitions from these levels to $n = 3$ levels in 71 F-like ions with $22 \leq Z \leq 92$ [38];
(6) 248 transitions from the ground level to $n = 4$ and $n = 5$ levels in 33 Ni-like ions with $60 \leq Z \leq 92$ [71];
(7) 45 $\Delta n = 0$ transitions with $n = 2$ in 85 Be-like ions with $8 \leq Z \leq 92$ [72];
(8) 105 $\Delta n = 0$ transitions with $n = 2$ in 85 B-like ions with $8 \leq Z \leq 92$ [73];
(9) Approximately 1650 $n = 2 - 3$ transitions in 85 B-like ions with $8 \leq Z \leq 92$ (only results for $Z = 14$, 26, 42 and 64 were published explicitly; all

data were made available in electronic format) [74];

(10) 185 $\Delta n = 0$ transitions with $n = 2$ in 46 C-like ions with $9 \leq Z \leq 54$ (only results for 32 Z values were published explicitly; all data were made available in electronic format) [75];

(11) Approximately 4000 $n = 2 - 3$ transitions in 46 C-like ions with $9 \leq Z \leq 54$ (only results for $Z = 12$, 26 and 54 were published explicitly; all data were made available in electronic format) [76];

(12) 105 $\Delta n = 0$ transitions with $n = 2$ in 81 N-like ions with $12 \leq Z \leq 92$ [77];

(13) 45 $\Delta n = 0$ transitions with $n = 2$ in 79 O-like ions with $14 \leq Z \leq 92$ [78].

We will refer to these publications according to the serial numbers listed above. For example, Paper 1 refers to the first publication on Ne-like ions [67]. The calculations were usually made for six scattered electron energies, in units of $Z_{\rm eff}^2$ Rydbergs, with

$$Z_{\rm eff} = Z - (5/6)(N-1)\,, \tag{4.93}$$

where N is the number of the bound electrons per ion. For example, in Papers 1, 2 and 5, for Ne-, Li- and F-like ions, respectively, the six energies were

$$\epsilon' = 0.008,\ 0.04,\ 0.1,\ 0.21,\ 0.41 \text{ and } 0.75\,, \tag{4.94}$$

and in Papers 7, 8, 10, 12 and 13, for the $\Delta n = 0$ transitions in Be-, B-, C-, N- and O-like ions, respectively, the energies were

$$\epsilon' = 0.03,\ 0.08,\ 0.2,\ 0.42,\ 0.80 \text{ and } 1.40\,. \tag{4.95}$$

For the six energies used in other publications, please see the corresponding references.

The procedures used in all of these large-scale calculations are very similar, with a few variations that are described below. In the earliest publications (Papers 1–6) we used our fully relativistic structure code, as described in chapter 2, to obtain bound orbital wave functions, level energies, mixing coefficients and line strengths or oscillator strengths. The potential used in obtaining the radial functions is the Dirac-Fock-Slater potential, given by eqs. (2.18)–(2.20). As stated previously, this potential is determined from a different set of fractional occupation numbers for each class of transitions. For the set, or sets, of fractional occupation numbers used in these calculations, the reader is referred to the respective publications. Since the same potential is used in determining

the radial functions for all bound and free electrons associated with a particular class of transitions, the resulting set of orbitals is automatically orthogonal and exchange can be handled in a simple, consistent manner. In the latter two of these earliest publications (Papers 5 and 6), the structure calculations also included the generalized Breit interaction and other corrections described in section 2.5.

As mentioned in Paper 7, and chapter 3 of the present work, our structure code introduced some slight numerical error in treating transitions involving s orbitals in ions with very large Z values. This discrepancy appeared to have a negligible effect on most oscillator strengths and collision strengths presented in Papers 1–6. A notable exception occurred in some $\Delta n = 0$ transitions in Papers 2–4, for which the transition energies differed significantly from those computed with the Grant code [6]. For this reason, energies calculated with the Grant code were used for the $\Delta n = 0$ transitions considered in Paper 5. Also for this reason, in Papers 7–13 we used the improvements described in section 4.4. That is, we used the Grant code with the "average level" option to obtain bound wave functions, level energies, mixing coefficients and oscillator strengths. Then we used Mann's potential, eqs. (4.37)–(4.40), in solving the Dirac equation for the free-electron orbitals. However, these later calculations are similar to the earlier ones, described in Papers 1–6, in that they continued to employ a set of fractional occupation numbers in order to obtain the electron density, and the resulting potential, for calculating free-electron wave functions. (Again, the reader is referred to the specific publication for a list of the fractional occupation numbers that were employed.) As pointed out in section 4.4, the continuum orbitals are no longer orthogonal to those of the bound electrons in this situation and an extra term had to be introduced in the appropriate exchange integral. The "post" form of this term, eq. (4.41), was used in Papers 7–13.

There was also some variation in the fitting procedure used to obtain values of Q^λ for the factorization method described in section 4.3. In most of our production calculations, in Papers 1–11 more specifically, in order to speed up the calculations, we made fits of Q^λ as a function of Z. As mentioned in Paper 1, Z^2Q^λ is a very slowly varying function of the nuclear charge, Z, and the number of bound electrons per ion, N. Therefore, we performed detailed relativistic distorted-wave calculations for six or eight values of Z, for each of the six scattered electron energies mentioned above. In each case, values of Q^λ were calculated for three incident-electron energies given by $\epsilon_i = \epsilon' + \Delta E_j$, where $j = 1$–3 and values of ΔE_j are chosen such that they span the range of fine-structure transition energies. Then, each value of Q^λ was fit to a power series in Z. For example, in Papers 1 and 5 concerning Ne-like and F-like ions, respectively, detailed calculations were made for the six Z values

$$Z = 22,\ 30,\ 42,\ 56,\ 74 \text{ and } 92\,. \tag{4.96}$$

Then, a power series of the form

$$Z^2 Q^\lambda = a_1 Z^3 + a_2 Z^2 + a_3 Z + a_4 + a_5 Z^{-1} + a_6 Z^{-2} \tag{4.97}$$

was used to obtain a set of fit parameters for each occurrence of Q^λ from the detailed results computed at the six Z vlaues. A different set of fit parameters, a_i, was determined for each Q^λ that can arise for a particular class of transitions (see eq. (4.32)). Then, we obtained the values of Q^λ at the exact energy associated with a given fine-structure transition by Lagrangian interpolation, as mentioned in section 4.6. However, in Papers 12 and 13 concerning N-like and O-like ions, we performed detailed calculations for every Z value considered in those respective publications, since the available computing power at that time was much greater than previously accessible. In this case, for a given value of Z, we still obtained the values of Q^λ at the exact transition energies via Lagrange interpolation on the values that were explicitly calculated at the three representative impact energies.

Finally, we mention the methods used to obtain the top-up contribution for the collision strengths. For optically allowed transitions, we used the partial-relativistic Coulomb-Bethe (PRCBe) approximation as described in section 4.9.1 to obtain the high partial-wave contribution. For forbidden transitions, the ratio approximation described in section 4.9.2 was used.

In addition to collisional excitation data, the above works also contain electric dipole oscillator strengths for optically allowed transitions. In Papers 1–6 our structure code was used to calculate oscillator strengths using the procedure described in chapter 3. In these early calculations, retardation effects were neglected. As mentioned in Papers 2 and 3, such an omission is acceptable for transitions involving orbitals with principal quantum number $n > 1$, since retardation effects are small in these cases, as confirmed by the comparisons provided in those publications. In the more recent Papers 7–13, as mentioned above, we used the Grant code for the structure calculations, which automatically included retardation in the oscillator-strength calculations.

4.12 Special simple cases

Similar to the situation for photoexcitation that was discussed in subsection 3.2.1, among the several cases for which there are initially no partially-filled subshells, in addition to the active one, there are two simple cases that are of particular interest for which the quantity f^λ in eq. (4.35) can be expressed in an especially simple form. These are: (1) the case in which the

active subshell initially contains a single electron, and (2) the case in which the active subshell is initially filled. The absence of partially-filled subshells, in addition to the active one, means that no extra angular factors enter in eq. (4.36).

As discussed in subsection 3.2.1, the first case is usually referred to as the pseudo-hydrogenic case. It applies to hydrogenic ions, as well as to the case in which transitions involve the valence electron outside of a closed-shell core, such as in Li-like and Na-like ions, provided that mixing is neglected between states belonging to different complexes. (There can be no mixing among initial, or final, states within the same complex if only the valence electron is considered to be active for a pseudo-hydrogenic ion.) This situation is a special case of the simple scenario considered in section 4.3, where initially there are only filled or empty subshells, in addition to the active one labeled a. In this special case, the CFP and w occupation number in eq. (4.36) are both unity. Also, $J_t'' = 0$ so that the 6-j symbol in eq. (4.36) becomes

$$\left\{ \begin{array}{ccc} j_a & \lambda & j_a' \\ J_t' & 0 & J_t \end{array} \right\} = \left\{ \begin{array}{ccc} j_a & J_t & 0 \\ J_t' & j_a' & \lambda \end{array} \right\} = \frac{(-1)^{j_a + J_t' + \lambda} \, \delta_{J_t j_a} \delta_{J_t' j_a'}}{[(2J_t + 1)(2J_t' + 1)]^{1/2}} \,. \tag{4.98}$$

Thus, f^λ reduces to $(-1)^{j_a + 3j_a' + \lambda}$, which is equal to ± 1 since j_a and j_a' are half integers and λ is an integer. Consequently, $B^\lambda = 1$ for all values of λ because the square of this phase factor is one and the relevant mixing coefficients in eq. (4.35) are all unity. Then, the collision strength takes the very simple form

$$\begin{aligned} \Omega(U - U') &\equiv \Omega_{\rm H}^{\rm ps}(n_a l_a j_a, n_a' l_a' j_a') \\ &= 8 \sum_\lambda Q^\lambda(n_a l_a j_a, n_a' l_a' j_a'; n_a l_a j_a, n_a' l_a' j_a') \\ &= 8 \sum_\lambda \sum_{\substack{l, l' \\ j, j'}} P^\lambda(n_a l_a j_a \epsilon l j; n_a' l_a' j_a' \epsilon' l' j')^2 \,, \end{aligned} \tag{4.99}$$

where the superscript "ps" and the subscript "H" indicate a pseudo-hydrogenic quantity, as in eqs. (3.37) and (3.38).

The second case applies to excitation from the ground state of systems such as He-like, Ne-like and Ni-like ions, which are very important in plasma applications, as stated in subsection 3.2.1. In this case, we assume no mixing between the ground configuration and any excited configurations, so that the ground state is pure and the CFP is again unity. Also, $J_t = 0$ so that the 6-j symbol in eq. (4.36) reduces to

$$\left\{ \begin{array}{ccc} j_a & \lambda & j_a' \\ J_t' & J_t'' & 0 \end{array} \right\} = \left\{ \begin{array}{ccc} j_a & J_t'' & 0 \\ J_t' & \lambda & j_a' \end{array} \right\} = \frac{(-1)^{j_a + J_t' + j_a'} \, \delta_{J_t'' j_a} \delta_{J_t' \lambda}}{[(2J_t' + 1)(2j_a + 1)]^{1/2}} \,. \tag{4.100}$$

Thus, eq. (4.36) becomes

$$f^{\lambda} = \frac{w^{1/2}}{(2j_a+1)^{1/2}}(-1)^{2(J'_t+j_a+j'_a)}\delta_{J'_t\lambda} = \delta_{J'_t\lambda}\,, \tag{4.101}$$

where the final expression results because $w = 2j_a + 1$ for a filled subshell, and $j_a + j'_a$ and J'_t are both integers. In this case, if we omit mixing in the ground state, then only mixing among the upper states needs to be considered. Hence, the collision strength obtained from eqs. (4.31) and (4.34) simplifies to

$$\Omega(U-U') = 8\sum_{S',S'_1} b(U',S')b(U',S'_1) \times Q^{\lambda=J'_t}(n_a l_a j_a, n'_a l'_a j'_a; n_{a_1} l_{a_1} j_{a_1}, n'_{a_1} l'_{a_1} j'_{a_1})\,. \tag{4.102}$$

4.13 Configuration-average cross sections for electron-impact excitation

When considering configuration-average quantities for electron-impact excitation, it is convenient to follow a similar approach to that used for photoexcitation in section 3.2.2. In particular, we begin with the collision strength and consider the single-configuration approximation by averaging over all possible SCSF transitions that can arise for a transition of the type displayed in eq. (3.42). Thus, the configuration-average collision strength between two configurations c and c' is given by

$$\Omega_{c-c'} \equiv \sum_{i\in c}\sum_{j\in c'} \Omega_{i-j}\,, \tag{4.103}$$

where Ω_{i-j} is the collision strength between two pure SCSFs labeled i and j. In order to reduce this expression to a useful form, one must introduce the additional approximation that the transition energy is the same for all SCSF transitions in the above summation so that the incident and scattered free-electron wave functions are also the same. In practice, it is convenient to assume that this transition energy can be accurately approximated by the configuration-average transition energy, $\Delta E_{c-c'}$. The result is that each SCSF collision strength in eq. (4.103) is described by a scattered electron with kinetic energy $\epsilon' = \epsilon - \Delta E_{c-c'}$, where $\Delta E_{c-c'} = E_{c'} - E_c$. This type of assumption was not necessary when considering the line strength in section 3.2.2 because that quantity involved only bound-electron wave functions. With this approximation, the collision strength can be reduced to the simple form

$$\Omega_{c-c'} = g_c \frac{w_\alpha(2j_\beta + 2 - w_\beta)}{(2j_\alpha+1)(2j_\beta+1)}\Omega_{\rm H}^{\rm ps}(n_\alpha l_\alpha j_\alpha, n_\beta l_\beta j_\beta)\,, \tag{4.104}$$

where the pseudo-hydrogenic collision strength, $\Omega_{\rm H}^{\rm ps}$, is given by eq. (4.99). We note that eq. (4.104) has the nice property that it is in exactly the same form as that given for the configuration-average line strength in eq. (3.44). As a point of reference, we also note that eq. (4.104) is the relativistic analog of eq. (15) given by Peyrusse [28].

Moving on to a consideration of the excitation cross section, we again assume that the transition energy between each pair of SCSFs can be approximated by the configuration-average transition energy, $\Delta E_{c-c'}$. Then, the configuration-average excitation cross section can be expressed according to

$$Q_{c-c'} \equiv \sum_{i\in c}\sum_{j\in c'} g_i Q_{i-j}/g_c = \frac{\pi}{k^2 g_c}\sum_{i\in c}\sum_{j\in c'}\Omega_{i-j} = \frac{\pi}{k^2 g_c}\Omega_{c-c'}\,, \tag{4.105}$$

where g_c is the statistical weight of the initial configuration, given by eq. (3.45). Thus, the relationship between the configuration-average excitation cross section and corresponding collision strength is formally identical to the relationship between the fine-structure (or SCSF) quantities, as given by eq. (4.1). With the use of eq. (4.104), the configuration-average excitation cross section can be expressed in the useful form

$$Q_{c-c'} = \frac{w_\alpha(2j_\beta + 2 - w_\beta)}{(2j_\beta+1)} Q_{\rm H}^{\rm ps}(n_\alpha l_\alpha j_\alpha, n_\beta l_\beta j_\beta)\,, \tag{4.106}$$

where the pseudo-hydrogenic excitation cross section is defined as

$$Q_{\rm H}^{\rm ps}(n_\alpha l_\alpha j_\alpha, n_\beta l_\beta j_\beta) = \frac{\pi}{k^2 g_\alpha}\Omega_{\rm H}^{\rm ps}(n_\alpha l_\alpha j_\alpha, n_\beta l_\beta j_\beta)\,, \tag{4.107}$$

with $g_\alpha = 2j_\alpha + 1$ being the statistical weight of subshell α. It is easily verified that all of the configuration-average quantities listed above reduce to the corresponding hydrogenic expressions for the case of hydrogenic ions (i.e. when $w_\alpha = w_\beta = 1$).

4.14 Rate coefficients for electron-impact excitation

In this section, we provide useful expressions for two quantities associated with electron-impact excitation: the rate coefficient and the effective collision strength. These quantities are temperature-dependent and are convenient for computing the collisional-excitation contribution to the rate equations that determine the atomic populations in plasma kinetics modeling. While no numerical results will be presented here, the expressions provided in this section will be applied in chapters 5, 7 and 8.

As in the description at the beginning of this chapter, we again consider a generic excitation transition, denoted by $i - f$, that could refer to a transition between configurations, states, fine-structure levels or magnetic sublevels. The expressions provided in this section are completely general in that they apply to any of these types of transitions. Then, for a transition $i - f$ that is caused by electron-impact excitation, the rate coefficient, C_{if}, is given by the average of the product of the electron speed, v, and the corresponding cross section, over the electron distribution function. For non-degenerate, Maxwellian electrons the result is given by

$$C_{if} = \frac{1}{N_e} \int_{p_0}^{\infty} n_e(p) v Q(i-f)\, dp = \frac{8\pi e^{-\eta}}{N_e h^3} \int_{p_0}^{\infty} e^{-\epsilon(p)/kT} p^2 v Q(i-f)\, dp\,, \quad (4.108)$$

where kT is the temperature expressed in the appropriate energy units, N_e is the electron number density and $n_e(p)\, dp$ is the number of electrons per unit volume that exist within a range of momenta between p and $p + dp$ The lower bound of the integral, p_0, is the momentum corresponding to the threshold of the transition, $\epsilon(p_0) = E_{if} = E_f - E_i$, with E_i and E_f being the initial and final energies of the configurations, states, etc., and the quantity η satisfies

$$e^{\eta} = \frac{8\pi}{N_e h^3} \int_0^{\infty} e^{-\epsilon(p)/kT} p^2\, dp\,, \quad (4.109)$$

which provides the appropriate normalization for the electron distribution function. The evaluation of the integral in eq. (4.109) can be expressed in terms of a known function or, alternatively, as a series expansion [79,80]. Specifically,

$$e^{\eta} = \frac{8\pi}{N_e} \left(\frac{mc}{h}\right)^3 \frac{e^a}{a} K_2(a) = \frac{2}{N_e h^3} (2\pi mkT)^{3/2} X\,, \quad (4.110)$$

where $a \equiv mc^2/kT$, $K_2(a)$ is the modified Bessel function of order 2 and the relativistic correction X is given by

$$X = 1 + \frac{15}{8} a^{-1} + \frac{105}{128} a^{-2} - \frac{315}{1024} a^{-3} + \frac{10395}{32768} a^{-4} + \cdots\,. \quad (4.111)$$

The series expansion is valid when $a > 1$ (or, equivalently, when $kT < mc^2$), which holds true for a wide range of cases that might be of practical interest.

When computing numerical data for large amounts of collisional excitation processes, it is often convenient to provide the effective collision strength, Υ_{if}, which varies more smoothly with temperature than the rate coefficient, C_{if}. The effective collision strength for direct excitation is defined by

$$\Upsilon_{if} \equiv \int_0^\infty \Omega(i-f)\,\mathrm{e}^{-\epsilon'/kT}\,\mathrm{d}(\epsilon'/kT)\,, \tag{4.112}$$

where $\epsilon' = \epsilon - E_{if}$ is the final, or scattered, electron kinetic energy.

From eqs. (4.108), (4.110) and (4.112), and the standard relationship between the cross section and the collision strength given by eq. (4.1), the connection between the rate coefficient and the effective collision strength is found to be

$$C_{if} = \frac{h^2}{g_i(2\pi m)^{3/2}(kT)^{1/2}X}\,\mathrm{e}^{-E_{if}/kT}\Upsilon_{if} \tag{4.113}$$

or, inserting numerical values,

$$C_{if} = \frac{8.629\times10^{-6}}{g_i T^{1/2} X}\,\mathrm{e}^{-E_{if}/kT}\Upsilon_{if} \quad \mathrm{cm}^3/\mathrm{s}\,, \tag{4.114}$$

where T is the temperature in Kelvin and X is given by eq. (4.111). This relationship is particularly useful because it is valid not only for the process of direct electron-impact excitation treated in this chapter, but also for resonance contributions to the total excitation rate coefficient described in section 7.4. This relationship is also valid for the total excitation rate coefficient itself, provided that the total effective collision strength is supplied on the right-hand side.

The expressions given in this section can also be easily applied to collisional de-excitation [81]. Rather than recompute the various de-excitation quantities from the analogous excitation equations given above, it is possible to obtain directly the desired results from the previously calculated excitation data. Specifically, if we consider the de-excitation transition $f - i$, with transition energy $E_{fi} = -E_{if} = E_i - E_f < 0$, then the corresponding rate coefficient can be determined from the detailed-balance relation

$$C_{fi} = \frac{g_i}{g_f}\,\mathrm{e}^{E_{if}/kT}C_{if}\,. \tag{4.115}$$

Inserting numerical values, and using the convenient property that the effective collision strength is symmetric (i.e. $\Upsilon_{fi} = \Upsilon_{if}$), the analog of eq. (4.114) can be written in the form

$$C_{fi} = \frac{8.629\times10^{-6}}{g_f T^{1/2} X}\Upsilon_{if} \quad \mathrm{cm}^3/\mathrm{s}\,. \tag{4.116}$$

As with excitation transitions, this last expression holds for both the direct and resonance contributions to the de-excitation rate coefficient.

5 Electron-impact ionization

Our basic approach for obtaining expressions for the electron-impact ionization cross sections follows in a straightforward manner from the electron-impact excitation theory described in the previous chapter. One must take into account the fact that the final bound electron in the excitation process is replaced by an ejected continuum electron, which shares the available energy with the scattered continuum electron in the form of kinetic energy. Consequently, the final ion is an $(N-1)$-electron system, rather than an N-electron system. The details of this approach have been described in ref. [82] for the non-factorized method and in ref. [32] for the factorized method. A summary of these two methods is provided in the next two subsections for transitions between fine-structure levels. Additional commentary is provided on the inclusion of the generalized Breit interaction, a method for obtaining convenient fit formulae for the ionization cross section, and the configuration-average approximation applied to collisional ionization. A treatment of transitions between magnetic sublevels is reserved for chapter 9.

5.1 The non-factorized approach to computing ionization cross sections

As described in ref. [82], five steps are required to extend the expression for the collisional excitation cross section, given by eq. (4.1) in the previous chapter, to the case of ionization. As mentioned previously, eq. (4.1) is valid for excitation transitions of any type. Here, we will consider transitions between fine-structure levels, for which eq. (4.6) applies in the case of excitation. Thus, the first step in obtaining the ionization cross section is to alter the final system wave function in eq. (4.6), Ψ_f, so that it represents an $(N+1)$-electron system comprised of an $(N-1)$-electron ion and two continuum electrons. For convenience, we first provide an explicit expression for Ψ_f as it applies to collisional excitation. Such an expression can be written in a manner similar to that used for the initial system wave function in eq. (4.8), and is given by

$$\Psi_f = \frac{1}{(N+1)^{1/2}} \sum_{p=1}^{N+1} (-1)^{N+1-p} \sum_{M_t', m'} C(J_t' j' M_t' m'; JM) \times \Psi_{\Delta_t' J_t' M_t'}(x_p^{-1}) u_{\epsilon' l' j' m'}(x_p) \,. \qquad (5.1)$$

The first required modification can be accomplished by replacing $\Psi_{\Delta_t' J_t' M_t'}(x_p^{-1})$ in eq. (5.1) with an antisymmetrized wave function for an N-electron system corresponding to the final $(N-1)$-electron ion plus an ejected electron. The appropriate expression is given by

$$\Psi_{\Delta_t' J_t' M_t'}(x_p^{-1}) = \frac{1}{N^{1/2}} \sum_{q \neq p}^{N+1} (-1)^{N-q} \sum_{M_t'', m''} C(J_t'' j'' M_t'' m''; J_t' M_t') \times \Psi_{\Delta_t'' J_t'' M_t''}(x_q^{-1}) u_{\epsilon'' l'' j'' m''}(x_q) , \quad (5.2)$$

where $\Psi_{\Delta_t'' J_t'' M_t''}$ is the antisymmetrized wave function that corresponds to the final $(N-1)$-electron ion with total angular momentum J_t'', and $u_{\epsilon'' l'' j'' m''}(x_q)$ is a Dirac spinor that represents the ejected electron. This spinor is analogous to the $u_{\epsilon l j m}$ spinor that represents the incident electron defined by eqs. (4.9)–(4.11). An important consequence of this last statement, when considered in concert with the specific form of eq. (5.2), is that the bound-electron radial functions, $P_{n_a' l_a' j_a'}$ and $Q_{n_a' l_a' j_a'}$, that appear in the direct and exchange radial integrals for excitation, given by eqs. (4.17) and (4.18), are simply replaced with $P_{\epsilon'' l'' j''}$ and $Q_{\epsilon'' l'' j''}$ when calculating the corresponding radial integrals for the ionization cross section.

The second required step is to sum eq. (4.6) over all possible values of J_t', which represents the total angular momentum of the N-electron system consisting of the final $(N-1)$-electron ion with total angular momentum J_t'' plus the ejected electron with total angular momentum j''. The third step is to also sum eq. (4.6) over all possible partial waves of the ejected electron, which are represented by κ'' or, equivalently, j'' and l''. The fourth step is to integrate eq. (4.6) over the appropriate range of the kinetic energy of the ejected electron, ϵ''. This range is obtained from a consideration of standard energy-conservation arguments and is found to be 0 to $(\epsilon - I)/2$, where I is the ionization energy and ϵ is the kinetic energy of the incident electron. The fifth, and final, step is to divide eq. (4.6) by a factor of π in order to take into account the fact that a final, bound-electron radial function with normalization

$$\int_0^\infty [P^2_{n_a' \kappa_a'}(r) + Q^2_{n_a' \kappa_a'}(r)] \, \mathrm{d}r = 1 \quad (5.3)$$

has been replaced with a continuum ejected electron radial function with normalization

$$\int_0^\infty [P_{\epsilon'' \kappa''}(r) P_{\epsilon''' \kappa'''}(r) + Q_{\epsilon'' \kappa''}(r) Q_{\epsilon''' \kappa'''}(r)] \, \mathrm{d}r = \pi \delta(\epsilon'' - \epsilon''') . \quad (5.4)$$

Combining these steps yields the relativistic distorted-wave ionization cross section for transitions between fine-structure levels,

$$Q(\Delta_t J_t - \Delta_t'' J_t'') = \frac{8}{k^2 g_i} \sum_J (2J+1)$$

$$\times \sum_{J_t'} \sum_{\kappa,\kappa'\kappa''} \int_0^{(\epsilon-I)/2} \mathrm{d}\epsilon'' \left| \left\langle \Psi_i \right| \sum_{\substack{p,q \\ p<q}}^{N+1} \frac{1}{r_{pq}} \left| \Psi_f \right\rangle \right|^2 , \quad (5.5)$$

with Ψ_i given by eq. (4.8) and Ψ_f given by eqs. (5.1) and (5.2).

Most of the practical issues that need to be considered when numerically evaluating the various pieces that comprise eq. (5.5) are similar to those described for excitation in chapter 4. For example, the continuum radial functions that represent the scattered and ejected electrons are determined from the same algorithm that is described in section 4.5. Also, some of the procedures that were described in section 4.6 also carry over to the case of collisional ionization. For example, a single mean configuration (which may contain fractional occupation numbers for certain subshells) is chosen to determine an appropriate central potential (see eqs. (2.18)–(2.20) in section 2.3) for a given class of transitions. In the case of ionization, a given class of transitions is typically denoted by the $n_a l_a j_a$ value of the active (ionized) electron. A method for determining the mean configuration that is analogous to the approached used for excitation is to split the occupation number of the active electron between the initial and final subshells. In the case of ionization, the final subshell is actually the ejected electron and, in order to mock up the effect of this ejected electron, we assume an occupation number of 0.5 for a very high-lying, bound subshell. As a specific example, we might consider the ionization of the 2s electron in the ground state of Li-like ions, for which we would choose a mean configuration of the form

$$1s^2 2s^{0.5} 6d_{5/2}^{0.5} . \quad (5.6)$$

An alternative approach that we often employed is to simply use the integer occupation numbers associated with the initial configuration of the target ion. For example, when considering either inner-shell ionization or ionization of the valence electron of Li-like ions in the ground level, the configuration $1s^2 2s$ was used in determining the DFS central potential. Similarly, for ionization of the $2p^*$ electron in Li-like ions the configuration $1s^2 2p^*$ was chosen.

Another important consideration from section 4.6 is the method for reducing the number of radial integrals that need to be calculated. For complex cases in which mixing among the initial or final bound states is strong, the set of radial integrals associated with a particular active orbital, denoted by $n_a l_a j_a$, will be used in different fine-structure transitions. The only difference between these integrals is that they must be evaluated with a different ionization energy for each fine-structure transition. However, the radial integrals vary smoothly as a function of the ionization energy and so we typically compute a set of radial integrals, for a given $n_a l_a j_a$ orbital, at three particular energies that span the range of actual, fine-structure ionization energies. Then we interpolate on

these three sets of results to obtain the radial integrals at a specific ionization energy of interest.

A consideration that applies to collisional ionization, but not collisional excitation, is that the relative phase of the scattered and ejected electrons is unknown when the central field approximation is employed in determining the wave functions that represent these electrons. The choice of phase used in our approach is sometimes referred to as the "natural"-phase approximation (see eq. (10) of ref. [83]). This choice corresponds to the $Z \rightarrow \infty$ limit in the non-relativistic case. Therefore, one might expect this choice to be a good approximation for highly charged ions.

As a numerical example, we provide in table 8 a portion of the comparisons that were originally presented in ref. [82] between our RDW ionization cross sections and results obtained from relativistic calculations performed by other researchers. The entries from ref. [84] were calculated with the RDW program that was used to compute the direct ionization contribution in ref. [85], as opposed to the indirect excitation-autoionization contribution computed in ref. [86]. This approach also uses the natural-phase approximation, but differs from our RDW approach only in that the bound and continuum radial functions are computed in a Dirac-Fock potential [6], rather than the more approximate Dirac-Fock-Slater potential used in our approach. For the highly charged ions considered here, this difference in potential typically makes very little difference because the nuclear potential dominates the electron-electron interaction. This statement is verified by noting the excellent agreement between our RDW results and those from refs. [84] and [85].

The results from refs. [87] and [88] were obtained in a manner very similar to that used in refs. [84] and [85], except that the "maximum-interference"-phase approximation (see eq. (11) of ref. [83]) was employed. The latter approximation yields smaller cross sections than the natural-phase approximation. Because of this difference, one can see from table 8 that the present RDW results are always larger than those from refs. [87] and [88]. Nevertheless, the agreement is still quite good when comparing with these results.

Finally, the results of ref. [83] differ from all of the others in two ways. First, these results were computed with the full lowest-order QED interaction for electrons scattering with a bound electron. In this case, the interaction was written in the Lorentz gauge and so the Møller interaction was used in these calculations (see eq. (2.29) and the surrounding discussion for details). The second difference in the data from ref. [83] is that the exchange and interference terms were excluded from the scattering matrix elements. This omission was expected to have no more than a 15% effect on the cross section. (However, this expectation was eventually shown to be false, as will be demonstrated in section 5.3, which concerns the generalized Breit interaction.) Thus, when

Table 8. Comparison of the ionization cross section (in units of cm^2) for various subshells between the present RDW results [82] and relativistic calculations performed by other workers. Results are presented for different ions, denoted by the nuclear charge Z, with varying number of bound electrons. The mean configuration used to determine the potential was chosen to be the ground configuration of the initial ion in all cases. $x[y] = x \times 10^y$.

Active subshell	Ion type	Z	Source	I (keV)	$u = \epsilon/I$ 1.25	1.351	1.448	1.50	1.552	1.737
3s	Na	34	present	1.036		9.72[-21]	1.09[-20]		1.18[-20]	1.29[-20]
			[84]	1.036		9.80[-21]	1.09[-20]		1.18[-20]	1.27[-20]
2p*	Ne	34	present	2.582	3.33[-21]			4.80[-21]		
			[84,85]	2.583	3.43[-21]			4.88[-21]		
2p	Ne	34	present	2.539	6.92[-21]			9.97[-21]		
			[84,85]	2.539	7.14[-21]			9.98[-21]		

Active subshell	Ion type	Z	Source	I (keV)	$u = \epsilon/I$ 1.05	1.125	1.25	1.50	2.00	2.50	3.00
3s	Na	79	present	8.373		7.70[-23]	1.26[-22]	1.79[-22]	2.13[-22]	2.16[-22]	2.12[-22]
			[84]	8.370		7.72[-23]	1.24[-22]	1.77[-22]	2.11[-22]	2.17[-22]	2.12[-22]
3s	Na	92	present	12.204	1.68[-23]	3.67[-23]					
			[84]	12.202	1.68[-23]	3.70[-23]					

Active subshell	Ion type	Z	Source	I (keV)	$u = \epsilon/I$ 1.10	1.50	2.00
2s	Li	92	present	32.96	4.20[-24]	1.24[-23]	1.55[-23]
			[87]	32.84	4.09[-24]	1.21[-23]	1.51[-23]
2s	Ne	92	present	25.31			1.34[-23]
			[88]	25.31			1.30[-23]
2p*	Ne	92	present	29.27			4.93[-23]
			[88]	29.27			4.77[-23]
2p	Ne	92	present	30.00			3.69[-23]
			[88]	29.95			3.57[-23]
1s	He	92	present[a]	130.4	0.54[-24]	1.95[-24]	2.79[-24]
			[83]	130.2	0.51[-24]	1.76[-24]	2.72[-24]

[a] Calculated with exchange and interference terms set to zero as in ref. [83].

comparing with these results, the corresponding terms were also omitted from our RDW calculations. The agreement between the two data sets is also very good in this case, which is somewhat surprising since the generalized Breit and Møller interactions were eventually shown to cause a substantial (~50%) increase in this cross section when all terms were properly included in the scattering matrix elements.

5.2 *Use of the factorization method to obtain simple expressions for the ionization cross section*

The factorized expression for the collisional ionization cross section can also be obtained from the corresponding excitation cross section via the five steps described in the previous section, and also described in ref. [32]. The factorized form of the collisional excitation cross section is easily obtained by substituting the collision strength in eq. (4.31) into eq. (4.1). Then, following the prescription in the previous section, the factorized form of the collisional ionization cross section is given by

$$Q(U-U'') = \frac{8}{(2J_t+1)k^2} \sum_{J_t'} \sum_{l'',j''} \sum_{\substack{S,S'' \\ S_1,S_1''}} \times \sum_{\lambda} B^{\lambda}[U, SS_1; (U''l''j''J_t'), (S''l''j''J_t')(S_1''l''j''J_t')] \times \sum_{(\epsilon-I)/2} \int_0 \mathrm{d}\epsilon''\, Q^{\lambda}(n_a l_a j_a, \epsilon'' l'' j''; n_{a_1} l_{a_1} j_{a_1}, \epsilon'' l'' j'') \,. \quad (5.7)$$

The quantities B^{λ} and Q^{λ} have the same basic definitions as those provided in section 4.3, except that the arguments have been modified appropriately for the case of ionization. The overall notation has been slightly modified to be consistent with that introduced in the previous section. In particular, the final ion level with total angular momentum J_t'' is now denoted by U'' rather than U'. Similarly, the sums over the states S' and S_1' have been replaced with sums over S'' and S_1''. The meaning of these symbols is completely analogous to their excitation counterparts, i.e. S'' and S_1'' are states with total angular momentum J_t'' that contribute to the mixing of the final ion level U'' with corresponding mixing coefficients $b(U'', S'')$ and $b(U'', S_1'')$. Also, for the case of ionization, both of the substitutions $n_a' l_a' j_a' \rightarrow \epsilon'' l'' j''$ and $n_{a_1}' l_{a_1}' j_{a_1}' \rightarrow \epsilon'' l'' j''$ are required. These substitutions appear explicitly in the argument of Q^{λ} and are understood in the corresponding expressions that comprise B^{λ} (i.e. in eqs. (4.35) and (4.36) for F^{λ} and f^{λ}, respectively). Thus, the appearance of $l''j''J_t'$ in the last three arguments of B^{λ} serves to emphasize the notion that each of those arguments refers to an N-electron system comprised of an ion in

the appropriate $(N-1)$-electron level, or state, that is coupled to the ejected electron, and described by total angular momentum J_t'.

Those two substitutions that concern the ejected electron, denoted by $\epsilon'' l'' j''$, result in certain simplifications [32] that do not arise for the excitation case. For illustrative purposes, we consider the same case that was treated in detail in section 4.3 for excitation, i.e. the case for which all subshells, apart from the active one labeled a, are initially filled or empty in the target ion. In this case, eq. (4.36) applies for the quantity f^λ. The phase factor in that expression, $(-1)^{J_t'+J_t''+j_a'}$, will not contribute to the ionization cross section because j_a' is replaced by j'' and J_t' is obtained by coupling j'' and J_t'', which represents the total angular momentum of the final ion with one less electron than the initial ion. Thus, $J_t'+J_t''+j''$ is an integer and, because the square of this phase factor appears in the cross section, the factor does not contribute. Additionally, the summation over J_t' in eq. (5.7) can be evaluated using an alternative form of eq. (4.30) given by

$$\sum_{J_t'}(2J_t'+1)\begin{Bmatrix} j_a & \lambda & j'' \\ J_t' & J_t'' & J_t \end{Bmatrix}\begin{Bmatrix} j_{a_1} & \lambda & j'' \\ J_t' & J_t'' & J_t \end{Bmatrix} = \frac{\delta_{j_a j_{a_1}}}{2j_a+1}\,. \tag{5.8}$$

Note that this result removes the dependence of f^λ (and, consequently, B^λ) on the index λ.

A further simplification results when one considers the fact that only bound states of the same parity can mix with each other. This statement applies to both the initial and final levels of the ion. In order for both this latter statement and eq. (5.8) to be simultaneously satisfied, it must also be true that $l_{a_1} = l_a$. Taking this result into account, we can define a κ''-summed version of Q^λ according to

$$\begin{aligned} &Q^\lambda(n_a n_{a_1} l_a j_a;\epsilon'') \\ &\qquad \equiv \sum_{\kappa''} Q^\lambda(n_a l_a j_a, \epsilon'' l'' j''; n_{a_1} l_{a_1} j_{a_1}, \epsilon'' l'' j'') \\ &\qquad = \sum_{\substack{l,l',l'' \\ j,j',j''}} P^\lambda(n_a l_a j_a \epsilon l j; \epsilon'' l'' j'' \epsilon' l' j') P^\lambda(n_{a_1} l_a j_a \epsilon l j; \epsilon'' l'' j'' \epsilon' l' j')\,. \end{aligned} \tag{5.9}$$

This quantity can be combined with the simplifications described above to express the factorized version of the ionization cross section in the simplified form

$$Q(U-U'') = \frac{8}{(2j_a+1)k^2} \sum_{\substack{S,S'' \\ S_1,S_1''}} B(U, SS_1; U'', S''S_1'')$$

$$\times \int_0^{(\epsilon-I)/2} \mathrm{d}\epsilon'' \sum_\lambda Q^\lambda(n_a n_{a_1} l_a j_a; \epsilon'') \,, \quad (5.10)$$

where

$$B(U, SS_1; U'', S''S_1'') = F(US, U''S'')F(US_1, U''S_1''), \quad (5.11)$$

$$F(US, U''S'') = b(U, S)f(S, S'')b(U'', S'') \,, \quad (5.12)$$

and

$$f(S, S'') = \sqrt{w}(j_a^{w-1}\alpha_a'' J_a'' \,|\}j_a^w \alpha_a J_a) \,. \quad (5.13)$$

Here, eqs. (5.10)–(5.12) apply to the general case, but eq. (5.13) is valid only for the present case under consideration for which all subshells, except the active one, are initially filled or empty. For more complex ions, eq. (5.13) must be multiplied by the appropriate factor, as discussed in subsection 3.2.1 and section 4.3, and also in ref. [32] where analytic expressions are provided. Alternatively, the value of $f(S, S'')$ that applies to an arbitrarily complex transition can be determined from the MCT package [34] of the Grant code. However, the relationship is not as straightforward as that provided for the case of photoexcitation (see the discussion following eq. (3.30)).

While it may seem odd that a factor of $2j_a+1$, rather than $2J_t+1$, now appears in the denominator of eq. (5.10), this choice is intentional as it lends itself to a particularly simple expression when mixing is limited to states that lie within the same complex. Up to this point, we have been considering the most general case for which the levels that describe the initial and final ions are allowed to include mixing of states that reside outside of a single complex. If mixing is limited to states within a complex, which is often a good approximation for highly charged ions, then there is only a single set of n values to describe the active electron so that $n_{a_1} = n_a$. We first consider the simplest possible case of this type, i.e. ionization of a hydrogenic ion with no mixing. In this case, the quadruple sum in eq. (5.10) reduces to a single term, with the surviving B coefficient replaced by one because the relevant mixing coefficients and the sole f coefficient all have a value of one. Then, the hydrogenic cross section for ionization can be written as

$$Q_{\mathrm{H}}(n_a l_a j_a) = \frac{8}{(2j_a+1)k^2} \int_0^{(\epsilon-I)/2} \mathrm{d}\epsilon'' \sum_\lambda Q^\lambda(n_a l_a j_a; \epsilon'') \quad (5.14)$$

with

$$Q^{\lambda}(n_a l_a j_a; \epsilon'') = \sum_{\substack{l,l',l'' \\ j,j',j''}} P^{\lambda}(n_a l_a j_a \epsilon l j; \epsilon'' l'' j'' \epsilon' l' j')^2 \,. \tag{5.15}$$

Next we consider an arbitrarily complex ion, but with mixing limited to states that reside within the same complex. Once again, the relationship $n_{a_1} = n_a$ is valid and eq. (5.10) can be rearranged into the convenient form

$$Q(U - U'') = \sum_{\substack{S,S'' \\ S_1,S_1''}} B(U, SS_1; U'', S''S_1'') Q_{\mathrm{H}}^{\mathrm{ps}}(n_a l_a j_a) \,, \tag{5.16}$$

where $Q_{\mathrm{H}}^{\mathrm{ps}}$ is a pseudo-hydrogenic ionization cross section of the same form as eq. (5.14). When evaluating $Q_{\mathrm{H}}^{\mathrm{ps}}$, the ionization energy I in eq. (5.14) is chosen to be the actual value associated with the fine-structure transition in question and the radial wave functions to be used in the integrals that comprise the P^{λ} values are calculated from the central potential that is appropriate for the complex ion under consideration.

The convenient form of eq. (5.16) can also be extended to the case when mixing is considered outside of a complex. Specifically, eq. (5.10) can be rewritten as

$$Q(U - U'') = \sum_{\substack{S,S'' \\ S_1,S_1''}} B(U, SS_1; U'', S''S_1'') Q_{\mathrm{H}}^{\mathrm{ps}}(n_a n_{a_1} l_a j_a) \,, \tag{5.17}$$

where $Q_{\mathrm{H}}^{\mathrm{ps}}(n_a n_{a_1} l_a j_a)$ is the same as $Q_{\mathrm{H}}^{\mathrm{ps}}(n_a l_a j_a)$, except that $Q^{\lambda}(n_a l_a j_a; \epsilon'')$ in eq. (5.14) should be replaced with $Q^{\lambda}(n_a n_{a_1} l_a j_a; \epsilon'')$ defined in eq. (5.9). Thus,

$$Q_{\mathrm{H}}^{\mathrm{ps}}(n_a n_{a_1} l_a j_a) = \frac{8}{(2j_a + 1)k^2} \int_0^{(\epsilon - I)/2} \mathrm{d}\epsilon'' \sum_{\lambda} Q^{\lambda}(n_a n_{a_1} l_a j_a; \epsilon'') \,. \tag{5.18}$$

The expressions provided in eqs. (5.16) and (5.17) are the main results of this section. The former is to be used when mixing is limited to states within a complex, while the latter is to be used when mixing outside of a complex is considered. These two formulae are particularly compact and very useful in computing RDW ionization cross sections for transitions involving arbitrarily complex ions. For completeness, we mention that additional commentary is provided in ref. [32] for computing the factorized ionization cross section in the LS-coupling scheme. In that case, an expression similar to that given in eq. (5.16) is obtained. See eq. (40) in ref. [32] and the surrounding discussion for further details.

As a numerical example, we provide in table 9 a portion of the comparisons that were originally presented in ref. [32] between our RDW ionization cross

sections computed with the factorization method and those obtained from relativistic calculations performed by Moores and Pindzola [85]. The mean

Table 9
Comparison of ionization cross sections (in units of 10^{-24} cm^2) for U^{85+} ions. The present RDW results are labeled SZ, while those of Moores and Pindzola [85] are labeled MP. The symbol $2\bar{p}$ in table II of ref. [32] has been changed to the present notation $2p^*$.

Transition	Threshold energy (keV)		Cross section at 2 th. units [a]	
	SZ	MP	SZ	MP
$2p^{*2}2p(3/2) \rightarrow 2p^{*2}(0)$ [b]	26.59	26.59	30.2	31.4
$2p^{*2}2p(3/2) \rightarrow 2p^*2p(1)$	30.57	30.57	16.8	17.4
$2p^{*2}2p(3/2) \rightarrow 2p^*2p(2)$	30.59	30.59	28.0	29.1
$2p^*2p^2(3/2) \rightarrow 2p^*2p(1)$	26.63	26.63	45.3	47.0
$2p^*2p^2(3/2) \rightarrow 2p^*2p(2)$	26.65	26.65	15.1	15.7
$2p^*2p^2(5/2) \rightarrow 2p^*2p(1)$	26.61	26.61	7.6	7.8
$2p^*2p^2(5/2) \rightarrow 2p^*2p(2)$	26.63	26.63	52.8	54.8
$2p^*2p^2(1/2) \rightarrow 2p^*2p(1)$	26.53	26.53	22.7	23.5
$2p^*2p^2(1/2) \rightarrow 2p^*2p(2)$	26.55	26.55	37.9	39.1
$2p^*2p^2(3/2) \rightarrow 2p^2(2)$	30.69	30.69	22.3	23.2
$2p^*2p^2(5/2) \rightarrow 2p^2(2)$	30.67	30.67	22.3	23.2
$2p^*2p^2(1/2) \rightarrow 2p^2(0)$	30.68	30.68	22.3	23.2
$2p^3(3/2) \rightarrow 2p^2(2)$	26.63	26.63	75.5	78.0
$2p^3(3/2) \rightarrow 2p^2(0)$	26.72	26.72	15.1	15.6

[a] "th. units" stands for threshold units, i.e. the incident energy divided by the threshold energy.
[b] The quantity in parentheses is the total angular momentum of the ion.

configuration used in determining the DFS central potential for these N-like uranium calculations was

$$1s^2 2s^2 2p^{*0.83} 2p^{1.67} 8f^{0.5} . \tag{5.19}$$

Numerical studies showed that the resulting cross sections are relatively insensitive to how the number of electrons was distributed among the subshells in the $n = 2$ shell. The results were also found to be insensitive to the precise high subshell that was chosen to mock up the effect of the ejected electron. For example, replacement of $8f^{0.5}$ with $6f^{0.5}$ or $10f^{0.5}$ had no effect on the results presented in table 9. As in the previous section, the calculations of Moores and Pindzola included the lowest-order QED effect in the scattering matrix elements, whereas this correction was not included in our RDW calculations. Although the agreement between the two data sets is generally quite good, the differences that occur at the higher of the two impact energies are probably due to this distinction in treating the QED effects. Our approach to including

QED effects in the ionization scattering matrix elements is discussed in the next section.

5.3 An option to include the generalized Breit interaction in the ionization scattering matrix elements

The initial decision to develop an option to include the generalized Breit interaction in our electron-impact ionization program was motivated by a desire to produce better agreement with (then-recent) EBIT measurements of ionization cross sections for the 1s electron in H-like and He-like uranium [89]. The measured results exceeded those produced by our non-factorized approach [82], described previously in section 5.1, by about 50%. Since the distorted-wave approach is expected to produce accurate results for such highly charged systems, it was postulated that QED effects might be responsible for the discrepancy between theory and experiment. An earlier theoretical study of collisional ionization of U^{91+} and U^{90+} ions, performed by Pindzola et al. [83], did not display a very strong effect on the ionization cross sections when the Møller interaction was included in the scattering matrix elements. However, that study employed the "no-exchange" approximation in which the exchange and interference terms were excluded from the cross section calculation. A subsequent study by Pindzola et al. [64] displayed a very similar plot of the various no-exchange, U^{91+} cross sections. However, that work also included a statement to the effect that an additional calculation, which did include the full exchange and interference terms, had been performed at a single impact energy (222 keV) and the resulting cross section increased by almost 50%. Therefore, it was desirable to perform a more complete study of the first-order QED correction to the Coulomb interaction between the bound and free electrons, i.e. the generalized Breit interaction (in the Coulomb gauge) or the Møller interaction (in the Lorentz gauge), at the EBIT experimental conditions.

In our case, we implemented logic in our collisional ionization program to include the generalized Breit interaction in the scattering matrix elements. The necessary modifications were made to the factorized version of the code described in section 5.2 and, as mentioned in ref. [90], the changes were relatively straightforward. Basically, the same changes that were described in subsection 4.10.2, regarding the addition of the generalized Breit interaction to the scattering matrix elements for collisional excitation, also apply to collisional ionization, with minor alterations. In brief, the two direct, Breit integrals given by eqs. (4.90) and (4.91) must be added to the standard Coulomb integral given by eq. (4.89). The same type of statement applies to the corresponding exchange integrals (see eq. (4.92) and the surrounding discussion). In order to apply these integrals to the case of ionization, the only change that needs to

be made is that the radial functions that represent the final (bound) excited electron must be replaced everywhere by radial functions that represent the continuum ejected electron. This change is easily accomplished by performing the substitution $n'_a l'_a j'_a \rightarrow \epsilon'' l'' j''$ in all of the excitation expressions.

Upon completion of these modifications, our ionization program contained a general capability for including the generalized Breit interaction in RDW calculations of the ionization cross section for transitions between fine-structure levels in arbitrarily complex ions. Calculations were subsequently performed of the 1s ionization cross section for U^{91+} and U^{90+} ions [90]. These results are reproduced in table 10, along with the corresponding EBIT measurements. The notation used to describe the various theoretical calculations is the same

Table 10
Comparison of electron-impact ionization cross sections (in units of 10^{-24} cm^2) for an electron in the 1s subshell of U^{90+} and U^{91+} ions. The incident-electron energy is 198 keV for both ion stages.

	Theory			Experiment
Ion	C	GB	GBI	
U^{90+}	1.95	2.90	2.94	2.82 ± 0.35
U^{91+}	0.93	1.38	1.40	1.55 ± 0.27

as that used in subsections 4.10.1 and 4.10.2. Hence, the label C refers to calculations that were performed with only the Coulomb interaction included in the scattering matrix elements, the GB-labeled results also included the real part of the generalized Breit interaction and the GBI-labeled results included both the real+imaginary parts of the generalized Breit interaction (labeled GBI). As was observed in the case of collisional excitation, the GB and GBI results agree to within a couple of percent, underscoring the lack of importance of the imaginary part of the generalized Breit interaction in these types of calculations. More importantly, the GB and GBI results display a significant (~50%) increase over the Coulomb-only cross sections for both U^{91+} and U^{90+} ions, and excellent agreement is observed when comparing the QED calculations with the EBIT measurements. Calculations that considered the Møller interaction, rather than the generalized Breit interaction, in computing the ionization cross section for U^{91+} ions were concurrently performed by Moores and Reed [91]. These Møller results were very similar to the U^{91+} cross sections computed by our RDW code, providing a fundamental test of gauge invariance and additional support of the excellent agreement between theory and experiment.

In the discussions that occur near the end of refs. [32] and [82], a method was outlined for producing reduced ionization cross sections from detailed RDW results and then fitting these reduced quantities to a particular functional form. The resulting fit parameters would make possible very rapid calculations that accurately reproduced detailed RDW results for fine-structure transitions in arbitrarily complex ions. A procedure of this type was previously implemented, for example, with respect to non-relativistic Coulomb-Born-exchange cross sections (see refs. [92–94] and the references therein).

Research of this type for RDW calculations was reported in three publications [95,96,79] that were organized according to the principal quantum number of the subshell in which the active electron resides. Transitions in highly charged ions involving active electrons with $n = 3$, 4 and 5 were first considered in ref. [95]. Ionization of electrons in these subshells were the simplest to consider because the reduced cross sections were relatively independent of Z and N, where N is the number of bound electrons in the target ion. Ionization of a 1s electron was next considered [96], followed by ionization of $n = 2$ electrons [79]. These last two cases exhibited strong dependence on Z and N, and the 1s-electron case also required special consideration due to the significant effect of the generalized Breit interaction on the shape of the reduced cross section.

The development of this fit procedure begins with a consideration of the simple, factorized form of the ionization cross section that appears in eq. (5.16), which is repeated here for convenience,

$$Q(U - U'') = \sum_{\substack{S,S'' \\ S_1,S_1''}} B(U, SS_1; U'', S''S_1'')Q_{\rm H}^{\rm ps}(nlj)\,. \tag{5.20}$$

The subscript "a", which denotes the active subshell, has also been omitted for convenience. The B coefficients depend only on the ion properties such as mixing coefficients and angular momenta, and can be rapidly computed. As mentioned previously, the pseudo-hydrogenic cross section, $Q_{\rm H}^{\rm ps}(nlj)$, has exactly the same form as the cross section for collisional ionization from subshell nlj in a hydrogenic ion, but is calculated with bound and continuum radial functions determined from the appropriate potential of the actual ion under consideration. For relatively low values of Z, for which LS coupling is appropriate, the dependence of $Q_{\rm H}^{\rm ps}(nlj)$ on j can generally be neglected so that

$$Q_{\rm H}^{\rm ps}(nlj) \rightarrow Q_{\rm H}^{\rm ps}(nl), \qquad Z \lesssim 30. \tag{5.21}$$

The basic concept that underlies the fit procedure is to design a simple, fast method for determining $Q_{\mathrm{H}}^{\mathrm{ps}}(nlj)$ for an arbitrary transition in any ion. The first step in achieving this goal is accomplished by defining a suitable reduced cross section. Such a quantity was defined for the non-relativistic, Coulomb-Born approach to collisional ionization of hydrogenic ions by taking advantage of the fact that the cross section scales perfectly as $1/I^2$ in the $Z \rightarrow \infty$ limit, where I is the ionization energy of the bound electron. This relationship was then extended to ionization in non-relativistic, complex ions (see, for example, refs. [92–94] and the references therein). An important quality exhibited by those reduced cross sections associated with ionization of an electron from a particular nl subshell is that they are approximately independent of the Z value and number of bound electrons, N, that describe the target ion.

5.4.1 Fits to $n = 3$, 4 and 5 ionization cross sections

In applying this approach to RDW ionization cross sections, we consider the same type of scaling and define a (dimensionless) reduced ionization cross section, Q_R, according to

$$Q_{\mathrm{H}}^{\mathrm{ps}}(nlj) = \frac{\pi}{[I(\mathrm{Ry})]^2} Q_R(nlj, u)\,, \tag{5.22}$$

where $I(\mathrm{Ry})$ is the ionization energy in Rydbergs and $u = \epsilon/I$ is the incident-electron kinetic energy in threshold units. In order to test the utility of such a reduced cross section for RDW calculations, we first considered ionization of electrons residing in subshells having principal quantum numbers $n = 3$, 4 and 5. The process of collisional ionization of electrons in these shells is expected to be less affected by relativistic effects, relative to ionization of the more tightly bound electrons residing in the $n = 1$ and 2 shells. Therefore, it was hoped that the previously mentioned approach, which was successfully applied to non-relativistic Coulomb-Born cross sections, would also work well for these electrons within an RDW framework.

To this end, we computed values of $Q_R(nlj, u)$ for a large number of cases involving the ionization of electrons residing in the $n = 3$, 4 and 5 shells [95]. A subset of these results is displayed in table 11 for the $n = 4$ values. The additional $n = 3$ and $n = 5$ data are available in ref. [95], along with a detailed description of how these reduced cross sections were calculated. From table 11 and ref. [95], one observes that the reduced cross section for ionization from a given subshell nlj is almost independent of Z, N and j for $n \geq 3$, despite the fact that the ionization energy, and hence the pseudo-hydrogenic cross section $Q_{\mathrm{H}}^{\mathrm{ps}}(nlj)$, differ greatly as a function of these quantities. Moreover, the reduced cross sections are reasonably close to the non-relativistic Coulomb-Born-exchange values for hydrogenic ions, except that the RDW values tend to

Table 11
Comparison of values for the reduced ionization cross section Q_R for electrons residing in the $n = 4$ shell.

Active				$u = \epsilon/I$					
subshell	Z	N	I(Ry)	1.125	1.250	1.500	2.250	4.000	6.000
4s		1[a]		0.359	0.580	0.807	0.937	0.800	0.651
	79	1	421.16	0.3624	0.5869	0.8276	0.9600	0.8447	0.6951
	26	11	18.74	0.3360	0.5473	0.7733	0.9020	0.7703	0.6203
	79	35	189.48	0.3276	0.5368	0.7668	0.9096	0.7821	0.6355
	79	45	144.28	0.3101	0.5099	0.7325	0.8858	0.7721	0.6286
4p*		1[a]		0.394	0.640	0.901	1.057	0.882	0.702
	79	1	421.08	0.3771	0.6145	0.8740	1.0421	0.9184	0.7518
	26	11	17.79	0.3570	0.5812	0.8223	0.9756	0.8492	0.6835
	79	35	181.40	0.3502	0.5703	0.8059	0.9469	0.8339	0.6810
	79	45	136.05	0.3439	0.5616	0.7975	0.9394	0.8133	0.6782
4p		1[a]		0.394	0.640	0.901	1.057	0.882	0.702
	79	1	400.65	0.3965	0.6448	0.9139	1.0913	0.9542	0.7758
	26	11	17.71	0.3582	0.5823	0.8218	0.9786	0.8512	0.6856
	79	35	171.26	0.3665	0.5968	0.8429	0.9984	0.8800	0.7218
	79	45	127.23	0.3607	0.5880	0.8349	0.9890	0.8644	0.7160
4d*		1[a]		0.488	0.785	1.083	1.205	0.963	0.755
	79	1	400.65	0.4945	0.7981	1.1084	1.2534	1.0367	0.8328
	26	11	16.46	0.4712	0.7617	1.0606	1.2061	0.9882	0.7805
	79	35	158.69	0.4549	0.7430	1.0501	1.2303	1.0356	0.8395
	79	45	113.85	0.4327	0.7105	1.0175	1.2226	1.0496	0.8601
4d		1[a]		0.488	0.785	1.083	1.205	0.963	0.755
	79	1	394.84	0.4977	0.8021	1.1102	1.2560	1.0358	0.8316
	26	11	16.46	0.4710	0.7609	1.0576	1.2057	0.9871	0.7801
	79	35	156.48	0.4585	0.7480	1.0544	1.2335	1.0339	0.8338
	79	45	112.01	0.4364	0.7162	1.0237	1.2271	1.0499	0.8492
4f*		1[a]		0.538	0.864	1.187	1.326	1.057	0.820
	79	1	394.84	0.5518	0.8856	1.2202	1.3794	1.1263	0.8936
	26	11	15.80	0.5362	0.8617	1.1857	1.3428	1.0799	0.8366
	79	35	142.00	0.5637	0.9096	1.2596	1.4394	1.1783	0.9263
	79	45	95.92	0.5797	0.9404	1.3126	1.5183	1.2638	1.0059
4f		1[a]		0.538	0.864	1.187	1.326	1.057	0.820
	79	1	392.05	0.5514	0.8849	1.2187	1.3787	1.1251	0.8925
	26	11	15.80	0.5359	0.8613	1.1846	1.3426	1.0796	0.8364
	79	35	141.34	0.5632	0.9086	1.2577	1.4374	1.1758	0.9238
	79	45	95.40	0.5792	0.9395	1.3109	1.5161	1.2613	1.0030

[a] Non-relativistic Coulomb-Born-exchange values for hydrogenic ions from refs. [92–94]. These values are independent of Z.

exceed the non-relativistic results for the higher values of Z and u, as expected. This separation is due to the RDW potential being somewhat different from a pure Coulomb potential and also due to the relativistic effects that are included in our RDW calculations.

Equipped with a reduced cross section that possesses the desired lack of dependence on Z and N (as well as j), we next considered fitting the reduced

cross section, for a given subshell nlj, to a functional form that is the same as that used for the non-relativistic case. Specifically, we considered

$$Q_R^{\rm fit}(nlj,u) = \frac{1}{u}\Big\{A(nlj)\,\ln(u) + D(nlj)\,\left(1-\frac{1}{u}\right)^2 + \left[\frac{c(nlj)}{u}+\frac{d(nlj)}{u^2}\right]\left(1-\frac{1}{u}\right)\Big\}, \tag{5.23}$$

where, as mentioned previously, the dependence on j was found to be small and can be neglected. The reasons for choosing this particular fit formula are discussed in more detail in subsection 5.4.4. The coefficients A, D, c and d are fit parameters to be determined from the computed values of the reduced cross sections discussed above. Once the fit parameters are determined, the cross section in eq. (5.20) for ionization between fine-structure levels can be approximated by

$$Q(U-U'') \approx \frac{\pi}{[I({\rm Ry})]^2}\sum_{\substack{S,S''\\ S_1,S_1''}} B(U,SS_1;U'',S''S_1'')Q_R^{\rm fit}(nlj,u)\,, \tag{5.24}$$

where I is the actual ionization energy for the fine-structure transition denoted by $U-U''$.

Returning to the reduced cross sections in table 11 (and the corresponding $n=3$ and $n=5$ results from ref. [95]), we considered the results for Br-like gold ($N=35$ and $Z=79$) to be a representative data set. These values of Q_R were then fit to the functional form given by eq. (5.23). In doing so, for subshells with $l \geq 1$, fits were made to the mean values

$$Q_R(nl,u) \equiv \tfrac{1}{2}[Q_R(nlj=l-\tfrac{1}{2},u)+Q_R(nlj=l+\tfrac{1}{2},u)] \tag{5.25}$$

since, as previously mentioned, the reduced cross sections do not exhibit a strong dependence on the j quantum number in this case. Of course, more accurate fits would result if each nlj reduced cross section had been considered individually. The resulting fit parameters are provided in ref. [95] and are reproduced here in table 12. These parameters fit the Br-like gold data set to within 2%, with the agreement typically much better than that.

A numerical example, which will not be reproduced here, was provided in ref. [95] to demonstrate the application of these parameters. Specifically, the fit parameters were used to compute fine-structure, inner-shell ionization cross sections from the ground state of Cu-like ($N=29$) gold ions to various final levels with $J=1$ in the Ni-like stage. The resulting fit data were compared with the actual RDW results and a maximum discrepancy of 6% was obtained

Table 12
Values for the parameters in the fits to the reduced cross sections $Q_R(nl, u)$ obtained from Br-like gold results. These parameters are to be used in eq. (5.23) and eq. (5.39).

nl	$A(nl)$	$D(nl)$	$c(nl)$	$d(nl)$	nl	$A(nl)$	$D(nl)$	$c(nl)$	$d(nl)$
3s	0.848	3.67	−0.24	2.70	4f	0.187	6.82	2.67	3.04
3p	0.711	5.06	0.03	3.02	5s	0.584	3.87	0.38	2.56
3d	0.342	7.31	0.90	4.16	5p	0.570	4.09	0.95	2.31
4s	0.686	3.38	1.22	1.45	5d	0.468	5.23	0.81	2.97
4p	0.640	4.17	0.49	2.64	5f	0.288	5.95	2.47	2.66
4d	0.474	5.48	1.78	2.48	5g	0.101	6.64	3.17	2.63

for strong and moderately strong transitions when comparing the two data sets. The reader is referred to ref. [95] for further details.

5.4.2 Fits to $n = 2$ ionization cross sections

Fits to $n = 2$ ionization cross sections were considered in ref. [79]. This study included a large number of calculations of $n = 2$ cross sections to get an idea of what sort of fit formulae and parameters would be required to accurately reproduce the associated reduced cross sections. A preliminary goal of this study was to determine the range of conditions under which the generalized Breit interaction had a significant effect on cross sections that represent ionization from the $n = 2$ subshells. It was found that this interaction became important for $Z \gtrsim 42$ and had a maximum effect of only 13% on the cross sections at the highest Z value of 92. Moreover, these tests indicated a maximum contribution of only 0.1% from the imaginary part of this interaction. Thus, only the real part of the generalized Breit interaction was included when computing the actual reduced cross sections that were used in the fit procedure described below.

The determination of an accurate fit formula and corresponding parameters is somewhat more complicated for ionization from the $n = 2$ subshells than for the $n = 3$–5 subshells described in the previous subsection. The complications arise from two separate considerations. First, the relativistic effects (and, to a lesser extent, the effects of the generalized Breit interaction) on Q_R become much stronger for $n = 2$ ionization as Z increases. From inspection, the relativistic effects start to become important for $Z \gtrsim 30$, which provides a dividing line for consideration of those effects. The second complication concerns the low-Z region for which the relativistic effects are not important. In this region, the ionization cross sections are of interest for a relatively large range of N values (about 1 to 12). This consideration introduces a strong N dependence into the reduced cross sections for low-Z ions, which requires some additional attention.

Based on this information, we chose $Z = 30$ as the approximate boundary for deciding whether weak/strong N dependence and relativistic effects must be considered. For $Z > 30$ the fits were somewhat simpler since they displayed only a weak dependence on N and so we begin with a discussion of those results. There is considerable discussion and detail provided in ref. [79], which will be summarized presently. An inspection of the various calculations for $Z > 30$ indicated that the weak N dependence could be split into two regions: $1 \leq N \leq 7$ and $8 \leq N \leq 12$. Data for the former region can be accurately represented by fitting reduced cross sections that were computed for $N = 4$, while the latter region is well represented by fitting $N = 10$ results. Next, a function $F(Z)$ must be chosen such that a modified reduced cross section, Q'_R, defined by

$$Q'_R(2lj, u) = Q_{\mathrm{R}}(2lj, u)/F(Z), \tag{5.26}$$

is independent of Z for low incident-electron energies. The choices

$$F(Z) = \begin{cases} [66 + (Z/30)^{2.3}]/67 & \text{for 2s} \\ [150 + (Z/30)^{2.5}]/151 & \text{for 2p}^* \\ [76 + (Z/30)^{2.3}]/77 & \text{for 2p} \end{cases} \tag{5.27}$$

were found to work well for the $N = 4$ case, while the choices

$$F(Z) = \begin{cases} [13.75 + (Z/30)^{1.3}]/14.75 & \text{for 2s} \\ [79 + (Z/30)^2]/80 & \text{for 2p}^* \\ [49 + (Z/30)^2]/50 & \text{for 2p} \end{cases} \tag{5.28}$$

worked well for the $N = 10$ case. Then, for $Z = 30$, where $Q'_R = Q_R$, the calculated results were fit to the form

$$Q'_R(2lj, u) = \frac{1}{u}\Big\{A\ln(u) + D\left(1 - \frac{1}{u}\right)^2 + Cu\left(1 - \frac{1}{u}\right)^4 + \left[\frac{c}{u} + \frac{d}{u^2}\right]\left(1 - \frac{1}{u}\right)\Big\}, \tag{5.29}$$

where D, C, c and d are free fit parameters and A is the known constant that reproduces the non-relativistic Bethe high-energy limit for hydrogenic ions. A comparison of eq. (5.29) with eq. (5.23) used in the previous subsection reveals an extra term containing the C parameter. This extra term provides additional flexibility in fitting the $n = 2$ reduced cross sections at high impact energies. It was originally introduced to better fit the high-energy behavior displayed by 1s ionization cross sections and will be discussed in more detail in the next subsection. The resulting fit parameters for the present case of

Table 13
Fit parameters for $n = 2$ ionization to be used in eq. (5.29) and eq. (5.43) when $Z > 30$. See also eqs. (5.30)–(5.32) for a prescription of how the C and D coefficients should be modified as a function of Z.

Subshell	Z	N	A	D	c	d	C
2s	30	4	0.82300	3.29272	1.29228	0.97231	0.12297
		10	0.82300	3.42429	0.74161	1.30061	0.10748
2p*	30	4	0.53000	4.70251	2.21302	1.39644	0.15751
		10	0.53000	5.08482	1.73067	1.75431	0.16469
2p	30	4	0.53000	4.69802	2.24186	1.38246	0.15499
		10	0.53000	5.08759	1.75208	1.75654	0.16191

$Z = 30$ and $N = 4$ are displayed in table 13. The previous procedure was also repeated for $Z = 30$ and $N = 10$, and the resulting fit parameters are also displayed in table 13.

In order to extend these fits beyond $Z = 30$, so that accurate reduced cross sections would be obtained, it was necessary to allow for some of the fit parameters to depend on Z. For the case of $N = 4$ the values of A, c and d were held fixed at their values for $Z = 30$ given in table 13. However, C was allowed to vary with Z, while D was fixed at its $Z = 30$ value over the range $30 \leq Z \leq 50$ and then allowed to vary with Z beyond this range. The choices used to represent this Z dependence were

$$C(Z) = \begin{cases} 0.12297 + [(Z-30)/122]^{1.35} & \text{for 2s} \\ 0.15751 + [(Z-30)/90]^{1.45} & \text{for 2p*} \\ 0.15499 + [(Z-30)/124]^{1.25} & \text{for 2p} \end{cases} \tag{5.30}$$

$$D(Z) = \begin{cases} 3.29272 + [(Z-50)/95]^2 & \text{for 2s} \\ 4.70251 + (Z-50)/100 & \text{for 2p*}. \\ 4.69802 + (Z-50)/170 & \text{for 2p} \end{cases} \tag{5.31}$$

For $N = 10$, the values of A, c and d were also held fixed at their values for $Z = 30$. No improvement was obtained when the D parameter was allowed to depend on Z, and so that parameter was also held fixed at its $Z = 30$ value. Thus, only the C parameter was allowed to vary with Z when $N = 10$ and the functional form was chosen to be

$$C(Z) = \begin{cases} 0.10748 + [(Z-30)/91.6]^{2.8} & \text{for 2s} \\ 0.16469 + [(Z-30)/79]^{2.3} & \text{for 2p*}. \\ 0.16191 + [(Z-30)/96]^{2.5} & \text{for 2p} \end{cases} \tag{5.32}$$

For $Z \leq 30$ we did not consider any explicit Z dependence in the fit formulae or parameters. Therefore, $F(Z) = 1$ and no Z dependence is included in the C and D parameters. However, the strong N dependence must be taken into

Table 14
Fit parameters for $n = 2$ ionization to be used in eq. (5.29) and eq. (5.43) when $Z \leq 30$. These results are to be used in conjunction with the information listed in tables 15 and 16.

Subshell	fit label	Z	N	A	D	c	d	C
2s	m	20	2	0.82300	3.25608	1.39689	0.90728	0.10312
	n	14	3	0.82300	3.19030	1.26373	0.92092	0.09837
	o	20	7	0.82300	3.40125	0.74015	1.28843	0.08671
	p	23	10	0.82300	3.47502	0.42973	1.47638	0.09090
	q	20	10	0.82300	3.49865	0.19704	1.61284	0.08620
	r	10	6	0.82300	3.25615	0.24498	1.42340	0.10526
	s	14	9	0.82300	3.37995	−0.16761	1.67916	0.10495
	t	16	12	0.82300	3.47813	−0.60240	1.90515	0.11514
2p	u	20	3	0.53000	4.63025	2.25094	1.33408	0.13207
	v	9	4	0.53000	5.11279	1.58909	1.88921	0.10317
	w	9	5	0.53000	5.49331	1.00456	2.34350	0.11167
	x	18	10	0.53000	5.46097	0.96675	2.13802	0.17920
	y	12	8	0.53000	5.33521	0.87126	1.95646	0.25035
	z	16	12	0.53000	5.41330	0.41832	2.08234	0.30398

account, particularly for large values of N and small values of u. To address this issue, we found it necessary to compute a number of different sets of fit parameters in order to accurately represent all of the relevant regimes of Z and N. In computing these sets of fit parameters, use was made of the observation that the Q_R values are approximately a function of Z/N when the dependence on N is strong. Hence, a single set of fit parameters can be used for all cases with nearly the same Z/N value.

In the first part of table 14, the recommended fit parameters to be used for 2s ionization, when $Z \leq 30$, are given. A lowercase letter is used to label each set of fit parameters and the corresponding values of Z and N denote from which explicitly calculated set of Q_R data the parameters were determined. Using these labels, the range of Z and N values for which each of these fits can be applied is indicated in table 15.

The lower part of table 14 contains the analogous fit parameters for ionization of a 2p electron when $Z \leq 30$. In this low-Z region, values of Q_R for the 2p* and 2p orbitals agree to within 0.5% and so the same fit parameters apply to both orbitals. The corresponding ranges of Z and N for which these parameters are to be applied are provided in table 16.

A nice summary that describes how to use the various sets of $n = 2$ fit parameters is provided in table A of ref. [79]. Some useful discussions of certain numerical comparisons are also provided in that reference.

Table 15
Regions of N and Z for which each set of 2s fit parameters given in table 14 applies.

Z \ N	1	2	3	4	5	6	7	8	9	10	11	12
4	m											
5	m											
6	m	n										
7	m	n	o									
8	m	n	o	q								
9	m	n	o	p	q							
10	m	n	o	o	q	r						
11	m	n	n	o	q	r	s					
12	m	m	n	o	p	q	r	s				
13	m	m	n	o	p	q	r	r	t			
14	m	m	n	n	o	p	q	r	s	t		
15	m	m	n	n	o	p	p	r	s	t	t	
16	m	m	n	n	o	o	p	q	r	s	t	t
17	m	m	n	n	o	o	p	q	r	s	s	t
18	m	m	n	n	o	o	p	q	r	r	r	s
19	m	m	n	n	n	o	o	p	q	r	r	r
20	m	m	n	n	n	o	o	p	p	q	q	r
21	m	m	m	n	n	n	o	p	p	q	q	r
22	m	m	m	n	n	n	o	o	p	p	q	q
23	m	m	m	n	n	n	o	o	p	p	p	q
24	m	m	m	n	n	n	o	o	o	p	p	q
25	m	m	m	n	n	n	o	o	o	p	p	p
26	m	m	m	m	n	n	n	o	o	p	p	p
27	m	m	m	m	n	n	n	o	o	o	p	p
28	m	m	m	m	n	n	n	o	o	o	o	p
29	m	m	m	m	n	n	n	o	o	o	o	p
30	m	m	m	m	n	n	n	n	o	o	o	o

5.4.3 Fits to 1s ionization cross sections

Our investigation into the fitting of ionization cross sections for a 1s electron [96] proceeded in a manner very similar to that described in the previous subsection for ions in the $n = 2$ shell. In fact, as mentioned earlier, our study of the 1s electron was actually performed before the $n = 2$ work. The first part of this study focused on determining the effect of the generalized Breit interaction on the 1s ionization cross section. Cross sections are displayed in table 17 for 1s ionization in a variety of hydrogenic ions with Z ranging from 10–92. Results are presented for Coulomb-only calculations and calculations that also included the real part of the generalized Breit interaction. As in previous calculations, the imaginary part of the generalized Breit interaction was found to make only a small contribution to the cross section, even at the highest Z value of 92. In that case, the contribution of the imaginary part was

Table 16
Regions of N and Z for which each set of 2p fit parameters given in table 14 applies.

Z \ N	1	2	3	4	5	6	7	8	9	10	11	12
4	u											
5	u											
6	u	u										
7	u	u	u									
8	u	u	u	v								
9	u	u	u	v	w							
10	u	u	u	v	w	x						
11	u	u	u	v	w	x	y					
12	u	u	u	v	v	w	x	y				
13	u	u	u	v	v	w	w	x	y			
14	u	u	u	u	v	w	w	x	y	z		
15	u	u	u	u	v	v	w	x	y	z	z	
16	u	u	u	u	v	v	w	x	y	y	z	z
17	u	u	u	u	v	v	w	w	x	y	y	z
18	u	u	u	u	v	v	v	w	w	x	y	y
19	u	u	u	u	v	v	v	w	w	x	x	x
20	u	u	u	u	v	v	v	w	w	w	x	x
21	u	u	u	u	v	v	v	w	w	w	w	x
22	u	u	u	u	v	v	v	w	w	w	w	x
23	u	u	u	u	v	v	v	w	w	w	w	w
24	u	u	u	u	v	v	v	v	w	w	w	w
25	u	u	u	u	v	v	v	v	w	w	w	w
26	u	u	u	u	v	v	v	v	v	w	w	w
27	u	u	u	u	v	v	v	v	v	w	w	w
28	u	u	u	u	v	v	v	v	v	w	w	w
29	u	u	u	u	v	v	v	v	v	w	w	w
30	u	u	u	u	v	v	v	v	v	v	w	w

only 1.6% for incident energies near threshold. The real part of the generalized Breit interaction, on the other hand, has a very significant effect. As expected, the effect increases with Z and incident energy, u, up to a maximum of 60% for $Z = 92$. For $Z = 30$, the effect dwindles to only a few percent and was omitted for $Z = 10$ and 20 because it was negligible.

The next step was to investigate the reduced 1s cross section for a range of ions in order to determine the best approach to fitting those results. The results used for this purpose are presented in table 18. In this table, results for H-like and He-like ions are presented for fine-structure transitions, while the results for Li-like and Be-like ions are based on the pseudo-hydrogenic cross section with the orbital binding energy chosen for the ionization energy. Exceptions to this latter description occur at $Z = 10$ for which results are also presented for fine-structure transitions when the final level is listed. From inspection

Table 17
Comparison of results for 1s ionization cross sections (in units of 10^{-24} cm^2) for hydrogenic ions for various incident electron energies u (in threshold units) and nuclear charge Z. Upper entries are values calculated with only the Coulomb interaction included, while lower entries are values calculated with the generalized Breit interaction also included.

	Z							
u	10	20	30	42	50	66	79	92
1.125	2490	155.7	30.8	8.04	4.01	1.327	0.649	0.355
			31.2	8.33	4.27	1.535	0.831	0.516
1.250	4219	264.0	52.3	13.65	6.82	2.259	1.106	0.605
			53.1	14.21	7.29	2.636	1.432	0.889
1.500	6374	399.3	79.2	20.74	10.37	3.453	1.695	0.926
			80.6	21.71	11.19	4.081	2.227	1.381
2.250	8624	542.5	108.3	28.67	14.46	4.897	2.429	1.331
			110.9	30.32	15.82	5.910	3.268	2.029
4.000	8453	538.9	109.9	30.03	15.51	5.503	2.815	1.569
			113.1	32.16	17.28	6.823	3.894	2.450
6.000	7266	471.2	98.6	27.96	14.83	5.512	2.903	1.647
			102.0	30.31	16.80	7.009	4.126	2.639

of these results, we chose $Z = 20$ to be the approximate value above which relativistic effects become significant. It is also noted that the N dependence is rather weak above this Z value, and so it was decided that the reduced cross sections for hydrogenic ions with $Z = 20$ would be used in determining the fit parameters for $Z \geq 20$. We will return to a discussion of ions with $Z < 20$ near the end of this subsection.

The final concern with choosing an appropriate fit formula for the 1s reduced cross section was the fact that the cross section does not fall off with the usual $\ln(u)/u$ dependence, which is the non-relativistic, Bethe high-energy limit. Instead, as demonstrated by the results in figure 2, the 1s cross section is roughly constant for the higher impact energies. This behavior is not unexpected because the standard $\ln(u)/u$ limit is not valid for such relativistic energies. In fact, Bethe's original formula, which was written in terms of velocities, is valid for both relativistic and non-relativistic energies. A more appropriate form of the relativistic Bethe formula is given by $\ln(\beta^2+G)/\beta^2$, where β has the usual definition of $\beta = v/c$ and G is a constant. It is easily verified that this last expression approaches a constant value for very high energies due to the fact that the velocity v of the incident electron is bounded by the speed of light. This expression is expected to describe the limiting behavior when only the Coulomb interaction is considered in the scattering matrix elements. If any of the various forms of the Breit interaction are also considered, then there is a predicted "relativistic rise" in the cross section that occurs at sufficiently high incident energies. In this case, extra terms, which grow with increasing impact energy, must be added to the standard Bethe formula. When specifically considering the original Breit interaction, a limiting behavior of the form

Table 18
Reduced cross sections $Q_R(1s, u)$ and ionization energies I(Ry) for ions in the ground state with various N and Z values. $x[y] = x \times 10^y$.

		Final		$u = \varepsilon/I$					
Z	N	level	I(Ry)	1.125	1.250	1.500	2.250	4.000	6.000
10	1		1.0013[2]	0.2837	0.4807	0.7264	0.9828	0.9632	0.8280
	2		8.7797[1]	0.2714	0.4580	0.7038	0.9682	0.9669	0.8396
	3		8.4376[1]	0.2636	0.4557	0.6951	0.9694	0.9768	0.8495
	3	$(1s2s)_0$	8.4793[1]	0.2647	0.4577	0.6982	0.9744	0.9819	0.8539
	3	$(1s2s)_1$	8.4007[1]	0.2626	0.4539	0.6923	0.9650	0.9721	0.8455
	4		8.0893[1]	0.2587	0.4434	0.6824	0.9600	0.9790	0.8574
	4	$(1s2s^2)_{1/2}$	8.0795[1]	0.2584	0.4430	0.6816	0.9588	0.9777	0.8563
20	1		4.0205[2]	0.2861	0.4851	0.7337	0.9968	0.9901	0.8657
	2		3.7688[2]	0.2793	0.4743	0.7217	0.9882	0.9896	0.8682
	3		3.6975[2]	0.2774	0.4722	0.7196	0.9886	0.9942	0.8733
	4		3.6213[2]	0.2730	0.4679	0.7142	0.9862	0.9960	0.8766
23	1		5.3261[2]	0.2873	0.4871	0.7369	1.0030	1.0017	0.8822
30	1		9.1063[2]	0.2943	0.5003	0.7602	1.0450	1.0659	0.9610
42	1		1.8062[3]	0.3091	0.5269	0.8051	1.1244	1.1927	1.1240
50	1		2.5869[3]	0.3245	0.5545	0.8509	1.2030	1.3143	1.2779
	2		2.5181[3]	0.3198	0.5469	0.8407	1.1904	1.3012	1.2642
	3		2.5036[3]	0.3192	0.5461	0.8400	1.1907	1.3027	1.2655
	4		2.4825[3]	0.3173	0.5432	0.8361	1.1869	1.2995	1.2623
66	1		4.6373[3]	0.3751	0.6444	0.9976	1.4447	1.6678	1.7134
	2		4.5389[3]	0.3702	0.6352	0.9850	1.4270	1.6468	1.6905
79	1		6.8591[3]	0.4446	0.7660	1.1912	1.7477	2.0825	2.2067
	2		6.7311[3]	0.4383	0.7554	1.1754	1.7248	2.0546	2.1764
92	1		9.7078[3]	0.5531	0.9522	1.4798	2.1740	2.6247	2.8273
	2		9.5422[3]	0.5455	0.9391	1.4599	2.1451	2.5903	2.7942
	3		9.5407[3]	0.5459	0.9394	1.4614	2.1481	2.5950	2.8024
	4		9.4934[3]	0.5431	0.9394	1.4545	2.1389	2.5845	2.7890

$\{\ln[\beta^2/(1-\beta^2)] - \beta^2 + G\}/\beta^2$ is obtained [97]. One can see from the data in figure 2 and table 17 that the results which include the generalized Breit interaction are increasing slightly faster than the Coulomb-only data as the incident energy and Z value increase. This behavior is an indication that the cross sections are approaching the region in which the relativistic rise occurs. Due to the numerical difficulties associated with obtaining converged cross sections for energies beyond $u = 6$, the highest energy for which detailed cross sections were calculated, we were not able to further explore this behavior. In any event, we do not expect our fits to be reliable for u values that are appreciably greater than 6, which is sufficiently large for most practical applications.

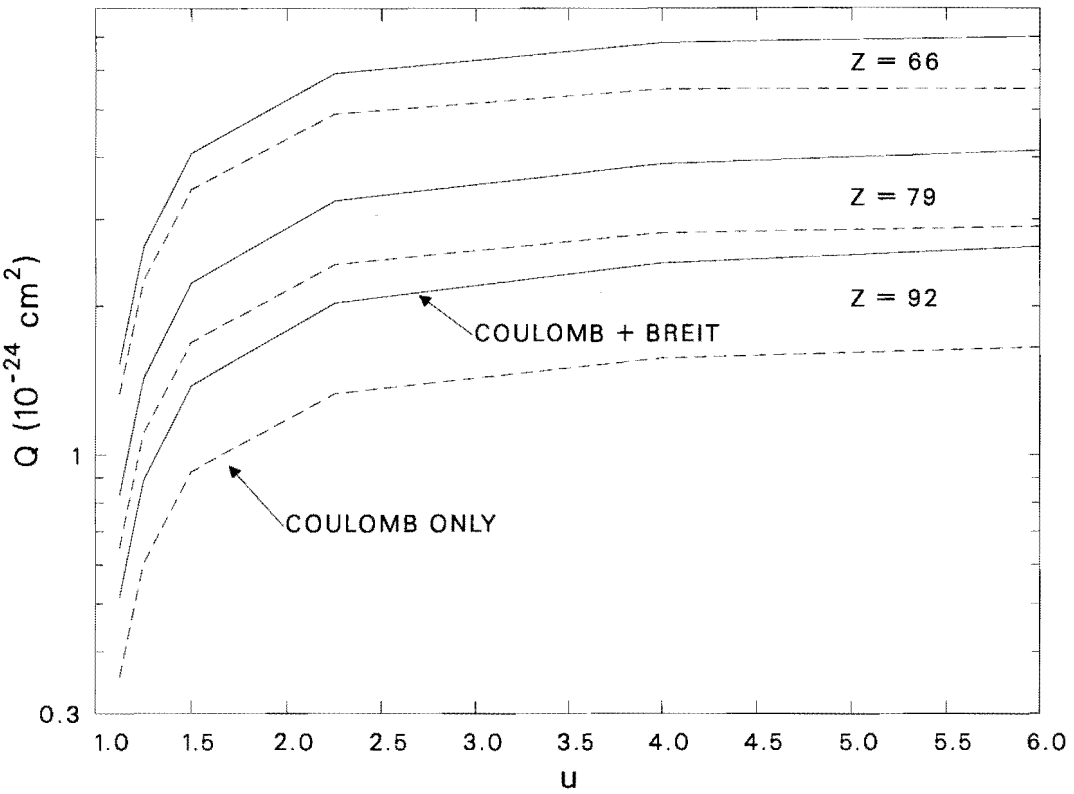

Fig. 2. Ionization cross sections for the 1s electron in hydrogenic ions as a function of incident energy in threshold units. Results are provided for $Z = 66$, 79 and 92. The dashed lines represent results calculated with only the Coulomb interaction included in the scattering matrix elements. The solid lines represent results calculated with both the Coulomb interaction and the real part of the generalized Breit interaction.

After taking these issues into account, the fitting procedure can proceed as described in the previous subsection. First, we define a modified reduced cross section

$$Q'_R(1\mathrm{s}, u) = Q_R(1\mathrm{s}, u)/F(Z), \tag{5.33}$$

where $F(Z)$ is chosen such that $Q'_{\mathrm{R}}(1\mathrm{s}, u)$ is independent of Z for low incident-electron energies (i.e. $u \approx 1$). The choice

$$F(Z) = [140 + (Z/20)^{3.2}]/141 \tag{5.34}$$

accomplishes this independence to within 1% for the explicitly calculated values of Q_R. Then, for $Z = 20$, where $Q'_R = Q_R$, we fit the calculated results for $N = 1$ to the form

$$Q'_R(1\mathrm{s}, u) = \frac{1}{u}\left\{A\ln(u) + D\left(1 - \frac{1}{u}\right)^2 + Cu\left(1 - \frac{1}{u}\right)^4\right.$$

$$+\left[\frac{c}{u}+\frac{d}{u^2}\right]\left(1-\frac{1}{u}\right)\Bigg\}, \qquad (5.35)$$

where $A = 1.13$ is the known constant that reproduces the non-relativistic, Bethe high-energy limit and D, C, c and d are free fit parameters. As stated in the previous subsection, the term that contains the C parameter was added to the standard fit formula in order to more accurately capture the (nearly constant) high-energy behavior of the 1s cross section for very high-Z ions. The fit parameters that resulted from this procedure are listed in the second row of table 19.

Table 19
Fit parameters for 1s ionization obtained from hydrogenic ions with $Z = 20$ and He-like ions with $Z = 10$. These parameters are to be used in eq. (5.35) and eq. (5.43). The first row of data should be used for ions with $Z < 20$ and the second row of data should be used for ions with $Z \geq 20$. The latter results should be used in conjunction with eqs. (5.36)–(5.38).

Z	N	A	D	c	d	C
10	2	1.1300	3.82652	−0.80414	2.32431	0.14424
20	1	1.1300	3.70590	−0.28394	1.95270	0.20594

For $Z > 20$, we first attempted to use eq. (5.35) with the coefficients A, D, c and d fixed at the same values as for $Z = 20$, but allowed C to be a free parameter in determining the best fits at each of the remaining test Z values. This approach led to fits that were accurate to within 2.4% or better at each of the test Z values. We then used these best values of C to express C as a function of Z. The resulting functions, which preserve the accuracy to within 2.4% at the test Z values, are given by

$$C(Z) = [(Z-20)/50.5]^{1.11} + C(Z=20),\ 20 \leq Z \leq 66 \qquad (5.36)$$

and

$$C(Z) = [(Z-20)/53]^{0.73} + C(Z=20),\ 67 \leq Z \leq 92. \qquad (5.37)$$

Furthermore, the single formula

$$C(Z) = [(Z-20)/55]^{0.92} + C(Z=20),\ 20 \leq Z \leq 92 \qquad (5.38)$$

gives only slightly worse accuracy over the entire range of Z values.

Although the $Z = 20$ fit parameters obtained from the above procedure also produce a fairly good reproduction of $Q_R(1s, u)$ for $Z < 20$, further numerical studies showed that fitting the He-like, $Z = 10$ results with eq. (5.35) gives an

improved overall accuracy for the low-Z region. In this region, there is no need to define a quantity like Q'_R (i.e. $F(Z) \equiv 1$), or to express C as a function of Z, because there is essentially no Z dependence exhibited by the reduced cross sections in this region. The fit parameters that resulted from this procedure are listed in the first row of table 19. Thus, we recommend that the first row of table 19 should be used for ions with $Z < 20$ and the second row should be used for ions with $Z \geq 20$. The latter set of parameters should be used in conjunction with eqs. (5.36)–(5.38).

5.4.4 The form of the fit formulae and ionization rate coefficients

As mentioned in refs. [92–94], which deal with the fitting of non-relativistic ionization cross sections, the particular fit formula appearing in eq. (5.23) was chosen for two reasons. First, it reproduces the appropriate physical behavior in the various incident-electron energy regimes. For example, the A coefficient multiplies the $\ln(u)/u$ term, which represents the well-known Bethe high-energy limit of the ionization cross section for non-relativistic electrons. Second, eq. (5.23) can be readily integrated over a Maxwellian distribution function, representing the velocity distribution of the continuum electrons at a temperature T, to obtain the ionization rate coefficient in terms of exponential integrals. The expression for the collisional excitation rate coefficient that corresponds to cross section $Q(i-f)$ was previously provided in eq. (4.108). This same expression holds for the ionization rate coefficient, provided that the excitation cross section is replaced with the ionization cross section.

For ionization of $n = 3$, 4 and 5 electrons, it is sufficient to consider the Maxwellian distribution in its non-relativistic form, as opposed to the relativistic approach taken in chapter 4. With this choice, the rate coefficient for ionization that corresponds to the cross section in eq. (5.24) is given (in regular units, rather than Rydberg atomic units) by

$$\begin{aligned} C(U-U'';kT) = \left(\frac{8kT}{\pi m}\right)^{1/2} \frac{\pi a_0^2}{[I(\mathrm{Ry})]^2}\, y \sum_{\substack{S,S'' \\ S_1,S_1''}} B(U,SS_1;U'',S''S_1'') \\ \times\{D(nlj)\mathrm{e}^{-y} - y\,d(nlj)E_3(y) \\ +[A(nlj)+y\,c(nlj)-2y\,D(nlj)]E_1(y) \\ +y[D(nlj)+d(nlj)-c(nlj)]E_2(y)\}\,, \end{aligned} \tag{5.39}$$

where m is the electron mass, I is the ionization energy of the actual fine-structure transition denoted by $U-U''$,

$$y = I/kT \tag{5.40}$$

with k being Boltzmann's constant, and $E_n(y)$ represents the exponential integrals

$$E_n(y) = \int_1^\infty \frac{\mathrm{e}^{-yx}}{x^n} dx \,. \tag{5.41}$$

Additional discussion is provided in ref. [95] concerning the application of continuum lowering to eq. (5.39). The details are relatively straightforward and, under such considerations, eq. (5.39) becomes eq. (9) of ref. [95].

The fit formula that was applied to the ionization of electrons residing in the $n = 1$ and $n = 2$ shells, eq. (5.29) or eq. (5.35), can also be integrated over a Maxwellian to obtain the associated rate coefficient in terms of exponential integrals. Recall that eqs. (5.29) and (5.35) differ from eq. (5.23) only in that they contain an extra term in order to better represent the high-energy behavior of the reduced cross section. This extra term requires some additional, but straightforward, work in determining the corresponding rate coefficient. Since the ionization of $n = 1$ and $n = 2$ electrons is potentially influenced by relativistic effects, we consider here the relativistic form of the Maxwellian that is described in chapter 4. Applying eq. (5.20) to eq. (4.108), we obtain the rate coefficient in the form

$$C(U - U''; kT) = \sum_{\substack{S,S'' \\ S_1,S_1''}} B(U, SS_1; U'', S''S_1'') C_{\mathrm{H}}^{\mathrm{ps}}(nlj; kT) \,, \tag{5.42}$$

where the pseudo-hydrogenic ionization rate coefficient for an $n = 1$ or $n = 2$ electron is given (again in regular units) by

$$\begin{aligned} &C_{\mathrm{H}}^{\mathrm{ps}}(nlj; kT) \\ &\quad = \frac{2I_{\mathrm{H}} F(Z) \mathrm{e}^{-\eta}}{N_{\mathrm{e}} h y} \Bigg[\Big\{ [\,(D - 3C) + C/y] \mathrm{e}^{-y} \\ &\qquad + [A + y(c - 2D + 6C)] E_1(y) \\ &\qquad + y(D - 4C + d - c) E_2(y) + y(C - d) E_3(y) \Big\} \\ &\qquad + \frac{\alpha^2}{4} I(\mathrm{Ry}) \Big\{ [(c - D + 3C) + \frac{1}{y}(A + D - 2C) + 2C/y^2] \mathrm{e}^{-y} \\ &\qquad + [y(D + d - c - 4C) + A/y] E_1(y) + y(C - d) E_2(y) \Big\} \Bigg] \,. \end{aligned} \tag{5.43}$$

Some of the symbols in eq. (5.43) have already been previously defined. For example, y is given by eq. (5.40), and the E_n are the exponential integrals from eq. (5.41). The symbol $I_{\mathrm{H}} = 1$ Ry is the ionization energy of the hydrogen atomic, h is Planck's constant and $\alpha = 1/137.036$ is the fine-structure

constant. The entire term containing α^2 can typically be ignored for ions with $Z \lesssim 26$. Finally, N_e is the electron number density and the inverse of the exponential $e^{-\eta}$, which is a normalization factor for the relativistic Maxwellian distribution, is provided in eq. (4.109). It should be noted that useful examples for $n = 1$ and $n = 2$ ionization have been provided in refs. [96] and [79], regarding certain simple cases for which the quadruple sum in eq. (5.42) reduces to a single B factor.

5.5 Configuration-average cross sections for electron-impact ionization

An expression for the configuration-average cross section for electron-impact ionization is determined in exactly the same manner as described in section 4.13 for the case of electron-impact excitation. Thus, we define the configuration-average ionization cross section between two configurations c and c'' as

$$Q_{c-c''} \equiv \sum_{i \in c} \sum_{j \in c''} g_i Q_{i-j} / g_c \,, \tag{5.44}$$

where Q_{i-j} is the cross section between two pure SCSFs labeled i and j, and g_c is the statistical weight of the initial configuration given by eq. (3.45). For ionization, the final configuration is denoted as c'' instead of c' to emphasize the fact that the final configuration has one fewer electron than the initial configuration. As in section 4.13, we again make the approximation that the ionization energy associated with each of the SCSF transitions can be accurately represented by the configuration-average transition energy, $\Delta E_{c-c''}$. The result is that each SCSF cross section in eq. (5.44) is described by a scattered and ejected electron with kinetic energies that satisfy the relation $\epsilon' + \epsilon'' = \epsilon - \Delta E_{c-c''}$, where $\Delta E_{c-c''} = E_{c''} - E_c$. With this assumption, eq. (5.44) can be rewritten in the very simple form

$$Q_{c-c'} = w_\alpha Q_{\mathrm{H}}^{\mathrm{ps}}(n_\alpha l_\alpha j_\alpha) \,, \tag{5.45}$$

where the form of the pseudo-hydrogenic ionization cross section is given by eq. (5.14). As usual, the pseudo-hydrogenic cross section should be computed with energies and radial wave functions that are appropriate to the particular ion under consideration.

For comparison, we note that, if eq. (5.45) were to be recast in the form of a collisional ionization strength, the result would be the relativistic analog of eq. (16) given by Peyrusse [28]. As a check, we note that it is trivial to verify that eq. (5.45) reduces to the correct hydrogenic expression for the case of hydrogenic ions ($w_\alpha = 1$). We also note that the form of eq. (5.45) is very similar to the analogous expression for excitation in eq. (4.106), except

that the leading statistical factor is simpler for the case of ionization. This simplification is due to the fact that, for the case of ionization, the active bound electron residing in subshell $n_\alpha l_\alpha j_\alpha$ is ionized to become a continuum electron that resides in an orbital denoted by the quantum numbers $l''j''$ with an occupancy that is always one. Setting $w_\beta = 1$ in eq. (4.106) produces the simplified statistical factor that appears in eq. (5.45) above.

6 Photoionization

Photoionization (PI) cross sections of atoms and ions are crucial in the modeling of astrophysical and laboratory plasmas in the presence of an external radiation field, or that are not optically thin. Among the many applications, the most extensive is perhaps the calculation of the opacity of the plasma under both local thermodynamic equilibrium (LTE) and non-LTE conditions. As in the case of electron-impact ionization, both the non-factorized and factorized methods for calculating fine-structure photoionization cross sections are described in this chapter. In addition, expressions are also provided for the configuration-average case. We note that the expressions for the cross section provided in this section are in the length form (see subsection 3.1.2) and with the effect of retardation (see sections 3.3 and 3.4) omitted.

6.1 General expressions for photoionization cross sections

In writing an expression for the relativistic photoionization cross section, we adopt the method that was outlined in ref. [98], which employs the generalized line strength. Thus, for a transition from a fine-structure level denoted by the quantum numbers $\Delta_t J_t$ in a given ion stage to a level denoted by $\Delta_t'' J_t''$ in the adjacent ion stage with one less electron, the photoionization cross section is given by

$$Q_{\rm PI}(\Delta_t J_t - \Delta_t'' J_t'') = \frac{4\pi\alpha E_{\rm p}}{3(2J_t+1)} \sum_{l',j',J'} \mathcal{S}(\Delta_t J_t, \Delta_t'' J_t'' \epsilon' l' j' J'), \tag{6.1}$$

where $E_{\rm p}$ is the photon energy in Rydbergs and ϵ' is the ejected-electron kinetic energy related to $E_{\rm p}$ and the ionization energy ΔE by

$$\epsilon' = E_{\rm p} - \Delta E(\Delta_t J_t - \Delta_t'' J_t'')\,. \tag{6.2}$$

The symbol $\mathcal{S}$ represents the generalized oscillator strength, which is a generalization of the line strength in eq. (3.14), and is given by

$$\mathcal{S}(\Delta_t J_t, \Delta_t'' J_t'' \epsilon' l' j' J') = |\langle \Delta_t J_t \parallel \boldsymbol{P}^{(1)} \parallel \Delta_t'' J_t'' \epsilon' l' j' J' \rangle|^2 . \tag{6.3}$$

Here, the symbol J' represents the total angular momentum of the final system formed by the final ion in level $\Delta_t'' J_t''$ and the free (ionized) electron composed of partial waves that are denoted by the usual notation $\epsilon' l' j'$. By analogy with eq. (3.17), the reduced matrix element can be written as

$$\begin{aligned}\langle \Delta_t J_t \parallel \boldsymbol{P}^{(1)} \parallel \Delta_t'' J_t'' \epsilon' l' j' J' \rangle = \sum_{\beta_t, \beta_t''} & b^{J_t}(\Delta_t, \beta_t) b^{J_t''}(\Delta_t'', \beta_t'') \\ & \times \langle \beta_t J_t \parallel \boldsymbol{P}^{(1)} \parallel \beta_t'' J_t'' \epsilon' l' j' J' \rangle , \end{aligned} \tag{6.4}$$

where β_t represents all quantum numbers in addition to J_t that are necessary to specify the pure SCSF basis state $\beta_t J_t$ with corresponding mixing coefficient $b^{J_t}(\Delta_t, \beta_t)$. (The omission of the magnetic quantum number in describing an SCSF is potentially confusing. See the explanatory note following eq. (3.17).) Double primes on symbols indicate corresponding quantities in the final state. Due to the presence of the reduced matrix element in eq. (6.4), the summation in eq. (6.1) spans all of the free-electron quantum numbers and values of the total angular momentum of the final system J' that are permitted by the selection rules provided in subsection 3.1.3 for an electric dipole transition. In particular, the relation

$$J_t - J' = \pm 1, \text{ or } 0 \tag{6.5}$$

must be satisfied, but $J_t = J' = 0$ is not permitted. Also, the parity must change between the initial state, denoted by $\beta_t J_t$, and the final system, denoted by $\beta_t'' J_t'' \epsilon' l' j' J'$.

In order to evaluate the reduced matrix element appearing on the right-hand side of eq. (6.4), we mirror the approach described in section 3.2 and first consider the case for which the target ion is in a state comprised of only empty or closed subshells, in addition to the active subshell designated by the subscript a. The completely antisymmetric wave function for w electrons in subshell a of the initial state is then given by eq. (3.20). The corresponding wave function for the final system of ion plus free electron can be obtained from eq. (3.22) by substituting free-electron quantities for the final, active-electron quantities in the appropriate places. The result is

$$\begin{aligned}&\Psi[(n_a l_a j_a)^{w-1} \alpha_a'' J_a'' \epsilon' l' j' J' M' \mid x_1 x_2 \cdots x_w] = \\ &\quad \frac{1}{\sqrt{w}} \sum_{p=1}^{w} (-1)^{w-p} \sum_{M_a'', m'} C(J_a'' j' M_a'' m'; J' M') \\ &\quad \times \Psi[(n_a l_a j_a)^{w-1} \alpha_a'' J_a'' M_a'' \mid x_1 x_2 \cdots x_{p-1} x_{p+1} \cdots x_w] u_{\epsilon' l' j' m'}(x_p) . \end{aligned} \tag{6.6}$$

Then, performing manipulations similar to those described in section 3.2, we obtain

$$\begin{aligned}\langle \beta_t J_t \parallel \boldsymbol{P}^{(1)} \parallel \beta_t'' J_t'' \epsilon' l' j' J' \rangle = \sqrt{w}[(2J_t+1)(2J'+1)]^{1/2}(-1)^{J'+J_t''+j'} \\ \times \begin{Bmatrix} j_a & 1 & j' \\ J' & J_t'' & J_t \end{Bmatrix} (j_a^{w-1}\alpha_a'' J_a'' \mid\} j_a^w \alpha_a J_a) \\ \times \langle j_a \parallel \boldsymbol{C}^{(1)} \parallel j' \rangle \langle n_a l_a j_a \mid r \mid \epsilon' l' j' \rangle \,, \end{aligned} \tag{6.7}$$

where the radial matrix element is given by

$$\begin{aligned}&\langle n_a l_a j_a \mid r \mid \epsilon' l' j' \rangle \\ &\qquad = \int_0^\infty [P_{n_a l_a j_a}(r) P_{\epsilon' l' j'}(r) + Q_{n_a l_a j_a}(r) Q_{\epsilon' l' j'}(r)] r \, \mathrm{d}r \,. \end{aligned} \tag{6.8}$$

We note that in eq. (6.7), for the present case of ions with initially only empty or closed subshells, in addition to the active subshell, the relationships $J_a'' = J_t''$ and $J_a = J_t$ are valid.

For more complex cases of additional partially filled subshells, the form of eq. (6.7) remains unchanged, except for inclusion of additional angular factors that arise from the presence of these extra partially filled subshells. The appropriate references for obtaining these extra factors are provided in section 3.2. Alternatively, as noted at the end of subsection 3.2.1, for the general case, one can also use the MCT module of the Grant code [34] to obtain the angular coefficient for the generalized line strength. In order to write an expression for the photoionization cross section for a general transition in terms of the MCT coefficients, we again follow the approach in section 3.2. Specifically, we use the simplified notation $U = \Delta_t J_t$ and $U'' = \Delta_t'' J_t''$ for the initial and final levels. Also, we let $S = \beta_t J_t$ indicate a pure SCSF state contributing to U, while $S'' = \beta_t'' J_t''$ indicates a pure SCSF state contributing to U''. (The omission of the magnetic quantum number in describing an SCSF is potentially confusing. See the explanatory note following eq. (3.17).) With this notation

$$U = \sum_S b(U,S)|S\rangle, \quad U'' = \sum_{S''} b(U'',S'')|S''\rangle \,, \tag{6.9}$$

where the b's are the mixing coefficients formerly called $b^{J_t}(\Delta_t, \beta_t)$ and $b^{J_t''}(\Delta_t'', \beta_t'')$ in eq. (6.4). After some manipulation, we arrive at the expression

$$\begin{aligned}\langle \Delta_t J_t \parallel \boldsymbol{P}^{(1)} \parallel \Delta_t'' J_t'' \epsilon' l' j' J' \rangle &\equiv \langle U \parallel \boldsymbol{P}^{(1)} \parallel U'' \epsilon' l' j' J' \rangle \\ &= \sum_{S,S''} b(U,S) b(U'',S'') d^{(1)}(S, S'' l' j' J') \\ &\qquad \times \mathcal{L}_{\mathrm{H}}^{\mathrm{ps}}(n_a l_a j_a, \epsilon' l' j') \,, \end{aligned} \tag{6.10}$$

where $d^{(1)}(\cdots)$ is the angular coefficient obtained from Grant's MCT package for the electric dipole operator and

$$\mathcal{L}_{\rm H}^{\rm ps}(n_a l_a j_a, \epsilon' l' j') = \langle n_a l_a j_a \mid r \mid \epsilon' l' j' \rangle \langle j_a \parallel \boldsymbol{C}^{(1)} \parallel j' \rangle \tag{6.11}$$

is the pseudo-hydrogenic electric dipole matrix element for the transition between the bound orbital $n_a l_a j_a$ and the orbital $\epsilon' l' j'$ associated with the photoionized continuum electron.

Finally, applying eqs. (6.10) and (6.3) to eq. (6.1), the photoionization cross section between levels U and U'' can be written as

$$Q_{\rm PI}(U - U'') = \frac{4\pi\alpha E_{\rm p}}{3(2J_t+1)} \sum_{l',j',J'} \left| \sum_{S,S''} b(U,S) b(U'',S'') \times d^{(1)}(S, S'' l' j' J') \mathcal{L}_{\rm H}^{\rm ps}(n_a l_a j_a, \epsilon' l' j') \right|^2 . \tag{6.12}$$

This non-factorized expression was implemented in a computer program to compute RDW photoionization cross sections [98]. The motivation for this work was to calculate high-energy photoionization cross sections to complement results computed at lower photon energies by members of the Opacity Project (OP) [99] using the close-coupling R-matrix method. As an illustration of this work, we note that RDW and R-matrix total PI cross sections for Be-like ions in the ground term $1s^2 2s^2\ ^1S$ with $Z = 4$–20 and 26 were presented in ref. [100]. The R-matrix results presented in this reference were computed with a more extensive target expansion than previously considered, and were compared with data computed from the present RDW approach and with R-mtarix data computed by Tully et al. [101], under the OP [99], when available. It was shown [100] that discernible differences in the background contribution to the cross section for neutral Be consistently decreased as one considered more highly charged Be-like ions. For example, in the case of neutral Be, the difference between the RDW cross sections and the R-matrix cross sections was around 18% at 5 Ry. However, for C III the difference was around 3% at 15 Ry. At energies above the inner-shell threshold, the difference between the results was consistently around 10% for the various ions under investigation. Comparisons for ions with $Z = 16$–20 and 26 are reproduced here in figure 3.

6.2 Factorized expressions for photoionization cross sections

As in the case of electron-impact ionization, the expression for the photoionization cross section can be written in a convenient factorized form. In fact, as will be shown, the form of such an expression is very similar to that provided

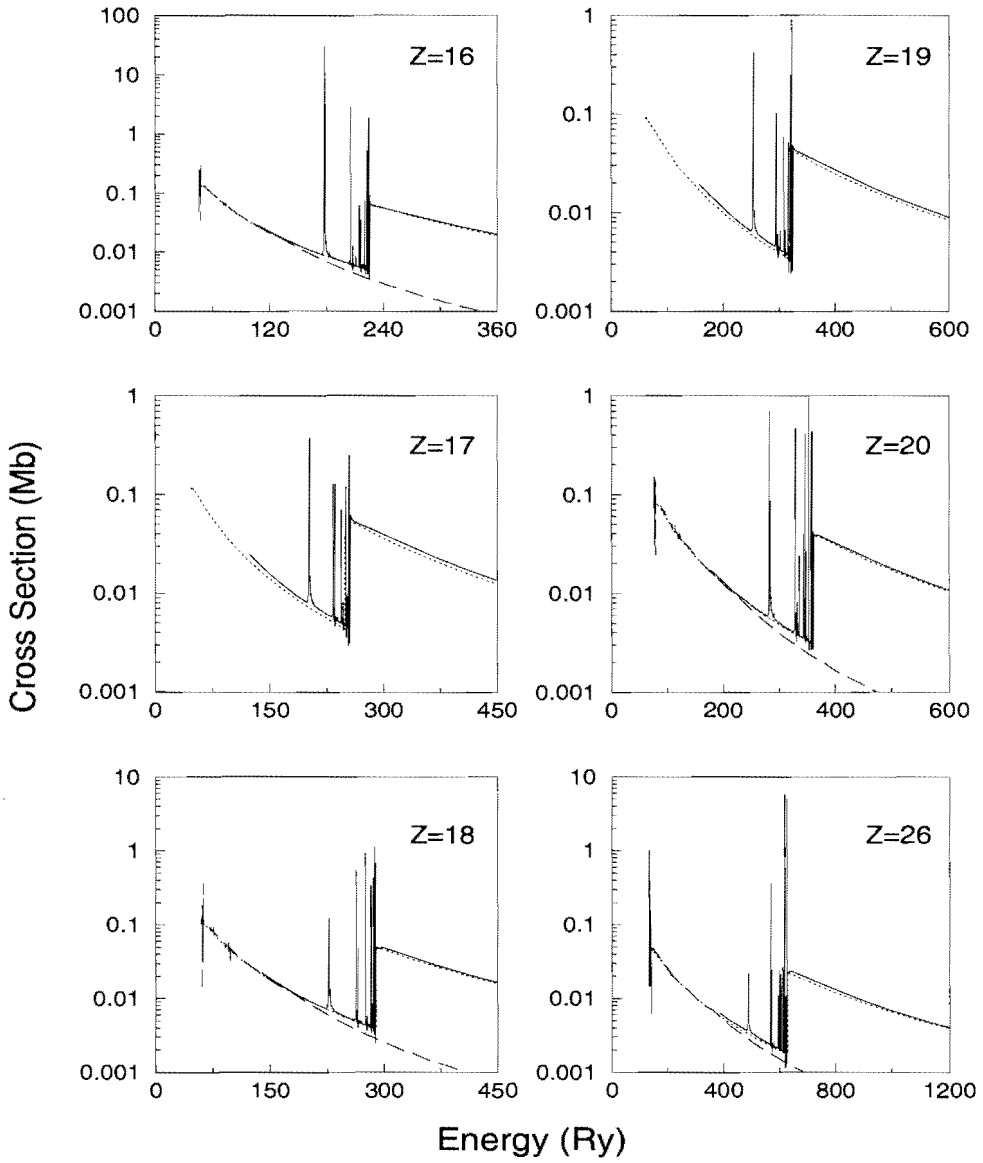

Fig. 3. Total photoionization cross sections for Be-like ions with Z = 16–20 and 26: — R-matrix results, $\cdots$ RDW results, $-\,-\,-$ OP results of Tully et al. [101] augmented with $1/(E_{\rm p})^3$ extrapolation at high energies.

for collisional ionization in eq. (5.17). In order to produce the factorized expression for photoionization, we again consider the case where the initial level of the target ion contains only empty or closed subshells, in addition to the active subshell a. With this assumption, the summation in eq. (6.1) can be expanded according to eqs. (6.3), (6.4), (6.7) and (6.11) to yield

$$\frac{1}{2J_t+1}\sum_{l',j',J'}\mathcal{S}(\Delta_t J_t, \Delta_t'' J_t'' \epsilon' l' j' J')$$

$$
\begin{aligned}
&= \frac{1}{2J_t+1}\sum_{l',j',J'}\left|\sum_{S,S'} b(U,S)b(U'',S'')\langle\beta_t J_t \parallel \boldsymbol{P}^{(1)} \parallel \beta''_t J''_t \epsilon' l' j' J'\rangle\right|^2 \\
&= \sum_{l',j',J'}\sum_{\substack{S,S''\\ S_1,S''_1}} b(U,S)b(U'',S'')b(U,S_1)b(U'',S''_1)\sqrt{w}\sqrt{w_1}(2J'+1) \\
&\quad\times(j_a^{w-1}\alpha''_a J''_a \,|\}j_a^w \alpha_a J_a)(j_{a_1}^{w_1-1}\alpha''_{a_1} J''_{a_1} \,|\}j_{a_1}^{w_1}\alpha_{a_1} J_{a_1}) \\
&\quad\times\begin{Bmatrix} j_a & 1 & j' \\ J' & J''_t & J_t \end{Bmatrix}\begin{Bmatrix} j_{a_1} & 1 & j' \\ J' & J''_t & J_t \end{Bmatrix} \\
&\quad\times\mathcal{L}^{\rm ps}_{\rm H}(n_a l_a j_a, \epsilon' l' j')\mathcal{L}^{\rm ps}_{\rm H}(n_{a_1} l_{a_1} j_{a_1}, \epsilon' l' j')\,. \qquad (6.13)
\end{aligned}
$$

Using the property of the 6-j symbol given by

$$
\sum_{J'}(2J'+1)\begin{Bmatrix} j_a & 1 & j' \\ J' & J''_t & J_t \end{Bmatrix}\begin{Bmatrix} j_{a_1} & 1 & j' \\ J' & J''_t & J_t \end{Bmatrix} = \frac{\delta_{j_a j_{a_1}}}{2j_a+1} \qquad (6.14)
$$

and the fact that $l_a = l_{a_1}$, since $j_a = j_{a_1}$ and only states with the same parity can mix, we obtain

$$
\begin{aligned}
&\frac{1}{2J_t+1}\sum_{l',j',J'}\mathcal{S}(\Delta_t J_t, \Delta''_t J''_t \epsilon' l' j' J') \\
&\qquad= \sum_{\substack{S,S''\\ S_1,S''_1}} b(U,S)b(U'',S'')b(U,S_1)b(U'',S''_1)\sqrt{w}\sqrt{w_1} \\
&\qquad\quad\times(j_a^{w-1}\alpha''_a J''_a \,|\}j_a^w \alpha_a J_a)(j_a^{w_1-1}\alpha''_{a_1} J''_{a_1} \,|\}j_a^{w_1}\alpha_{a_1} J_{a_1}) \\
&\qquad\quad\times\frac{1}{2j_a+1}\sum_{l',j'}\mathcal{L}^{\rm ps}_{\rm H}(n_a l_a j_a, \epsilon' l' j')\mathcal{L}^{\rm ps}_{\rm H}(n_{a_1} l_a j_a, \epsilon' l' j')\,. \qquad (6.15)
\end{aligned}
$$

This expression can be used to recast the photoionization cross section in a factorized form that is very similar to that given for collisional ionization in eq. (5.17). Specifically,

$$
Q_{\rm PI}(U-U'') = \sum_{\substack{S,S''\\ S_1,S''_1}} B^{(1)}(U, SS_1; U'', S''S''_1)Q^{(1)}(n_a n_{a_1} l_a j_a)\,, \qquad (6.16)
$$

where $B^{(1)}$ depends only on quantities related to the atomic structure of the initial and final ions and is given by

$$
B^{(1)}(U, SS_1; U'', S''S''_1) = F^{(1)}(US, U''S'')F^{(1)}(US_1, U''_1 S''_1)\,, \qquad (6.17)
$$

with

$$
F^{(1)}(US, U''S'') = b(U,S)f^{(1)}(S,S'')b(U'',S'')\,. \qquad (6.18)
$$

The radial quantity $Q^{(1)}$ appearing in eq. (6.16) depends only on the active, bound-electron and free-electron orbitals, and is given by

$$Q^{(1)}(n_a n_{a_1} l_a j_a) = \frac{4\pi\alpha E_{\rm p}}{3(2j_a+1)} \sum_{l',j'} \mathcal{L}_{\rm H}^{\rm ps}(n_a l_a j_a, \epsilon' l' j') \mathcal{L}_{\rm H}^{\rm ps}(n_{a_1} l_a j_a, \epsilon' l' j') \,, \quad (6.19)$$

which is the analog of the pseudo-hydrogenic quantity given in eq. (5.18) for collisional ionization. As discussed in more detail in the next section, eq. (6.19) reduces to the pseudo-hydrogenic cross section for photoionization when mixing is limited to states within a complex.

In the present special case,

$$f^{(1)}(S, S'') = \sqrt{w}(j_a^{w-1} \alpha_a'' J_a'' \,|\} j_a^w \alpha_a J_a) \,, \quad (6.20)$$

which is exactly the same expression as the result given in eq. (5.13) for the case of electron-impact ionization applied to the similar situation of an initial target ion in a level that is described by only empty or closed subshells, in addition to the active subshell. In fact, for more complex ions, $f^{(1)}(S, S'')$ will be identical to the corresponding value obtained for the same transition in the case of collisional ionization. Furthermore, the $\lambda = 1$ dependence can technically be removed in eq. (6.20) because the result is independent of λ, as shown for the case of collisional ionization (see the comment after eq. (5.8)). As usual, for these more complex cases that involve additional partially filled subshells, the form of eq. (6.16) remains unchanged, except for the inclusion in eq. (6.20) of additional angular factors that arise from the presence of these extra partially filled subshells. Alternatively, for these more complex cases, one can obtain numerical values of $f^{(1)}(S, S'')$ from the MCT package in Grant's atomic structure code [34], as discussed after eq. (3.30).

While no published results are available for photoionization cross sections computed with this factorization approach, it has been benchmarked and used extensively in creating massive data sets for large-scale plasma modeling (e.g. refs. [102] and [103]).

6.3 Pseudo-hydrogenic and configuration-average expressions for photoionization

The previous section dealt with the general case for which mixing between states outside of an n-complex was allowed. When mixing is limited to states within the same complex, the cross section in eq. (6.19) is transformed into the pseudo-hydrogenic cross section for photoionization. Specifically, when n_{a_1} is set equal to n_a in eq. (6.19), we obtain

$$Q_{\rm PI}^{\rm ps-H}(n_a l_a j_a) = \frac{4\pi\alpha E_{\rm p}}{3(2j_a+1)} \sum_{l'j'} \mathcal{S}_{\rm H}^{\rm ps}(n_a l_a j_a, \epsilon' l' j') \,, \tag{6.21}$$

with the generalized line strength for the pseudo-hydrogenic case given by

$$\mathcal{S}_{\rm H}^{\rm ps}(n_a l_a j_a, \epsilon' l' j') = \mid \mathcal{L}_{\rm H}^{\rm ps}(n_a l_a j_a, \epsilon' l' j') \mid^2 \,. \tag{6.22}$$

Eq. (6.21) represents the exact expression for the cross section when considering hydrogenic ions. As usual, for more complex ions, the pseudo-hydrogenic cross section should be computed with energies and radial wave functions that are appropriate to the ion under consideration.

Next, we consider the configuration-average case for photoionization. Using an equation analogous to eq. (3.43), the configuration-average, generalized line strength for a transition between initial configuration c and final configuration c'' is defined according to

$$\begin{aligned} \mathcal{S}_{c-c''}(\epsilon' l' j') &\equiv \sum_{S\in c} \sum_{S''\in c''} \mathcal{S}(S, S'' \epsilon' l' j') \\ &= \sum_{S\in c} \sum_{S''\in c''} \sum_{J'} \mathcal{S}(S, S'' \epsilon' l' j' J') \,, \end{aligned} \tag{6.23}$$

where $\mathcal{S}(S, S''\epsilon' l' j')$ is the J'-summed, generalized line strength for the transition between two pure SCSFs labeled S and S''. As in section 5.5 concerning collisional ionization, we denote the final configuration, c'', with two primes to emphasize that the final configuration has one fewer electron than the initial configuration. Eq. (6.23) can be simplified in a manner very similar to that used in arriving at eq. (3.44) for photoexcitation. Taking note of the fact that the final subshell for photoionization actually represents a free electron residing in the $l'j'$ orbital with an occupation number that is always one, the configuration-average, generalized line strength can be written in the compact form

$$\mathcal{S}_{c-c''}(\epsilon' l' j') = g_c \frac{w_\alpha}{(2j_\alpha+1)} \mathcal{S}_{\rm H}^{\rm ps}(n_\alpha l_\alpha j_\alpha, \epsilon' l' j') \,. \tag{6.24}$$

(See the discussion following eq. (5.45) concerning the configuration-average collisional ionization cross section for more details.) In writing the above expression, we have made the usual assumption that the ionization energy ΔE associated with each SCSF transition in the transition array is approximately equal to the configuration-average ionization energy $\Delta E_{c-c''} = E_{c''} - E_c$. This approximation allows for the same value of $\epsilon' = E_{\rm p} - \Delta E_{c-c''}$ to be used for the photoionized electron that occurs in all SCSF transitions within the transition array.

With the result from eq. (6.24) in hand, obtaining a useful expression for the configuration-average photoionization cross section is straightforward. Analogous to the definition in eq. (5.44) for collisional ionization, the configuration-average photoionization cross section can be written as

$$Q_{\rm PI}(c,c'') \equiv \sum_{S\in c}\sum_{S''\in c''} g_S\, Q_{\rm PI}(S,S'')/g_c = \frac{4\pi\alpha E_{\rm p}}{3g_c}\sum_{S\in c}\sum_{S''\in c''}\sum_{l',j'}\mathcal{S}(S,S''\epsilon' l' j')$$
$$= \frac{4\pi\alpha E_{\rm p}}{3g_c}\sum_{l',j'}\mathcal{S}_{c-c''}(\epsilon' l' j') = w_\alpha Q_{\rm PI}^{\rm ps-H}(n_\alpha l_\alpha j_\alpha)\,, \qquad (6.25)$$

where the final result follows from eqs. (6.21) and (6.24). As expected, the final result in eq. (6.25) has the same fundamental form as the corresponding configuration-average expression displayed in eq. (5.45) for collisional ionization. As a point of comparison, we note that the final result in eq. (6.25) is the relativistic analog of eq. (19) given by Peyrusse [28].

7 Resonances and dielectronic recombination

Resonances can be very important when considering the processes of electron-impact excitation and ionization, photoionization and photorecombination. As an alternative to the R-matrix close-coupling method in which resonances are included automatically, Cowan [104] developed an approximate method that considered resonances to be the result of a two-step process, with each process being calculated independent of the other. The first step consists of the creation of a doubly excited level by electron capture, photoexcitation or electron-impact excitation. The second step consists of autoionization or radiative decay to the desired final level. We have used this two-step approximation in our RDW work to obtain resonance contributions to electron-impact excitation and ionization, photoionization and photorecombination. The resonance contribution to this last process is also commonly referred to as dielectronic recombination. In this chapter, we first provide the relevant equations for electron capture and its inverse process, autoionization, as derived in ref. [105]. Then these expressions are considered for different applications.

7.1 Electron capture and autoionization

The collision strength for electron capture from an ion in an initial level i to form a doubly excited level d can be expressed in the form

$$\Omega_{id}^{\rm cap} = \widetilde{\Omega}_{id}^{\rm cap}\delta(\epsilon - E_{id})\,, \qquad (7.1)$$

where the delta function indicates that the captured-electron kinetic energy, ϵ, must be equal to the transition energy E_{id}. The electron-capture collision strength, $\Omega_{id}^{\rm cap}$, is explicitly distinguished from the quantity $\widetilde{\Omega}_{id}^{\rm cap}$, which can be obtained by modifying the expression for the electron-impact excitation collision strength given in eq. (4.6). Specifically, the summation over J is eliminated and J is set equal to the total angular momentum of the doubly excited level, J_d, while the summation over κ' is omitted since there is no outgoing free electron. The result is

$$\widetilde{\Omega}^{\rm cap}(\Delta_t J_t - \Delta_d J_d) = 2\pi(2J_d+1)\sum_{\kappa}\left|\left\langle \Psi_i \left| \sum_{\substack{p,q \\ p<q}}^{N+1} \frac{2}{r_{pq}} \right| \Psi_d \right\rangle\right|^2 , \tag{7.2}$$

where Ψ_i is given by eq. (4.8) and the wave function for the doubly excited level, Ψ_d, is of the general form given by eq. (2.11). An extra factor of π enters the above expression due to the different normalization for bound- and free-electron wave functions. This expression can be rewritten, as in section 4.1 for the electron-impact excitation collision strength, in terms of the reactance matrix $\boldsymbol{R}$ as

$$\widetilde{\Omega}^{\rm cap}(\Delta_t J_t - \Delta_d J_d) = 2\pi(2J_d+1)\sum_{l,j}\left|R(\Delta_t J_t \epsilon l j J_d,\ \Delta_d J_d)\right|^2 . \tag{7.3}$$

In general, the initial level and the doubly excited level are each comprised of mixtures of pure SCSF states, having the same total angular momentum and parity, as in eq. (2.11). Therefore, we can express the reactance matrix in terms of the pure-state basis according to

$$\begin{aligned} R(\Delta_t J_t \epsilon l j J_d,\ \Delta_d J_d) = \sum_{\beta_t,\beta_d} & b^{J_t}(\Delta_t,\beta_t) b^{J_d}(\Delta_d,\beta_d) \\ & \times R(\beta_t J_t \epsilon l j J_d,\ \beta_d J_d) , \end{aligned} \tag{7.4}$$

where the additional symbols have the same meanings as described in chapter 3, (see eq. (3.17), for example).

As in version 1 of our collision strength code described in section 4.2, the angular part of the reactance matrix elements can be evaluated with the MCP module of the Grant code [6]. The radial part of the reactance matrix elements is very similar to that for the excitation collision strength given in section 4.2, except that one of the free electrons is replaced with a bound electron. Specifically, the "direct" terms are given by

$$D^{\lambda}(n_a l_a j_a \epsilon l j; n'_a l'_a j'_a n'_b l'_b j'_b) =$$

$$\int_0^\infty \int_0^\infty [P_{n_a l_a j_a}(r_1) P_{n'_a l'_a j'_a}(r_1) + Q_{n_a l_a j_a}(r_1) Q_{n'_a l'_a j'_a}(r_1)] \times \frac{r_<^\lambda}{r_>^{\lambda+1}} [P_{\epsilon l j}(r_2) P_{n'_b l'_b j'_b}(r_2) + Q_{\epsilon l j}(r_2) Q_{n'_b l'_b j'_b}(r_2)] \, \mathrm{d}r_1 \mathrm{d}r_2 \qquad (7.5)$$

and the "exchange" terms are given by

$$E^\lambda(n_a l_a j_a \epsilon l j; n'_a l'_a j'_a n'_b l'_b j'_b) = \int_0^\infty \int_0^\infty [P_{n_a l_a j_a}(r_1) P_{n'_b l'_b j'_b}(r_1) + Q_{n_a l_a j_a}(r_1) Q_{n'_b l'_b j'_b}(r_1)] \times \frac{r_<^\lambda}{r_>^{\lambda+1}} [P_{\epsilon l j}(r_2) P_{n'_a l'_a j'_a}(r_2) + Q_{\epsilon l j}(r_2) Q_{n'_a l'_a j'_a}(r_2)] \, \mathrm{d}r_1 \mathrm{d}r_2 \,, \qquad (7.6)$$

where a indicates the active electron in the initial level i, and a' and b' indicate the active electrons in the doubly excited level d.

We next obtain the rate coefficients for electron capture and its inverse, autoionization. For the process of electron capture, the cross section, Q_{id}^{cap}, is related to the collision strength, $\Omega_{id}^{\mathrm{cap}}$, according to the usual expression

$$Q_{id}^{\mathrm{cap}} = \frac{\pi}{k^2 g_i} \Omega_{id}^{\mathrm{cap}} = \frac{\pi}{k^2 g_i} \widetilde{\Omega}_{id}^{\mathrm{cap}} \delta(\epsilon - E_{id}) \,. \qquad (7.7)$$

Substituting eq. (7.7) into eq. (4.108), and using the usual relativistic relationships between the electron kinetic energy, ϵ, the velocity, v, and the momentum, p, we obtain the electron-capture rate coefficient

$$C_{id}^{\mathrm{cap}} = \frac{2}{N_e h g_i} \mathrm{e}^{-(\eta + E_{id})/kT} \widetilde{\Omega}_{id}^{\mathrm{cap}} \,, \qquad (7.8)$$

where the quantity $\widetilde{\Omega}_{id}^{\mathrm{cap}}$ is given by eq. (7.2) or (7.3). The rate coefficient in eq. (7.8) can be written in the alternative form

$$C_{id}^{\mathrm{cap}} = \frac{h^2}{g_i (2\pi m k T)^{3/2} X} \mathrm{e}^{-E_{id}/kT} \widetilde{\Omega}_{id}^{\mathrm{cap}} \,, \qquad (7.9)$$

where use has been made of eq. (4.110) and X is given by eq. (4.111). If the temperature is sufficiently small ($kT \ll mc^2$), then $X \to 1$ and the standard non-relativistic expression is recovered.

The rate for the inverse process of autoionization, A_{di}^{a}, can be obtained from the principle of detailed balance, which can be expressed mathematically as

$$C_{id}^{\rm cap} = \frac{N_d}{N_{\rm e}N_i} A_{di}^{\rm a} = \frac{{\rm e}^{-\eta}}{N_{\rm e}} \frac{g_d}{g_i} {\rm e}^{-E_{id}/kT} A_{di}^{\rm a}$$
$$= \frac{h^3}{2(2\pi mkT)^{3/2}X} \frac{g_d}{g_i} {\rm e}^{-E_{id}/kT} A_{di}^{\rm a} \tag{7.10}$$

or, inserting numerical values,

$$C_{id}^{\rm cap} = \frac{2.071 \times 10^{-16}}{T^{3/2}X} \frac{g_d}{g_i} {\rm e}^{-E_{id}/kT} A_{di}^{\rm a} \quad {\rm cm}^3/{\rm s} \tag{7.11}$$

with the temperature T in Kelvin. Comparing eqs. (7.8) and (7.10), we obtain

$$A_{di}^{\rm a} = \frac{2}{hg_d} \tilde{\Omega}_{id}^{\rm cap} \,, \tag{7.12}$$

which, with the use of eq. (7.2) and $g_d = 2J_d + 1$, can be expanded to obtain

$$A_{di}^{\rm a} = \frac{2}{\hbar} \sum_{\kappa} \left| \left\langle \Psi_i \right| \sum_{\substack{p,q \\ p<q}}^{N+1} \frac{2}{r_{pq}} \left| \Psi_d \right\rangle \right|^2 \equiv \frac{2}{\hbar} \sum_{\kappa} |\langle i \mid V_{\rm int} \mid d \rangle|^2 \,, \tag{7.13}$$

where $V_{\rm int}$ represents the electrostatic interaction between the electrons. We note that eq. (7.13) is in a form that is very similar to Cowan's eq. (18.65) [8], except for a factor of π, which is due to different normalization conventions used for the free-electron wave function (see section 18.3 in ref. [8]).

7.2 Pseudo-hydrogenic and configuration-average expressions for electron capture and autoionization

In deriving an expression for the pseudo-hydrogenic electron-capture collision strength, we consider the specific case for which the initial system is a pseudo-hydrogenic ion in a state described by a configuration with a filled core plus an electron denoted by the quantum numbers $n_a l_a j_a$. The final, doubly excited state shall be described by a configuration with the same filled core plus two additional electrons denoted by the quantum numbers $n'_a l'_a j'_a$ and $n'_b l'_b j'_b$. As usual, for this situation, the total angular momentum of the initial level is $J_i = j_a$, where j_a is the total angular momentum of the active electron. However, the total angular momentum of the final, doubly excited level, J_d, can take on multiple values due to coupling among the two electrons denoted by $n'_a l'_a j'_a$ and $n'_b l'_b j'_b$. In this case, we perform a sum over all possible values of J_d to obtain the appropriate expression for the pseudo-hydrogenic, capture collision strength. If, in addition to this last consideration, mixing can be omitted

for the initial and final levels, then the capture collision strength can be obtained in a manner similar to that used previously in section 4.12 to derive the pseudo-hydrogenic, excitation collision strength. Specifically, the electron-capture collision strength can be obtained from eq. (4.99) by replacing $\epsilon' l' j'$ with $n'_b l'_b j'_b$ and multiplying by a factor of π to account for the different normalizations used for the free-electron and bound-electron wave functions. The resulting expression for the pseudo-hydrogenic version of the quantity $\widetilde{\Omega}^{\rm cap}$ is

$$\begin{aligned}\widetilde{\Omega}^{\rm cap}_{\rm ps-H}(n_a l_a j_a - n'_a l'_a j'_a n'_b l'_b j'_b) \\ = 8\pi(1-\tfrac{1}{2}\delta_{a'b'})\sum_{\lambda}\sum_{lj} P^{\lambda}(n_a l_a j_a \epsilon l j; n'_a l'_a j'_a n'_b l'_b j'_b)^2 \,, \quad (7.14)\end{aligned}$$

where the factor $(1-\frac{1}{2}\delta_{a'b'})$ takes into account the situation where a' and b' represent equivalent electrons. In the present case, the P^{λ} are given by

$$\begin{aligned}&P^{\lambda}(n_a l_a j_a \epsilon l j; n'_a l'_a j'_a n'_b l'_b j'_b) \\ &\quad = (2\lambda+1)^{-1/2} D^{\lambda}(n_a l_a j_a \epsilon l j; n'_a l'_a j'_a n'_b l'_b j'_b) \langle j_a \parallel \boldsymbol{C}^{(\lambda)} \parallel j'_a \rangle \langle j \parallel \boldsymbol{C}^{(\lambda)} \parallel j'_b \rangle \\ &\quad + \sum_t (-1)^{\lambda+t} (2\lambda+1)^{1/2} \begin{Bmatrix} j_a & j'_b & t \\ j & j'_a & \lambda \end{Bmatrix} \\ &\qquad \times E^t(n_a l_a j_a \epsilon l j; n'_a l'_a j'_a n'_b l'_b j'_b) \langle j_a \parallel \boldsymbol{C}^{(t)} \parallel j'_b \rangle \langle j \parallel \boldsymbol{C}^{(t)} \parallel j'_a \rangle \,, \quad (7.15)\end{aligned}$$

which is identical to eq. (4.33), provided the $\epsilon' l' j'$ free-electron quantum numbers are replaced by the $n'_b l'_b j'_b$ bound-electron quantum numbers in that earlier expression.

As demonstrated previously for all of the other fundamental processes, the configuration-average expression for a particular quantity can typically be expressed in a useful form in terms of the corresponding pseudo-hydrogenic quantity. A similar statement holds true for autoionization as well. In this case, the configuration-average autoionization rate can be expressed in terms of the pseudo-hydrogenic collision strength quantity in eq. (7.14). For definiteness we consider an autoionizing transition that involves the removal of an electron from subshells α' and β' in configuration c_d. The result is described by a configuration c_i that contains an extra electron in subshell α, along with a corresponding free electron. In the spirit of eq. (3.42), we represent this type of transition in the symbolic form

$$\begin{aligned}(n_\alpha \kappa_\alpha)^{w_\alpha - 1}(n'_\alpha \kappa'_\alpha)^{w'_\alpha}(n'_\beta \kappa'_\beta)^{w'_\beta}(n_\gamma \kappa_\gamma)^{w_\gamma} \cdots \longrightarrow \\ (n_\alpha \kappa_\alpha)^{w_\alpha}(n'_\alpha \kappa'_\alpha)^{w'_\alpha - 1}(n'_\beta \kappa'_\beta)^{w'_\beta - 1}(n_\gamma \kappa_\gamma)^{w_\gamma} \cdots + \mathrm{e} \,. \quad (7.16)\end{aligned}$$

The formal definition of the configuration-average autoionization rate, valid for transitions between arbitrarily complex configurations c_d and c_i, is

$$A^{\mathrm{a}}_{c_d-c_i} \equiv \sum_{d\in c_d}\sum_{i\in c_i} g_d A^{\mathrm{a}}_{di}/g_{c_d}\,, \tag{7.17}$$

where A^{a}_{di} is a fine-structure autoionization rate of the type given by eq. (7.13) and g_{c_d} is the statistical weight of the autoionizing configuration c_d. If the fine-structure rate, and corresponding sums, in eq. (7.17) are limited to only pure SCSF states, then the configuration-average approach described in subsection 3.2.2 and sections 4.13, 5.5 and 6.3 can be similarly applied to the process of autoionization. The resulting expression exhibits the typical form, i.e. it contains a statistical factor multiplying a pseudo-hydrogenic quantity, and is given by

$$A^{\mathrm{a}}_{c_d-c_i} = \frac{2}{h}\Big(\frac{w'_\alpha}{2j'_\alpha+1}\Big)\frac{(w'_\beta-\delta_{\alpha'\beta'})}{(2j'_\beta+1-\delta_{\alpha'\beta'})}\frac{(2j_\alpha+1)-(w_\alpha-1)}{2j_\alpha+1} \times\tilde{\Omega}^{\mathrm{cap}}_{\mathrm{ps-H}}(n_\alpha l_\alpha j_\alpha - n'_\alpha l'_\alpha j'_\alpha n'_\beta l'_\beta j'_\beta)\,. \tag{7.18}$$

As mentioned above, α' and β' are the labels of the active subshells of the doubly excited configuration, c_d, α is the label of the active subshell of the final configuration, c_i, and the presence of the Kronecker delta symbols takes into account the case of equivalent electrons ($\alpha' = \beta'$). For comparison, we note that eq. (7.18) is the relativistic analog of eq. (17) in ref. [28].

As with the configuration-average expressions that were previously presented for the other atomic processes, eq. (7.18) reduces to the correct hydrogenic expression when dealing with autoionization from a He-like ion to form a hydrogenic ion. In order to verify this statement, it must be shown that the appropriate form of eq. (7.12) is satisfied, i.e.

$$A^{\mathrm{a}}_{c_d-c_i} \to \frac{2}{hg_{c_d}}\tilde{\Omega}^{\mathrm{cap}}_{\mathrm{H}}(n_\alpha l_\alpha j_\alpha - n'_\alpha l'_\alpha j'_\alpha n'_\beta l'_\beta j'_\beta)\,, \tag{7.19}$$

or, equivalently,

$$\Big(\frac{w'_\alpha}{2j'_\alpha+1}\Big)\frac{(w'_\beta-\delta_{\alpha'\beta'})}{(2j'_\beta+1-\delta_{\alpha'\beta'})}\frac{(2j_\alpha+1)-(w_\alpha-1)}{2j_\alpha+1} \to \frac{1}{g_{c_d}}\,. \tag{7.20}$$

In order to show that eq. (7.20) is satisfied for the hydrogenic case, we first note that w_α is always one in this situation, which reduces the last term on the left-hand side of eq. (7.20) to one. Next, we must consider separately the two cases for which the active electrons in configuration c_d are either equivalent or non-equivalent. For the equivalent-electron case, there are two electrons occupying the same subshell in the doubly excited configuration so that $w'_\alpha = w'_\beta = 2$ and subshell $\alpha' = \beta'$ in general. Also, we note that the statistical weight of such a He-like configuration is given by the formula (see

eq. (3.45)) $g_{c_d} = (2j'_\alpha + 1)2j'_\alpha/2 = g'_\alpha(g'_\alpha - 1)/2$, where we have assumed that the sole active subshell in the doubly excited configuration is denoted by α'. Making the appropriate substitutions in the left-hand side of eq. (7.20) yields the expression $2/[(2j'_\alpha+1)2j'_\alpha]$, which is precisely the desired value of $1/g_{c_d}$. For non-equivalent electrons, $w'_\alpha = w'_\beta = 1$ (but $\alpha \neq \beta$) and the statistical weight of the doubly excited configuration is simply the product of the statistical weights of the individual subshells, i.e. $g_{c_d} = g'_\alpha g'_\beta$. Making the appropriate substitutions in the left-hand side of eq. (7.20) yields the expression $1/(g'_\alpha g'_\beta)$ which, again, is the desired value of $1/g_{c_d}$.

7.3 Approximate methods for electron capture and autoionization

In this section, we summarize two approximate methods presented in ref. [105] for calculating electron-capture collision strengths and autoionization rates. We consider electron capture for the transition

$$|J_t\rangle + \mathrm{e} \rightarrow |[(J''_t n'_a l'_a j'_a)_{J'_t} n'_b l'_b j'_b]_{J_d}\rangle \,, \tag{7.21}$$

where we assume that $n_a l_a j_a$ describes the active electron in the fine-structure level $|J_t\rangle$, and $|J''_t\rangle$ represents an inactive core.

As described in section 7.1, eq. (4.6) or (4.12), which apply to the process of collisional excitation, can be modified to obtain a general expression for the capture collision strength. The necessary changes are to replace $\epsilon' l' j'$ by $n'_b l'_b j'_b$, eliminate the sum over κ', eliminate the sum over J and let $J = J_d$, resulting in eq. (7.2) or (7.3). However, with the first approximate method described in ref. [105], the capture collision strength could instead be obtained by modifying the factorized expression for the excitation collision strength given in eq. (4.31). In this method, it is assumed that: 1) we are not interested in the total angular momentum of the final, doubly excited level ($J = J_d$) and therefore continue to sum over J as in eq. (4.6) or (4.12); 2) we neglect configuration mixing involving different values for $n'_b l'_b j'_b$ so that j'_b is considered to be a 'good' quantum number; 3) J'_t is also assumed to be a 'good' quantum number. As seen from eq. (7.21), J'_t is now the angular momentum obtained by coupling the total angular momentum of the inactive core J''_t to j'_a, the total angular momentum of the lower excited orbital of the doubly excited, final level. The autoionizing transition relevant to this approximate method can be written symbolically as

$$|J_t\rangle + \mathrm{e} \rightarrow |(J''_t n'_a l'_a j'_a)_{J'_t} n'_b l'_b j'_b\rangle \,. \tag{7.22}$$

In this case, eq. (4.30) applies, provided that j' is replaced by j'_b, and the

capture collision strength quantity $\widetilde{\Omega}^{\rm cap}$ can be expressed in the factorized form

$$\widetilde{\Omega}^{\rm cap}(U-U'n'_bl'_bj'_b) = 8 \sum_{\substack{S,S' \\ S_1,S'_1}} \sum_{\lambda} B^{\lambda}(U,SS_1;U',S'S'_1) \times Q^{\lambda}_{b'}(n_al_aj_a,n'_al'_aj'_a;n_{a_1}l_{a_1}j_{a_1},n'_{a_1}l'_{a_1}j'_{a_1})\,, \quad (7.23)$$

where exactly the same expressions given by eqs. (4.34)–(4.36) still apply for B^{λ}. However, in this case,

$$Q^{\lambda}_{b'}(n_al_aj_a,n'_al'_aj'_a;n_{a_1}l_{a_1}j_{a_1},n'_{a_1}l'_{a_1}j'_{a_1}) = \pi \sum_{lj} P^{\lambda}(n_al_aj_a\epsilon lj;n'_al'_aj'_an'_bl'_bj'_b) \times P^{\lambda}(n_{a_1}l_{a_1}j_{a_1}\epsilon lj;n'_{a_1}l'_{a_1}j'_{a_1}n'_bl'_bj'_b)\,, \quad (7.24)$$

where the P^{λ} are given by eq. (7.15). In eq. (7.23), $U = |J_t\rangle$ is the initial level and $U' = |J'_t\rangle$ has the form of an excited level of an ion with total angular momentum J'_t and the same number of electrons as contained in the initial level U. This approximate method is usually applicable to cases where the n'_b orbital is sufficiently high-lying so that levels of the form $|[(J''_tn'_al'_aj'_a)_{J'_t}n'_bl'_bj'_b]_{J_d}\rangle$ with different J_d values will be described by energies that are close to each other and can therefore be regarded as degenerate. For example, such conditions are valid for the levels that arise from the Li-like configuration in transitions of the form

$$(1s^2)_0 + e \rightarrow (1s2p_{3/2})_1 7d_{5/2}\,.$$

The second approximate method corresponds to going one step further and performing an additional summation over J'_t. In general, transitions of this type can be written in the symbolic form

$$|J_t\rangle + e \rightarrow |(J''_tn'_al'_aj'_a)n'_bl'_bj'_b\rangle\,,$$

for which a specific example might be

$$(1s^2)_0 + e \rightarrow 1s2p_{3/2}7d_{5/2}\,.$$

In conjunction with this choice, configuration mixing among different values of $n'_al'_aj'_a$ is neglected, so that j'_a is considered to be a 'good' quantum number. In addition, J''_t is also assumed to be a 'good' quantum number. Thus, the only mixing allowed for the final state is that occurring within the core state

$U'' = |J_t''\rangle$. With these approximations, the 6-j symbol in eq. (4.36) can be eliminated using an alternative form of eq. (4.30) given by

$$\sum_{J_t'}(2J_t'+1)\begin{Bmatrix} j_a & \lambda & j_a' \\ J_t' & J_t'' & J_t \end{Bmatrix}\begin{Bmatrix} j_{a_1} & \lambda & j_a' \\ J_t' & J_t'' & J_t \end{Bmatrix} = \frac{\delta_{j_a j_{a_1}}}{2j_a+1}\,. \tag{7.25}$$

Then, the capture collision strength quantity $\widetilde{\Omega}^{\rm cap}$ can be expressed in the simple form

$$\widetilde{\Omega}^{\rm cap}(U-U''n_a'l_a'j_a'n_b'l_b'j_b') = \sum_{\substack{S,S'' \\ S_1,S_1''}} \frac{2J_t+1}{2j_a+1} B(U,SS_1;U'',S''S_1'') \times \widetilde{\Omega}^{\rm cap}_{\rm ps-H}(n_a l_a j_a - n_a'l_a'j_a'n_b'l_b'j_b')\,, \tag{7.26}$$

where $\widetilde{\Omega}^{\rm cap}_{\rm ps-H}(n_a l_a j_a - n_a'l_a'j_a'n_b'l_b'j_b')$ is given by eq. (7.14). This approximate method is applicable when both the n_a' and n_b' values are sufficiently high.

For completeness, we mention that an expression analogous to eq. (7.26) has also been derived for the appropriate type of collisional-excitation transition in ref. [106]. The reader is referred to that reference for additional details.

7.4 Resonance contributions to electron-impact excitation

As in ref. [104], we treat the resonance contribution to electron-impact excitation as the two-step process of electron capture by an ion in the initial level $|i\rangle$, forming a doubly excited level $|d\rangle$, followed by autoionization to the final level of interest, denoted by $|f\rangle$. Through the use of a branching ratio, account is taken of the possibility that the doubly excited level autoionizes or radiatively decays to a final level other than $|f\rangle$. These various processes can be written symbolically as

$$|i\rangle + \mathrm{e} \rightarrow |d\rangle \begin{cases} \nearrow |f\rangle + \mathrm{e}' \\ \rightarrow |m'\rangle + \mathrm{e}'' \\ \searrow |k\rangle + h\nu\,, \end{cases} \tag{7.27}$$

where i and f represent the initial and final levels of the collisional excitation transition, d represents a doubly excited level resulting from capture of a free electron by level i, m' indicates other levels (besides f) to which d can autoionize, and k represents the levels to which d can radiatively decay. The total collision strength for the transition $i \rightarrow f$ can be written as

$$\Omega_{if}^{\text{total}} = \Omega_{if} + \Omega_{if}^{\text{res}}\,, \tag{7.28}$$

where Ω_{if} is the usual background (or direct) collision strength given, for example, by eq. (4.6), and the resonance contribution can be written as

$$\Omega_{if}^{\text{res}} = \sum_d \Omega_{id}^{\text{cap}} B_{df} = \sum_d \widetilde{\Omega}_{id}^{\text{cap}} B_{df} \delta(\epsilon - E_{id})\,. \tag{7.29}$$

In the above expression, B_{df} is the branching ratio for excitation,

$$B_{df} = \frac{A_{df}^{\text{a}}}{\sum\limits_m A_{dm}^{\text{a}} + \sum\limits_k A_{dk}^{\text{r}}}\,, \tag{7.30}$$

in which the autoionization rate A_{df}^{a} is given by eq. (7.12), A_{dk}^{r} is the radiative decay rate for the transition $d \rightarrow k$ (see eq. (3.2)), and m indicates all levels to which d can autoionize, including f. In order to delineate the resonance contribution when plotting the total collision strength, we typically replace the delta function in eq. (7.29) with a Lorentz profile. Hence,

$$\Omega_{if}^{\text{res}} = \sum_d \widetilde{\Omega}_{id}^{\text{cap}} B_{df} \frac{(\Gamma_d^{\text{a}} + \Gamma_d^{\text{r}})/2\pi}{(\epsilon - E_{id})^2 + (\Gamma_d^{\text{a}}/2 + \Gamma_d^{\text{r}}/2)^2}\,, \tag{7.31}$$

where the quantities Γ_d^{a} and Γ_d^{r} are given by

$$\Gamma_d^{\text{a}} = \hbar \sum_m A_{dm}^{\text{a}} \qquad \text{and} \qquad \Gamma_d^{\text{r}} = \hbar \sum_k A_{dk}^{\text{r}}\,. \tag{7.32}$$

Also, each value of E_{id} indicates the position of an individual resonance profile and $(\Gamma_d^{\text{a}} + \Gamma_d^{\text{r}})$ is its width.

Similar to eq. (7.28), the total, effective collision strength can be separated into a direct and resonance contribution

$$\Upsilon_{if}^{\text{total}} = \Upsilon_{if} + \Upsilon_{if}^{\text{res}}\,, \tag{7.33}$$

where Υ_{if} is the direct contribution, given by eq. (4.112), and $\Upsilon_{if}^{\text{res}}$ is the resonance contribution. An expression for Υ_{if} was previously provided in eq. (4.112). The resonance contribution can be obtained from an integral that is identical to that listed in eq. (4.112), except that the resonance collision strength from eq. (7.29) must be used in place of Ω_{if}. The resulting expression for the resonance contribution to the effective collision strength is

$$\Upsilon_{if}^{\rm res} = \sum_d \frac{1}{kT} \, {\rm e}^{-(E_{id}-E_{if})/kT} \widetilde{\Omega}_{id}^{\rm cap} B_{df} \, . \tag{7.34}$$

For completeness, we note that the total rate coefficient for electron-impact excitation, $C_{if}^{\rm total}$, can also be written as a sum of the direct and resonance contributions. An expression that is valid for each of these contributions was provided earlier in eq. (4.114), provided that the appropriate expression for the effective collision strength is used in each case. A useful, alternative expression for the resonance contribution to the total rate coefficient is given by

$$C_{if}^{\rm res} = \sum_d C_{id}^{\rm cap} B_{df} \, , \tag{7.35}$$

where the capture rate coefficient $C_{id}^{\rm cap}$ is given by eq. (7.9) or (7.10).

Previously unpublished RDW results concerning the resonance contribution to electron-impact excitation were performed in support of the Atomic Data and Analysis Structure (ADAS) Project [107]. Specifically, calculations were performed that considered the resonance contributions to excitation rate coefficients for transitions from the $(1s^2)_0$ ground level to the six $n = 2$ fine-structure levels arising from the $1s2l$ configurations in He-like ions with $4 \leq Z \leq 54$. Resonance contributions from the doubly excited levels of the $1s3l3l'$ complex were calculated using the procedure described above with the capture rate coefficients and autoionization rates obtained using the detailed method described in section 7.1. For resonance contributions from the $1s3ln'l'$ complexes with $n' = 4, 5$ and 6, capture rates and autoionization rates were obtained using the first approximate method described in section 7.3. Then the entire contribution from the $1s3ln'l'$ complexes with $7 \leq n' \leq \infty$ was obtained from the $1s3l6l'$ contribution by applying a standard $1/(n')^3$ scaling approximation [108]. We also note that the contributions from $1snln'l'$ complexes with $n \geq 4$ are negligible for this case and are not included. The rate coefficients and effective collision strengths needed to evaluate these resonance contributions were calculated for nine temperatures given by

$$T({\rm K})/Z^3 = 400, \ 600, \ 900, \ 1350, \ 2000, \ 3000, \ 4500, \ 6700 \text{ and } 10000 \, ,$$

where Z is the nuclear charge of the appropriate ion. These values are expected to cover the temperature ranges of interest for plasmas containing the various He-like ions mentioned above. It should be mentioned that our RDW results have been compared with those in ref. [81] and the agreement was found to be quite good. In table 20, a sample of these unpublished results is presented for He-like iron in the form of effective collision strengths.

One can also make comparisons of our RDW results with those calculated

Table 20
Effective collision strengths, computed from only the resonance contributions, as a function of temperature for electron-impact excitation in He-like iron. Results are presented for transitions from the $(1s^2)_0$ ground level to the six $n = 2$ fine-structure levels arising from the the 1s2l configurations. The numbers that appear immediately below the level labels are the transition energies in Ry. $x[y] = x \times 10^y$.

$T(\mathrm{K})/Z^3$	$(1s2s)_0$ 490.69	$(1s2s)_1$ 488.44	$(1s2p^*)_0$ 490.45	$(1s2p^*)_1$ 490.73	$(1s2p)_1$ 493.18	$(1s2p)_2$ 491.83
400	5.54[-5]	1.05[-4]	3.33[-5]	9.33[-5]	8.84[-5]	1.65[-4]
600	4.91[-5]	8.99[-5]	2.95[-5]	8.25[-5]	7.54[-5]	1.45[-4]
900	4.01[-5]	7.16[-5]	2.41[-5]	6.71[-5]	5.98[-5]	1.18[-4]
1350	3.07[-5]	5.40[-5]	1.87[-5]	5.14[-5]	4.50[-5]	9.00[-5]
2000	2.28[-5]	3.96[-5]	1.37[-5]	3.80[-5]	3.29[-5]	6.65[-5]
3000	1.62[-5]	2.80[-5]	9.73[-6]	2.70[-5]	2.32[-5]	4.73[-5]
4500	1.13[-5]	1.94[-5]	6.78[-6]	1.88[-5]	1.61[-5]	3.29[-5]
6700	7.81[-6]	1.34[-5]	4.69[-6]	1.30[-5]	1.11[-5]	2.27[-5]
10000	5.34[-6]	9.11[-6]	3.20[-6]	8.89[-6]	7.56[-6]	1.55[-5]

with the Breit-Pauli R-matrix (BPRM) codes [109,110]. In figure 4, a comparison is made of collision strengths, including both the direct and resonance contributions, for four transitions,

$$
\begin{aligned}
1\,^1\mathrm{S}_0 \rightarrow 2\,^3\mathrm{S}_1 \quad &\text{or} \quad (1s^2)_0 \rightarrow (1s2s)_1\,, \\
1\,^1\mathrm{S}_0 \rightarrow 2\,^3\mathrm{P}_1 \quad &\text{or} \quad (1s^2)_0 \rightarrow (1s2p^*)_1\,, \\
2\,^3\mathrm{S}_1 \rightarrow 2\,^1\mathrm{P}_1 \quad &\text{or} \quad (1s2s)_1 \rightarrow (1s2p)_1\,, \\
2\,^3\mathrm{P}_1 \rightarrow 2\,^1\mathrm{P}_1 \quad &\text{or} \quad (1s2p^*)_1 \rightarrow (1s2p)_1\,,
\end{aligned}
$$

in He-like iron. In the BPRM calculations, radiation damping was not included, resulting in some higher peaks in the resonance profiles. However, interference effects between the resonances were included, which are not considered in our RDW calculations. These interference effects produce small dips below the background contribution for some energies. Despite these differences, the BPRM and RDW results typically agree quite well.

7.5 Contributions of autoionization to electron-impact ionization

Autoionization rates calculated via the RDW approach can also be used to obtain the autoionization contribution to total ionization cross sections or rate coefficients. Similar to the previous section, this contribution is again obtained by a two-step process which, in this case, consists of innershell excitation followed by autoionization. This two-step process is typically referred to as

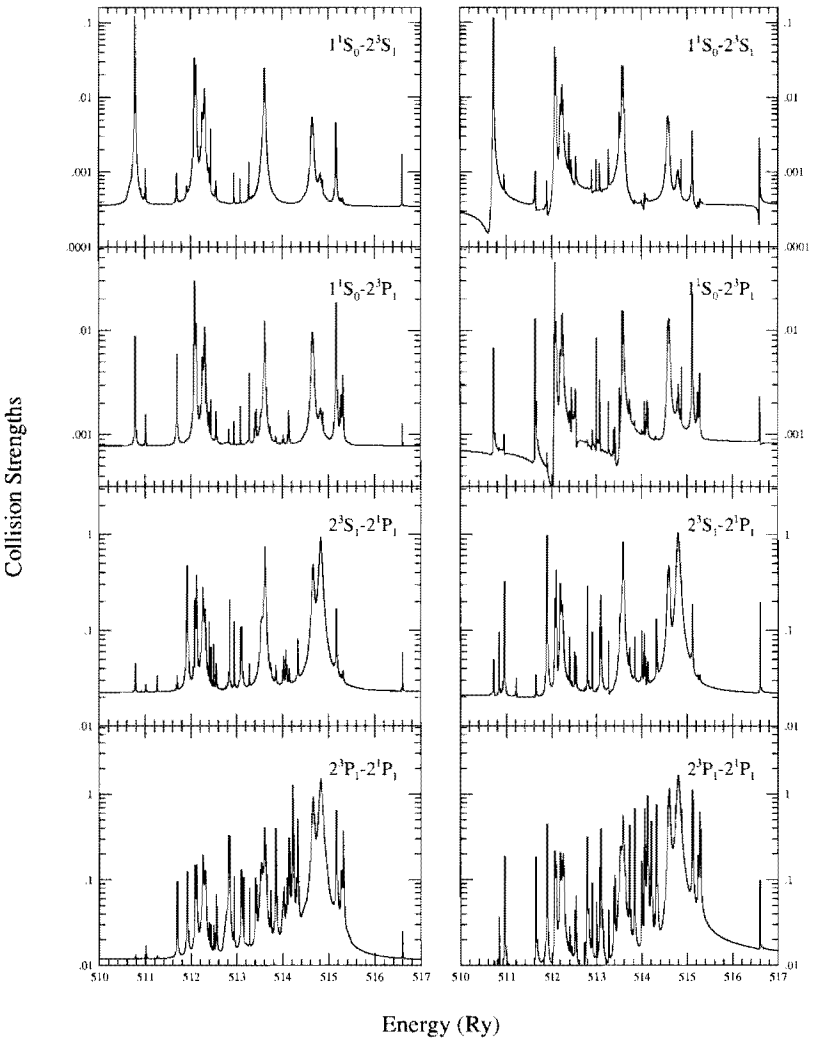

Fig. 4. Collision strengths as a function of impact energy for RDW (left panels) and BPRM (right panels) calculations. Results are presented for four transitions, as specified, in He-like iron.

excitation-autoionization. Cowan and Mann [111] investigated this approach and found that, for plasma temperatures at which Na-like iron is abundant, the autoionization contribution was twice as large as the direct collisional ionization. It is noted that Griffin et al. [112] used a similar method to obtain excitation-autoionization cross sections for Na-like Ti, Cr, Fe and Ni. Although we have not published any RDW data for this process, we describe this method briefly for completeness.

The excitation-autoionization process, with radiative decay taken into account, can be written symbolically as

$$|i\rangle + \mathrm{e} \rightarrow |d\rangle + \mathrm{e}' \begin{array}{l} \nearrow |f\rangle + \mathrm{e}' + \mathrm{e}'' \\ \rightarrow |m'\rangle + \mathrm{e}' + \mathrm{e}''' \\ \searrow |k\rangle + \mathrm{e}' + h\nu \,, \end{array} \tag{7.36}$$

where i and f are the initial and final levels of the collisional ionization transition under consideration, d is the doubly excited level resulting from innershell excitation of level i, m' indicates all levels (other than f) to which level d can autoionize, and k represents the levels to which level d can radiatively decay. The total ionization cross section from the initial level i to the final level f, which includes both the direct ionization cross section Q_{if}^{dir} (see eq. (5.5)) and the excitation-autoionization contribution, can be written as

$$Q_{if}^{\mathrm{total}} = Q_{if}^{\mathrm{dir}} + \sum_d Q_{id}^{\mathrm{exc}} B_{df} \,. \tag{7.37}$$

Here, Q_{id}^{exc} is an excitation cross section of the type displayed in eq. (4.1) for the transition $i \rightarrow d$, and B_{df} is the branching ratio for ionization given by

$$B_{df} = \frac{A_{df}^{\mathrm{a}}}{\sum_m A_{dm}^{\mathrm{a}} + \sum_k A_{dk}^{\mathrm{r}}} \,. \tag{7.38}$$

In this last expression, the autoionization rates A^{a} can be obtained from eq. (7.12), A_{dk}^{r} is the radiative decay rate for the transition $d \rightarrow k$ (see eq. (3.2)) and the index m indicates all levels to which level d can autoionize, including level f.

One is often interested in the total ionization cross section from the initial level i to all possible final levels, instead of a specific final level f, as considered in refs. [111] and [112]. In this case, the total cross section from level i is given by

$$Q_i^{\mathrm{total}} = \sum_f Q_{if}^{\mathrm{dir}} + \sum_d Q_{id}^{\mathrm{exc}} B_d \,, \tag{7.39}$$

where the branching ratio B_d is given by

$$B_d = \frac{\sum_m A_{dm}^{\mathrm{a}}}{\sum_m A_{dm}^{\mathrm{a}} + \sum_k A_{dk}^{\mathrm{r}}} \,. \tag{7.40}$$

As pointed out by Cowan [104], the excitation-autoionization contribution does not produce obvious resonance structures in the ionization cross section because the only restriction placed on the incident-electron kinetic energy is that it be equal to or greater than the excitation energy required to create a doubly excited level d. In contrast, for the case of resonance contributions to excitation discussed in the previous section, the electron energy must be equal to the precise energy difference $E_{id} = E_d - E_i$. Therefore, in the case of excitation-autoionization, when the kinetic energy of the incident electron surpasses the excitation energy required to form a doubly excited level d, this level will contribute to indirect ionization for all subsequent energies, producing a step-function increase in the total ionization cross section.

7.6 Resonance contributions to photoionization

Many authors in the Opacity Project have calculated photoionization cross sections using the close-coupling R-matrix method and demonstrated the importance of resonance contributions to this process (e.g. ref. [113]; see table 2 therein). In those calculations, resonances are generated automatically. In our RDW approach, one can obtain the resonance contribution to photoionization by again using Cowan's two-step approach [104]. In this method, an atom or ion in a level k absorbs a photon, making a transition to a doubly excited level d. This level then autoionizes to a level i, producing a resonance contribution to the total photoionization transition $k \rightarrow i$. Of course, the doubly excited level could also radiatively decay to compete with autoionization. This competing process is often referred to as radiation damping of the resonances. The resonance contribution to photoionization described above, with allowance for radiative decay, can be written symbolically as

$$|k\rangle + h\nu \rightarrow |d\rangle \begin{cases} \nearrow |i\rangle + \mathrm{e} \\ \rightarrow |m'\rangle + \mathrm{e}' \\ \searrow |k'\rangle + h\nu' \,, \end{cases} \tag{7.41}$$

where m' represents all levels (other than i) to which level d can autoionize and k' represents all levels to which level d can radiatively decay.

In ref. [114], our RDW approach was used to obtain resonance contributions to photoionization and its inverse process, photorecombination, in order to compare with Breit-Pauli R-matrix results. In that study, the photoexcitation cross section from a level k to a doubly excited level d is obtained from the absorption radiative rate A^{r}_{kd} or the radiative width

$$\Gamma^{\mathrm{r}}_{kd} \equiv \hbar A^{\mathrm{r}}_{kd} \,. \tag{7.42}$$

The photoexcitation (PE) cross section is given by

$$Q_{\mathrm{PE}}(k-d) = \frac{4\pi^2}{\alpha^2 (E_{\mathrm{p}})^2} \Gamma^{\mathrm{r}}_{kd}\, \delta(E_{\mathrm{p}} - E_{kd}) \,, \tag{7.43}$$

where E_{p} and $E_{kd} = E_d - E_k$ are the photon energy and transition energy, respectively, and α is the fine-structure constant. The delta function indicates that the photon energy E_{p} must be equal to the transition energy E_{kd} in order for the photoexcitation transition to occur. The doubly excited level d then has two channels for stabilization, as mentioned previously. Taking these two possibilities into account, the resonance cross section is given by

$$Q^{\mathrm{res}}_{\mathrm{PI}}(k-i) = \frac{4\pi^2}{\alpha^2 (E_{\mathrm{p}})^2} \sum_d \Gamma^{\mathrm{r}}_{kd} B_{di}\, \delta(E_{\mathrm{p}} - E_{kd}) \,, \tag{7.44}$$

where B_{di} is the branching ratio for PI and is given by

$$B_{di} = \frac{A^{\mathrm{a}}_{di}}{\sum\limits_m A^{\mathrm{a}}_{dm} + \sum\limits_{k'} A^{\mathrm{r}}_{dk'}} \,. \tag{7.45}$$

Here, the index m includes all levels (including i) to which level d can autoionize and the index k' includes all levels that are accessible from level d via radiative decay.

We forgo the presentation of numerical examples in this section, since our calculations concerning the resonance contribution to photoionization have been used primarily to obtain the resonance contribution to the inverse process of photorecombination. Our two methods for computing this type of resonance contribution are discussed in the next section.

7.7 Resonance contributions to photorecombination—dielectronic recombination

As mentioned in the previous section, the process of photorecombination (PR) is the inverse of photoionization. This process can be considered as the capture of a free electron by a target ion in level i to form a new ion in level k, with one more electron, and an accompanying photon. The resonance contribution to photorecombination is typically referred to as dielectronic recombination (DR). The DR process can be very important in non-local thermodynamic equilibrium plasmas, as demonstrated by the multitude of references in the

literature. Among these, Seaton and Storey [115] and Hahn and LaGattuta [116] give detailed reviews of the history, theoretical developments and applications of DR. In our RDW approach, we use two different methods to compute the resonance contribution to photorecombination, as described below.

The first calculational method that we used to obtain DR cross sections is based on Cowan's two-step paradigm [8,104]. This approach was used, for example, in performing most of the calculations in ref. [105]. The two-step process can be written symbolically as

$$|i\rangle + \mathrm{e} \longrightarrow |d\rangle \begin{cases} \nearrow |k\rangle + h\nu \\ \longrightarrow |m'\rangle + h\nu' \\ \searrow |i'\rangle + \mathrm{e}' \,. \end{cases} \tag{7.46}$$

In this case, the capture of an electron by the ion in level i to form a doubly excited level d is followed by radiative decay to the final level k. Through the use of a branching ratio, account is taken of the possibility that the doubly excited level d autoionizes to a level i', or radiatively decays to a final level m' that is different from level k.

Using eqs. (7.7) and (7.12), the electron-capture cross section for the transition $i \longrightarrow d$ can be written as

$$Q_{id}^{\mathrm{cap}} = \frac{\pi^2}{k^2 g_i} g_d \hbar A_{di}^{\mathrm{a}} \, \delta(\epsilon - E_{id}) \,. \tag{7.47}$$

Applying the appropriate branching ratio yields the DR cross section

$$Q_{\mathrm{DR}}(i-k) = \sum_d Q_{id}^{\mathrm{cap}} B_{dk} = \sum_d \frac{\pi^2}{k^2 g_i} g_d \hbar A_{di}^{\mathrm{a}} B_{dk} \, \delta(\epsilon - E_{id}) \,. \tag{7.48}$$

This branching ratio for DR is given by

$$B_{dk} = \frac{A_{dk}^{\mathrm{r}}}{\sum_{i'} A_{di'}^{\mathrm{a}} + \sum_{k'} A_{dk'}^{\mathrm{r}}} \,, \tag{7.49}$$

where index i' includes all levels to which d can autoionize and index k' includes all levels that are accessible for radiative decay, including level k. The corresponding rate coefficient for DR is given by

$$C_{\mathrm{DR}}(i-k) = \sum_d C_{id}^{\mathrm{cap}} \, B_{dk} \,, \tag{7.50}$$

where $C_{id}^{\rm cap}$ can be obtained from eq. (7.10).

We now present some numerical results, originally published in ref. [105], for the process of DR that were computed with this first method. Specifically, eqs. (7.50) and (7.49) were used to obtain DR rate coefficients. The results that we present here are the contributions from two different n complexes, $n_b' = 5$ and 7, to the total DR rate coefficients of the $(1s^2)_0$ ground level in He-like ions. More specifically, we considered processes of the type

$$(1s^2)_0 + e \rightarrow (1s2l_a'j_a')_{J_t'} n_b' l_b' j_b' \rightarrow (1s^2)_0 n_b' l_b' j_b' + h\nu\,,$$

where the total angular momentum of both the doubly excited levels and the final recombined levels have been purposefully omitted. This choice was made in order to calculate the required capture rate coefficients using the first approximate method described in section 7.3 (referred to as "Approx" below), in addition to the detailed method described in section 7.1 (referred to as "Full DW" below). In this way, we can also assess the accuracy of the former method.

We note that, in this case, the final configuration for the process of dielectronic recombination was chosen to always be of the form $1s^2 n_b' l_b' j_b'$. That is, we assumed that it is the $2l_a'j_a' = 2p^*$ or 2p electron that radiatively decays from the autoionizing level, which is the most probable outcome. However, it is also possible for the more highly excited electron to decay, which we have neglected in the present calculations. When performing detailed plasma kinetics calculations, these additional cascading transitions can be taken into account in a straightforward manner according to the method described above. Under the above assumption, eq. (7.50) reduces to the simpler form

$$C_{\rm DR}(i-k) \approx \sum_d C_{id}^{\rm cap} \frac{A_{dk}^{\rm r}}{A_{di}^{\rm a} + A_{dk}^{\rm r}}\,. \tag{7.51}$$

The results for these calculations are given in table 21 for iron, molybdenum and gold, with nuclear charges $Z = 26$, 42 and 79, respectively. In each case, the results are given for a temperature near that for which the dielectronic recombination rate is a maximum, but additional calculations indicate that the accuracy of the "Approx" entries appears to be nearly independent of temperature. It is understood that the values for each $n_b' l_b' j_b'$ entry represent the partial sum associated with the $1s2l_a'j_a'n_b'l_b'j_b'$ contributions from all possible doubly excited levels that arise from the two allowed choices for $2l_a'j_a'$. The row labeled "Sum" indicates values of the DR rate coefficients that were obtained by adding the appropriate partial sums. Thus, these summed rate coefficients take into account all of the processes described above that radiatively decay

Table 21
A comparison of contributions to the dielectronic recombination rate coefficient, C_{DR} (in units of cm^3/s), due to electron capture by He-like ions in the ground level $(1s^2)_0$ to form doubly excited levels arising from the $1s2l'_aj'_an'_bl'_bj'_b$ configurations of Li-like ions, followed by radiative stabilization to levels arising from the $1s^2n'_bl'_bj'_b$ configurations. $x[y] = x \times 10^y$.

	Z=26, T=3×10^7 K		Z=42, T=1.5×10^8 K		Z=79, T=5×10^8 K	
$n'_bl'_bj'_b$	Approx	Full DW	Approx	Full DW	Approx	Full DW
5s	9.82[-16]	1.98[-15]	3.19[-16]	7.71[-16]	7.08[-17]	2.21[-16]
5p*	2.88[-15]	3.58[-15]	8.73[-16]	1.15[-15]	1.27[-16]	2.11[-16]
5p	6.75[-15]	7.65[-15]	2.02[-15]	2.68[-15]	2.58[-16]	3.77[-16]
5d*	2.49[-15]	1.48[-15]	7.51[-16]	1.39[-15]	9.71[-17]	1.52[-16]
5d	3.76[-15]	5.92[-15]	1.08[-15]	1.51[-15]	1.11[-16]	2.27[-16]
5f*	3.61[-16]	3.78[-16]	1.10[-16]	2.29[-16]	1.13[-17]	3.36[-17]
5f	4.72[-16]	8.13[-16]	1.37[-16]	2.79[-16]	1.15[-17]	2.13[-17]
5g*	1.16[-17]	1.87[-17]	3.15[-18]	4.36[-18]	3.35[-19]	4.07[-19]
5g	1.42[-17]	2.79[-17]	3.69[-18]	1.03[-17]	3.32[-19]	3.74[-19]
Sum	1.77[-14]	2.19[-14]	5.29[-15]	8.02[-15]	6.88[-16]	1.24[-15]
7s	3.28[-16]	1.12[-15]	1.08[-16]	2.10[-16]	2.33[-17]	7.23[-17]
7p*	9.80[-16]	1.12[-15]	3.02[-16]	4.23[-16]	4.31[-17]	6.05[-17]
7p	2.33[-15]	2.50[-15]	6.98[-16]	8.82[-16]	8.92[-17]	1.38[-16]
7d*	9.04[-16]	5.19[-16]	2.80[-16]	4.19[-16]	3.60[-17]	9.13[-17]
7d	1.37[-15]	1.91[-15]	4.02[-16]	6.55[-16]	4.14[-17]	5.51[-17]
7f*	1.63[-16]	1.72[-16]	5.07[-17]	7.87[-17]	5.31[-18]	6.57[-18]
7f	2.13[-16]	2.52[-16]	6.34[-17]	1.39[-16]	5.43[-18]	1.07[-17]
7g*	9.76[-18]	1.50[-17]	2.81[-18]	3.46[-18]	2.88[-19]	3.38[-19]
7g	1.20[-17]	2.02[-17]	3.29[-18]	5.72[-18]	2.86[-19]	3.22[-19]
7h*	2.26[-19]	5.12[-19]	6.89[-20]	7.44[-20]	6.35[-21]	5.19[-21]
7h	2.67[-19]	4.18[-19]	7.85[-20]	9.76[-20]	6.17[-21]	5.04[-21]
7i*	1.99[-21]	1.57[-20]	1.06[-21]	3.46[-22]	4.42[-23]	5.23[-23]
7i	2.29[-21]	2.49[-21]	1.19[-21]	4.02[-22]	4.22[-23]	5.11[-23]
Sum	6.31[-15]	7.62[-15]	1.91[-15]	2.82[-15]	2.44[-16]	4.35[-16]

into any of the levels arising from configurations of the form $1s^2n'_bl'_bj'_b$ ($n'_b = 5$ or 7).

One observes that the "Approx" values underestimate the "Full DW" values in nearly all cases. Furthermore, on a percentage basis, this underestimation is roughly the same when considering the summed rate coefficients associated with $n'_b = 5$ versus 7 for a particular value of Z. Specifically, the sum of the "Approx" entries are about 0.82, 0.67 and 0.56 times the corresponding "Full DW" values for $Z = 26$, 42 and 79, respectively. Calculations were also made in which configuration mixing was completely omitted in obtaining both "Approx" and "Full DW" results. The agreement between the results obtained from these latter two calculations, and also the "Approx" values given in the

table, was almost perfect. This agreement indicates that: (1) mixing between the $(1s2p^*)_1$ and $(1s2p)_1$ levels, which is the only mixing included in obtaining the "Approx" entries in the table, has little effect on the $C_{\rm DR}$ values and (2) the individual single-configuration (i.e. no mixing) rate coefficients produced by the "Approx" and "Full DW" calculations, which are based on completely different angular formulations, are consistent (as verified by detailed inspection). This type of test provides a good check that no errors were made in either of the two computational approaches.

The principal reason for the differences between the "Approx" and "Full DW" results in the table is that only doubly excited levels corresponding to $(1s2p^*)_1 n'_b l'_b j'_b$ and $(1s2p)_1 n'_b l'_b j'_b$ can contribute to the "Approx" results. However, due to mixing of these levels with $(1s2p^*)_0 n'_b l'_{b1} j'_{b1}$, $(1s2p)_2 n'_b l'_{b1} j'_{b1}$ and $(1s2s)_{0,1} n'_b l'_{b1} j'_{b1}$ levels having the same parity and total angular momentum, one obtains contributions from many more doubly excited levels in the "Full DW" results. In general, for lower Z values, where the value of $A^{\rm a}_{di}$ in the denominator of eq. (7.51) tends to be significantly larger than the corresponding value of $A^{\rm r}_{dk}$, these extra contributions that arise from mixing are rather small since they are comprised primarily of radiative decay rates rather than autoionizing rates. However, as Z increases, the radiative rates $A^{\rm r}_{dk}$ increase rapidly and eventually tend to dominate the sum over the autoionization rates $A^{\rm a}_{di}$ even for very weak radiative transitions. Thus, for very large values of Z

$$C_{\rm DR}(i-k) \rightarrow \sum_d C^{\rm cap}_{id} \,, \tag{7.52}$$

where the summation over d includes essentially all doubly excited levels for which there exists a non-zero value of $A^{\rm r}_{dk}$. This property results in a summation that includes many more doubly excited levels in the case of the "Full DW" calculations.

Our second calculational method for obtaining DR cross sections was motivated by a desire to compare with then-recent Breit-Pauli R-matrix (BPRM) results produced by Pradhan and Zhang [114]. This BPRM work used an approach that was based on earlier R-matrix work by Nahar and Pradhan [117], in which total photorecombination cross sections, which include both the direct photorecombination and resonance DR contributions, were obtained from photoionization cross sections using the detailed-balance (Milne relation) method.

In this second RDW method, we also use the detailed-balance approach, but only to obtain the DR contribution to the total PR cross section, rather than to obtain the total PR cross section, as in the BPRM work mentioned above. Specifically, we consider the DR process to be the inverse of the resonance contribution to photoionization displayed in eq. (7.41). The resonance contri-

bution to the photoionization cross section is computed with eq. (7.44) and then the result is used in the detailed-balance method to obtain DR cross sections. In this case, the Milne detailed-balance relation can be written in relativistic form and Rydberg atomic units as

$$Q_{\mathrm{PR}}^{\mathrm{res}}(i-k) = \frac{g_k}{g_i}\frac{\alpha^2 (E_{\mathrm{p}})^2}{4k^2} Q_{\mathrm{PI}}^{\mathrm{res}}(k-i)\,, \tag{7.53}$$

where α is the fine-structure constant, E_{p} is the photon energy, and k is the wavenumber related to the free-electron kinetic energy, ϵ, by eq. (4.2). Using eq. (7.44), we obtain

$$Q_{\mathrm{PR}}^{\mathrm{res}}(i-k) = \frac{g_k}{g_i}\frac{\pi^2}{k^2}\sum_d \Gamma_{kd}^{\mathrm{r}} B_{di}\,\delta(E_{\mathrm{p}} - E_{kd})\,, \tag{7.54}$$

where B_{di} is the branching ratio given by eq. (7.45). The right-hand side of eq. (7.54) can be shown to be identical to that of eq. (7.48) by noting eq. (7.42) and the additional relationships

$$g_k A_{kd}^{\mathrm{r}} = g_d A_{dk}^{\mathrm{r}} \equiv g A^{\mathrm{r}}$$

$$E_{\mathrm{p}} - E_{kd} = \epsilon + E_{ki} - E_{kd} = \epsilon - E_{id}$$

$$A_{di}^{\mathrm{a}} B_{dk} = A_{dk}^{\mathrm{r}} B_{di}\,.$$

In order to delineate the resonance contributions when plotting the total PR cross section, we replace the delta function in eq. (7.54), first with the equivalent expression $\delta(\epsilon - E_{id})$, then with a Lorentz profile. Hence,

$$Q_{\mathrm{PR}}^{\mathrm{res}}(i-k) = \frac{g_k}{g_i}\frac{\pi^2}{k^2}\sum_d \Gamma_{kd}^{\mathrm{r}} B_{di}\frac{(\Gamma_d^{\mathrm{a}} + \Gamma_d^{\mathrm{r}})/2\pi}{(\epsilon - E_{id})^2 + (\Gamma_d^{\mathrm{a}}/2 + \Gamma_d^{\mathrm{r}}/2)^2}\,, \tag{7.55}$$

where

$$\Gamma_d^{\mathrm{a}} = \sum_m \Gamma_{dm}^{\mathrm{a}} = \hbar \sum_m A_{dm}^{\mathrm{a}} \qquad \text{and} \qquad \Gamma_d^{\mathrm{r}} = \sum_{k'} \Gamma_{dk'}^{\mathrm{r}} = \hbar \sum_{k'} A_{dk'}^{\mathrm{r}}\,.$$

As written, eq. (7.55) includes the effect of radiation damping of the resonances. A number of methods have also been developed which take into account this effect when computing photorecombination cross sections within the R-matrix framework [114,118,119]. However, for light elements that are

not too highly charged, the error that results from neglecting radiation damping is small since the radiative rates are much smaller than the autoionization rates for those systems [120]. Nevertheless, it is possible to modify eq. (7.55) in order to perform calculations that can be used to determine the relative importance of radiation damping, and also to compare with BPRM calculations that did not take this effect into account. The modifications require that all values of $A^{\rm r}$ be set to zero in both the branching ratio B_{di} and the Lorentz profile in eq. (7.55) to obtain

$$Q_{\rm PR}^{\rm res}(i-k) = \frac{g_k}{g_i}\frac{\pi^2}{k^2}\sum_d \Gamma_{kd}^{\rm r}\frac{\Gamma_{di}^{\rm a}/2\pi}{(\epsilon - E_{id})^2 + (\Gamma_d^{\rm a}/2)^2}\,. \tag{7.56}$$

Eqs. (7.55) and (7.56) have been used to compute resonance contributions, with and without inclusion of radiation damping, to the total PR cross sections for recombination of He-like ions and compared with BPRM results in refs. [114] and [120]. Good overall agreement was obtained in these comparisons and, to illustrate this behavior, we reproduce figure 1 from ref. [114] as figure 5 in the present work. In this figure, a comparison is provided between RDW and BPRM total photorecombination cross sections that were computed with and without radiation damping for the $n = 2$ (KLL) group of the Fe XXV recombination. As stated above, the agreement is observed to be very good.

8 Hyperfine-structure transitions

Our work on collision strengths for hyperfine-structure transitions was motivated by a remark [121] that the 3.071 mm hyperfine line of Li-like ^{57}Fe is of interest in the study of cooling flows in clusters of galaxies, and that rate coefficients were needed to investigate the role of electron-impact excitation as a mechanism for populating the upper, $F = 1$ hyperfine-structure level of this transition. Also, Syunyaev and Churazov [122] considered the possible astrophysical interest in this hyperfine line, as well as hyperfine transitions in other ions, such as Li-like Na, Mg, Al and Si, and H-like C and N.

In order to calculate collision strengths and effective collision strengths for transitions between hyperfine-structure levels, our relativistic distorted-wave approach described in chapter 4 was expanded and applied to these Li-like and H-like ions [123,124]. Since resonance contributions to the total collision strengths and effective collision strengths are expected to be important, we also developed the theory and corresponding computer code [125] for calculating electron-capture rate coefficients to form a doubly excited hyperfine-structure level, as well as for calculating rates for the inverse process of autoionization.

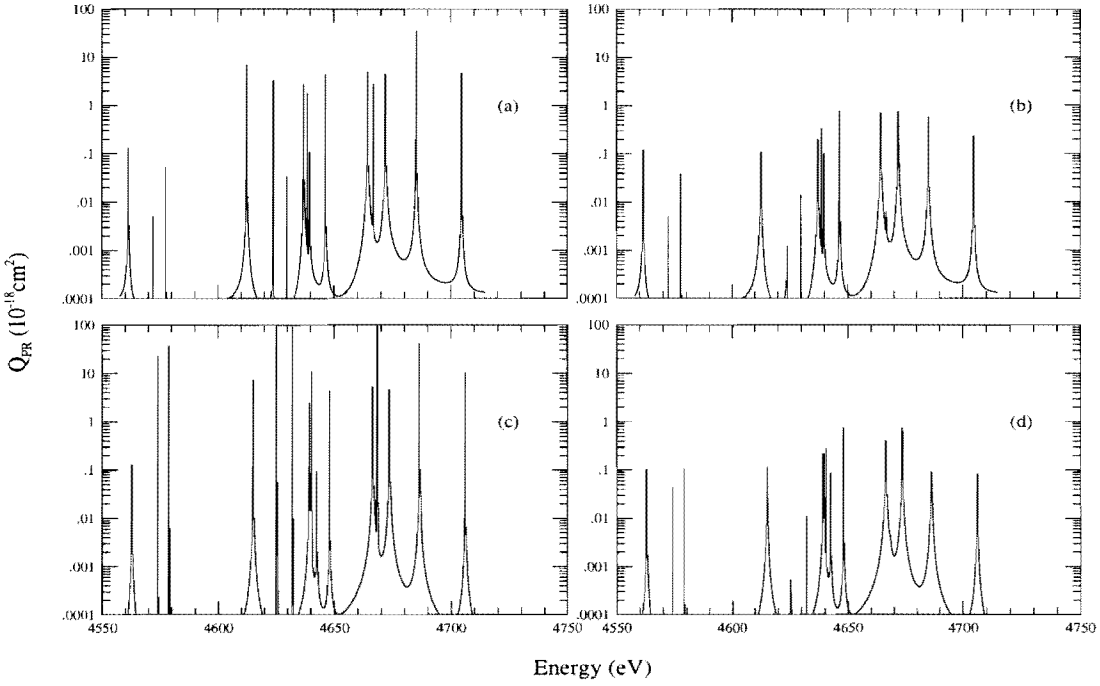

Fig. 5. Comparison of the $n = 2$ (KLL) group of resonances in photorecombination of Fe XXV: Breit-Pauli R-matrix (BPRM) cross sections without (a) and with (b) radiation damping; relativistic distorted-wave (RDW) cross sections without (c) and with (d) radiation damping.

These capabilities can then be applied to obtain resonance contributions to the total collision strengths and effective collision strengths. Our RDW approach for including the resonance contributions to hyperfine transitions in this manner has been applied to a variety of H-like and Li-like systems of astrophysical interest [125,126].

8.1 The background contribution to hyperfine-structure collision strengths

The calculation of collision strengths for transitions between hyperfine-structure levels follows the factorization method described in section 4.3. We consider a hyperfine-structure transition of the form

$$U - U' \equiv \mid \Delta_t J_t I F\rangle - \mid \Delta'_t J'_t I F'\rangle \,,$$

where I is the nuclear spin, and F and F' are the total angular momenta for the initial and final hyperfine-structure levels, respectively. (The meaning of the Δ_t, J_t and Δ'_t, J'_t quantum numbers associated with the initial and final fine-structure levels, respectively, is identical to that provided in chapters 3 and 4.) The hyperfine interaction can be treated perturbatively in this application because it is extremely weak relative to the nuclear and electron-electron potentials. Hence, the interaction has no effect on the radial part of the wave function and the only substantive effect is on the angular portion of the scattering matrix elements.

In order to derive a factorized form for the collision strength in this case, we start, as in section 4.3, by treating in detail the case of subshells that are initially filled or empty, in addition to the active one labeled a. By analogy with eq. (4.20), we write the direct part of the reactance matrix element in this case as

$$\begin{aligned} &R^d(\beta_t J_t I F \epsilon l j J;\, \beta'_t J'_t I F' \epsilon' l' j' J) \\ &= 2\sqrt{w} \sum_{J_1,\alpha_1} (j_a^{w-1} \alpha_1 J_1 \mid\} j_a^w \alpha_a J_a) \sum_{\lambda=0}^{\infty} D^\lambda(n_a l_a j_a \epsilon l j;\, n'_a l'_a j'_a \epsilon' l' j') \qquad (8.1) \\ &\times \langle j_a^{w-1} \alpha_1 J_1 j_a J_t I F j J M \mid \boldsymbol{C}^{(\lambda)}(\hat{\boldsymbol{r}}_w) \cdot \boldsymbol{C}^{(\lambda)}(\hat{\boldsymbol{r}}_{w+1}) \mid j_a^{w-1} \alpha''_a J''_a j'_a J'_t I F' j' J M\rangle \,, \end{aligned}$$

where all of the symbols for the quantum numbers, except I and F, have been previously specified in sections 3.2 and 4.3. In eq. (8.1), the angular matrix element is now given by

$$\begin{aligned} &\langle j_a^{w-1} \alpha_1 J_1 j_a J_t I F j J M \mid \boldsymbol{C}^{(\lambda)}(\hat{\boldsymbol{r}}_w) \cdot \boldsymbol{C}^{(\lambda)}(\hat{\boldsymbol{r}}_{w+1}) \mid j_a^{w-1} \alpha''_a J''_a j'_a J'_t I F' j' J M\rangle \\ &\quad = \delta_{\alpha_1 \alpha''_a} \delta_{J_1 J''_a} (-1)^{J+j+j'_a+J''_t+I+2(F'+J_t+\lambda)} \\ &\qquad \times [(2F+1)(2F'+1)(2J_t+1)(2J'_t+1)]^{1/2} \\ &\qquad \times \begin{Bmatrix} F & \lambda & F' \\ j' & J & j \end{Bmatrix} \begin{Bmatrix} J_t & \lambda & J'_t \\ F' & I & F \end{Bmatrix} \begin{Bmatrix} j_a & \lambda & j'_a \\ J'_t & J''_t & J_t \end{Bmatrix} \\ &\qquad \times \langle j_a \parallel \boldsymbol{C}^{(\lambda)} \parallel j'_a\rangle \langle j \parallel \boldsymbol{C}^{(\lambda)} \parallel j'\rangle \,, \qquad (8.2) \end{aligned}$$

which is the analog of eqs. (4.21) and (4.22). The exchange matrix element R^e can be written as

$$\begin{aligned} &R^e(\beta_t J_t I F \epsilon l j J;\, \beta'_t J'_t I F' \epsilon' l' j' J) \\ &= 2\sqrt{w} \sum_{J_1,\alpha_1} (j_a^{w-1} \alpha_1 J_1 \mid\} j_a^w \alpha_a J_a) \sum_{\lambda=0}^{\infty} E^\lambda(n_a l_a j_a \epsilon l j;\, n'_a l'_a j'_a \epsilon' l' j') \qquad (8.3) \\ &\times \langle j_a^{w-1} \alpha_1 J_1 j_a J_t I F j J M \mid \boldsymbol{C}^{(\lambda)}(\hat{\boldsymbol{r}}_w) \cdot \boldsymbol{C}^{(\lambda)}(\hat{\boldsymbol{r}}_{w+1}) \mid j_a^{w-1} \alpha''_a J''_a j'_a J'_t I F' j' J M\rangle^{\mathrm{e}} \,, \end{aligned}$$

where, as seen from the description preceding eq. (4.25), electrons in the wave function represented by the ket $|\cdots\rangle^{\rm e}$ are in the order $1, 2, ..., w+1, w$. This ordering corresponds to electrons $w+1$ and w being in orbitals j'_a and j', respectively, and we indicate this convention by adding a superscript "e" to the ket that represents the final state above. In order to use irreducible tensor techniques to manipulate this matrix element, we must first recouple the final system wave function according to the same argument that precedes eq. (4.25). The result is

$$
\begin{aligned}
&|\, j_a^{w-1}\alpha''_a J''_a j'_a J'_t I F' j' J M\rangle^{\rm e} \\
&\qquad = \sum_{F''}\sum_{F_2}\sum_{J_2}(-1)^{2(I+j'_a+j'+F'')+J'_t+F_2+F'+J_2}(2F''+1) \\
&\qquad\qquad \times[(2J'_t+1)(2F_2+1)(2F'+1)(2J_2+1)]^{1/2} \\
&\qquad\qquad \times \begin{Bmatrix} J''_a & I & F'' \\ F' & j'_a & J'_t \end{Bmatrix} \begin{Bmatrix} F'' & j' & F_2 \\ J & j'_a & F' \end{Bmatrix} \\
&\qquad\qquad \times \begin{Bmatrix} J''_a & j' & J_2 \\ F_2 & I & F'' \end{Bmatrix} |\, j_a^{w-1}\alpha''_a J''_a j' J_2 I F_2 j'_a J M\rangle \,, \qquad (8.4)
\end{aligned}
$$

where the electrons in the wave function represented by the ket on the right-hand side are now in the standard order $1, 2, ..., w, w+1$. If eq. (8.4) is substituted into eq. (8.3), the angular factor involving the recoupled final state appears in the resulting expression. This factor can be written in a form that is very similar to eq. (8.2) and is given by

$$
\begin{aligned}
&\langle j_a^{w-1}\alpha_1 J_1 j_a J_t I F j J M \mid \boldsymbol{C}^{(\lambda)}(\hat{\boldsymbol{r}}_w)\cdot\boldsymbol{C}^{(\lambda)}(\hat{\boldsymbol{r}}_{w+1}) \mid j_a^{w-1}\alpha''_a J''_a j' J_2 I F_2 j'_a J M\rangle \\
&\qquad = \delta_{\alpha_1\alpha''_a}\delta_{J_1 J''_a}(-1)^{J+j+j'+J''_a+I+2(F_2+J_t+\lambda)} \\
&\qquad\quad \times[(2F+1)(2F_2+1)(2J_t+1)(2J_2+1)]^{1/2} \\
&\qquad\quad \times \begin{Bmatrix} F & \lambda & F_2 \\ j'_a & J & j \end{Bmatrix} \begin{Bmatrix} J_t & \lambda & J_2 \\ F_2 & I & F \end{Bmatrix} \begin{Bmatrix} j_a & \lambda & j' \\ J_2 & J''_a & J_t \end{Bmatrix} \\
&\qquad\quad \times \langle j_a \parallel \boldsymbol{C}^{(\lambda)} \parallel j'\rangle\langle j \parallel \boldsymbol{C}^{(\lambda)} \parallel j'_a\rangle \,. \qquad (8.5)
\end{aligned}
$$

The exchange matrix element in eq. (8.3) can now be written as a rather lengthy expression that contains a product of the angular factor in eq. (8.5) and the triple summation plus angular factors that precede the ket on the right-hand side of eq. (8.4). This cumbersome result can be greatly simplified using the properties of the 6-j symbol (see ref. [123] for more detail) to produce a compact form for the exchange matrix element R^e. This new result for R^e is then combined with the expression for R^d in eq. (8.2), according to eq. (4.14), to yield an expression for the reactance matrix elements for transitions between pure hyperfine-structure states in the form

$$R(\beta_t J_t I F \epsilon l j J;\ \beta'_t J'_t I F' \epsilon' l' j' J)$$

$$
\begin{aligned}
&= 2\sqrt{w}(j_a^{w-1}\alpha_a'' J_a'' \,|\}\, j_a^w \alpha_a J_a)(-1)^{2J_t+I-F+j_a'+J_t''} \\
&\quad \times[(2F+1)(2F'+1)(2J_t+1)(2J_t'+1)]^{1/2} \\
&\quad \times\Bigg[\sum_\lambda D^\lambda(n_a l_a j_a \epsilon l j; n_a' l_a' j_a' \epsilon' l' j') \\
&\qquad \times\begin{Bmatrix} F & \lambda & F' \\ j' & J & j \end{Bmatrix}\begin{Bmatrix} J_t & \lambda & J_t' \\ F' & I & F \end{Bmatrix}\begin{Bmatrix} j_a & \lambda & j_a' \\ J_t' & J_t'' & J_t \end{Bmatrix} \\
&\qquad \times\langle j_a \parallel \boldsymbol{C}^{(\lambda)} \parallel j_a'\rangle\langle j \parallel \boldsymbol{C}^{(\lambda)} \parallel j'\rangle \\
&\qquad +\sum_{\lambda'}\sum_\tau (-1)^{\lambda'+\tau}(2\tau+1)E^{\lambda'}(n_a l_a j_a \epsilon l j; n_a' l_a' j_a' \epsilon' l' j')\begin{Bmatrix} F & \tau & F' \\ j' & J & j \end{Bmatrix} \\
&\qquad \times\begin{Bmatrix} J_t & \tau & J_t' \\ F' & I & F \end{Bmatrix}\begin{Bmatrix} j_a & \tau & j_a' \\ J_t' & J_a'' & J_t \end{Bmatrix}\begin{Bmatrix} j_a & j' & \lambda' \\ j & j_a' & \tau \end{Bmatrix} \\
&\qquad \times\langle j_a \parallel \boldsymbol{C}^{(\lambda')} \parallel j'\rangle\langle j \parallel \boldsymbol{C}^{(\lambda')} \parallel j_a'\rangle\Bigg]. \qquad (8.6)
\end{aligned}
$$

At this point, eq. (8.6) can be substituted into expressions similar to eqs. (4.13) and (4.12) to obtain the collision strength for the hyperfine transition $U - U'$ in non-factorized form. Since the effect of the hyperfine interaction on the mixing coefficients is neglected, those quantities remain unchanged in eq. (4.13). Thus, the non-factorized form of the collision strength can be written as a combination of the two equations

$$
\begin{aligned}
&\Omega(\Delta_t J_t I F - \Delta_t' J_t' I F') \\
&\qquad = 2\sum_J (2J+1)\sum_{\substack{l,j \\ l',j'}} |R(\Delta_t J_t I F \epsilon l j J;\ \Delta_t' J_t' I F \epsilon' l' j' J)|^2 \qquad (8.7)
\end{aligned}
$$

and

$$
\begin{aligned}
&R(\Delta_t J_t I F \epsilon l j J;\ \Delta_t' J_t' I F \epsilon' l' j' J) \\
&\qquad = \sum_{\beta_t,\beta_t'} b^{J_t}(\Delta_t,\beta_t) b^{J_t'}(\Delta_t',\beta_t') R(\beta_t J_t I F \epsilon l j J;\ \beta_t' J_t' I F' \epsilon' l' j' J)\,. \qquad (8.8)
\end{aligned}
$$

In order to obtain the collision strength in factorized form, we proceed according to the discussion presented after eq. (4.29). Specifically, we interchange the labeling λ' and τ in eq. (8.6) above so that the result looks more like the expression for P^λ given by eq. (4.33). Since F, F', j and j' are all 'good' quantum numbers, the summation over J in eq. (8.7) can be performed using the formula [41]

$$
\sum_J (2J+1)\begin{Bmatrix} F & C & F' \\ j' & J & j \end{Bmatrix}\begin{Bmatrix} F & C' & F' \\ j' & J & j \end{Bmatrix} = \frac{\delta_{CC'}}{2C+1}\,. \qquad (8.9)
$$

From this result, one sees that the factorized form of the collision strength,

given by eqs. (4.31)–(4.35), is also applicable to hyperfine-structure transitions $U - U'$ provided that the following substitution

$$\begin{aligned} f^{\lambda}(S,S') \rightarrow & f^{\lambda}(S,S';I,F,F') \\ = & [(2F+1)(2F'+1)(2J_t+1)(2J_t'+1)]^{1/2} \\ & \times(-1)^{2J_t+I-F+j_a'+J_t''}\sqrt{w}(j_a^{w-1}\alpha_a''J_a''\,|\}j_a^{w}\alpha_a J_a) \\ & \times\left\{\begin{array}{ccc} J_t & \lambda & J_t' \\ F' & I & F \end{array}\right\}\left\{\begin{array}{ccc} j_a & \lambda & j_a' \\ J_t' & J_t'' & J_t \end{array}\right\} \end{aligned} \tag{8.10}$$

is made for the expression appearing in eq. (4.36). The above equation can be written in a more compact form by noting that, since the effect of the hyperfine interaction on mixing coefficients is neglected, J_t and J_t' can be considered to be 'good' quantum numbers and an extra 'hyperfine-structure corrective' (hfsc) factor of the form

$$f^{\lambda}_{\rm hfsc} = (-1)^{2J_t+I-F-J_t'}[(2F+1)(2F'+1)]^{1/2}\left\{\begin{array}{ccc} J_t & \lambda & J_t' \\ F' & I & F \end{array}\right\} \tag{8.11}$$

can be separated out. The remaining piece is simply the fine-structure expression for f^{λ} given by eq. (4.36), which allows us to write

$$f^{\lambda}(S,S';I,F,F') = f^{\lambda}_{\rm hfsc} \times f^{\lambda}(S,S')\,. \tag{8.12}$$

An alternative factorized expression can be obtained if eq. (8.12) is substituted into eq. (4.35) and then eq. (4.34) is evaluated to obtain the B^{λ} coefficients. Since $J_t + I - F$ and $J_t - J_t'$ are integers, the square of the resulting phase factors can be ignored. The final result is that the factorized expression for the hyperfine-structure collision strength can be obtained from the full set of fine-structure eqs. (4.31)–(4.36), provided that a corrective factor

$$B^{\lambda}_{\rm hfsc} = (2F+1)(2F'+1)\left\{\begin{array}{ccc} J_t & \lambda & J_t' \\ F' & I & F \end{array}\right\}^2 \tag{8.13}$$

is applied to the B^{λ} coefficients so that

$$\begin{aligned} B^{\lambda}(U,SS_1;U',S'S_1') \rightarrow & B^{\lambda}(U,SS_1;U',S'S_1';I,F,F') \\ = & B^{\lambda}_{\rm hfsc} \times B^{\lambda}(U,SS_1;U',S'S_1') \end{aligned} \tag{8.14}$$

in eq. (4.34).

We emphasize that eq. (8.10) applies only for the case of filled, and closed, spectator subshells. However, as discussed in section 4.3, all that is required

to describe more complex cases is to include some extra angular factors. The correction factor for hyperfine transitions, given by eq. (8.11) or (8.13), is not affected and the MCT module in the Grant code [6,11] can still be used to calculate f^λ values for the relevant fine-structure transition. Then, one simply multiplies by the appropriate correction factor, $f^\lambda_{\rm hfsc}$ or $B^\lambda_{\rm hfsc}$, to produce the f^λ or B^λ values, respectively, that are necessary to compute the hyperfine-structure result.

Once the collision strength has been obtained for a particular hyperfine-structure transition according to the above description, other quantities of interest are readily computed. For example, the cross section can be obtained from eq. (4.1), the effective collision strength from eq. (4.112) and the rate coefficient from eq. (4.114), with the statistical weight now given by $g_i = 2F+1$.

As a numerical example, collision strengths and effective collision strengths have been calculated for the ions with the properties listed in table 22. In this

Table 22
Ions to be considered and their hyperfine-structure properties: the isotope abundance A (relative to one for ^{1}H), the nuclear magnetic moment μ, the nuclear spin I, the initial and final total angular momentum quantum numbers F and F', the hyperfine-structure corrective factor $B^\lambda_{\rm hfsc}$, the wavelength λ and the transition energy ΔE. Values of A, μ, I and λ for all isotopes are taken from ref. [122].

Ion	$A\times10^6$	μ	I	F	F'	$B^\lambda_{\rm hfsc}$	λ (mm)	ΔE (Ry)$\times10^5$
$^{13}C^{5+}$	3.3	0.7024	1/2	0	1	0.500	3.87	2.35
$^{14}N^{6+}$	91.0	0.4036	1	1/2	3/2	0.889	5.64	1.62
$^{23}Na^{8+}$	1.8	2.2180	3/2	1	2	1.250	3.11	2.93
$^{25}Mg^{9+}$	2.6	−0.8553	5/2	3	2	1.944	6.71	1.36
$^{27}Al^{10+}$	2.5	3.6414	5/2	2	3	1.944	1.21	7.53
$^{29}Si^{11+}$	1.6	−0.5553	1/2	1	0	0.500	3.74	2.44
$^{57}Fe^{23+}$	0.88	0.0907	1/2	0	1	0.500	3.07	2.97

case, we are considering transitions between hyperfine levels belonging to the fine-structure ground level of each ion. Thus, $J_t = J'_t = 1/2$ in all cases. We note that a negative value for the nuclear magnetic moment, μ, indicates a transition for which $F > F'$, so that the initial level is actually described by the larger quantum number in those cases.

The corresponding collision strengths, Ω, are presented as a function of scattered electron energy ϵ'(Ry) in table 23, while the effective collision strengths, Υ, are presented as a function of electron temperature T in degrees Kelvin in table 24. The latter results are expected to cover the complete range of temperatures of interest. We note that it is generally expected that the collision strength, or the effective collision strength, for a given transition will decrease with Z when mixing effects are small or non-existent. However, in the present case, these quantities for either the H-like or Li-like ions differ for different

isotopes by the factor $B^{\lambda}_{\rm hfsc}$ given in table 22. When this point is taken into account, the results in tables 23 and 24 are seen to vary with Z in the expected manner.

Table 23

Collision strengths, Ω, for the hyperfine excitation transition $F \rightarrow F'$ (see table 22) given as a function of scattered electron energy ϵ'(Ry) for various ions.

	$\Omega\times10^2$							$\Omega\times10^3$
ϵ'(Ry)	$^{13}C^{5+}$	$^{14}N^{6+}$	$^{23}Na^{8+}$	$^{25}Mg^{9+}$	$^{27}Al^{10+}$	$^{29}Si^{11+}$	ϵ'(Ry)	$^{57}Fe^{23+}$
0.15	4.836	6.327	7.948	9.933	8.153	1.751	1.0	4.187
0.75	4.727	6.222	7.544	9.520	7.870	1.700	5.0	3.986
3.0	4.350	5.850	6.284	8.187	6.936	1.527	25.0	3.181
7.0	3.784	5.268	4.730	6.445	5.656	1.281	60.0	2.276
15.0	2.944	4.340	2.984	4.324	3.994	0.944	125.0	1.398
30.0	1.975	3.159	1.576	2.441	2.392	0.595	240.0	0.734
55.0	1.175	2.045	0.753	1.235	1.277	0.334	450.0	0.330
90.0	0.671	1.260	0.372	0.634	0.680	0.185	800.0	0.139
140.0	0.374	0.746	0.160	0.296	0.338	0.096	1400.0	0.054
210.0	0.174	0.367	0.055	0.110	0.137	0.040		
300.0	0.112	0.245	0.029	0.060	0.076	0.024		

8.2 Resonance contributions to hyperfine-structure collision strengths

It is expected that, for the hyperfine-structure transitions considered in the previous section, the resonance contribution would be important, since these are forbidden transitions. In this section, we provide the relevant equations for electron-capture collision strengths from a hyperfine-structure level to fine-structure levels, along with equations for the inverse autoionization rates from a fine-structure level to a hyperfine-structure level. These results are then applied in obtaining resonance contributions to the collision strengths and effective collision strengths.

Resonance contributions to the total collision strength for a hyperfine-structure

Table 24

Effective collision strengths, Υ, for the hyperfine excitation transition $F \rightarrow F'$ (see table 22) given as a function of temperature T(K) for various ions.

	$\Upsilon\times10^2$							$\Upsilon\times10^3$
T(K)/10^5	$^{13}C^{5+}$	$^{14}N^{6+}$	$^{23}Na^{8+}$	$^{25}Mg^{9+}$	$^{27}Al^{10+}$	$^{29}Si^{11+}$	T(K)/10^6	$^{57}Fe^{23+}$
1.0	4.747	6.241	7.625	9.600	7.924	1.709	1.0	3.934
1.5	4.694	6.189	7.443	9.409	7.791	1.685	1.5	3.807
2.5	4.592	6.087	7.111	9.055	7.541	1.639	2.5	3.585
4.0	4.449	5.943	6.681	8.589	7.206	1.575	4.0	3.309
6.0	4.278	5.765	6.205	8.058	6.818	1.501	6.0	3.017
10.0	3.982	5.450	5.471	7.216	6.186	1.377	10.0	2.589
15.0	3.680	5.115	4.805	6.429	5.578	1.255	15.0	2.221
25.0	3.219	4.582	3.917	5.341	4.713	1.076	25.0	1.755
40.0	2.739	3.997	3.113	4.322	3.876	0.898	40.0	1.356
60.0	2.307	3.444	2.474	3.486	3.171	0.744	60.0	1.053
100.0	1.781	2.737	1.780	2.553	2.361	0.563	100.0	0.737
150.0	1.403	2.204	1.330	1.933	1.810	0.436		

transition can again be treated as the same two-step process that is symbolically represented by eq. (7.27). Of course, in the present case, i and f represent hyperfine-structure levels. From a practical perspective, it is possible to obtain the desired hyperfine quantities from the corresponding fine-structure results. For example, as shown in the Appendix of ref. [125], the capture collision strength for a transition from a hyperfine-structure level $i = |J_t F\rangle$ to a doubly excited fine-structure level $d = |J_d\rangle$ can be obtained from the capture collision strength for the fine-structure transition of the type $|J_t\rangle \rightarrow |J_d\rangle$ according to the relationship

$$\widetilde{\Omega}^{\rm cap}_{\rm hfs}(F \rightarrow J_d) = \sum_{F_d} \widetilde{\Omega}^{\rm cap}_{\rm hfs}(F \rightarrow F_d) = \frac{2F+1}{2J_t+1} \widetilde{\Omega}^{\rm cap}_{\rm fs}(J_t \rightarrow J_d)\,. \tag{8.15}$$

This result can be combined with the relevant equations in section 7.1 to obtain similar relationships for capture cross sections, capture rate coefficients and autoionization rates.

For the capture cross section, one obtains

$$\begin{aligned} Q^{\rm cap}_{\rm hfs}(F \rightarrow J_d) &= \frac{\pi}{(2F+1)k^2} \frac{2F+1}{2J_t+1} \widetilde{\Omega}^{\rm cap}_{\rm fs}(J_t \rightarrow J_d) \delta(\epsilon - E_{id}) \\ &= Q^{\rm cap}_{\rm fs}(J_t \rightarrow J_d) \end{aligned} \tag{8.16}$$

with a similar expression for the capture rate coefficient given by

$$C^{\rm cap}_{\rm hfs}(F \rightarrow J_d) = C^{\rm cap}_{\rm fs}(J_t \rightarrow J_d)\,. \tag{8.17}$$

For autoionization, we first note that, for the present case involving transitions between hyperfine-structure levels, the statistical weight for the doubly excited fine-structure level is given by

$$g_d = \sum_{F_d} (2F_d + 1) = (2J_d + 1)(2I + 1)\,. \tag{8.18}$$

From eqs. (7.12) and (8.15) we obtain

$$\begin{aligned} A^{\rm a}_{\rm hfs}(J_d \rightarrow F) &= \frac{2(2F+1)}{h(2J_t+1)(2I+1)(2J_d+1)} \widetilde{\Omega}^{\rm cap}_{\rm fs}(J_t \rightarrow J_d) \\ &= \frac{(2F+1)}{(2J_t+1)(2I+1)} A^{\rm a}_{\rm fs}(J_d \rightarrow J_t)\,. \end{aligned} \tag{8.19}$$

The resonance contribution to the transition from $i = |J_t F\rangle$ to $f = |J'_t F'\rangle$

can then be obtained in the usual manner (see eq. (7.35)), and is expressed according to

$$C^{\rm res}_{\rm hfs}(F \rightarrow F') = \sum_d C^{\rm cap}_{\rm hfs}(F \rightarrow J_d) B_{\rm hfs}(J_d \rightarrow F') \,, \tag{8.20}$$

where the branching ratio is

$$B_{\rm hfs}(J_d \rightarrow F') = \frac{A^{\rm a}_{\rm hfs}(J_d \rightarrow J'_t F')}{\sum\limits_m A^{\rm a}_{dm} + \sum\limits_k A^{\rm r}_{dk}} \,. \tag{8.21}$$

In this last expression, the quantities without the subscript "hfs" refer to fine-structure transitions and are written with the same notation as in chapter 7. Using an expression for the autoionization rate associated with the transition $|J_d\rangle \rightarrow |J'_t F'\rangle$ that is analogous to eq. (8.19), and employing eq. (7.30), one obtains the relationship

$$B_{\rm hfs}(J_d \rightarrow F') = \frac{(2F'+1)}{(2J'_t+1)(2I+1)} B_{\rm fs}(J_d \rightarrow J'_t) \tag{8.22}$$

between the hyperfine-structure and fine-structure branching ratios, where $B_{\rm fs}$ is a fine-structure branching ratio of the type displayed in eq. (7.30). Thus, the relationship between the hyperfine-structure and fine-structure expressions for the resonance contribution to the impact-excitation rate coefficient is found to be

$$C^{\rm res}_{\rm hfs}(F \rightarrow F') = \frac{(2F'+1)}{(2J'_t+1)(2I+1)} C^{\rm res}_{\rm fs}(J_t \rightarrow J'_t) \,, \tag{8.23}$$

where $C^{\rm res}_{\rm fs}$ is the quantity $C^{\rm res}_{if}$ in eq. (7.35). Similarly, the relationship for the resonance contribution to the effective collision strength is found to be

$$\Upsilon^{\rm res}_{\rm hfs}(F \rightarrow F') = \frac{(2F+1)}{(2J_t+1)} \frac{(2F'+1)}{(2J'_t+1)(2I+1)} \Upsilon^{\rm res}_{\rm fs}(J_t \rightarrow J'_t) \tag{8.24}$$

and to the total collision strength is given by

$$\Omega^{\rm res}_{\rm hfs}(F \rightarrow F') = \frac{(2F+1)}{(2J_t+1)} \frac{(2F'+1)}{(2J'_t+1)(2I+1)} \Omega^{\rm res}_{\rm fs}(J_t \rightarrow J'_t) \,. \tag{8.25}$$

In the above expression, $\Upsilon^{\rm res}_{\rm fs}$ is given by the quantity $\Upsilon^{\rm res}_{if}$ in eq. (7.34), and $\Omega^{\rm res}_{\rm fs}$ is given by the quantity $\Omega^{\rm res}_{if}$ in eq. (7.29), respectively. Hence, in order to

obtain the hyperfine-structure resonance contributions to these various quantities, it is only necessary to calculate the corresponding fine-structure quantities and then multiply by the extra angular factors appearing in eq. (8.19) and eqs. (8.23)–(8.25).

As a numerical example, we reproduce some of the results from ref. [125]. In particular, we present effective collision strengths for Li-like ^{57}Fe and H-like ^{14}N ions in their fine-structure ground levels. In these cases, the hyperfine-structure transition energies, E_{if}, are so small that the quantity E_{if}/kT in the exponent of eq. (7.34) can be neglected.

First, we consider Li-like ^{57}Fe for the transition described by $F = 0$, $F' = 1$ and $J_t = J'_t = I = 1/2$. Applying these values to eqs. (8.24) and (8.25) yields

$$\Upsilon^{\rm res}_{\rm hfs} = \tfrac{3}{8}\Upsilon^{\rm res}_{\rm fs}, \qquad \Omega^{\rm res}_{\rm hfs} = \tfrac{3}{8}\Omega^{\rm res}_{\rm fs}. \tag{8.26}$$

Only contributions from the $1s^2nln'l'$ doubly excited levels with $n = 2$ and 3 are significant in this example. Based on energy considerations, for $n = 2$, only levels with $n' \geq 11$ can contribute, while for $n = 3$ contributions, all levels with $n' \geq 3$ are energetically possible. For $3 \leq n' \leq 6$, a full distorted-wave treatment was used, while results were computed with the rapid, first approximation method described in section 7.3 to obtain accurate contributions for $n' > 6$ up to some prescribed value of n' for the two possible values of n. The contributions for $n' > 20$ when $n = 2$, and for $n' > 10$ when $n = 3$, were then estimated by assuming that they scaled as $1/(n')^3$ for large values of n' [108]. In the discussion below, the background or "direct" contributions are indicated by BG or by adding "dir" as a superscript.

Values for the total effective collision strength, $\Upsilon^{\rm total} = \Upsilon^{\rm dir} + \Upsilon^{\rm res}$, are shown in figure 6. The direct contribution to this quantity, labeled BG in the figure, was taken from table 24. The resonance contributions from the $1s^22ln'l'$ and $1s^23ln'l'$ doubly excited levels are indicated by $2ln'l'$ and $3ln'l'$, respectively. One indeed observes that the resonance contributions are important over the entire temperature range of interest. The dashed lines in figure 6 are results when radiative decay is neglected. One also observes that inclusion of radiative decay is not highly important, but does have nearly a 10% effect on the total effective collision strength at the highest temperatures.

Next, we consider H-like ^{14}N ions in the fine-structure ground level that undergo a hyperfine transition described by the quantum numbers $F = 1/2$, $F' = 3/2$, $I = 1$ and again $J_t = J'_t = 1/2$. In this case, eqs. (8.24) and (8.25) give

$$\Upsilon^{\rm res}_{\rm hfs} = \tfrac{2}{3}\Upsilon^{\rm res}_{\rm fs}, \qquad \Omega^{\rm res}_{\rm hfs} = \tfrac{2}{3}\Omega^{\rm res}_{\rm fs}. \tag{8.27}$$

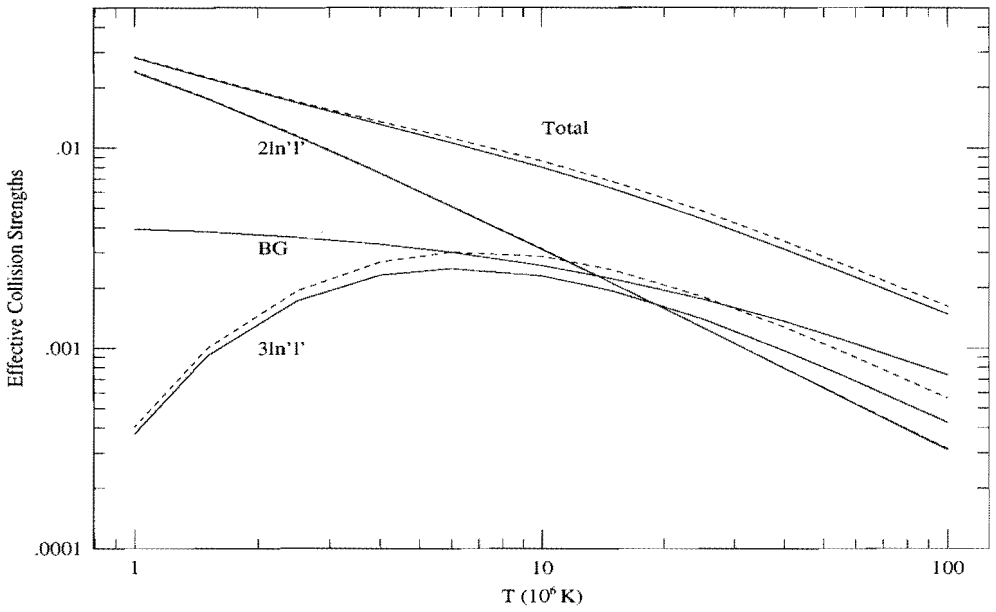

Fig. 6. Effective collision strengths, Υ, as a function of temperature, $T(10^6\mathrm{K})$, for the transition $(1s^2 2s)_{1/2}F - (1s^2 2s)_{1/2}F'$, with $F = 0$ and $F' = 1$, in Li-like ^{57}Fe. The dashed and solid lines represent the results with radiative decay neglected and included, respectively. The curve labeled BG represents the background contribution and the curves labeled Total represent the sum of the background and resonance contributions.

Furthermore, only contributions from the $2ln'l'$ doubly excited levels are significant. For $2 \leq n' \leq 6$, a full distorted-wave treatment was used, for $6 < n' \leq 10$ the first approximate method of section 7.3 was again used, and for $n' > 10$ results were estimated by assuming a $1/(n')^3$ dependence. Due to the fact that the initial free electron must have a rather large energy in order to excite the 1s electron to the $n = 2$ shell when forming a doubly excited level during the capture process, resonances contribute only at quite high energies. Hence, they are significant only for high temperatures. Even then, the resonances are not highly important as can be seen from the effective collision strengths listed as a function of $T(\mathrm{K})$ in table 25. In this case, the background (BG) contribution was taken from table 24. One observes that, at the highest temperature considered in the present work, the resonance contribution to $\Upsilon^{\mathrm{total}}$ has risen to only 17%. The entries labeled as "NRD" and "RD" in the table correspond to neglect and inclusion, respectively, of the effect of radiative decay. In this case, the maximum effect of radiative decay on $\Upsilon^{\mathrm{total}}$ is only about 2%.

In addition to the numerical examples provided above, resonance contributions were also considered for the case of electron-impact excitation to the

Table 25
Effective collision strengths as a function of temperature, T(K), for the transition $1s_{1/2}F - 1s_{1/2}F'$, with $F = 1/2$ and $F' = 3/2$, in H-like ^{14}N. Results are presented for the background (BG) values, the resonance contributions from the $2ln'l'$ levels, and the total collision strengths. The entries labeled NRD and RD are results calculated with radiative decay neglected and included, respectively.

		$n = 2$ Resonances		Total	
T(K)	BG	NRD	RD	NRD	RD
1.0E+05	6.24E-02	1.75E-19	1.73E-19	6.24E-02	6.24E-02
1.5E+05	6.19E-02	1.53E-13	1.51E-13	6.19E-02	6.19E-02
2.5E+05	6.09E-02	7.53E-09	7.44E-09	6.09E-02	6.09E-02
4.0E+05	5.94E-02	2.92E-06	2.87E-06	5.94E-02	5.94E-02
6.0E+05	5.77E-02	7.45E-05	7.24E-05	5.77E-02	5.77E-02
1.0E+06	5.45E-02	8.97E-04	8.54E-04	5.54E-02	5.54E-02
1.5E+06	5.12E-02	2.79E-03	2.62E-03	5.39E-02	5.38E-02
2.5E+06	4.58E-02	5.87E-03	5.44E-03	5.17E-02	5.13E-02
4.0E+06	4.00E-02	7.51E-03	6.89E-03	4.75E-02	4.69E-02
6.0E+06	3.44E-02	7.47E-03	6.82E-03	4.19E-02	4.13E-02
1.0E+07	2.74E-02	6.19E-03	5.62E-03	3.36E-02	3.30E-02
1.5E+07	2.20E-02	4.84E-03	4.39E-03	2.69E-02	2.64E-02

upper hyperfine-structure levels associated with the ground level of H-like ^{13}C and Li-like ^{23}Na, ^{25}Mg, ^{27}Al and ^{29}Si ions, and the resulting effective collision strengths were provided in ref. [126]. In that work, it was found that the resonance contributions were very important for the Li-like ions, considerably more so than for the Li-like ^{57}Fe example shown in figure 6, while the contributions for H-like ^{13}C ions were found to be rather unimportant.

9 Transitions between magnetic sublevels due to impact with an electron beam

In this chapter, we discuss our work concerning transitions between magnetic sublevels caused by an electron beam. The chapter is organized into two sections. The first section deals with collisional excitation while the second deals with collisional ionization.

9.1 Transitions between magnetic sublevels due to electron-impact excitation

It is well known that the radiation emitted from ions excited by a directed electron beam can be strongly polarized. In order to predict the polarization of the emitted radiation, one must know the values of the cross sections for

transitions between specific magnetic sublevels of the ion. Another motivation concerning our interest in obtaining electron-impact excitation cross sections for magnetic sublevel transitions was to compare our results with the EBIT experiments at LLNL [127]. Often, these experiments involved highly charged ions of heavy elements, such as Ba, for which a fully relativistic description is necessary. In this section, the pertinent equations for these cross sections or collision strengths, obtained in ref. [128], are given. Additional discussion is provided concerning the calculation of the top-up contribution, an option for including the generalized Breit interaction and the calculation of the resonance contribution to electron-impact excitation. Numerical examples, and comparisons with results computed by other workers, are provided throughout. Comparisons with experimentally determined values are also provided for the specific application of the magnetic sublevel cross sections in determining the polarization of the emitted radiation.

9.1.1 General formulae for electron-impact excitation between magnetic sublevels

The procedure we use for calculating cross sections for excitation by an electron beam has been given in ref. [128] and is summarized here. The relativistic amplitude, $B^{m_s}_{m'_s}$, for scattering an incident electron with spin magnetic quantum number m_s, wavenumber k, and direction $\hat{\boldsymbol{k}}$ into direction $\hat{\boldsymbol{k}}'$ with wavenumber k' and final spin magnetic quantum number m'_s, accompanied by a change in the magnetic sublevel of the target ion from $\Delta_t J_t M_t$ to $\Delta'_t J'_t M'_t$, can be written [3,129]

$$\begin{aligned} B^{m_s}_{m'_s}(\Delta_t J_t M_t - \Delta'_t J'_t M'_t) \\ = \frac{2\pi}{k} \sum_{\substack{l,m_l,j,m \\ l',m'_l,j',m'}} & \mathrm{i}^{l-l'+1} \exp[\mathrm{i}(\delta_\kappa + \delta_{\kappa'})] Y^*_{lm_l}(\hat{\boldsymbol{k}}) Y_{l'm'_l}(\hat{\boldsymbol{k}}') \\ & \times C(l\tfrac{1}{2}m_l m_s; jm) C(l'\tfrac{1}{2}m'_l m'_s; j'm') T(\alpha, \alpha'), \end{aligned} \tag{9.1}$$

where

$$\alpha = \Delta_t J_t M_t k l j m, \quad \alpha' = \Delta'_t J'_t M'_t k' l' j' m'. \tag{9.2}$$

As usual, the symbol Y denotes spherical harmonics, C denotes Clebsch-Gordan coefficients and the quantum numbers (l, m_l, j, m) and (l', m'_l, j', m') refer to the angular momenta of the incident and scattered free electrons. The appearance of k and k' in eq. (9.2), rather than the energies ϵ and ϵ' that appear in previous chapters, is merely a reminder that we are also concerned with the direction of the incident and scattered electrons for the current case of transitions between magnetic sublevels. The δ quantities are the relativistic

distorted-wave phase shifts of the incident and scattered free electrons described by eq. (A1) of ref. [128]. For highly charged ions, these shifts differ from the corresponding relativistic Coulomb phase shifts by a small correction, as described in the appendix of ref. [128]. The quantum numbers J_t and M_t represent the total angular momentum and corresponding z-component associated with the initial sublevel, while Δ_t represents all additional quantum numbers required to specify the initial sublevel of the ion. Analogous primed quantities apply to the final sublevel of the ion. The quantity $T(\alpha, \alpha')$ represents specific elements of the transmission matrix, $\boldsymbol{T}$, that was mentioned in section 4.1.

Before considering an expression for the excitation cross section, we note that the scattering amplitude in eq. (9.1) was derived for the specific case in which the spin of the incident electron can be in the positive or negative z direction, with a similar statement applying to the spin of the scattered electron. This choice results from using plane waves of the type given in eq. (4.50) or eq. (4.58) when describing the asymptotic form of the incident- and scattered-electron wave functions in order to obtain the scattering amplitude. Those 4-vector plane waves contain the 2-component Pauli spinors, χ^{m_s}, which corresponds to the electron spin being in one of the two possible directions $\pm\hat{\boldsymbol{z}}$. However, an expression for the scattering amplitude that applies to the situation in which the spins of the incident and scattered electrons are in arbitrary directions can be handled in a straightforward manner. For this general case, the 2-component spinors in eq. (4.50) or eq. (4.58) are to be replaced with an arbitrary linear combination of those spinors [3,129], i.e.

$$\chi^{m_s} \rightarrow \chi = \sum_{m_s} c_{m_s} \chi^{m_s} = \begin{pmatrix} c_{1/2} \\ c_{-1/2} \end{pmatrix} \qquad \text{where} \qquad \sum_{m_s} |c_{m_s}|^2 = 1\,. \tag{9.3}$$

A similar expression, in which all appropriate quantities are primed, applies to the 2-component spinors appearing in the wave function associated with the scattered electron. Then, the scattering amplitude in eq. (9.1) takes on the more general form [129]

$$B^{m_s}_{m'_s} \rightarrow (\chi')^\dagger \boldsymbol{B} \chi = \sum_{m_s, m'_s} c_{m_s} c^*_{m'_s} B^{m_s}_{m'_s}\,, \tag{9.4}$$

where $\boldsymbol{B}$ is the 2×2 matrix given by

$$\boldsymbol{B} = \begin{pmatrix} B^{1/2}_{1/2} & B^{-1/2}_{1/2} \\ B^{1/2}_{-1/2} & B^{-1/2}_{-1/2} \end{pmatrix}\,. \tag{9.5}$$

In our work, we choose to use the amplitude in eq. (9.1) because that form is more convenient when deriving an expression for the excitation cross section

for the case of an unpolarized beam of electrons [129]. Also, eq. (9.1) can be used to derive an expression for the cross section when a beam is composed of electrons with a specific spin polarization, such as the case of longitudinally polarized electrons, which is discussed next.

Thus, assuming that one is not interested in the z-component of the spin of the scattered electron, the excitation cross section is given by

$$Q_{m_s}(\Delta_t J_t M_t - \Delta'_t J'_t M'_t) = \sum_{m'_s} \int \mathrm{d}\hat{\boldsymbol{k}}' \, |B^{m_s}_{m'_s}|^2 \,. \tag{9.6}$$

In evaluating eq. (9.6), we choose $\hat{\boldsymbol{k}}$ to be in the direction of the z axis so that $m_l = 0$ (as a consequence $m = m_s$) and

$$Y_{lm_l}(\hat{\boldsymbol{k}}) = Y_{l0}(\hat{\boldsymbol{k}}) \underset{\theta=0}{\longrightarrow} \left(\frac{2l+1}{4\pi}\right)^{1/2} . \tag{9.7}$$

Choosing $\hat{\boldsymbol{k}}$ to be in the direction of the z axis corresponds to an electron that is longitudinally polarized because the spin and direction of the electron are either parallel or anti-parallel. After squaring eq. (9.1) and substituting the result in eq. (9.6), the integration over the scattered-electron direction yields a factor of the form

$$\int \mathrm{d}\hat{\boldsymbol{k}}' \; Y^*_{l'_1 m'_{l_1}}(\hat{\boldsymbol{k}}') Y_{l' m'_l}(\hat{\boldsymbol{k}}') = \delta_{l'_1 l'} \delta_{m'_{l_1} m'_l} \,. \tag{9.8}$$

Additional quantum numbers with a subscript "1" have been introduced here in order to distinguish the various sets of summation indices that arise from taking the square of eq. (9.1). After performing the summation over m'_{l_1} and l'_1, another simplification,

$$\sum_{m'_s, m'_l} C(l' \tfrac{1}{2} m'_l m'_s; j'_1 m'_1) C(l' \tfrac{1}{2} m'_l m'_s; j' m') = \delta_{j'_1 j'} \delta_{m'_1 m'} \,, \tag{9.9}$$

occurs due to the properties of the Clebsch-Gordan coefficients. This last result eliminates the dependence on the final phase shifts denoted by $\delta_{\kappa'}$. Also, we express the $\boldsymbol{T}$ matrix in terms of the reactance matrix, $\boldsymbol{R}$, according to eq. (4.4). Combining these last several results, we obtain an expression for the cross section for excitation between magnetic sublevels, due to collisions with a longitudinally polarized beam of electrons, that can be written in the form

$$Q_{m_s}(\Delta_t J_t M_t - \Delta'_t J'_t M'_t)$$

$$= \frac{4\pi}{k^2} \sum_{\substack{l,l_1,j,j_1 \\ l',j',m'}} \mathrm{i}^{l-l_1}[(2l+1)(2l_1+1)]^{1/2} \times \exp[\mathrm{i}(\delta_\kappa - \delta_{\kappa_1})] C(l\tfrac{1}{2}0m_s; jm) C(l_1\tfrac{1}{2}0m_s; j_1 m) \times R(\alpha, \alpha') R(\alpha_1, \alpha') \,, \tag{9.10}$$

where α_1 differs from α in that l_1 and j_1 replace l and j, respectively. In writing eq. (9.10), the summation over m was eliminated because, as mentioned previously, $m \equiv m_s$. This restriction is made explicit by the fact that the Clebsch-Gordan coefficients can only be non-zero if $m = m_s$.

Finally, it is sometimes convenient to consider reactance matrix elements in the coupled representation denoted by

$$\gamma = \Delta_t J_t k l j \, JM \text{ and } \gamma' = \Delta'_t J'_t k' l' j' \, JM \tag{9.11}$$

because the matrix elements are independent of M in this coupling scheme. Therefore, the corresponding equations provided in sections 4.1–4.2 for fine-structure levels can be immediately applied to the present case. The transformation between matrix elements in the uncoupled and the coupled representations is given by

$$R(\alpha, \alpha') = \sum_{J,M} C(J_t j M_t m; JM) C(J'_t j' M'_t m'; JM) R(\gamma, \gamma') \tag{9.12}$$

and

$$R(\alpha_1, \alpha') = \sum_{J_1, M_1} C(J_t j_1 M_t m_1; J_1 M_1) C(J'_t j' M'_t m'; J_1 M_1) R(\gamma_1, \gamma'_1) \,, \tag{9.13}$$

where γ_1 differs from γ in that J_1, l_1 and j_1 replace J, l and j, respectively, while γ'_1 differs from γ' in that only J_1 replaces J. Due to the lack of dependence on M mentioned above, we note that $R(\gamma, \gamma')$ in eq. (9.12) is identical to the left-hand side of eq. (4.13), which applies to fine-structure levels. As with eq. (9.2), the use of k and k', instead of ϵ and ϵ', in eq. (9.11) is an intentional choice to denote the consideration of directional electrons in the present case.

Using eqs. (9.12) and (9.13) in eq. (9.10), we obtain

$$Q_{m_s}(\Delta_t J_t M_t - \Delta'_t J'_t M'_t) = \frac{4\pi}{k^2} \sum_{\substack{l,l_1,j,j_1 \\ l',j',m'}} \sum_{J,J_1,M} \mathrm{i}^{l-l_1}[(2l+1)(2l_1+1)]^{1/2} \times \exp[\mathrm{i}(\delta_\kappa - \delta_{\kappa_1})] C(l\tfrac{1}{2}0m_s; jm) C(l_1\tfrac{1}{2}0m_s; j_1 m) \times C(J_t j M_t m; JM) C(J_t j_1 M_t m; J_1 M)$$

$$\times C(J_t' j' M_t' m'; JM) C(J_t' j' M_t' m'; J_1 M)$$
$$\times R(\gamma, \gamma') R(\gamma_1, \gamma_1') \,. \tag{9.14}$$

In writing eq. (9.14), the summation over M_1 was eliminated due to the fact that $M_1 \equiv M$ because both quantum numbers must be simultaneously equal to $M_t + m_s$ (recall that $m = m_1 = m_s$ in this case), as well as $M_t' + m'$, if the Clebsch-Gordan coefficients are to be non-zero.

In practice, it is computationally more efficient to first obtain the $\boldsymbol{R}$ matrix elements in the uncoupled representation using eqs. (9.12) and (9.13), and then to calculate the cross section via eq. (9.10), rather than using eq. (9.14) directly. However, obtaining the cross section directly from eq. (9.14) can be used as a convenient check on the former procedure.

While eqs. (9.10) and (9.14) give the cross section between magnetic sublevels when the electron beam is longitudinally polarized, one is often interested in impact excitation by an unpolarized electron beam. In that case, the initial spin orientations must be averaged over and the cross section of interest becomes

$$Q(\Delta_t J_t M_t - \Delta_t' J_t' M_t') = \tfrac{1}{2} \sum_{m_s} Q_{m_s}(\Delta_t J_t M_t - \Delta_t' J_t' M_t') \,. \tag{9.15}$$

Additionally, in most applications the target ions are randomly oriented so the cross section of interest is given by averaging eq. (9.10) or eq. (9.14) over initial sublevels. Therefore, the cross section for a transition from a fine-structure level to a magnetic sublevel is given by

$$Q_{m_s}(\Delta_t J_t - \Delta_t' J_t' M_t') = \frac{1}{2J_t + 1} \sum_{M_t} Q_{m_s}(\Delta_t J_t M_t - \Delta_t' J_t' M_t') \tag{9.16}$$

when the incident beam is comprised of longitudinally polarized electrons, and by

$$Q(\Delta_t J_t - \Delta_t' J_t' M_t') = \frac{1}{2(2J_t + 1)} \sum_{m_s, M_t} Q_{m_s}(\Delta_t J_t M_t - \Delta_t' J_t' M_t') \tag{9.17}$$

when the beam is unpolarized. Of course, substituting eq. (9.14) into eq. (9.17) and summing over M_t' leads to the standard expression for the excitation cross section for transitions between fine-structure levels (see eqs. (4.1) and (4.12)), which provides a useful check on our equations.

The RDW formalism described above has been used to compute excitation cross sections for transitions to specific magnetic sublevels for a variety of applications. For example, Inal et al. have used the appropriate RDW cross

sections to predict the degree of polarization for various spectral lines emitted by different ions. These calculations include a prediction of the circular polarization of lines from He-like iron excited by longitudinally polarized, directional electrons [130] and a study of the effects of the hyperfine interaction on the circular polarization of various x-ray lines from Sc XX [131]. As a specific numerical application of eq. (9.10) or eq. (9.14), we consider here the collisional data for excitation to magnetic sublevels by impact with an unpolarized electron beam that were presented in ref. [128]. In that work, collision strengths were presented for He-like, Li-like and Ne-like iron, as well as for Ne-like molybdenum. Comparisons were also provided with results from other works when available. We note that for magnetic sublevel transitions, the usual relationship holds between the collision strength, Ω, and the cross section, Q, (see, specifically, eq. (4.1), or eq. (9.18) in the next subsection). However, the statistical weight associated with the initial sublevel, g_i, is always one in this case.

In table 26, we present a sample of those results from ref. [128]. In this table, our results for collision strengths for excitation from the ground level to the magnetic sublevels M_t' of the 1s2p levels in He-like iron are compared with two different sets of semi-relativistic results produced by Inal and Dubau [132] and the Los Alamos excitation code ACE [46]. As can be seen from the table, the agreement between the three sets of calculations is very good. Therefore, the relativistic effects are not particularly significant for iron ions and a semi-relativistic treatment is adequate.

9.1.2 The relativistic Coulomb-Bethe approximation

As pointed out in section 4.9, when considering optically allowed $\Delta n = 0$ transitions, which generally have small transition energies, very large values of the angular momentum quantum numbers l and l' that are associated with the incident and scattered electrons, respectively, can contribute significantly to the excitation collision strength. In subsection 4.9.1, we briefly described the partial-relativistic Coulomb-Bethe (PRCBe) and relativistic Coulomb-Bethe (RCBe) approximations as a way to estimate the top-up contribution in order to obtain converged collision strengths for fine-structure transitions. However, those formulations of the PRCBe and RCBe approximations can not be directly applied to collision strengths associated with transitions between magnetic sublevels. For example, the presence of the Coulomb phase shifts associated with the continuum partial waves must be considered explicitly. Also, a useful form of the PRCBe method can not be readily obtained for magnetic sublevel transitions because one is not allowed to perform a sum over the magnetic quantum numbers associated with the initial and final target states. Furthermore, for moderate and high values of the nuclear charge Z, a relativistic treatment should be used, especially since more detailed (i.e. less

Table 26
Comparison of collision strengths for excitation from the ground level to the magnetic sublevels M_t' of various 1s2p levels in He-like iron. In each case, upper entries represent our fully relativistic (RDW) values, second entries are from the code of ref. [46], and third entries are from ref. [132]. The results from ref. [132] were all computed with the same transition energy $\Delta E = 493$ Ry. Also, as discussed in ref. [128], for most transitions, the present RDW results were calculated at slightly different values of the incident-electron energy, ϵ, than those listed in the table. $x[y] = x \times 10^y$.

Excited			ϵ (Ry)				
Level	M_t'	ΔE (Ry)	550	700	900	1200	2000
1s2p $^1P_1$	0	493.2	1.69[-3]	2.37[-3]	3.09[-3]	3.85[-3]	4.94[-3]
or		493.0	1.69[-3]	2.39[-3]	3.07[-3]	3.76[-3]	4.68[-3]
$(1s_{1/2}2p_{3/2})_1$			1.69[-3]	2.38[-3]	3.06[-3]	3.76[-3]	4.69[-3]
	1		4.19[-4]	6.12[-4]	8.84[-4]	1.30[-3]	2.32[-3]
			4.18[-4]	6.20[-4]	8.98[-4]	1.31[-3]	2.30[-3]
			4.06[-4]	5.84[-4]	8.87[-4]	1.35[-3]	2.39[-3]
1s2p $^3P_1$	0	490.7	2.08[-4]	2.42[-4]	2.85[-4]	3.37[-4]	4.20[-4]
or		490.6	2.19[-4]	2.55[-4]	2.99[-4]	3.47[-4]	4.16[-4]
$(1s_{1/2}2p_{1/2})_1$							
	1		2.65[-4]	2.09[-4]	1.76[-4]	1.69[-4]	2.16[-4]
			2.66[-4]	2.09[-4]	1.78[-4]	1.72[-4]	2.20[-4]
1s2p $^3P_2$	0	491.9	2.91[-4]	1.98[-4]	1.27[-4]	7.35[-5]	2.50[-5]
or		491.7	3.08[-4]	2.10[-4]	1.35[-4]	7.76[-5]	2.63[-5]
$(1s_{1/2}2p_{3/2})_2$							
	1		2.37[-4]	1.61[-4]	1.04[-4]	6.04[-5]	2.12[-5]
			2.50[-4]	1.70[-4]	1.10[-4]	6.36[-5]	2.23[-5]
			2.45[-4]	1.65[-4]	1.05[-4]	6.05[-5]	2.10[-5]
	2		7.46[-5]	5.00[-5]	3.32[-5]	2.11[-5]	9.70[-6]
			7.63[-5]	5.13[-5]	3.42[-5]	2.19[-5]	1.02[-5]
			7.55[-5]	4.96[-5]	3.28[-5]	2.09[-5]	9.74[-6]

averaged) collision strengths, such as those associated with transitions between magnetic sublevels, tend to be more sensitive to any approximation made. Based on these considerations, we provide in this section some of the details associated with the RCBe approximation and its application to obtaining the top-up contribution to collision strengths that describe transitions

between magnetic sublevels produced by impact with directional electrons. A more detailed description of this approach is provided in ref. [55].

For values of the angular momentum quantum numbers l or $l' \geq l_0$, where l_0 is some suitably large number, the continuum partial waves can be accurately described by relativistic Coulomb functions and the RCBe approximation becomes valid. That is, the Coulomb interaction between the active bound electron, with coordinate label N, and the free electron, with coordinate label $N+1$, can be approximated by eq. (4.60). In addition, exchange is neglected in the $\boldsymbol{R}$ matrix elements and relativistic Coulomb functions are used to represent the free electrons. These approximations can be applied directly to the cross section that describes a transition between magnetic sublevels that appears in eq. (9.10) or eq. (9.14). Here, we choose to apply these approximations to the collision strength, which is related to the cross section in the usual way, i.e.

$$Q(\Delta_t J_t M_t - \Delta'_t J'_t M'_t) = \frac{\pi}{k^2}\Omega(\Delta_t J_t M_t - \Delta'_t J'_t M'_t)\,. \tag{9.18}$$

In the present case, the statistical weight of the initial sublevel that would normally appear in the denominator of the right-hand side of eq. (9.18) is always one. We note that this expression is also valid for the quantities Q_{m_s} and Ω_{m_s}, which apply to excitation by a beam of longitudinally polarized electrons. Applying the previous approximations to the cross section in eq. (9.10) and using the appropriate version of eq. (9.18), the corresponding RCBe collision strength can be written in the form

$$\begin{aligned}
&\Omega^{\mathrm{RCBe}}_{m_s}(\Delta_t J_t M_t - \Delta'_t J'_t M'_t) \\
&\quad = 16\, S(\Delta_t J_t, \Delta'_t J'_t) \sum_{\substack{l,l_1,j,j_1 \\ l',j',m'}} \mathrm{i}^{l-l_1}[(2l+1)(2l_1+1)]^{1/2} \\
&\qquad \times \exp[\mathrm{i}(\delta_{\kappa c} - \delta_{\kappa_1 c})] C(l\tfrac{1}{2}0m_s; jm) C(l_1\tfrac{1}{2}0m_s; j_1 m) \\
&\qquad \times (-1)^{j+j_1-2m_s}\, I(\epsilon l j, \epsilon' l' j')\, I(\epsilon l_1 j, \epsilon' l' j') \\
&\qquad \times \langle j \parallel \boldsymbol{C}^{(1)} \parallel j' \rangle \langle j_1 \parallel \boldsymbol{C}^{(1)} \parallel j' \rangle \\
&\qquad \times \sum_q \begin{pmatrix} j & 1 & j' \\ -m & q & m' \end{pmatrix} \begin{pmatrix} j_1 & 1 & j' \\ -m & q & m' \end{pmatrix} \begin{pmatrix} J_t & 1 & J'_t \\ -M_t & q & M'_t \end{pmatrix}^2 ,
\end{aligned} \tag{9.19}$$

where the reduced matrix elements of the form $\langle j_a \parallel \boldsymbol{C}^{(1)} \parallel j'_a \rangle$ are given by eq. (3.26) and the $(\cdots)$ are Wigner 3-j symbols. The I symbols represent relativistic Coulomb integrals given by eq. (4.62), $\delta_{\kappa c}$ is the relativistic Coulomb phase shift given by eq. (A2) in ref. [128] and S is the fine-structure line strength given by eq. (3.14). As mentioned in the previous subsection, one is often interested in impact excitation by an unpolarized beam. In that case, the appropriate RCBe collision strength is given by

$$\Omega^{\mathrm{RCBe}}(\Delta_t J_t M_t - \Delta'_t J'_t M'_t) = \tfrac{1}{2} \sum_{m_s} \Omega^{\mathrm{RCBe}}_{m_s}(\Delta_t J_t M_t - \Delta'_t J'_t M'_t)\,. \tag{9.20}$$

We note that, if eq. (9.19) is summed over the magnetic quantum numbers M_t and M'_t associated with the initial and final sublevels, and also averaged over the two possible spin polarizations of the incident electron represented by m_s, then one should obtain the RCBe expression for the fine-structure collision strength given by eq. (4.61) in subsection 4.9.1. This outcome is relatively straightforward to verify, as follows. The double summation over M_t and M'_t eliminates the squared 3-j symbol and replaces it with a value of $\frac{1}{3}$. The summations over q and m' can next be performed, which eliminates the remaining two 3-j symbols and replaces them with a factor of $\delta_{jj_1}/(2j+1)$. Next, the summation over m_s (recall that $m = m_s$ for the case of longitudinally polarized electrons) removes the two Clebsch-Gordan coefficients and replaces them with a value of $\delta_{ll_1}[(2j+1)/(2l+1)]$. The factor of $\frac{1}{2}$ that remains from taking the average over m_s is combined with the factor of 16 to yield 8, the remaining three phase factors can be set to one for obvious reasons, and the final result is

$$\begin{aligned}\Omega^{\mathrm{RCBe}}(\Delta_t J_t - \Delta'_t J'_t) = {} & \tfrac{8}{3}\, S(\Delta_t J_t - \Delta'_t J'_t) \\ & \times \sum_{\substack{l,j \\ l',j'}} I^2(\epsilon l j, \epsilon' l' j') \langle j \parallel \boldsymbol{C}^{(1)} \parallel j' \rangle\,,\end{aligned} \tag{9.21}$$

which is precisely the expression in eq. (4.61).

The procedure we follow in order to calculate the complete collision strength between magnetic sublevels is similar to the second method described in subsection 4.9.1 for transitions between fine-structure levels, except that it is more convenient to make the final summation over the final orbital quantum number l', rather than l. As noted in the last paragraph of subsection 4.9.1, the outcome is the same as what would be obtained if the final summation were performed over l. In the present illustration, we consider the case of an unpolarized electron beam, but the same basic logic can also be applied to the polarized case. We begin with eq. (9.18), along with eqs. (9.15) and (9.14), to calculate the relativistic distorted-wave collision strength up to some large value of $l' = l_0 - 1$. This contribution is denoted by $\Omega^{\mathrm{RDW}}_{0,l_0-1}$, where the argument that denotes the magnetic sublevel transition from eq. (9.18) has been omitted here and in the subsequent discussion for brevity.

Next, we employ the RCBe collision strength given by eq. (9.20), along with eq. (9.19), to approximate the contribution from $l' = l_0$ up to some much higher value $l_0^* - 1$, usually chosen to be the maximum value that can be attained before encountering numerical difficulties on a given computer platform. This contribution is denoted by $\Omega^{\mathrm{RCBe}}_{l_0,l_0^*-1}$. Finally, as noted in subsection 4.9.1, for

sufficiently large values of l', the ratio of successive partial-wave contributions becomes very nearly constant. Assuming this ratio is exactly constant when $l' = l_0^* - 1$, and equal to the specific value C for a given transition and incident (or scattered) electron energy, then the contribution of all partial waves with $l' \geq l_0^*$ is given by

$$\Omega_{l_0^*,\infty}^{\mathrm{RATIO}} = \Omega_{l_0^*-1}^{\mathrm{RCBe}} \frac{C}{1-C}\,, \tag{9.22}$$

where $\Omega_{l_0^*-1}^{\mathrm{RCBe}}$ is the partial-wave RCBe value for $l' = l_0^* - 1$. Hence, the complete collision strength for transitions between magnetic sublevels is given by

$$\Omega^{\mathrm{RDW}} \approx \Omega_{0,l_0-1}^{\mathrm{RDW}} + \Omega_{l_0,l_0^*-1}^{\mathrm{RCBe}} + \Omega_{l_0^*,\infty}^{\mathrm{RATIO}}\,, \tag{9.23}$$

which is identical in form to the expression given by eq. (4.72) in subsection 4.9.1 that applies to fine-structure transitions.

As a numerical example of the application of eq. (9.23), we consider the results presented in ref. [55]. In that work, we calculated and presented results for transitions from the sublevels of $(1s2s)_1$ to the sublevels of $(1s2p^*)_0$, $(1s2p^*)_1$, $(1s2p)_1$ and $(1s2p)_2$ for He-like neon, iron, barium and gold. Here, we reproduce a portion of those barium data in table 27. The atomic structure data used in those calculations were obtained from our DFS structure code described in chapter 2, with the improvements described in section 2.5 also included. As described in ref. [55], results between some sublevels are not presented because they can be obtained from the symmetry relation

$$\Omega(\Delta_t J_t M_t - \Delta_t' J_t M_t') = \Omega(\Delta_t J_t(-M_t) - \Delta_t' J_t'(-M_t'))\,. \tag{9.24}$$

The Σ entries that appear in the table represent the collision strengths associated with the corresponding fine-structure-level transitions. These results are obtained by summing over all possible pairs of M_t and M_t'. We also list the values of l_0 and l_0^* that were used in the top-up calculations for each of the three scattered-electron energies.

9.1.3 The Kummer transformation applied to transitions between magnetic sublevels

Recent attempts to obtain a more accurate approximation of the top-up contribution for excitation between magnetic sublevels [133] have involved an extension of the relativistic plane-wave-Born (RPWB) approach, or Kummer transformation, described in subsection 4.9.3 for transitions between fine-structure

Table 27
Collision strengths for $\Delta n = 0$ optically allowed transitions between magnetic sublevels with $n = 2$ in He-like barium. Results are presented for three scattered energies, ϵ', along with the corresponding values of l_0 and l_0^* used in eq. (9.23). The transition energy, ΔE, is also provided for each transition. $x[y] = x \times 10^y$.

		ϵ'(eV)					ϵ'(eV)		
M_t	M_t'	1000	4500	22000	M_t	M_t'	1000	4500	22000
		$l_0 = 23$	33	58			$l_0 = 23$	33	58
		$l_0^* = 50$	100	190			$l_0^* = 50$	100	190
		$(1s2s)_1$ - $(1s2p^*)_1$, ΔE = 82.0 eV					$(1s2s)_1$ - $(1s2p)_1$, ΔE = 575 eV		
-1	-1	9.10[-3]	6.57[-3]	2.23[-3]	-1	-1	3.11[-3]	2.82[-3]	2.23[-3]
-1	0	5.63[-3]	1.04[-2]	1.59[-2]	-1	0	1.70[-3]	2.50[-3]	4.42[-3]
-1	1	5.26[-8]	5.50[-8]	2.95[-8]	-1	1	4.73[-5]	4.41[-5]	2.29[-5]
0	-1	5.65[-3]	1.04[-2]	1.59[-2]	0	-1	1.62[-3]	2.45[-3]	4.42[-3]
0	0	8.98[-5]	6.23[-5]	1.78[-5]	0	0	1.75[-4]	1.08[-4]	2.03[-5]
	Σ	4.08[-2]	5.50[-2]	6.80[-2]		Σ	1.31[-2]	1.57[-2]	2.22[-2]

levels. The basic concept associated with the Kummer transformation is symbolized by eq. (4.75). In order to implement this approach, one must obtain an analytic expression for the RPWB collision strength, $\Omega^{\rm RPWB}$ (or the corresponding cross section). Then the appropriate partial-wave, RPWB collision strength is subtracted from the analytic expression to obtain the top-up contribution, which is to be added to the corresponding partial-wave, RDW value of the collision strength.

A partial-wave approach to computing the RPWB collision strength for transitions between magnetic sublevels is relatively straightforward and follows directly from the RDW prescription in subsection 4.8.2. Specifically, for magnetic sublevel transitions, a partial-wave, RPWB calculation can be performed with the same computer code that is used for the corresponding RDW calculation. The main difference is that the radial wave functions associated with the partial waves of the incident and scattered electrons in the RDW calculation must be replaced with the appropriate spherical Bessel functions implied by eq. (4.58). Also, only the direct Slater integrals are retained when computing the reactance matrix elements, due to the use of product wave functions in the RPWB approach. Additionally, the normalization of the plane waves is chosen according to eq. (4.59), in order to be consistent with the normalization of the RDW radial wave functions. Thus, taking these considerations into account, eqs. (9.10) and (9.14) can also be used to compute the RPWB excitation cross section for transitions between magnetic sublevels when the beam of impact electrons is longitudinally polarized. Alternatively, eq. (9.15) can be used if the beam of electrons is unpolarized.

The remaining task is to determine an analytic expression for the RPWB excitation cross section for magnetic sublevel transitions. As stated in subsection 4.8.1, the excitation cross section depends on the square of the RPWB

matrix element in eq. (4.48). By analogy with the scattering amplitude in eq. (9.1), we consider a magnetic sublevel transition, denoted by $\Delta_t J_t M_t - \Delta'_t J'_t M'_t$, that is caused by relativistic plane waves, rather than distorted waves. The incident plane wave is characterized by momentum $\boldsymbol{k}$ and spin magnetic quantum number m_s, while the scattered electron is characterized by momentum $\boldsymbol{k}'$ and spin magnetic quantum number m'_s. If one is not interested in the spin polarization of the scattered electron, then eq. (9.6) applies and the RPWB form of the excitation cross section can be written as

$$Q_{m_s}^{\mathrm{RPWB}}(\Delta_t J_t M_t - \Delta'_t J'_t M'_t) = \sum_{m'_s} \int \mathrm{d}\hat{\boldsymbol{k}}' \left| \left[B_{m'_s}^{m_s} \right]^{\mathrm{RPWB}} \right|^2 , \tag{9.25}$$

where the scattering amplitude is given by

$$\left[B_{m'_s}^{m_s} \right]^{\mathrm{RPWB}} (\Delta_t J_t M_t - \Delta'_t J'_t M'_t) = \frac{1}{4\pi} \sqrt{\left(\frac{EE'}{m^2 c^4} \right) \frac{k'}{k}} \, H_{\alpha\alpha'} \tag{9.26}$$

and the matrix element $H_{\alpha\alpha'}$ is given by eq. (4.48). The factor $EE'/(m^2c^4)$, which is written in standard units for clarity, is the extra kinematic factor (see ref. [52]) that was mentioned in subsection 4.8.1. This factor takes into account the relativistic relationship between the velocity and momentum, $\boldsymbol{v} = \boldsymbol{p}c^2/E$, for the incident and scattered electrons. Aside from this extra factor, eq. (9.26) is identical in form to the standard non-relativistic expression (see eq. (18.154) of Cowan [8]).

However, as discussed in subsection 4.8.1, the matrix element $H_{\alpha\alpha'}$ also contains an extra factor that does not appear in the non-relativistic case. In particular, this matrix element factors into two pieces: a scalar product between the 4-vector amplitudes of the incident and scattered plane waves, given by eq. (4.52), and another matrix element that has exactly the same form as the corresponding non-relativistic RPWB matrix element (see eq. (18.140) of Cowan [8]). Thus, we write the square of eq. (4.48) as

$$\begin{aligned} |H_{\alpha\alpha'}|^2 = {} & \frac{64\pi^2}{K^4} \left| U^\dagger(\boldsymbol{k}, m_s) U(\boldsymbol{k}', m'_s) \right|^2 \\ & \times \left| \langle \Delta_t J_t M_t | \sum_q e^{i\boldsymbol{K}\cdot\boldsymbol{r}_q} | \Delta'_t J'_t M'_t \rangle \right|^2 , \end{aligned} \tag{9.27}$$

where $\boldsymbol{K} = \boldsymbol{k}' - \boldsymbol{k}$ is the momentum transfer. As stated above, the matrix element containing the initial and final sublevels has exactly the same form as the result that is encountered in the non-relativistic case, but it is understood that the wave functions are represented as 4-vector quantities. For the case of transitions between magnetic sublevels currently under consideration, this ma-

trix element can be expanded according to well-established techniques, which are summarized below when considering the generalized oscillator strength.

In order to reduce eq. (9.27) to a more useful form, we first focus on the square of the scalar-product factor, $U^{\dagger}U$, which contains the entire dependence on the spin magnetic quantum numbers, m_s and m_s', associated with the incident and scattered electrons. Thus, we can apply the $\sum_{m_s'}$ that appears in eq. (9.25) to this factor. Expanding the square of the scalar product, as it appears in eq. (4.52), and repeatedly applying the relationship

$$(\boldsymbol{\sigma}\cdot\boldsymbol{p})(\boldsymbol{\sigma}\cdot\boldsymbol{p}') = \boldsymbol{p}\cdot\boldsymbol{p}' + \mathrm{i}\boldsymbol{\sigma}\cdot(\boldsymbol{p}\times\boldsymbol{p}')\,, \tag{9.28}$$

we obtain

$$\sum_{m_s'} \left|U^{\dagger}(\boldsymbol{k}, m_s)U(\boldsymbol{k}', m_s')\right|^2 = (N_k N_k')^2 \left[\left(1 + \frac{c^2}{D}\boldsymbol{p}\cdot\boldsymbol{p}'\right)^2 + \frac{c^4}{D^2}(\boldsymbol{p}\times\boldsymbol{p}')^2\right], \tag{9.29}$$

where $D \equiv (E + mc^2)(E' + mc^2)$. An expression for the normalization factor associated with the incident plane wave, N_k, is presented in the text after eq. (4.50), with a similar expression valid for the scattered-electron factor, N_k'. Eq. (9.29) is a particularly useful result because its derivation does not require any assumption about the direction of the incident or scattered electrons, and it is independent of the spin magnetic quantum number associated with the incident electron, m_s. This latter characteristic is a consequence of the use of product, rather than antisymmetrized, wave functions in the RPWB approach. Thus, eq. (9.29) applies equally well to excitation caused by a beam that contains either spin-polarized or unpolarized electrons. Furthermore, in the case of a spin-polarized beam, there is no constraint between the direction of the spin of the incident electron, $\boldsymbol{s}$, and the direction of the incident or scattered electrons, $\hat{\boldsymbol{k}}$ or $\hat{\boldsymbol{k}}'$, respectively.

Before proceeding with a discussion of the RPWB excitation cross section in eq. (9.25), we next define the generalized oscillator strength (GOS) for the case of transitions between magnetic sublevels. An expression that is appropriate for magnetic sublevels can be defined in a manner analogous to the GOS presented in eq. (4.54) for fine-structure levels in subsection 4.8.1. The details for obtaining this quantity are provided in ref. [133] and are only summarized here.

As usual, the derivation of an expression for the GOS begins with the matrix element containing the magnetic sublevels on the right-hand side of eq. (9.27),

which can be reduced to a more useful form according to standard irreducible-tensor techniques (see eq. (18.144) of Cowan [8]). The square of this expression is subsequently expanded and further simplifications ensue. An important difference that occurs in expressing the GOS for magnetic sublevels versus fine-structure levels is a dependence on the direction of the *vector* momentum transfer, $\boldsymbol{K}$, rather than a dependence on the magnitude of the momentum transfer, K. Specifically, the GOS for the magnetic sublevel transition $\Delta_t J_t M_t - \Delta'_t J'_t M'_t$, with transition energy ΔE, can be written in the form

$$\begin{aligned}
&f(\Delta_t J_t M_t - \Delta'_t J'_t M'_t; \boldsymbol{K}) \\
&\quad \equiv \frac{\Delta E}{K^2} \left| \langle \Delta_t J_t M_t | \sum_q e^{\mathrm{i}\boldsymbol{K}\cdot\boldsymbol{r}_q} | \Delta'_t J'_t M'_t \rangle \right|^2 \\
&\quad = \frac{2\Delta E}{K^2} \sum_{\substack{\nu,\nu' \\ (\nu-\nu')\,\text{even}}} \mathrm{i}^{\nu-\nu'} \sqrt{(2\nu+1)(2\nu'+1)} \\
&\qquad \times \sum_{\tau,\tau'} \mathcal{P}_\nu^{(\tau)}(\cos\theta_K)\, \mathcal{P}_{\nu'}^{(\tau')}(\cos\theta_K) \\
&\qquad \times \begin{pmatrix} J_t & \nu & J'_t \\ -M_t & \tau & M'_t \end{pmatrix} \begin{pmatrix} J_t & \nu' & J'_t \\ -M_t & \tau' & M'_t \end{pmatrix} \\
&\qquad \times \langle \Delta_t J_t || \sum_{q=1}^{N} j_\nu(Kr_q) \boldsymbol{C}_q^{(\nu)} || \Delta'_t J'_t \rangle \langle \Delta_t J_t || \sum_{q'=1}^{N} j_{\nu'}(Kr_{q'}) \boldsymbol{C}_{q'}^{(\nu')} || \Delta'_t J'_t \rangle,
\end{aligned} \tag{9.30}$$

with

$$\cos\theta_K = \frac{1}{2kK}[(k')^2 - K^2 - k^2]. \tag{9.31}$$

In eq. (9.30), the symbols appearing in the reduced matrix elements have the same meaning as those appearing in eq. (4.54) for the fine-structure GOS. For example, j_ν is the spherical Bessel function of order ν and $\boldsymbol{C}_q^{(\nu)}$ is the renormalized spherical harmonic of rank ν. The dependence on the direction of $\boldsymbol{K}$ appearing in the argument of the magnetic sublevel GOS is contained within the expression $\cos\theta_K$, where θ_K defines the angle between $\boldsymbol{K}$ and $\boldsymbol{k}$, and is measured with respect to the direction of the incident beam, $\hat{\boldsymbol{k}}$. Here, $\cos\theta_K$ appears as the argument of the normalized associated Legendre functions of degree ν and order τ, which are denoted by $\mathcal{P}_\nu^{(\tau)}$ [134]. The origin of the relationship expressed in eq. (9.31) can be more easily understood by applying the law of cosines to the triangle formed by the vectors $-\boldsymbol{k}$, $\boldsymbol{k}'$ and $\boldsymbol{K}$ to obtain the standard relationships

$$(k')^2 = K^2 + k^2 - 2kK\cos(\pi - \theta_K) = K^2 + k^2 + 2kK\cos\theta_K. \tag{9.32}$$

Similar to eq. (3.13), which represents the line strength for a transition between

magnetic sublevels, we note that the summations over τ and τ' in eq. (9.30) are unnecessary because of the properties of the 3-j symbols. For *fixed* values of M_t and M_t', which is the case currently under consideration, the 3-j symbols are non-zero only when $\tau = \tau' = (M_t - M_t')$. However, this more general expression of the GOS is useful when performing certain reductions, as illustrated in the next paragraph. We also note that, unlike the fine-structure GOS that appears in eq. (4.54), the GOS in eq. (9.30) does not contain the statistical weight symbol g because, as stated previously, the statistical weight of any magnetic sublevel is one.

As a check on eq. (9.30), we can show that it reduces to the correct fine-structure result in eq. (4.54). The reduction is performed in the standard way [8], i.e. by summing over the initial and final magnetic quantum numbers M_t and M_t', but there is a slight difference in this case due to the presence of the normalized associated Legendre functions. Proceeding in the usual way, we note that the summations over M_t and M_t' act only on the product of the 3-j symbols, which can be reduced according to

$$\sum_{M_t, M_t'} \begin{pmatrix} J_t & \nu & J_t' \\ -M_t & \tau & M_t' \end{pmatrix} \begin{pmatrix} J_t & \nu' & J_t' \\ -M_t & \tau' & M_t' \end{pmatrix} = \frac{\delta_{\nu\nu'}\delta_{\tau\tau'}}{2\nu + 1} . \tag{9.33}$$

This result can be used to greatly simplify eq. (9.30), which can be rewritten as

$$\begin{aligned} &\sum_{M_t, M_t'} f(\Delta_t J_t M_t - \Delta_t' J_t' M_t'; \boldsymbol{K}) \\ &\qquad = \frac{2\Delta E}{K^2} \sum_{\nu} \sum_{\tau} [\mathcal{P}_\nu^{(\tau)}(\cos\theta_K)]^2 \, \langle \Delta J_t || \sum_{q=1}^{N} j_\nu(Kr_q) \boldsymbol{C}_q^{(\nu)} || \Delta' J_t' \rangle^2 . \end{aligned} \tag{9.34}$$

The $\sum_\tau$ of the square of the normalized associated Legendre functions can be performed for arbitrary values of ν. The result can be expressed in the compact form

$$\sum_{\tau=-\nu}^{\nu} [\mathcal{P}_\nu^{(\tau)}(\cos\theta_K)]^2 = \frac{2\nu + 1}{2} , \tag{9.35}$$

which conveniently removes the dependence of the fine-structure GOS on the direction of $\boldsymbol{K}$. This last relation readily follows from the well-known sum rule for the spherical harmonics [8]

$$\sum_{m=-l}^{l} |Y_{lm}(\theta, \phi)|^2 = \frac{2l + 1}{4\pi} \tag{9.36}$$

and the fact that the spherical harmonics can be expressed in terms of the normalized associated Legendre functions according to [134]

$$Y_{lm}(\theta,\phi) = \frac{(-1)^m}{\sqrt{2\pi}} \mathcal{P}_l^{(m)}(\cos\theta)\, \mathrm{e}^{\mathrm{i}m\phi} \,. \tag{9.37}$$

If eq. (9.35) is then substituted into eq. (9.34), we obtain

$$\begin{aligned} &\sum_{M_t, M_t'} f(\Delta_t J_t M_t - \Delta_t' J_t' M_t'; \boldsymbol{K}) \\ &\qquad = \frac{\Delta E}{K^2} \sum_{\nu} (2\nu+1) |\langle \Delta J_t || \sum_{q=1}^{N} j_\nu(K r_q) \boldsymbol{C}_q^{(\nu)} || \Delta' J_t' \rangle|^2 \,, \end{aligned} \tag{9.38}$$

which is precisely the expression for the fine-structure GOS given by eq. (4.54).

With the GOS defined as in eq. (9.30), the determination of a useful, analytic expression for the RPWB excitation cross section for transitions between magnetic sublevels proceeds in a manner very similar to that presented for the fine-structure case. Returning to eq. (9.25), the integration over $\hat{\boldsymbol{k}}'$ can be performed in the standard way. Specifically, the polar axis is chosen to be in the direction of the unit vector $\hat{\boldsymbol{k}}$ (which is not required to be in the direction of the z axis for this application) and the integration is carried out over all angles θ' and ϕ' that describe $\hat{\boldsymbol{k}}'$ in this coordinate system. The integral over ϕ' is trivial, producing a factor of 2π, because the integrand has azimuthal symmetry about the $\hat{\boldsymbol{k}}$ direction. The remaining integral over θ' can be converted into an integral over the magnitude of the momentum transfer, K, in the standard way [8]. At this point, it is convenient to substitute eqs. (9.26), (9.27), (9.29) and (9.30) into eq. (9.25). After various manipulations, the resulting cross section can be used to obtain an expression for the corresponding collision strength according to

$$\begin{aligned} &\Omega_{m_s}^{\mathrm{RPWB}}(\Delta_t J_t M_t - \Delta_t' J_t' M_t') \\ &\qquad \equiv \frac{k^2}{\pi} Q_{m_s}^{\mathrm{RPWB}}(\Delta_t J_t M_t - \Delta_t' J_t' M_t') \\ &\qquad = \frac{8}{\Delta E} \int_{K_{\min}}^{K_{\max}} F_{\mathrm{rel}}(K) f(\Delta_t J_t M_t - \Delta_t' J_t' M_t'; \boldsymbol{K})\, \mathrm{d}(\ln K) \,. \end{aligned} \tag{9.39}$$

We note that eq. (9.39) is almost identical in form to the collision strength in eq. (4.53), which applies to fine-structure transitions. As stated previously, the statistical weight associated with the initial sublevel, g_i, has been omitted above because it has a value of one for any magnetic sublevel. Additionally,

the quantity $f(\cdots;\boldsymbol{K})$ represents the GOS for magnetic sublevels given by eq. (9.30). Aside from these two differences, the expressions for the magnetic sublevel and fine-structure RPWB collision strengths are identical. Hence, the quantity $F_{\rm rel}(K)$, which represents the relativistic correction factor that was previously discussed for the case of transitions between fine-structure levels, is again given by eq. (4.56). Also, the limits of integration are still given by eqs. (4.55a) and (4.55b).

Thus, the integral in eq. (9.39) can be evaluated with the same numerical techniques that were used in the fine-structure case. However, when considering the $K \to 0$ limit of the magnetic sublevel GOS, the dependence on the direction of $\boldsymbol{K}$ does require some additional attention. In the fine-structure case, this limit is unambiguous and readily produces the corresponding dipole oscillator strength, as mentioned in the discussion following eq. (4.54). In the case of transitions between magnetic sublevels, the situation is more complicated due to the dependence of the GOS on $\boldsymbol{K}$. A discussion of this issue is provided in ref. [133] and the reader is referred to that work for further details.

As written, the subscript m_s in eq. (9.39) denotes that the collision strength is valid for the case of excitation between magnetic sublevels due to collisions with a beam of spin-polarized electrons. More precisely, this expression is valid for arbitrary orientations between the electron spin, $\boldsymbol{s}$, and the direction of the incident beam, $\hat{\boldsymbol{k}}$, not just for the case of longitudinally polarized electrons in which $\boldsymbol{s}$ and $\hat{\boldsymbol{k}}$ are parallel. This general outcome is obtained because the derivation above did not require the specification of a particular direction for $\hat{\boldsymbol{k}}$. Furthermore, because the final expression on the right-hand side of eq. (9.39) is independent of the spin magnetic quantum m_s (see the discussion following eq. (9.29)), this result also applies to the case of excitation caused by impact with a beam of unpolarized electrons. Thus, eq. (9.39) can be used to obtain the top-up contribution for transitions between magnetic sublevels, via eq. (4.75), for either an arbitrarily polarized beam of electrons or an unpolarized beam.

As a specific numerical example, we consider the case of excitation between magnetic sublevels caused by a beam of unpolarized electrons. In table 28, we reproduce results from ref. [133] for certain magnetic sublevel transitions associated with the $(1s^2)_0 \to (1s2p^*)_1$ fine-structure transition in He-like ions for $Z = 10$, 26, 56 and 79. Collision strengths for all possible magnetic sublevel transitions arising from this fine-structure transition were previously presented in table 27 for Ba^{54+} ions. Those results were calculated using the RCBe top-up approach presented in eq. (9.23). (As mentioned previously, some transitions were omitted from table 27 due to symmetry arguments. See eq. (9.24). Also, slight differences between those results and the RCBe collision strengths presented in table 28 are due to calculations having been performed on different computing platforms.) In table 28, results are presented for only two of the

Table 28. Comparison of collision strengths for the magnetic sublevel transitions denoted by $(1s^2)_0\,(M_t = -1) \rightarrow (1s2p^*)_1\,(M_t' = -1, 0)$, due to impact with an unpolarized electron beam in the following He-like ions: Ne^{8+}, Fe^{24+}, Ba^{54+} and Au^{77+}. Two different top-up methods are considered: the relativistic Kummer transformation (KUM) in eq. (4.75) and the relativistic Coulomb-Bethe approximation (RCBe) in eq. (9.23). The final, or scattered, electron energy is denoted by ϵ'. $x[y] = x \times 10^y$.

Ne^{8+}					Fe^{24+}				
	$M_t' = -1$		$M_t' = 0$			$M_t' = -1$		$M_t' = 0$	
ϵ'(keV)	KUM	RCBe	KUM	RCBe	ϵ'(keV)	KUM	RCBe	KUM	RCBe
0.04	4.08[-1]	4.22[-1]	2.38[-1]	2.42[-1]	0.25	5.42[-2]	5.99[-2]	3.25[-2]	3.47[-2]
0.1	3.58[-1]	3.52[-1]	3.29[-1]	3.35[-1]	0.6	4.48[-2]	5.30[-2]	4.72[-2]	5.06[-2]
0.2	2.98[-1]	3.49[-1]	4.65[-1]	4.72[-1]	1.25	3.85[-2]	3.79[-2]	6.35[-2]	6.78[-2]
0.5	2.64[-1]	3.15[-1]	5.79[-1]	5.98[-1]	2.5	3.36[-2]	2.36[-2]	8.01[-2]	8.27[-2]
0.8	2.48[-1]	2.55[-1]	6.57[-1]	6.80[-1]	4.0	3.11[-2]	1.61[-2]	9.13[-2]	9.09[-2]
1.25	2.38[-1]	1.92[-1]	7.27[-1]	7.44[-1]	6.0	2.96[-2]	1.11[-2]	1.01[-1]	9.71[-2]
1.6	2.34[-1]	5.83[-2]	7.65[-1]	7.03[-1]	9.0	2.87[-2]	3.59[-3]	1.10[-1]	8.56[-2]
2.0	2.30[-1]	4.71[-2]	7.98[-1]	7.18[-1]	13.0	2.84[-2]	2.45[-3]	1.18[-1]	8.99[-2]
2.5	2.29[-1]	3.84[-2]	8.30[-1]	7.32[-1]	18.0	2.84[-2]	1.75[-3]	1.26[-1]	9.41[-2]
3.2	2.27[-1]	2.98[-2]	8.66[-1]	7.45[-1]	24.0	2.87[-2]	1.35[-3]	1.34[-1]	9.69[-2]
4.0	2.26[-1]	2.50[-2]	8.97[-1]	7.51[-1]	30.0	2.92[-2]	1.07[-3]	1.40[-1]	9.92[-2]
5.5	2.26[-1]	1.83[-2]	9.43[-1]	7.55[-1]	40.0	3.01[-2]	8.12[-4]	1.50[-1]	1.03[-1]

Ba^{54+}					Au^{77+}				
	$M_t' = -1$		$M_t' = 0$			$M_t' = -1$		$M_t' = 0$	
ϵ'(keV)	KUM	RCBe	KUM	RCBe	ϵ'(keV)	KUM	RCBe	KUM	RCBe
1.0	8.18[-3]	9.14[-3]	5.05[-3]	5.61[-3]	2.0	3.53[-3]	3.90[-3]	2.19[-3]	2.45[-3]
2.2	7.12[-3]	8.51[-3]	7.34[-3]	7.85[-3]	5.0	3.03[-3]	3.57[-3]	3.43[-3]	3.62[-3]
4.5	6.15[-3]	6.57[-3]	9.98[-3]	1.05[-2]	10.0	2.64[-3]	2.82[-3]	4.60[-3]	4.71[-3]
9.0	5.32[-3]	4.30[-3]	1.28[-2]	1.30[-2]	16.0	2.40[-3]	2.18[-3]	5.47[-3]	5.55[-3]
15.0	4.89[-3]	2.96[-3]	1.49[-2]	1.47[-2]	25.0	2.23[-3]	1.64[-3]	6.37[-3]	6.31[-3]
22.0	4.68[-3]	2.22[-3]	1.66[-2]	1.59[-2]	35.0	2.15[-3]	1.33[-3]	7.12[-3]	6.90[-3]
30.0	4.60[-3]	6.38[-4]	1.82[-2]	1.22[-2]	50.0	2.12[-3]	4.13[-4]	8.06[-3]	5.74[-3]
50.0	4.69[-3]	3.91[-4]	2.11[-2]	1.38[-2]	70.0	2.16[-3]	3.15[-4]	9.11[-3]	6.43[-3]
75.0	4.97[-3]	2.67[-4]	2.41[-2]	1.57[-2]	100.0	2.29[-3]	2.39[-4]	1.05[-2]	7.40[-3]
100.0	5.32[-3]	2.07[-4]	2.70[-2]	1.74[-2]	150.0	2.58[-3]	1.79[-4]	1.29[-2]	8.90[-3]
150.0	6.15[-3]	1.52[-4]	3.27[-2]	2.06[-2]	250.0	3.33[-3]	1.32[-4]	1.78[-2]	1.18[-2]
200.0	7.07[-3]	1.27[-4]	3.86[-2]	2.37[-2]	400.0	4.70[-3]	1.13[-4]	2.61[-2]	1.65[-2]

possible nine magnetic sublevel transitions in order to illustrate the differences that can arise when the top-up contribution is computed with the Kummer transformation in eq. (4.75) versus the RCBe approach. In particular, the initial magnetic quantum number is fixed at a value of $M_t = -1$, while two values of the final magnetic quantum, $M_t' = -1$ and 0, are considered. The behavior observed for these two transitions was indicative of the entire set.

For both magnetic sublevel transitions under consideration, the Kummer results are lower than the RCBe results for all of the ions considered when examining the lowest few energies. The differences range from approximately 2–10%. This behavior indicates that the Kummer results are inaccurate due to the use of plane waves, rather than Coulomb waves, at these energies. For slightly higher energies, the two sets of data become comparable and then the Kummer results start to exceed the RCBe values, particularly for the heavier Ba^{54+} and Au^{77+} ions. For the highest energies, the Kummer results are greater than the RCBe results for both transitions and for all ions. The discrepancies for the $(M_t = -1) \rightarrow (M_t' = -1)$ transition are particularly sensitive to the method used to compute the top-up contribution, while the $(M_t = -1) \rightarrow (M_t' = 0)$ transition is not quite so strongly affected. For example, the Au^{77+} values differ by more than a factor of 40 at the highest energy for the $M_t' = -1$ transition, but display a more benign, yet still significant, 60% difference for the $M_t' = 0$ transition. Similar trends are observed for Ba^{54+} ions. The discrepancies in this high-energy region are due to convergence problems associated with the RCBe approach. It can be numerically challenging to compute the RCBe contributions up to a sufficiently high value of l_0^* when evaluating eq. (9.23). If the value of l_0^* is too small, then the ratio approximation does not provide an accurate estimate of the remaining partial-wave contribution. On the other hand, the Kummer transformation is designed to automatically reproduce the correct RPWB behavior in the collision strength at such high energies, as illustrated in figure 1 for the $(1s\,2s)_1 \rightarrow (1s\,2p^*)_1$ fine-structure transition in He-like iron.

9.1.4 Comparisons with EBIT experiments at LLNL

The degree of polarization associated with the emission of a particular line can be obtained from the magnetic sublevel excitation cross sections described in the previous subsections. For example, comparisons of polarization results obtained from cross sections produced by our codes and data obtained from EBIT measurements have been made by Beiersdorfer and coworkers at LLNL. Generally, the agreement between theory and experiment was found to be good in those cases [135,136]. As a specific example, we include comparisons between measured and calculated values of the polarization in tables 29 and 30. These results were taken from refs. [137] and [138], and expressions for computing the polarization from the magnetic sublevel cross sections are provided, for

example, in ref. [137]. Table 29 displays polarization results for He-like iron for the w, y and z lines described in subsection 4.10.1, as well as the x line, which represents the transition

$$2\,^3P_2 \rightarrow 1\,^1S_0 \quad \text{or} \quad (1s2p)_2 \rightarrow (1s^2)_0\,.$$

Values labeled "Shlyaptseva and coworkers" are predictions based on Coulomb-Born calculations from refs. [139] and [140]. The values labeled "Inal and Dubau" are based on excitation calculations using the semi-relativistic distorted-wave programs of refs. [132] and [141]. The values labeled "Present calculations" are based on calculations from our RDW excitation code. One sees that there is very good agreement between theory and measurements with the exception of the Coulomb-Born calculations. Table 30 gives similar comparisons of the predicted polarization based on calculations from our RDW excitation code and the EBIT experiments for titanium. In this case, results for the Li-like line $1s2s2p\ ^2P_{3/2} \rightarrow 1s^22s\ ^2S_{1/2}$ (called q) are also provided. The agreement is again very good, with the exception of a larger discrepancy for the w line.

Table 29
Comparison of calculated and measured values of the polarization of lines w, x, y and z at an excitation energy of 6800 eV. Results are for He-like iron.

Line	Shlyaptseva and coworkers	Inal and Dubau	Present calculations	Measurements
P_w	+0.82	+0.584	+0.599	$+0.56^{+0.17}_{-0.08}$
P_x	−0.75	−0.518	−0.515	$-0.53^{+0.05}_{-0.02}$
P_y	−0.23	−0.196	−0.192	$-0.22^{+0.05}_{-0.02}$
P_z (no cascades)	0.000	0.000	0.000	
P_z (with cascades)		−0.078	−0.074	$-0.076^{+0.007}_{-0.007}$

Table 30
Intensities (adjusted for the spectrometer response function) and inferred linear polarization of the helium-like lines w, x, y and z, and of the lithium-like line q for titanium measured with Si(220) and Si(111) crystals. Theoretical (predicted) polarization values, computed with our RDW code, are given for comparison.

Line	Ion	Si(220) (counts)	Si(111) (counts)	Predicted polarization	Measured polarization
w	Ti^{20+}	18976	1820	+0.608	$+0.43^{+0.14}_{-0.12}$
x	Ti^{20+}	3628	185	−0.519	$-0.48^{+0.06}_{-0.06}$
y	Ti^{20+}	4468	268	−0.339	$-0.33^{+0.07}_{-0.07}$
z	Ti^{20+}	6511	470	−0.106	$-0.101^{+0.014}_{-0.013}$
q	Ti^{19+}	5999	569	+0.341	$+0.40^{+0.15}_{-0.10}$

9.1.5 *Inclusion of the generalized Breit interaction in excitation between magnetic sublevels*

The need to include the generalized Breit interaction in calculating excitation cross sections between magnetic sublevels was motivated by possible EBIT experiments to be performed on highly charged ions of heavy elements at LLNL. As discussed previously in subsection 4.10.1, the generalized Breit interaction was (unexpectedly) found to provide a stronger effect on excitation cross sections between fine-structure levels for more complex ions. Here, we are specifically referring to complexity as a measure of how much fine-structure splitting occurs among the various levels under consideration. For example, the effect of the generalized Breit interaction on the $n = 1$ to 2 excitation cross sections for hydrogenic xenon ions was shown to be less than 1% for near-threshold impact energies. On the other hand, the effect was observed to be as large as 28% in the corresponding transitions for He-like xenon ions. Summing the He-like cross sections in the appropriate way to obtain hydrogenic-type results produced results that displayed a much smaller sensitivity to the generalized Breit interaction, on a par with the true hydrogenic results. This behavior suggested that the additional splitting associated with magnetic sublevels might result in cross sections that displayed an even stronger sensitivity to the generalized Breit interaction, relative to cross sections associated with the corresponding fine-structure transitions.

As described near the beginning of section 4.10, the generalized Breit interaction can be included in electron-impact excitation processes by replacing the standard Coulomb interaction with an appropriate expression for the more complete interaction. This replacement is described by eqs. (4.76) and (4.77) and, in the present case of excitation between magnetic sublevels, must be applied to the cross section in eq. (9.10) (or eq. (9.14)). As usual, the replacement is specifically performed in the reactance matrix elements of eq. (9.10). However, because the expression for the generalized Breit interaction has an imaginary part, the product of reactance matrix elements displayed in eq. (9.10), $R(\alpha, \alpha')R(\alpha_1, \alpha')$, must be replaced with the more general result $R(\alpha, \alpha')R^*(\alpha_1, \alpha')$, so that the complex conjugate of the second element is taken. In the discussion to follow, we write these complex matrix elements using the abbreviations

$$R(\alpha, \alpha') \rightarrow R = R_{\rm r} + {\rm i}R_{\rm i} \tag{9.40}$$

and

$$R^*(\alpha_1, \alpha') \rightarrow R_1^* = R_{1\rm r} - {\rm i}R_{1\rm i}\,, \tag{9.41}$$

where the subscripts r and i denote the real and imaginary parts of the appro-

priate matrix element. An evaluation of the real matrix elements involves the usual Slater integrals given in eqs. (4.17) and (4.18), plus the Breit integrals given in eqs. (4.78)–(4.82). The imaginary matrix elements involve only Breit integrals, and are obtained by the prescription that precedes eq. (4.83).

In order to obtain an expression for the cross section that is convenient and efficient to evaluate numerically, it is useful to consider the remaining complex quantities that appear in eq. (9.10). The phase factor i^{l-l_1} is actually a real quantity because $l - l_1$ is always an even integer due to restrictions on the allowed values of the impact-electron orbital angular momenta l and l_1. Thus, the only remaining complex quantity to consider is the phase factor $\exp[\mathrm{i}(\delta_\kappa - \delta_{\kappa_1})]$, which shall be abbreviated as $\exp(\mathrm{i}D)$. The product of this phase factor with the two reactance matrix elements can be rearranged as

$$\begin{aligned}
&\exp[\mathrm{i}(\delta_\kappa - \delta_{\kappa_1})]R(\alpha,\alpha')R^*(\alpha_1,\alpha') \\
&\quad\rightarrow [\cos D + \mathrm{i}\,\sin D][R_\mathrm{r} + \mathrm{i}\,R_\mathrm{i}][R_{1\mathrm{r}} - \mathrm{i}\,R_{1\mathrm{i}}] \\
&\quad= (\cos D)(R_\mathrm{r}R_{1\mathrm{r}} + R_\mathrm{i}R_{1\mathrm{i}}) + (\sin D)(R_\mathrm{r}R_{1\mathrm{i}} - R_\mathrm{i}R_{1\mathrm{r}}) \\
&\qquad+\mathrm{i}[(\sin D)(R_\mathrm{r}R_{1\mathrm{r}} + R_\mathrm{i}R_{1\mathrm{i}}) - (\cos D)(R_\mathrm{r}R_{1\mathrm{i}} - R_\mathrm{i}R_{1\mathrm{r}})]\,. \qquad (9.42)
\end{aligned}$$

Since the cross section is a real quantity, the contribution of the imaginary part contained within the square brackets of the final term in eq. (9.42) must be zero. In fact, we have verified numerically that this statement is true. Therefore, the expression that we use for including the generalized Breit interaction in the excitation cross section for transitions between magnetic sublevels, caused by collisions with a beam of longitudinally polarized electrons, has the explicit form

$$\begin{aligned}
&Q_{m_s}(\Delta_t J_t M_t - \Delta'_t J'_t M'_t) \\
&= \frac{4\pi}{k^2} \sum_{\substack{l,l_1,j,j_1 \\ l',j',m'}} \mathrm{i}^{l-l_1}[(2l+1)(2l_1+1)]^{1/2} \\
&\qquad\times C(l\tfrac{1}{2}0m_s;jm)C(l_1\tfrac{1}{2}0m_s;j_1m) \\
&\qquad\times\{\cos(\delta_\kappa - \delta_{\kappa_1})[R_\mathrm{r}(\alpha,\alpha')R_\mathrm{r}(\alpha_1,\alpha') + R_\mathrm{i}(\alpha,\alpha')R_\mathrm{i}(\alpha_1,\alpha')] \\
&\qquad\;+\sin(\delta_\kappa - \delta_{\kappa_1})[R_\mathrm{r}(\alpha,\alpha')R_\mathrm{i}(\alpha_1,\alpha') - R_\mathrm{i}(\alpha,\alpha')R_\mathrm{r}(\alpha_1,\alpha')]\}\,. \qquad (9.43)
\end{aligned}$$

Again, we stress that the subscripts r and i refer to the real and imaginary parts of the appropriate reactance matrix element, with the real parts containing both Coulomb and Breit radial integrals, while the imaginary parts contain only Breit radial integrals.

As a numerical application of eq. (9.43), we consider the case in which the electron beam is unpolarized, so that $\frac{1}{2}\sum_{m_s}$ is applied to eq. (9.43), as in eq. (9.15). In table 31, we reproduce a portion of the results of this type that were originally presented in ref. [142]. The data presented in the table are actually collision strengths, which are related to the corresponding cross sections

in the usual way (e.g. eq. (9.18)). These collision strengths pertain to transitions starting from the ground state of He-like xenon ions to specific magnetic sublevels that contain an $n = 2$ electron. Results are presented for five impact energies ranging from near-threshold to about 4.5 times the ionization energy of a given transition. As in all of the previous studies involving the generalized Breit interaction, we observe the usual behavior that the imaginary part of this interaction does not contribute much to the collision strengths. The largest effect is a few-percent change in the near-threshold collision strength for a couple of the transitions. Therefore, the imaginary part of the interaction can typically be ignored, which amounts to almost a factor of two reduction in the computing time for these types of calculations.

Further investigation of table 31 indicates the expected trend of an increase in the importance of the generalized Breit interaction with increasing impact energy. In the near-threshold region, the change associated with this interaction ranges from about 5–20%, signifying a relatively modest effect. On the other hand, for the largest impact energy, the collision strengths associated with the weaker transitions display enhancements that are greater than a factor of two. Even the stronger $J = 1$ collision strengths exhibit relatively large changes of 30–40%. We note that the effect of the generalized Breit interaction for these strong $J = 1$ transitions is to increase or decrease the collision strength for the corresponding magnetic sublevel transitions. Finally, as postulated at the beginning of this subsection, the collision strengths associated with the corresponding fine-structure transitions, obtained by summing the appropriate values over M_i' and denoted by Σ in table 31, show a decreased sensitivity to the generalized Breit interaction.

9.1.6 Resonance contributions to magnetic sublevel collision strengths

In chapter 7, we stressed the importance of resonances and described a procedure for including those contributions when considering various processes. In this subsection, we are concerned with resonances for excitation transitions between magnetic sublevels caused by impact with directional electrons. We again treat the resonance contribution as the two-step process of electron capture followed by autoionization, as symbolized in eq. (7.27). Thus, we consider electron capture by an N-electron ion, in an initial magnetic sublevel i, followed by autoionization occurring in an $(N+1)$-electron ion. The intermediate autoionizing sublevel is denoted by d and the final sublevel is denoted by f. The pertinent equations for this two-step process have been derived for magnetic sublevel transitions in ref. [143] and we now summarize those results in this subsection.

The notation used in this subsection is similar to that used in chapter 7. Specifically, the quantities pertaining to the initial sublevel i will be unprimed,

Table 31
Comparison of collision strengths for excitation of He-like xenon ions from the ground level to specific magnetic sublevels M_t' for various incident-electron energies ϵ. Values of the transition energy, ΔE, are also provided for each transition. The Σ entries are the total collision strengths obtained from summing the contribution from all possible values of M_t'. In each case, the upper, middle and lower entries represent data computed with inclusion of only the Coulomb interaction, the Coulomb plus real part of the generalized Breit interaction and the Coulomb plus the full generalized Breit interaction, respectively. $x[y] = x \times 10^y$.

Excited Level	M_t'	ΔE(Ry)	ϵ(Ry) 2400	3000	4000	6000	10000
1s2s $^3S_1$	0	2214.6	3.084[-5]	2.425[-5]	1.716[-5]	9.917[-6]	4.559[-6]
or			3.312[-5]	2.718[-5]	2.070[-5]	1.384[-5]	8.356[-6]
$(1s_{1/2}2s_{1/2})_1$			3.306[-5]	2.713[-5]	2.066[-5]	1.382[-5]	8.345[-6]
	1		3.085[-5]	2.428[-5]	1.720[-5]	9.969[-6]	4.612[-6]
			3.358[-5]	2.777[-5]	2.140[-5]	1.473[-5]	9.866[-6]
			3.376[-5]	2.791[-5]	2.150[-5]	1.478[-5]	9.886[-6]
	Σ		9.255[-5]	7.280[-5]	5.157[-5]	2.986[-5]	1.378[-5]
			1.003[-4]	8.272[-5]	6.350[-5]	4.331[-5]	2.809[-5]
			1.006[-4]	8.296[-5]	6.366[-5]	4.339[-5]	2.812[-5]
1s2p $^3P_1$	0	2220.4	1.309[-4]	1.767[-4]	2.426[-4]	3.436[-4]	4.877[-4]
or			1.245[-4]	1.584[-4]	2.027[-4]	2.568[-4]	3.016[-4]
$(1s_{1/2}2p_{1/2})_1$			1.238[-4]	1.571[-4]	2.007[-4]	2.546[-4]	2.995[-4]
	1		8.201[-5]	8.168[-5]	9.230[-5]	1.310[-4]	2.266[-4]
			9.394[-5]	9.645[-5]	1.141[-4]	1.737[-4]	3.278[-4]
			9.447[-5]	9.730[-5]	1.153[-4]	1.751[-4]	3.292[-4]
	Σ		2.949[-4]	3.400[-4]	4.272[-4]	6.056[-4]	9.410[-4]
			3.124[-4]	3.513[-4]	4.310[-4]	6.042[-4]	9.573[-4]
			3.127[-4]	3.517[-4]	4.314[-4]	6.047[-4]	9.579[-4]
1s2p $^1P_1$	0	2251.5	2.785[-4]	3.926[-4]	5.540[-4]	7.946[-4]	1.136[-3]
or			2.588[-4]	3.585[-4]	4.897[-4]	6.550[-4]	8.123[-4]
$(1s_{1/2}2p_{3/2})_1$			2.545[-4]	3.529[-4]	4.829[-4]	6.474[-4]	8.047[-4]
	1		8.419[-5]	1.096[-4]	1.589[-4]	2.690[-4]	5.012[-4]
			7.737[-5]	1.069[-4]	1.668[-4]	3.106[-4]	6.425[-4]
			7.984[-5]	1.101[-4]	1.706[-4]	3.150[-4]	6.470[-4]
	Σ		4.469[-4]	6.119[-4]	8.717[-4]	1.333[-3]	2.138[-3]
			4.135[-4]	5.723[-4]	8.233[-4]	1.276[-3]	2.097[-3]
			4.142[-4]	5.731[-4]	8.241[-4]	1.277[-3]	2.099[-3]
1s2p $^3P_2$	0	2248.9	6.709[-5]	4.724[-5]	2.874[-5]	1.317[-5]	4.392[-6]
or			8.316[-5]	6.155[-5]	4.058[-5]	2.161[-5]	9.421[-6]
$(1s_{1/2}2p_{3/2})_2$			8.248[-5]	6.108[-5]	4.031[-5]	2.150[-5]	9.386[-6]
	1		5.507[-5]	3.876[-5]	2.364[-5]	1.096[-5]	3.777[-6]
			5.873[-5]	4.272[-5]	2.755[-5]	1.446[-5]	6.836[-6]
			5.841[-5]	4.250[-5]	2.743[-5]	1.442[-5]	6.827[-6]
	2		1.866[-5]	1.298[-5]	8.078[-6]	4.180[-6]	1.867[-6]
			1.936[-5]	1.409[-5]	9.604[-6]	6.242[-6]	4.986[-6]
			2.007[-5]	1.458[-5]	9.879[-6]	6.352[-6]	5.015[-6]
	Σ		2.146[-4]	1.507[-4]	9.219[-5]	4.345[-5]	1.568[-5]
			2.393[-4]	1.752[-4]	1.149[-4]	6.302[-5]	3.307[-5]
			2.394[-4]	1.752[-4]	1.149[-4]	6.304[-5]	3.307[-5]

or denoted with a subscript t, those pertaining to the doubly excited sublevel d will have a subscript d, and those pertaining to the final sublevel f will be primed, or primed with a subscript t. First we treat the capture of an electron from a directional beam. In doing so, we start with the scattering amplitude for electron capture (see eq. (2.1) in ref. [143]),

$$B^{m_s} = \frac{2\pi^{3/2}}{k} \sum_{l,m_l,j,m} \mathrm{i}^{l+1} \exp(\mathrm{i}\delta_\kappa) Y^*_{lm_l}(\hat{\boldsymbol{k}}) C(l\tfrac{1}{2}m_l m_s; jm) T(\alpha, \alpha_d), \tag{9.44}$$

which was obtained by modifying the scattering amplitude for electron-impact excitation, i.e. eq. (9.1) of the present work. (See ref. [143] for more detail.) In eq. (9.44), $\hat{\boldsymbol{k}}$ is the direction of the incident electron, and α and α_d are given by

$$\alpha = \Delta_t J_t M_t k l j m, \qquad \alpha_d = \Delta_d J_d M_d \,. \tag{9.45}$$

As in subsection 9.1.1, we choose $\hat{\boldsymbol{k}}$ to be in the direction of the z axis so that eq. (9.7) applies. Also, we express the $\boldsymbol{T}$ matrix in terms of the $\boldsymbol{R}$ matrix using eq. (4.4). Then we transform the $\boldsymbol{R}$ matrix elements from the uncoupled representation to the coupled representation according to

$$R(\alpha, \alpha_d) = C(J_t j M_t m; J_d M_d) R(\gamma, \gamma_d), \tag{9.46}$$

where γ and γ_d are given by

$$\gamma = \Delta_t J_t k l j J_d M_d, \qquad \gamma_d = \alpha_d \,. \tag{9.47}$$

(We note that in eq. (9.46), unlike eq. (9.12) or eq. (9.13), there is no summation required because J_d and M_d are fixed in the sense that electron capture to a specific doubly excited sublevel is being considered.) Thus, we obtain

$$\begin{aligned} B^{m_s} = \frac{2\pi}{k} \sum_{l,j,m} & \mathrm{i}^l (2l+1)^{1/2} \exp(\mathrm{i}\delta_\kappa) C(l\tfrac{1}{2}0 m_s; jm) \\ & \times C(J_t j M_t m; J_d M_d) R(\gamma, \gamma_d), \end{aligned} \tag{9.48}$$

where $m = m_s$ because $m_l = 0$.

The capture cross section for a beam of unpolarized electrons is given by

$$Q^{\mathrm{cap}}(\Delta_t J_t M_t - \Delta_d J_d M_d)$$

$$
\begin{aligned}
&= \tfrac{1}{2} \sum_{m_s} |B^{m_s}|^2 \, \delta(\epsilon - E_{id}) \\
&= \frac{2\pi^2}{k^2} \sum_{\substack{l,l_1, \\ j,j_1,m_s}} \mathrm{i}^{l-l_1} [(2l+1)(2l_1+1)]^{1/2} \\
&\quad \times \exp[\mathrm{i}(\delta_\kappa - \delta_{\kappa_1})] C(l\tfrac{1}{2}0m_s; jm) C(l_1\tfrac{1}{2}0m_s; j_1 m) \\
&\quad \times C(J_t j M_t m; J_d M_d) C(J_t j_1 M_t m; J_d M_d) \\
&\quad \times R(\gamma, \gamma_d) R(\gamma_1, \gamma_d) \delta(\epsilon - E_{id}) \ , \qquad (9.49)
\end{aligned}
$$

where γ_1 differs from γ only in that l_1 and j_1 replace l and j, ϵ is the kinetic energy of the incident electron and E_{id} is the transition energy.

As a check on eq. (9.49), we use eq. (C.13c) of Messiah [7],

$$
\begin{aligned}
&C(J_t j M_t m; J_d M_d) \\
&\qquad = (-1)^{j - J_d - M_t} \left(\frac{2J_d + 1}{2j+1} \right)^{1/2} C(J_t J_d \ -M_t M_d; jm) \, , \quad (9.50)
\end{aligned}
$$

along with the analogous expression applied to $C(J_t j_1 M_t m; J_d M_d)$. Then, we operate with $1/(2J_t+1) \sum_{M_t, M_d}$ on eq. (9.49), keeping in mind that the $\boldsymbol{R}$ matrix elements expressed in the coupled representation are independent of M_t and M_d; that is, we average over initial magnetic sublevels and sum over final magnetic sublevels, which eliminates the last two Clebsch-Gordan coefficients and gives a factor of $\delta_{jj_1}(2J_d+1)/[(2J_t+1)(2j+1)]$. Then, after summing over j_1, we apply eq. (C.13b) of Messiah to the remaining two Clebsch-Gordan coefficients and perform the sum over $m_s = m$. This procedure eliminates those two Clebsch-Gordan coefficients and yields a factor of $[(2j+1)/(2l+1)]\delta_{ll_1}$. Finally, after summing over l_1, we obtain an expression for the capture cross section associated with a transition between fine-structure levels,

$$
Q^{\mathrm{cap}}(\Delta_t J_t - \Delta_d J_d) = \frac{2\pi^2}{k^2} \, \frac{2J_d + 1}{2J_t + 1} \sum_{l,j} |R(\gamma, \gamma_d)|^2 \, \delta(\epsilon - E_{id}) \, . \qquad (9.51)
$$

This result is seen to be equivalent to the expression given by eqs. (7.1) and (7.3), after taking into account the relationship between the electron-capture cross section and collision strength given by eq. (7.7).

We next consider an appropriate expression for the autoionization rate for the sublevel transition denoted by $d \rightarrow f$. As usual, this rate is related to the capture collision strength for the inverse process via the appropriate form of eq. (7.12). We emphasize here that eq. (9.49) applies to the capture of directional electrons. It does not apply to the capture of randomly oriented electrons because the impact electron need not be moving in the z direction. Thus, eq. (9.49) can not be used to obtain autoionization rates for the case in

which ejected electrons are randomly oriented. For capture or autoionization involving randomly oriented electrons, a different treatment is required. We first consider the cross section for the electron-capture transition $f \rightarrow d$ and subsequently obtain an expression for the autoionization rate for the inverse transition $d \rightarrow f$.

Thus, we begin by considering an amplitude that is analogous to the expression given in eq. (9.44), but for the specific sublevel transition $\Delta_t' J_t' M_t' - \Delta_d J_d M_d$. In this case, an expression that is analogous to eq. (9.7) for l' and m_l' can not be used because $m_l' = 0$ is not always true. Using the relation between the $\boldsymbol{T}$ and $\boldsymbol{R}$ matrices given in eq. (4.4), and making a similar transformation on the $\boldsymbol{R}$ matrix elements from the uncoupled representation, $R(\alpha', \alpha_d)$, to the coupled representation, $R(\gamma', \gamma_d)$, where

$$\alpha' = \Delta_t' J_t' M_t' k' l' j' m' \tag{9.52}$$

and

$$\gamma' = \Delta_t' J_t' k' l' j' J_d M_d \,, \tag{9.53}$$

we obtain the scattering amplitude

$$B^{m_s'} = \frac{4\pi^{3/2}}{k'} \sum_{l', m_l', j', m'} \mathrm{i}^{l'} \exp(\mathrm{i}\delta_{\kappa'}) Y_{l' m_l'}^*(\hat{\boldsymbol{k}}') C(l' \tfrac{1}{2} m_l' m_s'; j' m') \times C(J_t' j' M_t' m'; J_d M_d) R(\gamma', \gamma_d). \tag{9.54}$$

For capture of randomly oriented electrons, one must average over the electron direction $\hat{\boldsymbol{k}}'$. Specifically, the amplitude above should be substituted in the first expression for the cross section that appears in eq. (9.49) and then an integration over $\hat{\boldsymbol{k}}'$ combined with a division by 4π is performed. The resulting expression for the capture cross section is

$$Q^{\mathrm{cap}}(\Delta_t' J_t' M_t' - \Delta_d J_d M_d) = \frac{1}{8\pi} \sum_{m_s'} \int |B^{m_s'}|^2 \, \mathrm{d}\hat{\boldsymbol{k}}' \; \delta(\epsilon' - E_{fd}) \,. \tag{9.55}$$

Using the orthonormality relation

$$\frac{1}{4\pi} \int Y_{l' m_l'}^*(\hat{\boldsymbol{k}}') Y_{l_1' m_{l_1}'}(\hat{\boldsymbol{k}}') \, \mathrm{d}\hat{\boldsymbol{k}}' = \delta_{m_l' m_{l_1}'} \delta_{l' l_1'} / 4\pi \,, \tag{9.56}$$

and performing the summations over m_{l_1}' and l_1', we have

$$Q^{\rm cap}(\Delta'_t J'_t M'_t - \Delta_d J_d M_d)$$
$$= \frac{2\pi^2}{(k')^2} \sum_{\substack{l',m'_{l'},j',m' \\ j'_1,m'_1,m'_s}} \exp[\mathrm{i}(\delta_{\kappa'} - \delta_{\kappa'_1})]$$
$$\times C(l'\tfrac{1}{2} m'_l m'_s; j' m') C(l'\tfrac{1}{2} m'_l m'_s; j'_1 m'_1)$$
$$\times C(J'_t j' M'_t m'; J_d M_d) C(J'_t j'_1 M'_t m'_1; J_d M_d)$$
$$\times R(\gamma', \gamma_d) R(\gamma'_1, \gamma_d) \delta(\epsilon' - E_{fd}) \,, \qquad (9.57)$$

where γ'_1 differs from γ' only in that j'_1 replaces j' and similarly κ'_1 differs from κ' only in that j'_1 replaces j'. Next, the summations over m'_l and m'_s are performed using

$$\sum_{m'_s, m'_l} C(l'\tfrac{1}{2} m'_l m'_s; j' m') C(l'\tfrac{1}{2} m'_l m'_s; j'_1 m'_1) = \delta_{j' j'_1} \delta_{m' m'_1} .$$

Then the summations over m'_1 and j'_1 are performed to obtain the final result

$$Q^{\rm cap}(\Delta'_t J'_t M'_t - \Delta_d J_d M_d)$$
$$= \frac{2\pi^2}{(k')^2} \sum_{l',j',m'} C(J'_t j' M'_t m'; J_d M_d)^2 \left| R(\gamma', \gamma_d) \right|^2 \delta(\epsilon' - E_{fd}) \,. \qquad (9.58)$$

Using eq. (7.7), with the label i replaced by f, ϵ and k replaced by the corresponding primed values, and noting that $g_f = 1$ for any magnetic sublevel, we obtain an expression for the collision strength quantity $\widetilde{\Omega}^{\rm cap}$ associated with the capture of randomly oriented electrons that can be written as

$$\widetilde{\Omega}^{\rm cap}(\Delta'_t J'_t M'_t - \Delta_d J_d M_d)$$
$$= 2\pi \sum_{l',j',m'} C(J'_t j' M'_t m'; J_d M_d)^2 \left| R(\gamma', \gamma_d) \right|^2 . \qquad (9.59)$$

As a check on eq. (9.59), one can perform additional summations over M'_t and M_d to see if the correct expression for the fine-structure expression is obtained. In this case, the sums over m' and M'_t can be used to eliminate the square of the Clebsch-Gordan coefficient, and then the sum over M_d yields a factor of $(2J_d + 1)$. The resulting expression,

$$\widetilde{\Omega}^{\rm cap}(\Delta'_t J'_t - \Delta_d J_d) = \sum_{M'_t, M_d} \widetilde{\Omega}^{\rm cap}(\Delta'_t J'_t M'_t - \Delta_d J_d M_d)$$
$$= 2\pi (2J_d + 1) \sum_{l',j'} \left| R(\gamma', \gamma_d) \right|^2 , \qquad (9.60)$$

applies to the collision strength for transitions between fine-structure levels, which is identical in form to eq. (7.3).

In order to obtain the autoionization rate for the transition $d \rightarrow f$, eq. (7.12) can be applied to the present case of transitions between magnetic sublevels. Using eq. (9.59), which describes the inverse process of electron capture, and also recalling that the statistical weight $g_d = 1$ for the case of magnetic sublevels, we obtain an expression for the autoionization rate according to

$$A^{\mathrm{a}}(\Delta_d J_d M_d - \Delta'_t J'_t M'_t) = \frac{2}{\hbar} \sum_{l',j',m'} C(J'_t j' M'_t m'; J_d M_d)^2 \, |R(\gamma', \gamma_d)|^2. \quad (9.61)$$

The above discussion provides all of the pieces that are necessary to obtain the resonance contribution to the total cross section for excitation between magnetic sublevels. The process can again be symbolically represented by eq. (7.27), except that all labels representing fine-structure levels in that expression now denote magnetic sublevels. The total cross section, in analogy to eq. (7.28) for the collision strength, can be written as

$$Q_{if}^{\mathrm{total}} = Q_{if} + Q_{if}^{\mathrm{res}}, \quad (9.62)$$

where Q_{if} is the usual background (or direct) excitation cross section, given by eq. (9.15) for an unpolarized beam, or by eq. (9.14) for a longitudinally polarized electron beam, and the resonance contribution can be written as

$$Q_{if}^{\mathrm{res}} = \sum_d Q_{id}^{\mathrm{cap}} B_{df}. \quad (9.63)$$

The branching ratio is given by (see eq. (7.30))

$$B_{df} = \frac{A_{df}^{\mathrm{a}}}{\sum_m A_{dm}^{\mathrm{a}} + \sum_k A_{dk}^{\mathrm{r}}}, \quad (9.64)$$

where the denominator takes into account the possibility that, instead of autoionizing to the final magnetic sublevel f of the transition under consideration, the doubly excited sublevel d autoionizes or radiatively decays to some other sublevel. In applying eq. (9.64) to eq. (9.63), the autoionization rates A_{df}^{a} and A_{dm}^{a} are given by the appropriate form of eq. (9.61). However, the summation of the A_{dm}^{a} values in the denominator of eq. (9.64) can be further simplified. Since the summation of A_{dm}^{a} implicitly includes a summation over M'_t, that summation plus the explicit summation over the ejected-electron quantum number m' can be used to eliminate the Clebsch-Gordan coefficient that appears in eq. (9.61). Therefore, in this case, one can replace the sum of magnetic sublevel autoionization rates with the corresponding sum of fine-structure autoionization rates because

$$A^{\rm a}(\Delta_d J_d - \Delta'_t J'_t) \equiv \frac{1}{2J_d+1} \sum_{M_d, M'_t} A^{\rm a}(\Delta_d J_d M_d - \Delta'_t J'_t M'_t)$$
$$= \frac{2}{\hbar} \sum_{l',j'} |R(\gamma', \gamma_d)|^2$$
$$= \sum_{M'_t} A^{\rm a}(\Delta_d J_d M_d - \Delta'_t J'_t M'_t)\,. \qquad (9.65)$$

Here, the second line is just the standard fine-structure expression of the form given in eq. (7.13), while the connection between the second and third lines becomes evident after summing eq. (9.61) over M'_t to eliminate the Clebsch-Gordan coefficient, as mentioned above. Thus, we have shown that the extra summation over M_d in the formal definition on the right-hand side of eq. (9.65) simply produces a factor of $(2J_d+1)$, which cancels the $(2J_d+1)^{-1}$ factor. (A corollary of this relationship is that the values of $A^{\rm a}$ on the right-hand side of the equation must be independent of the quantum number M_d.) Similar results apply for the summation of the $A^{\rm r}_{dk}$ values in eq. (9.64), and so only radiative decay rates between fine-structure levels need to be considered in this particular application.

In ref. [143], some calculated results were presented in graphical form for the total collision strengths, which included both the background and resonance contributions, for He-like and Be-like oxygen and iron. In making those plots, the $\delta(\epsilon - E_{id})$ factor in eq. (9.49) was replaced with a Lorentz profile, as in eq. (7.31). This work dealt with spin-change transitions for which the resonance contributions are generally more important. Here, we provide total collision strengths involving transitions from the ground level of He-like iron in figure 7, which is a reproduction of fig. 5 from ref. [143]. In this case, resonance contributions from the doubly excited levels arising from the $1s3l3l'$ configurations are included for transitions between the magnetic sublevels associated with the two transitions

$$1\,^1{\rm S}_0 - 2\,^3{\rm S}_1 \quad \text{or} \quad (1{\rm s}^2)_0 - (1{\rm s}2{\rm s})_1$$

and

$$1\,^1{\rm S}_0 - 2\,^3{\rm P}_1 \quad \text{or} \quad (1{\rm s}^2)_0 - (1{\rm s}2{\rm p}^*)_1\,.$$

As another numerical example, we provide in table 32 a comparison of our RDW excitation rate coefficients with the semi-relativistic results computed by Inal and Dubau [141] for certain transitions from the ground level of He-like iron. As mentioned in section 4.14, the expression used to compute the rate coefficient for a general transition denoted by $i \rightarrow f$ has the general form

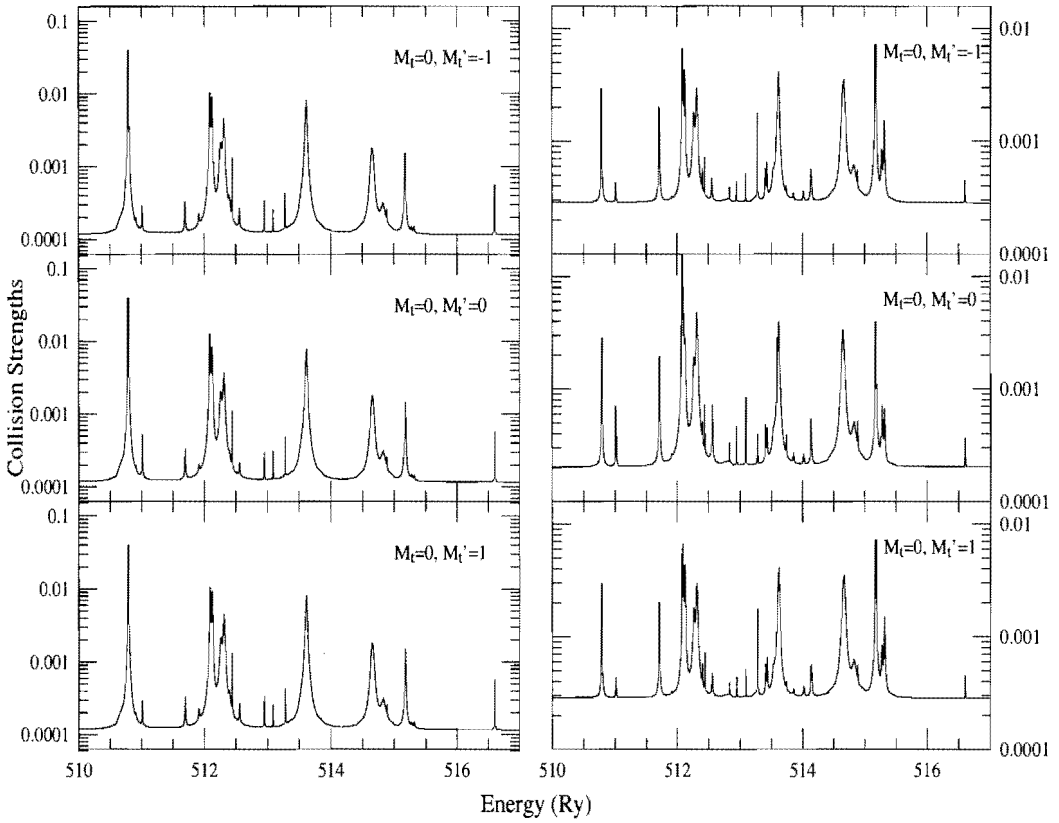

Fig. 7. Total RDW collision strengths as a function of impact energy for transitions between the magnetic sublevels of the $1\,^1S_0 - 2\,^3S_1$ or $(1s^2)_0 - (1s2s)_1$ transition (the left panels) and the $1\,^1S_0 - 2\,^3P_1$ or $(1s^2)_0 - (1s2p^*)_1$ transition (the right panels), in He-like iron. Only the resonances associated with the doubly excited levels involving the $1s3l3l'$ configurations are included for the impact-electron energy range considered.

$$C_{if} = \langle vQ_{if} \rangle \,. \tag{9.66}$$

In order to obtain RDW results similar to those provided in ref. [141], we averaged the collision strength for both the background (or direct) and resonance contributions over the resonance region, assuming a free-electron energy distribution that was uniform over the $1s3l3l'$ resonance region, and zero outside of this region. For $Z \leq 26$ the use of non-relativistic relations between the quantities v, k and ϵ is a good approximation. Making this choice, in combination with inserting numerical values for the physical constants and using a mean value for the electron energy in the narrow resonance region, yields a practical expression for the rate coefficient for these transitions of interest in He-like iron. The result is

Table 32
Comparison of direct and resonance contributions, $C_{\rm dir}$ and $C_{\rm res}$, respectively, to the rate coefficients (in units of $10^{-13}{\rm cm}^3/{\rm s}$) for excitation from the ground level to magnetic sublevels of the $n = 2$ levels in He-like iron. Superscripts RDW and ID indicate present RDW results and semi-relativistic results from ref. [141], respectively. The free-electron energy distribution was assumed to be constant over the $1s3l3l'$ resonance region, and zero otherwise.

	$1\,^1S_0 - 2\,^3P_2$		$1\,^1S_0 - 2\,^1P_1$		$1\,^1S_0 - 2\,^3P_1$		$1\,^1S_0 - 2\,^3S_1$	
	$M_t' = 1$	$M_t' = 2$	$M_t' = 0$	$M_t' = 1$	$M_t' = 0$	$M_t' = 1$	$M_t' = 0$	$M_t' = 1$
$C_{\rm dir}^{\rm RDW}$	2.22	0.707	12.7	3.19	1.72	2.41	0.985	0.985
$C_{\rm dir}^{\rm ID}$	2.31	0.726	12.7	3.21	1.70	2.39	0.959	0.959
$C_{\rm res}^{\rm RDW}$	2.51	1.107	2.71	1.67	2.15	1.94	2.888	2.905
$C_{\rm res}^{\rm ID}$	2.26	0.987	2.82	1.42	1.77	1.86	2.851	2.864

$$C_{if} = \frac{8.493^{-10}}{g_i}\langle\Omega_{if}\rangle \quad {\rm cm}^3/{\rm s}\ , \tag{9.67}$$

where

$$\langle\Omega_{if}\rangle = \frac{1}{\epsilon_b - \epsilon_a}\int_{\epsilon_a}^{\epsilon_b}\Omega_{if}\,{\rm d}\epsilon\,. \tag{9.68}$$

Here, $\epsilon_b - \epsilon_a$ covers the $1s3l3l'$ resonance region, and $g_i = 1$ for the He-like ground level currently under consideration.

The data listed in table 32 provide a comparison of our results (labeled RDW) with those from table IV of ref. [141], computed by Inal and Dubau (labeled ID). Results are presented for both the direct contribution, $C_{\rm dir}$, and the $1s3l3l'$ resonance contribution, $C_{\rm res}$, to the rate coefficient for excitation from the $1s^2\,^1S_0$ ground level of He-like iron to various magnetic sublevels. One sees that the agreement is generally good for the direct contribution, but is somewhat worse for the resonance contribution. The largest discrepancies are 21% and 18% for excitation to the $M_t' = 0$ sublevel of the $2\,^3P_1$ level and excitation to the $M_t' = 1$ sublevel of the $2\,^1P_1$ level, respectively.

9.2 Transitions between magnetic sublevels due to electron-impact ionization

In this section, the fully relativistic treatment of electron-impact excitation that was described in section 9.1 is extended to the case of ionization. Ionization between specific magnetic sublevels by impact with either a longitudinally polarized or unpolarized electron beam, as described in ref. [144], is considered.

We consider an ionizing transition from the magnetic sublevel M_t of the level $\Delta_t J_t$ to the magnetic sublevel M_t'' of the level $\Delta_t'' J_t''$. By analogy with the scattering amplitude for excitation displayed in eq. (9.1), we can define an ionization scattering amplitude $B^{m_s}_{m_s' m_s''}$ for the scattering of an electron with spin magnetic quantum number m_s, wave number k and direction $\hat{\boldsymbol{k}}$ into direction $\hat{\boldsymbol{k}}'$ with wave number k' and final spin magnetic quantum number m_s'. This scattering is accompanied by a change in the magnetic sublevel of the target ion from $\Delta_t J_t M_t$ to $\Delta_t'' J_t'' M_t''$ with one less bound electron, which has been ejected into direction $\hat{\boldsymbol{k}}''$ with wave number k'' and spin magnetic quantum number m_s''. The scattering amplitude for this process can be written as

$$
\begin{aligned}
B^{m_s}_{m_s' m_s''} = \frac{2\pi^{1/2}}{k} \sum_{\substack{l,m_l,j,m \\ l',m_l',j',m' \\ l'',m_l'',j'',m''}} & \mathrm{i}^{l-l'-l''} \exp[\mathrm{i}(\delta_\kappa + \delta_{\kappa'} + \delta_{\kappa''})] \\
& \times Y^*_{l m_l}(\hat{\boldsymbol{k}}) Y_{l' m_l'}(\hat{\boldsymbol{k}}') Y_{l'' m_l''}(\hat{\boldsymbol{k}}'') \\
& \times C(l \tfrac{1}{2} m_l m_s; j m) C(l' \tfrac{1}{2} m_l' m_s'; j' m') \\
& \times C(l'' \tfrac{1}{2} m_l'' m_s''; j'' m'') T(\alpha, \alpha') \,, \qquad (9.69)
\end{aligned}
$$

where the quantity

$$
Y_{l'' m_l''}(\hat{\boldsymbol{k}}'')\, \mathrm{i}^{-l''} \exp(\mathrm{i}\, \delta_{\kappa''})\, C(l'' \tfrac{1}{2} m_l'' m_s''; j'' m'')
$$

pertains to the ejected electron, and the extra factor of $\pi^{-1/2}$ relative to eq. (9.1) is due to the different normalization of the extra (ejected) free electron (see eq. (5.4) for the continuum normalization), which has replaced the final active bound electron. The notation for the uncoupled states α and α' is given by

$$
\alpha = \Delta_t J_t M_t k l j m, \quad \alpha' = \Delta_t'' J_t'' M_t'' k'' l'' j'' m'' k' l' j' m' \,, \qquad (9.70)
$$

which is very similar to eq. (9.2) for excitation.

The integrated cross section for ionization from one specific sublevel to a final specific sublevel by directional electrons with spin magnetic quantum number m_s can be obtained from the scattering amplitude according to the relation

$$
Q^{m_s}(\Delta_t J_t M_t - \Delta_t'' J_t'' M_t'') = \sum_{m_s', m_s''} \int_0^{(\epsilon - I)/2} \mathrm{d}\epsilon'' \int \mathrm{d}\hat{\boldsymbol{k}}' \int \mathrm{d}\hat{\boldsymbol{k}}'' |B^{m_s}_{m_s' m_s''}|^2 \,, \qquad (9.71)
$$

assuming one is not interested in the values of m_s' and m_s'' associated with the scattered and ejected electrons, respectively. In the above expression, ϵ and ϵ'' are the kinetic energies of the incident and ejected electrons, respectively, and I is the ionization energy. In evaluating eq. (9.71), we again choose $\hat{\boldsymbol{k}}$ to be in the z direction (i.e. longitudinal polarization), as in subsection 9.1.1, so that eqs. (9.7)–(9.9) apply. Expressions similar to eqs. (9.8) and (9.9) also apply to the analogous double-primed quantities that describe the ejected electron. Then, using eq. (4.4) and making similar manipulations as in section 9.1, we obtain an expression for the ionization cross section in terms of the reactance matrix elements according to

$$\begin{aligned} Q^{m_s}(\Delta_t J_t M_t - \Delta_t'' J_t'' M_t'') \\ = \frac{4}{k^2} \sum_{\substack{l,l_1,j,j_1 \\ l',j',m' \\ l'',j'',m''}} & \mathrm{i}^{l-l_1}[(2l+1)(2l_1+1)]^{1/2} \exp[\mathrm{i}(\delta_\kappa - \delta_{\kappa_1})] \\ & \times C(l\tfrac{1}{2}0m_s; jm) C(l_1\tfrac{1}{2}0m_s; j_1 m) \\ & \times \int_0^{(\epsilon-I)/2} \mathrm{d}\epsilon'' R(\alpha, \alpha') R(\alpha_1, \alpha') \,, \end{aligned} \tag{9.72}$$

where α_1 differs from α in that l_1 and j_1 replace l and j, respectively, and $m = m_s$ due to one of the standard properties of the Clebsch-Gordan coefficient.

The matrix elements in the uncoupled representation in eq. (9.72) can be written in terms of the matrix elements in the fully coupled representation by performing a transformation analogous to eq. (9.12), i.e.

$$\begin{aligned} R(\alpha, \alpha') = \sum_{J,M,J_t',M_t'} & C(J_t j M_t m; JM) C(J_t' j' M_t' m'; JM) \\ & \times C(J_t'' j'' M_t'' m''; J_t' M_t') R(\gamma, \gamma') \,, \end{aligned} \tag{9.73}$$

where γ and γ' are given by

$$\gamma = \Delta_t J_t k l j \; JM \text{ and } \gamma' = \Delta_t'' J_t'' k'' l'' j'' J_t' k' l' j' \; JM \,. \tag{9.74}$$

One could express the cross section in eq. (9.72) in terms of matrix elements in the fully coupled representation by applying the appropriate forms of eq. (9.73). However, as noted in subsection 9.1.1, it is computationally more efficient to calculate reactance matrix elements in the uncoupled representation, using eq. (9.73) in the present case, and then using eq. (9.72) to calculate the cross section for ionization by impact with a beam of longitudinally polarized electrons. In fact, the efficiency is greater for the present case of ionization because there are many more matrix elements to evaluate and many more summations to perform than in the case of excitation.

In most applications, the target ions are initially randomly oriented so the cross section of interest is given by averaging eq. (9.72) over initial target-ion sublevels. The corresponding cross section is given by

$$Q^{m_s}(\Delta_t J_t - \Delta_t'' J_t'' M_t'') = \frac{1}{2J_t + 1} \sum_{M_t} Q^{m_s}(\Delta_t J_t M_t - \Delta_t'' J_t'' M_t'') \,. \qquad (9.75)$$

If the ionization is also due to impact with unpolarized directional electrons, then the cross section of interest is

$$Q(\Delta_t J_t - \Delta_t'' J_t'' M_t'') = \frac{1}{2(2J_t + 1)} \sum_{m_s, M_t} Q^{m_s}(\Delta_t J_t M_t - \Delta_t'' J_t'' M_t'') \,. \quad (9.76)$$

Finally, if one is not interested in a particular, final magnetic sublevel M_t'', then the ionization cross section for transitions between fine-structure levels is obtained by further summing eq. (9.76) over the final ion sublevels M_t'' and is given by

$$Q(\Delta_t J_t - \Delta_t'' J_t'') = \frac{1}{2(2J_t + 1)} \sum_{m_s, M_t, M_t''} Q^{m_s}(\Delta_t J_t M_t - \Delta_t'' J_t'' M_t'') \,. \quad (9.77)$$

It is easily verified that, by applying eq. (9.73) to eq. (9.72) and using the properties of the Clebsch-Gordan coefficients, eq. (9.77) can be expressed in the form

$$\begin{aligned} &Q(\Delta_t J_t - \Delta_t'' J_t'') \\ &\qquad = \frac{2}{k^2(2J_t + 1)} \sum_J (2J + 1) \sum_{\substack{l, j, l', j' \\ J_t', l'', j''}} \int_0^{(\epsilon - I)/2} \mathrm{d}\epsilon'' \, |R(\gamma, \gamma')|^2 \,. \end{aligned} \quad (9.78)$$

One sees that eq. (9.78) agrees with the expression for the ionization cross section associated with transitions between fine-structure levels given by eq. (5.5), which provides an important check on the fundamental expression displayed in eq. (9.72).

As with the excitation cross sections described in the previous section, ionization cross sections computed with the RDW formalism described in this section have been used for a variety of applications. For example, Inal et al. have applied cross sections for ionization to specific magnetic sublevels, which were computed with the procedures described herein, to study the effect of ionization on the degree of polarization for various spectral lines from different

ions. Examples of this type include predictions of the degree of linear polarization of Ne-like Se lines [144] and a study of the effect of inner-shell ionization on the circular polarization of the Fe^{24+} $(1s2s)_1 \rightarrow 1s^2$ line produced by collisions with a longitudinally polarized electron beam [145]. The latter study also provides numerical examples for which the generalized Breit interaction was included when computing excitation cross sections for magnetic sublevel transitions, as previously discussed in subsection 9.1.5. The reader is referred to the respective publications for further details.

10 Concluding remarks

A complete review has been provided of the fully relativistic methods and procedures that we have developed and published over the past two decades. The ultimate goal of this work has been to provide high quality atomic physics data for applications in plasma modeling. Many of the methods described above have been implemented within the relativistic capabilities of the Los Alamos suite of atomic physics codes and applied to a variety of plasma modeling applications (e.g. refs. [102] and [103]). We hope that this review will offer some useful assistance to future research efforts in fundamental atomic physics, astrophysics, fusion energy, the modeling of high-temperature plasmas and other related fields.

Acknowledgements

While a research project of this breadth involves interactions with a large number of people, we would like to explicitly acknowledge contributions from the following colleagues: R.D. Cowan, I.P. Grant, C. Bottcher, R.E.H. Clark, A.K. Mohanty, M.K. Inal, M.H. Chen, P. Beiersdorfer and K.J. Reed. Funding is gratefully acknowledged from the following sources: Department of Energy (Office of Fusion Energy), Lawrence Livermore National Laboratory, the former Innovative Science and Technology Office of the Strategic Defense Initiative Organization and the ADAS Project. We would also like to thank J. Colgan and D.P. Kilcrease for a critical reading of this manuscript. A portion of this work was performed under the auspices of the U.S. Department of Energy through the Los Alamos National Laboratory.

References

[1] D.H. Sampson, H.L. Zhang, A.K. Mohanty and R.E.H. Clark, Phys. Rev. A40 (1989) 604.

[2] H.A. Bethe and E.E. Salpeter, Quantum Mechanics of One- and Two-Electron Systems, Springer-Verlag, Berlin, 1957.

[3] M.E. Rose, Relativistic Electron Theory, Wiley, New York, 1961.

[4] I.P. Grant, Relativistic Quantum Theory of Atoms and Molecules, Springer, New York, 2007.

[5] W.R. Johnson, Atomic Structure Theory: Lectures on Atomic Physics, Springer-Verlag, Berlin, 2007.

[6] I.P. Grant, B.J. McKenzie, P.H. Norrington, D.F. Mayers and N.C. Pyper, Comput. Phys. Commun. 21 (1980) 207.

[7] A. Messiah, Quantum Mechanics, vol. II, Amsterdam, North-Holland, 1962.

[8] R.D. Cowan, The Theory of Atomic Structure and Spectra, University of California Press, Berkeley, 1981.

[9] J.C. Slater, Phys. Rev. 81 (1951) 385.

[10] W. Kohn and L.J. Sham, Phys. Rev. 140 (1965) A1133.

[11] B.J. McKenzie, I.P. Grant and P.H. Norrington, Comput. Phys. Commun. 21 (1980) 233.

[12] P. Beiersdorfer et al., Phys. Rev. A37 (1988) 4153.

[13] G. Breit, Phys. Rev. 34 (1929) 553.

[14] G. Breit, Phys. Rev. 36 (1930) 383.

[15] G. Breit, Phys. Rev. 39 (1932) 616.

[16] C. Møller, Ann. Phys. (Leipzig) 14 (1932) 531.

[17] J.B. Mann and W.R. Johnson, Phys. Rev. A4 (1971) 41.

[18] I.P. Grant, Adv. Phys. 19 (1970) 747.

[19] I.P. Grant and N.C. Pyper, J. Phys. B9 (1976) 761.

[20] I.P. Grant and B.J. McKenzie, J. Phys. B13 (1980) 2671.

[21] J. Hata and I.P. Grant, J. Phys. B17 (1984) L107.

[22] L.W. Fullerton and G.A. Rinker, Phys. Rev. A13 (1976) 1283.

[23] P.J. Mohr, Ann. Phys. (N.Y.) 88 (1974) 52.

[24] P.J. Mohr, Phys. Rev. Lett. 34 (1975) 1050.

[25] K.G. Dyall, I.P. Grant, C.T. Johnson, F.A. Parpia and E.P. Plummer, Comput. Phys. Commun. 55 (1989) 425.

[26] M.H. Chen, B. Crasemann, M. Aoyagi, K.-N. Huang and H. Mark, At. Data Nucl. Data Tables 26 (1981) 561.

[27] M.S. Pindzola, D.C. Griffin and C. Bottcher, in: F. Brouillard (Ed.), Atomic Processes in Electron-Ion and Ion-Ion Collisions, vol. 145 of NATO Advanced Studies Institute Series B: Physics, Plenum, New York, 1986, p. 75.

[28] O. Peyrusse, J. Phys. B32 (1999) 683.

[29] A. Bar-Shalom, J. Oreg, M. Klapisch and T. Lehecka, Phys. Rev. E59, (1999) 3512.

[30] D.H. Sampson, Phys. Rev. A34 (1986) 986.

[31] A. Bar-Shalom, M. Klapisch and J. Oreg, Phys. Rev. A38 (1988) 1773.

[32] D.H. Sampson and H.L. Zhang, Phys. Rev. A45 (1992) 1657.

[33] H.L. Zhang and D.H. Sampson, Phys. Rev. A47 (1993) 208.

[34] N.C. Pyper, I.P. Grant and N. Beatham, Comput. Phys. Commun. 15 (1978) 387.

[35] K.J. Reed, Phys. Rev. A37 (1988) 1791.

[36] P.L. Hagelstein and R.K. Jung, At. Data Nucl. Data Tables 37 (1987) 121.

[37] I.P. Grant, J. Phys. B7 (1974) 1458.

[38] D.H. Sampson, H.L. Zhang and C.J. Fontes, At. Data Nucl. Data Tables 48 (1991) 25.

[39] F.A. Babushkin, Opt. Spectr. 13 (1962) 77; Acta. Phys. Polon. 25 (1964) 749; Opt. Spectr. 19 (1965) 1.

[40] H.L. Zhang, D.H. Sampson and A.K. Mohanty, Phys. Rev. A40 (1989) 616.

[41] A. De-Shalit and I. Talmi, Nuclear Shell Theory, Academic, London, 1963.

[42] D.L. Moores, (Personal communication).

[43] M.E. Riley and D.G. Truhlar, J. Chem. Phys. 63 (1975) 2182.

[44] J.M. Peek and J.B. Mann, Phys. Rev. A25 (1982) 749.

[45] J.B. Mann, At. Data Nucl. Data Tables 29 (1984) 407.

[46] R.E.H. Clark, J. Abdallah Jr., G. Csanak, J.B. Mann and R.D. Cowan, LANL Manual LA-11436-M, vol. II (Dec. 1988).

[47] C. Bottcher, D.C. Griffin and M.S. Pindzola, J. Phys. B16 (1983) L65.

[48] C.J. Fontes and H.L. Zhang, Phys. Rev. A76 (2007) 040703(R).

[49] H. Bethe, Ann. Phys. (Leipzig) 5 (1930) 325.

[50] H. Bethe, Z. Phys. 76 (1932) 293.

[51] H. Bethe, in: H. Geiger, K. Scheel (Eds.), Handbuch der Physik, vol. 24, part 1, Springer, Berlin, 1933, p. 273.

[52] M. Inokuti, Rev. Mod. Phys. 43 (1971) 297.

[53] U. Fano, Annu. Rev. Nucl. Sci. 13 (1963) 1.

[54] A. Burgess and V.B. Sheorey, J. Phys. B7 (1974) 2403.

[55] H.L. Zhang and D.H. Sampson, Phys. Rev. A52 (1995) 3827.

[56] A. Burgess, J. Phys. B7 (1974) L364.

[57] M. Abramowitz and I.A. Stegun, Handbook of Mathematical Functions, Dover, New York, 1972.

[58] Y.-K. Kim and P.S. Bagus, Phys. Rev. A8 (1973) 1739.

[59] C.J. Fontes, D.H. Sampson and H.L. Zhang, Phys. Rev. A47 (1993) 1009.

[60] C.J. Fontes, D.H. Sampson and H.L. Zhang, Phys. Rev. A49 (1994) 3704.

[61] M.H. Mittleman, Phys. Rev. A4 (1971) 893; Phys. Rev. A5 (1972) 2395; Phys. Rev. A24 (1981) 1167.

[62] J.D. Jackson, Classical Electrodynamics, John Wiley & Sons, New York, 1975.

[63] D.W. Walker, J. Phys. B8 (1975) 760.

[64] M.S. Pindzola, N.R. Badnell, D.L. Moores and D.C. Griffin, Z. Phys. D Suppl. 21 (1991) S23.

[65] D.L. Moores and M.S. Pindzola, J. Phys. B25 (1992) 4581.

[66] K. Widmann, P. Beiersdorfer, G.V. Brown, J.R. Crespo Lopez-Urrutia, A.L. Osterheld, K.J. Reed, J.H. Scofield and S.B. Utter, in: D.S. Gemmell et al. (Eds.), X-Ray and Inner-Shell Processes, AIP Conference Proceedings No. 506, AIP, New York, 2000, p. 444.

[67] H.L. Zhang and D.H. Sampson, At. Data Nucl. Data Tables 43 (1989) 1.

[68] H.L. Zhang, D.H. Sampson and C.J. Fontes, At. Data Nucl. Data Tables 44 (1990) 31.

[69] D.H. Sampson, H.L. Zhang and C.J. Fontes, At. Data Nucl. Data Tables 44 (1990) 209.

[70] H.L. Zhang, D.H. Sampson and C.J. Fontes, At. Data Nucl. Data Tables 44 (1990) 273.

[71] H.L. Zhang, D.H. Sampson and C.J. Fontes, At. Data Nucl. Data Tables 48 (1991) 91.

[72] H.L. Zhang and D.H. Sampson, At. Data Nucl. Data Tables 52 (1992) 143.

[73] H.L. Zhang and D.H. Sampson, At. Data Nucl. Data Tables 56 (1994) 41.

[74] H.L. Zhang and D.H. Sampson, At. Data Nucl. Data Tables 58 (1994) 255.

[75] H.L. Zhang and D.H. Sampson, At. Data Nucl. Data Tables 63 (1996) 275.

[76] H.L. Zhang and D.H. Sampson, At. Data Nucl. Data Tables 65 (1997) 183.

[77] H.L. Zhang and D.H. Sampson, At. Data Nucl. Data Tables 72 (1999) 153.

[78] H.L. Zhang and D.H. Sampson, At. Data Nucl. Data Tables 82 (2002) 357.

[79] C.J. Fontes, D.H. Sampson and H.L. Zhang, At. Data Nucl. Data Tables 72 (1999) 217.

[80] D.H. Sampson, Astrophys. J. 129 (1959) 734.

[81] H.L. Zhang and D.H. Sampson, Astrophys. J. Suppl. 63 (1987) 487.

[82] H.L. Zhang and D.H. Sampson, Phys. Rev. A42 (1990) 5378.

[83] M.S. Pindzola, D.L. Moores and D.C. Griffin, Phys. Rev. A40 (1989) 4941.

[84] D.L. Moores and M.S. Pindzola, (1990, Personal communication).

[85] D.L. Moores and M.S. Pindzola, Phys. Rev. A42 (1990) 5384.

[86] K.J. Reed, M.H. Chen and D.L. Moores, Phys. Rev. A41 (1990) 550.

[87] M.S. Pindzola and M.J. Buie, Phys. Rev. A37 (1988) 3232.

[88] M.S. Pindzola and M.J. Buie, Phys. Rev. A39 (1989) 1029.

[89] R.E. Marrs, S.R. Elliot and D.A. Knapp, Phys. Rev. Lett. 72 (1994) 4082.

[90] C.J. Fontes, D.H. Sampson and H.L. Zhang, Phys. Rev. A51 (1995) R12.

[91] D.L. Moores and K.J. Reed, Phys. Rev. A51 (1995) R9.

[92] D.L. Moores, L.B. Golden and D.H. Sampson, J. Phys. B13 (1980) 385.

[93] L.B. Golden and D.H. Sampson, J. Phys. B13 (1980) 2645.

[94] R.E.H. Clark and D.H. Sampson, J. Phys. B17 (1984) 3311.

[95] C.J. Fontes, D.H. Sampson and H.L. Zhang, Phys. Rev. A48 (1993) 1975.

[96] C.J. Fontes, D.H. Sampson and H.L. Zhang, Phys. Rev. A59 (1999) 1329.

[97] U. Fano, Phys. Rev. 102 (1956) 385.

[98] H.L. Zhang, Phys. Rev. A57 (1998) 2640.

[99] M.J. Seaton, C.J. Zeippen, J.A. Tully, A.K. Pradhan, C. Mendoza, A. Hibbert and K.A. Berrington, Rev. Mex. Astron. Astrofis. 23 (1992) 19.

[100] K. Berrington, L. Quigley and H.L. Zhang, J. Phys. B30 (1997) 5409.

[101] J.A. Tully, M.J. Seaton and K.A. Berrington, J. Phys. B23 (1990) 3811.

[102] J. Abdallah Jr., H.L. Zhang, C.J. Fontes, D.P. Kilcrease and B.J. Archer, J. Quant. Spect. Radiat. Trans. 71 (2001) 107.

[103] C.J. Fontes, J. Colgan, H.L. Zhang and J. Abdallah Jr., J. Quant. Spect. Radiat. Trans. 99 (2006) 175.

[104] R.D. Cowan, J. Phys. B13 (1980) 1471.

[105] D.H. Sampson and H.L. Zhang, J. Quant. Spect. Radiat. Trans. 54 (1995) 345.

[106] D.H. Sampson and H.L. Zhang, J. Quant. Spect. Radiat. Trans. 55 (1996) 279.

[107] H.P. Summers, The ADAS User Manual, Version 2.6 (2004), http://www.adas.ac.uk/.

[108] Y. Hahn, Adv. At. Molec. Phys. 21 (1985) 123.

[109] M.P. Scott and K.T. Taylor, Comput. Phys. Commun. 25 (1982) 347.

[110] K.A. Berrington, W. Eissner, P.H. Norrington, Comput. Phys. Commun. 92 (1995) 290.

[111] R.D. Cowan and J.B. Mann, Astrophys. J. 232 (1979) 940.

[112] D.C. Griffin, M.S. Pindzola and C. Bottcher, Phys. Rev. A36 (1987) 3642.

[113] M.J. Seaton, Y. Yu, D. Mihalas and A.K. Pradhan Mon. Not. R. Astr. Soc. 266 (1994) 805.

[114] A.K. Pradhan and H.L. Zhang, J. Phys. B30 (1997) L571.

[115] M.J. Seaton and P.J. Storey, in: P.G. Burke, B.L. Moiseiwitsch (Eds.), Atomic Processes and Applications, North-Holland, Amsterdam, 1976, p. 133.

[116] Y. Hahn and K.J. LaGattuta, Physics Reports 166 (1988) 195.

[117] S.N. Nahar and A.K. Pradhan, Phys. Rev. A49 (1994) 1816.

[118] F. Robicheaux, T.W. Gorczyca, M.S. Pindzola and N.R. Badnell, Phys. Rev. A52 (1995) 1319.

[119] T.W. Gorczyca and N.R. Badnell, J. Phys. B29 (1996) L283.

[120] H.L. Zhang, S.N. Nahar and A.K. Pradhan, J. Phys. B32 (1999) 1459.

[121] N. D'Cruz and C. Sarazin, (Personal communication).

[122] R.A. Syunyaev and E.M. Churazov, Soviet Astron. Lett. 10 (1983) 201.

[123] D.H. Sampson and H.L. Zhang, J. Phys. B30 (1997) 1449.

[124] H.L. Zhang and D.H. Sampson, Mon. Not. R. Astron. Soc. 292 (1997) 133.

[125] H.L. Zhang and D.H. Sampson, Phys. Rev. A61 (2000) 022707.

[126] H.L. Zhang and D.H. Sampson, Mon. Not. R. Astron. Soc. 322 (2001) 433.

[127] R.E. Marrs, M.A. Levine, D.A. Knapp and J.R. Henderson, Phys. Rev. Lett. 60 (1988) 1715.

[128] H.L. Zhang, D.H. Sampson and R.E.H. Clark, Phys. Rev. A41 (1990) 198.

[129] G.D. Carse and D.W. Walker, J. Phys. B6 (1973) 2529.

[130] M.K. Inal, H.L. Zhang and D.H. Sampson, Phys. Rev. A46 (1992) 2449.

[131] M.K. Inal, D.H. Sampson, H.L. Zhang and J. Dubau, Physica Scripta 55 (1997) 170.

[132] M.K. Inal and J. Dubau, J. Phys. B20, 4221 (1987).

[133] C.J. Fontes and H.L. Zhang, Phys. Rev. A (to be published).

[134] G. Arfken, Mathematical Methods for Physicists 3rd Edition, Academic Press, New York, 1985, p. 681.

[135] K.L. Wong, P. Beiersdorfer, K.J. Reed and D.A. Vogel, Phys. Rev. A51 (1995) 1214.

[136] S. Chantrenne, P. Beiersdorfer, R. Cauble and M.B. Schneider, Phys. Rev. Lett. 69 (1992) 265.

[137] P. Beiersdorfer, D.A. Vogel, K.J. Reed, V. Decaux, J.H. Scofield, K. Widmann, G. Hölzer, E. Förster, O. Wehrhan, D.W. Savin and L. Schweikhard, Phys. Rev. A53 (1996) 3974.

[138] P. Beiersdorfer, G. Brown, S. Utter, P. Neill, K.J. Reed, A.J. Smith and R.S. Thoe, Phys. Rev. A60 (1999) 4156.

[139] A.S. Shlyaptseva, A.M. Urno and A.V. Vinogradov, P.N. Lebedev Physical Institute of the USSR Academy of Sciences Report No. 194 (1981) (unpublished).

[140] A.V. Vinogradov, A.M. Urno and A.S. Shlyaptseva, in: I.I. Sobelman (Ed.), Atomic and Ionic Spectra and Elementary Processes in Plasma, Proceedings of the Lebedev Institute Academy of Sciences of Russia Vol. 192, Nova Science, Commack, New York, 1992, p. 93.

[141] M.K. Inal and J. Dubau, J. Phys. B47 (1993) 4794.

[142] C.J. Fontes, H.L. Zhang and D.H. Sampson, Phys. Rev. A59 (1999) 295.

[143] H.L. Zhang and D.H. Sampson, Phys. Rev. A66 (2002) 042704.

[144] H.L. Zhang, D.H. Sampson and M.K. Inal, Phys. Rev. A63 (2001) 052713.

[145] M.K. Inal, H.L. Zhang, D.H. Sampson and C.J. Fontes, Phys. Rev. A65 (2002) 032727.